Enhanced Uplink Packet Access in WCDMA

Combined Performance of Advanced Packet Scheduling Techniques, Fast L1 HARQ, Interference Cancellation, and 4-Branch Antenna Diversity

Rosa, Claudio

Publication date:
2008

Document Version
Publisher's PDF, also known as Version of record

Enhanced Uplink Packet Access in WCDMA

Combined Performance of Advanced Packet Scheduling Techniques, Fast L1 HARQ, Interference Cancellation, and 4-Branch Antenna Diversity

Ph.D. thesis by Claudio Rosa

December 2004

Department of Communication Technology
Institute for Electronic Systems, Aalborg University

Supervisors:
Research professor Ph.D. Preben E. Mogensen, Aalborg University
Ph.D. Jeroen Wigard, Nokia Networks R&D, Aalborg
Associate professor Ph.D. Troels B. Sørensen, Aalborg University

R04-1028
ISSN 0908-1224
ISBN 87-90834-72-0

Abstract

In the last years the focus in the evolution of WCDMA has been given to the downlink (base station to mobile) direction of transmission. This has led to the development of the high speed downlink packet access (HSDPA) concept. The main target of HSDPA has been to increase user peak data rates, quality of service, and generally improve spectral efficiency for downlink asymmetrical and bursty packet data services. However, the introduction of new and more demanding uplink services such as image/data upload, interactive gaming with rapid response patterns, etc., has directed concern to the possible limitation of uplink capacity and quality of service.

This thesis investigates the most promising technologies for the enhancement of WCDMA uplink performance, and in particular, their combined performance. This includes fast Node B scheduling, fast physical layer (L1) hybrid ARQ (HARQ) retransmission schemes, 4-branch antenna diversity, and interference cancellation (IC). Much the same techniques are considered for the high speed uplink packet access (HUSPA) concept currently under standardisation for Release 6 of the 3GPP specifications.

The system architecture according to the basic WCDMA, or Release 99 of the 3GPP, specifications is selected as a reference scenario in which the uplink packet access is under control of a packet scheduler located in the Radio Network Controller (RNC). Due to the long scheduling delays and a significant radio resource control signalling overhead, this system architecture is not optimal when considering packet data applications characterised by bursty data transmission and instantaneous requirements for relatively high data transmission rates. Therefore, as for HSDPA, the possibility of moving part of the packet scheduling functionality from the RNC to the Node B is considered.

With the packet scheduler moved to the Node B, packet scheduling can be performed more dynamically and uplink resources redistributed among the users more rapidly based on near instantaneous knowledge of their actual requirements. A scheduling algorithm that performs resource management based on the utilisation of the allocated radio resources is proposed and its performance investigated. Also, the impact on system performance of L1 HARQ schemes is assessed. Given specific outage constraints for both network load and user performance, the gain over the reference RNC scenario from jointly deploying the proposed fast Node B scheduling algorithm and fast L1 HARQ schemes in a macro-cell environment is approximately 25% (from 1.1 Mbps to 1.4 Mbps) and 60% (from 800 kbps to 1.3 Mbps) for a mobile speed of 3 and 50 km/h, respectively.

With the combination of a reduced scheduling rate down to the duration of a single data frame, a reduction of the frame size to 2 ms, and the introduction of frame synchronous transmission in uplink, it is possible to develop a Node B scheduling concept based on a time division multiplex. With time scheduling users can be allocated for transmission with high instantaneous data rates, and potentially when they experience favourable channel conditions. With these changes, the performance of different scheduling algorithms deploying time-division scheduling is investigated. With low user mobility, the capacity gain of the proposed channel-dependent schedulers over the reference RNC-located packet scheduler is 50% (from 1.1 to 1.65 Mbps) in a macro-cell environment, and 80% (from 1.05 to 1.9 Mbps) in a pedestrian micro-cell environment.

Finally, 4-branch antenna diversity and IC increase the cell throughput by 140% compared to a conventional Node B receiver configuration. These additional techniques, combined with advanced packet scheduling and fast L1 HARQ schemes, are shown to give a total cell throughput gain over basic Release 99 uplink packet access of approximately 250%.

Dansk Resumé

Udviklingen af WCDMA has i de sidste år haft speciel fokus på transmissionsretningen fra basisstationen til mobilen, den såkaldte downlink. Det har ført til udviklingen af High Speed Downlink Packet Access (HSDPA) konceptet. Hovedformålet har været at forøge den maksimale datarate, servicekvaliteten, og generelt spektraleffektiviteten for asymmetriske downlink pakkedata services. Introduktionen af nye og mere krævende services såsom overførsel af billede/data og interaktive spil i den modsatte transmissionsretning, uplink, har imidlertid rettet fokus mod potentielle kapacitets- og servicekvalitets-problemer i uplink.

Denne ph.d. afhandling undersøger de mest lovende teknikker til forbedring af WCDMA uplink, herunder specielt deres indvirkning i kombination. Teknikkerne inkluderer hurtig Node B pakkeskedulering, hurtig fysisklags (L1) hybrid ARQ (HARQ) retransmission, 4-grens antennediversitet og interferensudligning (IC). Tilsvarende teknikker er under overvejelse i forbindelse med High Speed Uplink Packet Access; HSUPA er p.t. under standardisering i 3GPP forumet for Release 6 af 3GPP specifikationerne.

Som referencescenario er der valgt en systemarkitektur svarende til Release 99 af 3GPP specifikationerne; i denne arkitektur er uplink pakkedata acces under kontrol af en pakkeskeduler placeret i radionetværkskontrolleren (RNC). På grund af de lange tidsforsinkelser, og et betydeligt overhead til signalering, er denne arkitektur ikke optimal under betragtning af pakkedata applikationer karakteriseret ved kraftigt varierende datarate, og som kræver momentant høje datarater. Som for HSDPA er der derfor overvejet en arkitektur hvor dele af pakkeskeduler funktionaliteten er flyttet til Node B.

Med pakkeskeduleren placeret i Node B kan skeduleringen foregå hurtigere og mere dynamisk og således tilsigte en fordeling af uplink radio resurserne mellem brugerne i overensstemmelse med deres momentane transmissionsbehov. Specifikt foreslås og undersøges der en algoritme til resursekontrol baseret på udnyttelsen af de allokerede resurser, og i sammenhæng hermed, indvirkningen af L1 HARQ metoder. Med givne krav for både den opnåelige netværks trafikbelastning og bruger servicekvalitet i et makrocellulært udbredelsesmiljø er det vist at kapacitetsforøgelsen over RNC referencescenariet for de to teknikker i kombination er henholdsvis 25% (fra 1.1 Mbps til 1.4 Mbps) i tilfældet af lav mobilitet og 60% (fra 800 kbps til 1.3 Mbps) i tilfældet af høj bruger mobilitet.

Med yderligere reduktion af tidsintervallet for pakkeskedulering, d.v.s hurtigere skedulering, en reduktion af rammetidsintervallet ned til 2 ms, og introduktionen af rammesynkron uplink transmission, er det muligt at udvikle et Node B skeduleringskoncept baseret på et tidsmultipleks af brugere. Med tidsbaseret skedulering kan brugerne allokeres meget høje momentane datarater, og potentielt når deres radiokanal er specielt favorabel. Med disse ændringer er der undersøgt forskellige skeduleringsalgoritmer baseret på tidsmultipleksing. Kapacitetsforøgelsen over RNC referencescenariet i tilfældet af lav brugermobilitet er henholdsvis 50% (from 1.1 to 1.65 Mbps) i et makrocellulært udbredelsesmiljø og 80% (fra 1.05 til 1.9 Mbps) i et mikrocellulært udbredelsesmiljø.

Endeligt er der i afhandlingen inkluderet 4-grens antennediversitet og IC der tillader en forøgelse af netværkskapaciteten med 140% i sammenligning med en konventionel Node B modtagerkonfiguration. I kombination med avanceret pakkeskedulering og hurtig L1 HARQ er det vist at disse teknikker kan give en total kapacitetsforøgelse på cirka 250% i sammenligning med Release 99 uplink pakkedata acces.

Preface and Acknowledgments

This Ph.D. thesis is the result of a three-year project carried out at the Division for Cellular Systems (Csys), Department of Communication Technology, Aalborg University. The thesis work has been completed in parallel with the mandatory courses and teaching/working obligations required in order to obtain the Ph.D. degree. The investigation has been conducted under the supervision of Research Professor Ph.D. Preben E. Mogensen (Aalborg University), and the co-supervision of Ph.D. Jeroen Wigard (Nokia Networks) and Associate Professor Ph.D. Troels B. Sørensen (Aalborg University). This Ph.D. research has been fully sponsored by Nokia Networks.

The thesis investigates new techniques to enhance the performance of uplink packet access in WCDMA systems, with a particular focus on their combined performance. In the very early stages of the Ph.D. study the project concentrated on investigating the performance of uplink common channels, specifically the Random Access Channel (RACH). Later on the scope was moved to the enhancement of uplink dedicated transport channels due to the increasing interest that this research area progressively gained within the 3rd Generation Partnership Project (3GPP). The study is primarily based on computer simulations, taking many practical system aspects into account. The reader is expected to have a basic knowledge about system level aspects of UMTS, as well as radio propagation.

There are many people I would like to thank for the help they gave me during these last three years. Without their contribution and support this project would have never been possible.

First of all I am deeply grateful to my supervisor Preben E. Mogensen for his guidance and wise advices during the completion of this Ph.D. work. Also, I would like to thank him for believing in me when about four years ago he gave me the opportunity to extend my stay at Aalborg University to complete the MSc programme in Mobile Communications. This has significantly changed my life both from a personal and from a professional point of view, therefore I will always be grateful to him.

I am also deeply thankful to Jeroen Wigard, who together with Preben has been helping me and devoting me much of his time since my first day in Aalborg. He also encouraged me in many situations, and gave me an inestimable support in the review of this report. For the same reason many appreciations are paid to Troels B. Sørensen, whom I would also like to thank for an unnumbered amount of enlightening and productive discussions.

I would also like to express my gratitude to my colleagues and former Ph.D. students Konstantinos Dimou and José Outes, whom I have worked in close collaboration with for a time period of approximately one year; they surely contributed to inspire a great part of the work presented in this thesis.

The help of all my colleagues and former colleagues at the Cellular System group at Aalborg University has been deeply appreciated. I would like to thank Laurent Schumacher for his technical support during the first year of my Ph.D. study. Thanks to Lisbeth S. Larsen for helping me every time I needed it, and for significantly contributing to my improvements in speaking Danish. Thanks also to Lars T. Berger and Oumer Teyeb for sharing with me the experience of being a Ph.D. student at Aalborg University.

I am also thankful to all the employees at Nokia Networks R&D for their inestimable contribution to my personal and professional growth. In particular, thanks to Klaus I. Pedersen and Troels E. Kolding for sharing with me some of their invaluable knowledge, to Frank Frederiksen for providing the link level results used during the Ph.D. investigation and

for reviewing part of this thesis, and to Tako F. Lootsma for his kindness and always appreciated good humour.

Moreover, I am sincerely grateful to ‘my Danish family’; thanks to Kirsten and Enoch, Morten and Karin, Lone and Thomas for making me feel like I was home, and for making me understand and appreciate what Denmark is really about.

I am infinitely thankful to my parents Elide and Attilio and to my sister Laura, who with their unconditional love have supported me since the first day I left Italy. With them I would also like to thank the rest of my family and friends, to whom I will always be grateful for the affection and friendship they offered me.

Foremost, I would like to thank my girlfriend Lise, who has been by my side day after day, giving me love and support especially in the difficult moments. She has also designed the cover of this Ph.D. report, for which reason I am once more grateful to her.

Claudio Rosa

December 2004

Table of Contents

Abbreviations

3G	3rd generation mobile communications
3GPP	3rd generation partnership project
4G	4th generation mobile communications
AC	Admission control
ACK	Positive acknowledgement
AMC	Adaptive modulation and coding
ARQ	Automatic repeat request
AVI	Actual value interface
AWGN	Additive white Gaussian noise
BER	Bit error rate
BFT	Blind fair throuhgput
BLER	Block error rate
CC	Chase combining
CD	Code division
CDF	Cumulative distribution function
CDM	Code division multiplexing
CDMA	Code division multiple access
CN	Core network
CPCH	Common packet channel
CQI	Channel quality indicator
CRC	Cyclic redundancy check
CSAFT	Channel-state aware fair throughput
CWD	Congestion window
DCH	Dedicated channel
DPCCH	Dedicated physical control channel
DPDCH	Dedicated physical data channel
DS-CDMA	Direct sequence code division multiple access
E_b/N_0	Data bit energy to interference ratio
E-DCH	Enhanced dedicated channel
EDGE	Enhanced data rates for global evolution
FAHC	Forward access channel
FDD	Frequency division duplex
FEC	Forward error correction

FTP	File transfer protocol
GGSN	Gateway GPRS support node
GPRS	General packet radio service
GSM	Global system for mobile communications
HARQ	Hybrid automatic repeat request
HC	Handover control
HSDPA	High speed downlink packet access
HSUPA	High speed uplink packet access
IC	Interference cancellation
IMT-2000	International mobile telephony
IP	Internet protocol
I-Q	In-phase and quadrature phase
IR	Incremental redundancy
IRC	Interference rejection combining
ITU	International telecommunications union
L1	Layer 1 (physical layer)
L2	Layer 2 (data layer)
L3	Layer 3 (network layer)
LC	Load control
MAC	Medium access control
MAI	Multiple access interference
MIMO	Multiple-input-multiple-output
MRC	Maximal ratio combining
MTPE	Maximise transmission power efficiency
MUD	Multi-user detection
NACK	Negative acknowledgement
NBAP	Node B application protocol
NR	Noise rise
NRT	Non-real time
OLPC	Outer loop power control
P2P	Peer-to-peer
PAR	Peak-to-average ratio
PC	Power control
PCT	Packet call throughput
PDCP	Packet data convergence protocol

PDF	Probability density function
PDU	Packet data unit
PHY	Physical layer (Layer 1)
PIE	Power increase estimator
PS	Packet scheduler
QoS	Quality of service
RACH	Random access channel
RB	Radio bearer
RLC	Radio link control
RNC	Radio network controller
RNS	Radio network sub-system
RRC	Radio resource control
RRM	Radio resource management
RT	Real time
RTT	Round trip time
RUF	Resource utilisation factor
SAW	Stop-and-wait
SHO	Soft handover
SINR	Signal-to-interference plus noise ratio
TB	Transport block
TCP	Transmission control protocol
TDD	Time division duplex
TDM	Time division multiplexing
TFC	Transport format combination
TFCI	Transport format combination indicator
TFCS	Transport format combination set
TTI	Transmission time interval
TVMR	Traffic volume measurement report
UCQI	Uplink channel quality indicator
UE	User equipment
UMTS	Universal mobile telecommunications system
UTRA	UMTS terrestrial radio access
UTRAN	UMTS terrestrial radio access network
VSF	Variable spreading factor
WCDMA	Wideband code division multiple access

Chapter 1

Introduction

1.1 WCDMA: A Technology About Services

Since its first launch in year 1992, GSM (Global System for Mobile communications) has grown to be the most successful mobile communication system for digital cellular networks, delivering high-quality voice and simple text messaging services to mobile users. In more recent years, the great popularity gained by the fixed Internet together with the significant growth of mobile subscribers all around the world has suggested network operators to introduce mobile-Internet packet-based services in wireless communication systems. Moreover, in a market where the average revenue per user of basic voice services is predicted to decline during the next years [UMTS03], network operators and content providers are compelled to offer new and attractive services to ensure they deliver business growth in regions where the market for voice services is already saturated.

GPRS (General Packet Radio Service) introduces the packet core to GSM networks and can provide users with an average data throughput of about 30-40 kbps [Erik01], thus playing an important role in bringing to market evolved messaging services and speeding up e-mail and the Internet experience. EDGE (Enhanced Data Rates for Global Evolution) enhances the capabilities of the GPRS air interface and makes it possible to experiencing data transmission rates in the order of 120 kbps [Furu99], thus enabling the provision of e-newspapers, images and sound files. However, both GPRS and EDGE do not allow multiplexing of services with different quality requirements on a single connection, e.g. speech, video and packet data.

Third-generation (3G) mobile communication systems were mainly introduced to address the limited data handling and multimedia capabilities of second-generation systems. Specifically, one of the most important aspects of 3G is enhanced packet-data access. 3G systems are covered under the IMT-2000 umbrella, and in Europe are referred to as UMTS (Universal Mobile Telecommunication System). UMTS is based on the WCDMA (Wideband Code Division Multiple Access) air interface, providing simultaneous support for a wide range of services with different characteristics on a common 5 MHz carrier. UMTS is composed of two different but related modes: (i) UMTS Terrestrial Radio Access (UTRA) Frequency Division Duplex (FDD), and (ii) UTRA Time Division Duplex (TDD).

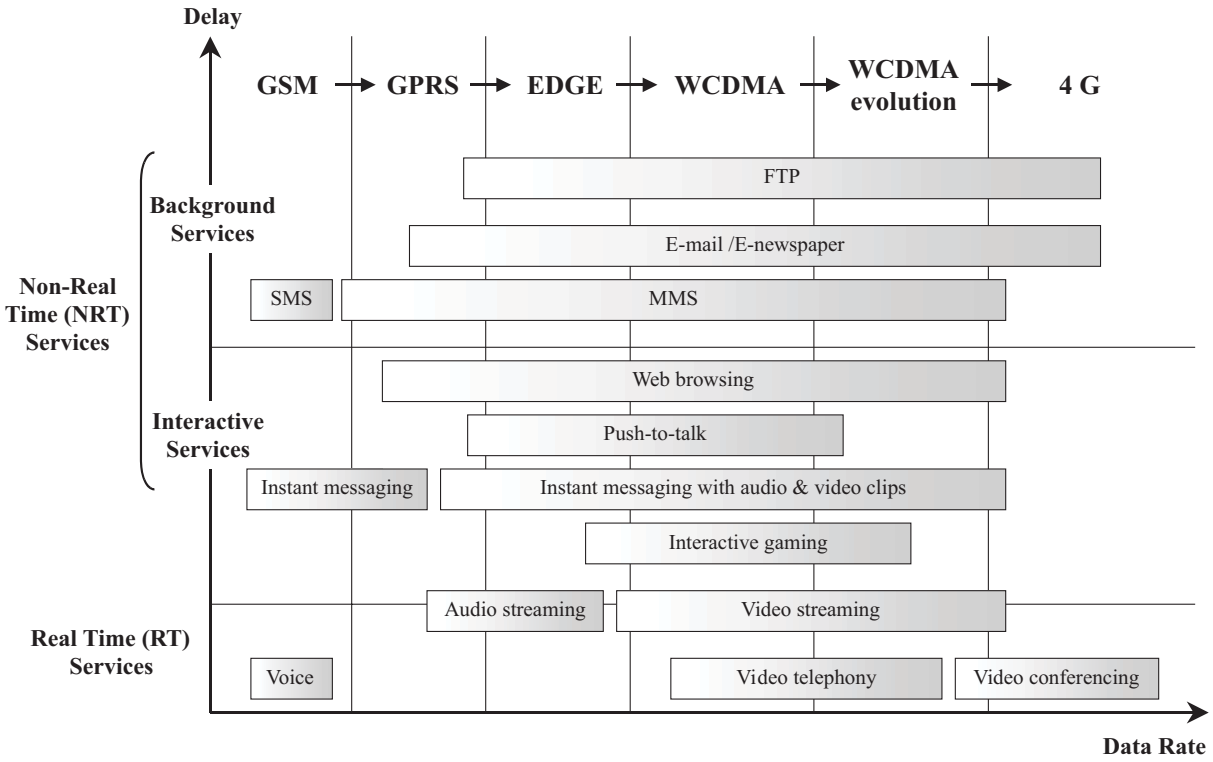

Figure 1.1: 3G Services and enabling technologies, based on information from [UMTS03] *and* [UMTS00].

Understanding the nature of the traffic that will flow across the UMTS networks is a key issue for the development of optimised solutions and advanced technologies for 3G systems. Figure 1.1 shows a few examples of services and application categories which users expect, and the enabling technologies that will support them [UMTS03] [UMTS00]. The diagram shows how the higher data rates of the WCDMA radio access technology are absolutely necessary to achieve the full multimedia experience.

Figure 1.1 also illustrates that 3G applications can be characterised both by their data rate and transfer delay requirements. For example, web browsing and video streaming have comparable bandwidth requirements, but video streaming requires much lower transfer delays. In terms of delivery requirements, a Real Time (RT) application is one that requires information delivery for immediate consumption. RT services demand the transfer delay and the required bandwidth to be guaranteed with a high probability. Typical examples of RT services are voice telephony and live video transmission (video telephony).

For Non-Real Time (NRT) services such as file transfer and e-mail, the main target is for the data to eventually arrive at its destination (best effort transmission) with a certain probability of successful transmission. This may imply data being transmitted across the system at varying bit rates, and also the retransmission of data if packets are lost. NRT services can be further differentiated between interactive and background services, the latter having less severe delay requirements.

The contrasting latency and reliability requirements of RT and NRT services suggest that these services should be handled in different ways. Specifically, the intrinsic packet-switched nature of NRT applications introduces flexibility in the system, which can be exploited by a more efficient allocation of the limited radio resources available in mobile communication systems.

With respect to the 3G services illustrated in Figure 1.1, the main focus of this Ph.D. investigation is on NRT applications.

1.2 WCDMA Evolution: The Way Towards Enhanced Packet Access

The 3rd Generation Partnership Project (3GPP) is a collaboration agreement whose scope is to produce globally applicable technical specifications for 3rd generation mobile systems based on evolved GSM core networks and the radio access technologies that they support (WCDMA). The American complement is 3GPP2. In the beginning of this Ph.D. study, the 3GPP had already frozen the Release 99 specifications; Release 99 includes support for data rates up to 2 Mbps in indoor or small-cell outdoor environments, wide-area coverage at rates up to 384 kbps, and support for high-rate packet-data and circuit-switched services [Hedb01].

WCDMA Release 5 has later extended the Release 99 specifications with, among other things, a new downlink transport channel that enhances support for interactive, background, and to some extent, streaming services. It yields a considerable increase in both capacity and user performance compared to Release 99 by significantly reducing delays and providing peak data rates up to 10 Mbps. This WCDMA downlink evolution, which goes under the name of High Speed Downlink Packet Access (HSDPA), is the first step of evolving WCDMA to provide enhanced packet access performance [Kold03] [Park03].

The particular focus on improving performance in the downlink of WCDMA systems is justified by the fact that a large majority of wireless data services are inherently causing a much heavier load in the downlink direction of the communication path. However, as new services such as interactive gaming and FTP upload are introduced, the delay and data rate requirements of the uplink are also expected to increase [Chau99]. Therefore, to further improve the support of packet data services in third-generation systems, uplink enhancements are also needed.

With this scope, a study item on uplink enhancements for dedicated transport channels started in September 2002 within 3GPP [TR25896]. The goal was to investigate enhancements that could be applied to the Release 99 specifications in order to improve the performance of uplink dedicated transport channels, with focus on packet-data services like interactive gaming, video streaming, image and video-clip upload, peer-to-peer (P2P) applications, and so on. In the standardisation process, the study item has later evolved to become a work item in March 2004. At the moment of writing, an evolution of WCDMA uplink packet access named High Speed Uplink Packet Access (HSUPA) is targeted for the Release 6 of the 3GPP specifications, with the aim of reducing delays, increasing the data rates and improve the capacity of the uplink [Park04].

The Ph.D. work was initiated concurrently with the 3GPP study item on uplink enhancements for dedicated transport channels with the same overall goal for improving WCDMA uplink packet access.

1.3 Spectral Efficiency and Quality of Service: The Network Operator and the User Perspectives

One of the main objectives 3G network operators need to accomplish in order to succeed is to provide their subscribers with services they are willing to purchase. The term Quality of Service (QoS) refers to the collective effect of service performance that determines the degree of satisfaction of the end user. The demand imposed by a certain service on the system to provide a satisfactory user QoS completely depends on the inherent characteristics of the service itself. For voice services, a good experience usually means that the voice is clearly

understandable with no gaps. For streamed video, a good experience could indicate that the picture is of good quality with little interruption of the video frames. For a web page, a good experience could mean that the web page is received in eight to ten seconds [Bouch00].

QoS is introduced to take into consideration the subscriber's perspective. On the other hand, network operators need sufficient reward to prosper and wish to maximise the utilisation of the network resources (air interface, transmission and network elements). Hence, there is the necessity to develop solutions allowing for a more efficient utilisation of such resources. To this end, in mobile communication systems the spectral efficiency (the amount of information that is carried by a wireless system per unit of spectrum and per unit of area) is often used as the figure of merit, since it directly affects an operator's cost structure: For a given service and QoS requirement, the spectral efficiency determines the required amount of spectrum, the required number of base stations, and the required number of sites and associated site maintenance. As a consequence, increased spectral efficiency improves operator economics by reducing the required equipment per subscriber, and improves the end-user affordability, since the cost of service delivery directly reflects in service pricing.

1.4 Technologies to Enhance Uplink Spectral Efficiency: State of the Art

So far, plenty of effort has been dedicated to the research of new techniques to increase the spectral efficiency of WCDMA systems. However, as previously introduced, most of the work has concentrated on the downlink direction of the communication path, mainly due to the asymmetrical properties of the traffic that is expected to flow in early deployments of WCDMA networks. For what concerns uplink transmission, several approaches have been considered to increase the uplink performance by means of new advanced techniques. Some of these approaches are schematically illustrated in Figure 1.2.

Antenna Arrays – Conventionally, antenna arrays can be operated in one of two distinct modes: (i) Diversity mode or (ii) Beamforming mode. Diversity techniques rely on the statistical independence between the antenna elements to reduce the likelihood of deep fades, and are additionally able to provide an average signal-to-interference plus noise ratio (SINR) gain by coherently combining the signals received at each antenna element [Jakes74]. The performance of 2-branch antenna diversity in WCDMA uplink is reviewed in [Holma04], showing that the diversity gain reduces as the inherent multi-path diversity of the mobile

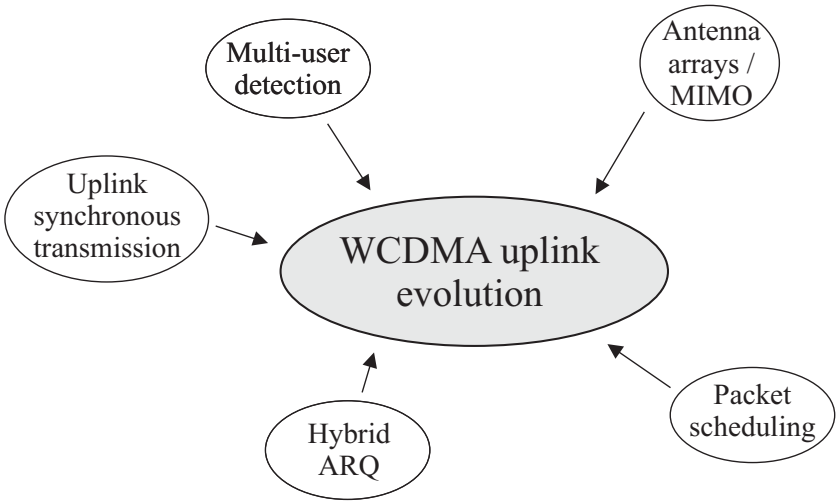

Figure 1.2: Technologies supporting WCDMA uplink evolution.

propagation channel increases. The performance of 4-branch antenna diversity is studied in [Holma01]. In this case the diversity gain compared to 2-branch antenna diversity is practically negligible, especially in presence of frequency-selective channels; still, 4-branch antenna diversity provides an overall gain of approximately 3 dB due to coherent combining.

Beamforming techniques create narrow beams towards each user in such a way that the multiple access interference is reduced by means of spatial filtering and potential suppression of interfering signals. In [Ylit00], it is shown that the diversity and beamforming concepts perform similarly with small number of antennas, but the beamforming approaches start to overcome the diversity techniques with large number of antennas and low azimuth spread. In [Rami03], beamforming techniques are proven to represent a real promise for enhancing the performance of WCDMA uplink, with a capacity gain over single-antenna reception up to 350% with eight antenna elements at the base station receiver.

The possibility of deploying antenna arrays both at the base station receiver and at the mobile terminal enables the use of multiple-input-multiple-output (MIMO) schemes in WCDMA uplink. The performance of some uplink diversity MIMO schemes are investigated in [Tiir03], showing that for uplink transmission doubling the number of receiving antennas is much more efficient than introducing the second transmitting antenna at the mobile terminal. There are also proposals in the open literature to utilise the MIMO systems so that several parallel spatially multiplexed data streams are transmitted between two transceivers equipped with antenna arrays, the so-called information MIMO [Fosc96].

Multi-User Detection – In a conventional CDMA system, all users interfere with each other. Theoretically, significant capacity increase and near-far resistance [Duel95] can be achieved if the negative effect that each user has to the others can be cancelled. A more fundamental view of this is multi-user detection [Verdu98], where the signals from different users are jointly used to better detect the signal from each individual user. The main drawback of the optimal multi-user detector introduced in [Verdu86] is that the complexity of the receiver grows exponentially with the number of users in the system. Therefore, over the last two decades, a lot of research has focused on finding suboptimal multi-user detector solutions which are more feasible to implement. A survey of different multi-user detection techniques for DS-CDMA systems is presented in [Duel95] and [Mosh96], where the trade-off between performance and complexity of multi-user detectors is also discussed. In [Bueh00], a performance comparison between some of the receiver structures most often discussed in the literature is presented on the basis of common assumptions. Theoretical analysis and simulation results show that parallel interference-cancellation receivers can offer significant performance increase with limited complexity.

Since the base station receiver has information on the chip sequences of all users served in the corresponding cell, and due to its potential to mitigate the near-far problem, multi-user detection is particularly suited for enhanced uplink performance of CDMA systems. The uplink capacity increase from interference cancellation in a multi-cell CDMA scenario is specifically addressed in [Hämä96] and [Meng03]. Both papers predict a capacity gain of approximately 100% compared to the performance with a conventional matched filter receiver. More recently, a study based on both system level simulations and measurements from a prototype parallel interference cancellation receiver has been presented in [Hage04]. The authors conclude that under realistic assumptions for the performance of the interference cancellation receiver, the capacity increase compared to the conventional Rake receiver in a multiple-cell typical urban radio environment is approximately 40%.

Uplink Synchronous Transmission Scheme – Synchronising the received signals at the Node B can potentially increase the capacity in the uplink of CDMA systems. The idea behind

uplink synchronisation is to use a similar approach as in the downlink, where the signals from the same cell are separated by means of orthogonal codes, thus reducing the multiple access interference [Outes04].

According to the results in [Kim01], uplink synchronous transmission can provide a theoretical capacity gain of 400%. However, these results are obtained for a single-cell scenario, without considering the effect of background noise power, and under the assumption of unlimited available orthogonal codes. Taking all these effects into account, the gain figure of uplink synchronous transmission reduces considerably to approximately 13% [Outes02a]. The gain can be increased up to 29% [Outes02b] with the introduction of variable modulation and coding. However, due to the significant changes required in the specifications compared to e.g. multi-user detection, uplink synchronous transmission has not been considered as a candidate technique for WCDMA enhanced uplink packet access [TR25896].

Hybrid ARQ – Schemes that incorporate error detection with automatic-repeat-request (ARQ) have been widely used for error control in wireline data communication systems since the early seventies. These schemes go under the name of hybrid ARQ [Lin84]. However, in the presence of wireless channels more spectrally efficient redundancy schemes than in wired networks are desirable. The first step in this direction has been taken with schemes such as chase combining [Chase85] and incremental redundancy [Mand74].

In the last years, hybrid ARQ schemes have been introduced as one of the core features of HSDPA, in order to ensure robustness and higher spectral efficiency [Kold03]. This has lead to quite a significant effort on hybrid ARQ schemes [Malk01] [Das01] [Fren01] [Fred02]. In [Malk01], for instance, the authors demonstrate that hybrid ARQ schemes can provide a capacity increase of 35% in the downlink of WCDMA systems compared to ARQ strategies that do not perform soft combining of information received at different transmission instants.

The question is whether or not hybrid ARQ schemes can provide the uplink of WCDMA systems with the same gain as in HSDPA. Hybrid ARQ for WCDMA uplink evolution has recently been subject of some research activity, showing some potential gain when combined with fast retransmission of erroneously received data frames [Mall04] [Park04]. However, since combining techniques are particularly suited for channels with a non-stationary bit error rate [Lin84], it is still to clarify which is the overall effect in the uplink from using hybrid ARQ schemes in combination with link adaptation based on fast closed loop power control. Some indications on the interaction between soft combining and power control are given in [Rait98], but also this work concentrates on the downlink direction of transmission.

Packet Scheduling – Circuit-switched systems are normally designed to meet absolute delay constraints, whereas the delay for data traffic normally is constrained in the statistical sense (e.g. average delay). The latter type of constraints implies an extra degree of freedom in the resource allocation procedure, leading to the possibility of a better resource utilisation [Zand97]. This inherent flexibility of packet-data services has opened for the possibility to perform data scheduling in wireless communication systems based on information on the instantaneous channel quality of the users [Knopp95] [Bhag96]. Based on this idea, different channel-dependent scheduling algorithms have been developed with the specific aim of increasing the spectral efficiency and/or QoS of HSDPA. In [Ameg03], the gain from channel-dependent scheduling compared to ‘blind’ allocation schemes in a macro-cell environment with low user mobility is estimated around 70%. More recently, several studies have considered the achievable scheduling gain by optimal resource allocation in the uplink of WCDMA systems [Jänt03] [Kuma03] [Oh03]. These papers show there is a potential for increasing the spectral efficiency in uplink by performing channel-dependent allocation of the available radio resources. However, the conducted research mainly makes use of an

information-theoretic approach. In this perspective, the development and performance assessment of channel-dependent packet scheduling strategies appositely designed for WCDMA uplink is needed.

Another way to enhance the uplink capacity of WCDMA systems by means of improved radio resource management is decentralised and faster packet scheduling operation. With decentralised packet scheduling, the entity controlling the allocation of the radio resources to NRT users is moved closer to the radio interface. Decentralised and faster packet scheduling operation is currently considered as one of the main modifications to the Release 99 standards to enable high-speed uplink packet access [TR25896]. Recently, papers investigating the uplink packet access performance with Release 6 WCDMA [Ghosh04] [Park04] and with the CDMA2000 1x EV-DV system [Pi03] have shown the potential for increased capacity due to decentralised and faster packet scheduling operation.

1.5 Ph.D. Objective

The main objective of this Ph.D. thesis is to investigate the potential enhancements in WCDMA uplink packet access compared to the Release 99 standard, both in terms of spectral efficiency and QoS.

The Ph.D. objective is illustrated in Figure 1.3, showing how the techniques investigated in this Ph.D. thesis to enhance uplink packet access performance can be used to increase the spectral efficiency while maintaining the user QoS, or to improve the user experienced QoS without decreasing the spectral efficiency in the system, or alternatively to increase both spectral efficiency and QoS.

The analysis of the most promising techniques introduced in Section 1.4 has confirmed that there is potential room for a substantial capacity enhancement in the uplink of WCDMA systems. In particular, the focus of this Ph.D. work is on the gain achievable when some of these techniques are used in combination with each other. More specifically, the following solutions are considered:

Fast L1 Retransmission Schemes – In Release 99, the entity controlling the retransmission of erroneously received data frames is located in the Radio Network Controller (RNC), and consequently the delay associated with the retransmissions of erroneous data frames is quite

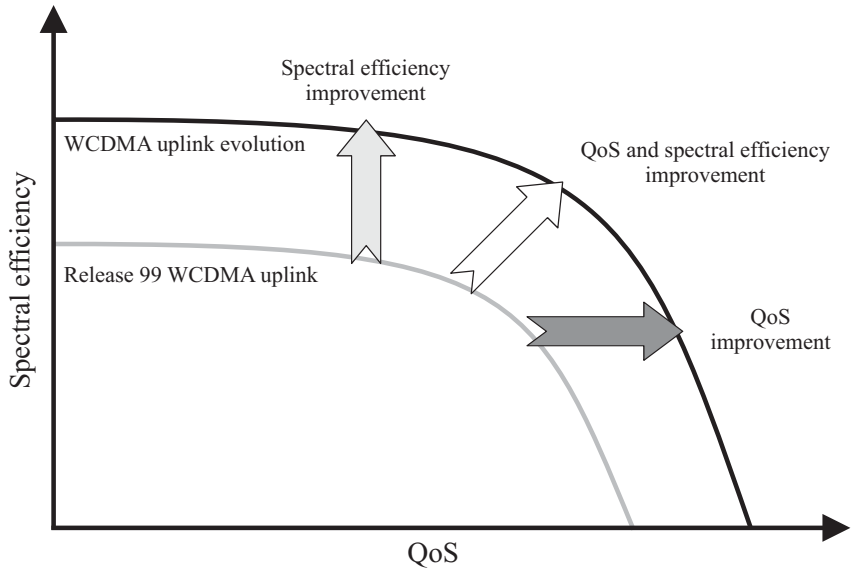

Figure 1.3: Spectral efficiency vs. QoS in WCDMA Release 99 and Release 99 WCDMA evolution.

significant. With the introduction of Node B-controlled retransmission schemes (Node B is the name used in 3GPP to indicate a base station), the retransmission delay is reduced, thus the physical channel can be operated at a higher error probability compared to Release 99. This results in increased spectral efficiency. Soft combining techniques can further improve the performance of Node B-controlled retransmission schemes.

In this thesis, the impact from Node B-controlled retransmission schemes (both with and without combining techniques) on the uplink spectral efficiency of WCDMA systems is investigated. In particular, the focus is on the interaction between Node B-controlled retransmission schemes, fast closed loop power control and fast Node B packet scheduling.

Fast Node B Packet Scheduling – In Release 99 uplink packet access the entity controlling the allocation of the radio resources to NRT users is also located in the RNC. With fast Node B packet scheduling tighter control of the total received power in uplink is possible compared to RNC scheduling. Moreover, the radio resources can be allocated to NRT users more dynamically based on near instantaneous information on their capacity requirements. Both these features have the potential to improve the performance of uplink packet access.

In this Ph.D. thesis, a new fast Node B scheduling algorithm for enhanced uplink performance is proposed, and its performance assessed and compared to the performance of a system using basic Release 99 features.

Channel-Dependent Scheduling – Channel-dependent radio resource allocation in the uplink of WCDMA systems has the potential for scheduling users for transmission when they experience favourable channel conditions. This results in reduced interference generated to other cells, hence in increased spectral efficiency.

This thesis presents an analysis of the advantages and disadvantages of introducing channel-dependent scheduling in WCDMA uplink. In this perspective, the thesis addresses the design and performance assessment of advanced scheduling strategies that perform channel-dependent radio resources allocation in WCDMA uplink.

4-Branch Antenna Diversity and Interference Cancellation – Antenna arrays and multi-user detection are among the most promising techniques for increased uplink performance. These technologies can be introduced in WCDMA uplink with limited cost compared to the downlink, mainly due to the fact that their complexity is concentrated at the receiver, i.e. at the base station for uplink transmission.

This work finally presents an investigation of the performance of 4-branch antenna diversity and interference cancellation in combination with advanced packet scheduling techniques and fast Node B-controlled retransmission schemes. The goal is to estimate the overall performance gain over Release 99 achievable with WCDMA uplink evolution, both in terms of spectral efficiency and QoS.

1.6 Assessment Methodology

Different options exist to evaluate the performance of a cellular network. Some of them are: (i) Analytic approach based on mathematical models, (ii) computer-aided simulations, and (iii) field trials in operational networks.

Analytic studies based on mathematical models have the advantage of low cost and high flexibility, but have the disadvantage of simple and incomplete modelling of real mobile communication systems; this is especially true with the additional randomness introduced by packet-data services.

On the other hand, field trials in an operational network can provide the most accurate performance assessment but require the availability of the network itself (high cost), and have the drawback of a strong dependence on the particular network configuration (low flexibility).

Computer-aided network simulations represent an appealing trade-off between the low cost and high flexibility of an approach based on theoretical analysis, and the high level of accuracy of field trials in an operational network. For this reason, computer-aided system level simulations are used in this Ph.D. thesis as the main performance assessment methodology, sometimes supported by theoretical analysis to more clearly understand the system behaviour and provide appreciation for the simulation results. A customised implementation of a dynamic system level simulator for the performance assessment of enhanced uplink packet access has been carried out as part of the Ph.D. work.

In order to assess the performance of enhanced uplink packet access in WCDMA, throughout the thesis the spectral efficiency and QoS previously introduced are quantified in terms of objective (engineering) measures. The most important are:

- The *cell throughput* is introduced to include the network operator's perspective. The cell throughput is defined as the number of bits per unit of time correctly received at the base station receiver.
- Similarly, the *packet call throughput* is introduced to allow for the user's perspective. It is defined as the number of bits per unit of time correctly delivered by a user during a packet-data session.

A more exhaustive definition of these and other key performance indicators used in the Ph.D. thesis can be found in Appendix A, Section A.2.

The general approach used for the evaluation of WCDMA uplink evolution starts from the performance assessment of a system deploying basic Release 99 features. The scope is to get a general understanding of the system functioning, and also to obtain a reference case for performance comparison. Then, the proposed modifications and advanced scheduling algorithms are introduced and analysed on a case-by-case basis. UTRA FDD mode is considered as a reference study case throughout the thesis.

The level of accuracy of the most relevant key performance indicators to the presented work is addressed in Appendix A, Section A.3.

1.7 Ph.D. Outline

The Ph.D. report is organised as follows:

Chapter 2: presents a general description of the uplink packet access procedure according to the Release 99 of the WCDMA specifications. It also gives an overview of the main network elements involved in uplink packet access, and of their respective functionality.

Chapter 3: introduces a specific implementation of the uplink packet access procedure in the system level simulator. The chapter aims at addressing the inherent trade-off between spectral efficiency and QoS in presence of high data rate NRT services in a system with basic Release 99 features. It also introduces some of the most relevant performance measures. The work presented in this chapter has been conducted together with former Ph.D. student Konstantinos Dimou (Ecole Nationale Supérieure des Télécommunications, France), to whom I must recognise 30% of the work.

Chapter 4: provides an evaluation of two techniques proposed to increase the performance of WCDMA uplink compared to the Release 99 specifications, namely fast L1 retransmission

schemes and fast Node B packet scheduling. A new algorithm for the allocation of radio resources to NRT users in the context of fast Node B packet scheduling operation is proposed and its performance assessed. The work presented in this chapter has been conducted together with former Ph.D. students Konstantinos Dimou and José Outes (Aalborg University), to whom I must recognise 50% of the work.

Chapter 5: a new scheduling concept for WCDMA uplink packet access based on combined time and code division scheduling is introduced. Time division multiplexing in the uplink of WCDMA yields to the possibility of exploiting multi-user diversity by means of channel-dependent scheduling The chapter first gives a general introduction to the main advantages and disadvantages of the proposed scheme. Then a comprehensive set of simulation results is presented to assess the performance enhancement that the proposed scheduling algorithms can provide compared to a basic implementation according to the Release 99 WCDMA specifications. The work presented in this chapter has been conducted together with former Ph.D. student José Outes, to whom I must recognise 30% of the work.

Chapter 6: gives an evaluation of the uplink performance enhancement achievable by deploying 4-branch antenna diversity and interference cancellation in combination with the advanced scheduling schemes presented in the previous chapters. A semi-analytical study is also presented that derives the theoretical cell throughput gain from interference cancellation, and compares it with the pole capacity (see definition [A 2.13]) gain derived in previous literature. The chapter also aims at addressing the potential performance enhancement when the users can be instantaneously allocated peak data rates up to 768 kbps. For other parts, peak data rates are limited to 384 kbps. The work presented in this chapter has been conducted without the contribution of others.

Chapter 7: draws the main conclusions of the Ph.D. investigation and discusses future research topics.

A number of appendices is also included with additional information to clarify certain aspects not comprehensively detailed in the main chapters of the Ph.D. report.

1.8 Publications

The following articles have been published during the Ph.D. study:

- K. Dimou, C. Rosa, T.B. Sørensen, J. Wigard, and P.E. Mogensen. *Performance of Uplink Packet Services in WCDMA*. IEEE Proceedings of the 57th Vehicular Technology Conference, Vol. 3, pp. 2071-2075, April 2003.
- C. Rosa, J. Outes, K. Dimou, T.B. Sørensen, J. Wigard, F. Frederiksen, and P.E. Mogensen. *Performance of Fast Node B Scheduling and L1 HARQ Schemes in WCDMA Uplink Packet Access*. IEEE Proceedings of the 59th Vehicular Technology Conference, May 2004.
- C. Rosa, J. Outes, T.B. Sørensen, J. Wigard, and P.E. Mogensen. *Combined Time and Code Division Scheduling for Enhanced Uplink Packet Access in WCDMA*. IEEE Proceedings of the 60th Vehicular Technology Conference, September 2004.
- C. Rosa, T.B. Sørensen, J. Wigard, and P.E. Mogensen. *Interference Cancellation and 4-branch Antenna Diversity for WCDMA Uplink Packet Access*. To appear in IEEE Proceedings of the 61st Vehicular Technology Conference, May 2005.

Chapter 2

Overview of Uplink Packet Access in WCDMA Release 99

2.1 Introduction

This chapter presents an overview of the main features taking part in the uplink packet access procedure in WCDMA Release 99. Sections 2.2 and 2.3 describe the system architecture, the Radio Resource Management (RRM) functions and the RRM functional split among the different network elements .The scope is to give an overall picture of uplink packet access in the WCDMA system, as well as to present the possible interactions between different RRM functions during the uplink packet access procedure. The emphasis is on packet scheduling for NRT radio bearers and on related issues. One of the tasks of the packet scheduler (PS) is to decide on what type of channel the transmission of NRT data should occur. For this reason, the channel type selection issue is shortly introduced in Section 2.4.1, describing upon which generic information the choice of the channel type is made. The focus is then moved to packet scheduling on dedicated channels, whose main mechanisms are introduced and discussed in detail in Section 2.4.2. Notice that the packet access procedure presented in Section 2.4.2 is a generalisation of the Nokia uplink packet access concept. See [NOK02] as a general reference.

2.2 The UMTS System Architecture

The UMTS system consists of a number of logical network elements, each one with a defined functionality. Functionally, the network elements are grouped into the UMTS Terrestrial Radio Access Network (UTRAN) that handles all radio-related functions, and the Core Network (CN), which is responsible for switching and routing data connections to external networks. To complete the system, the User Equipment (UE) that interfaces with the user and the radio interface is defined. The UMTS high level system architecture is shown in Figure 2.1. UTRAN consists of one or more Radio Network Sub-systems (RNS). An RNS is a sub-network within UTRAN and consists of a Radio Network Controller (RNC) and one or more Node Bs. RNCs may be connected to each other via an Iur interface. RNCs and Node Bs are connected through an Iub interface.

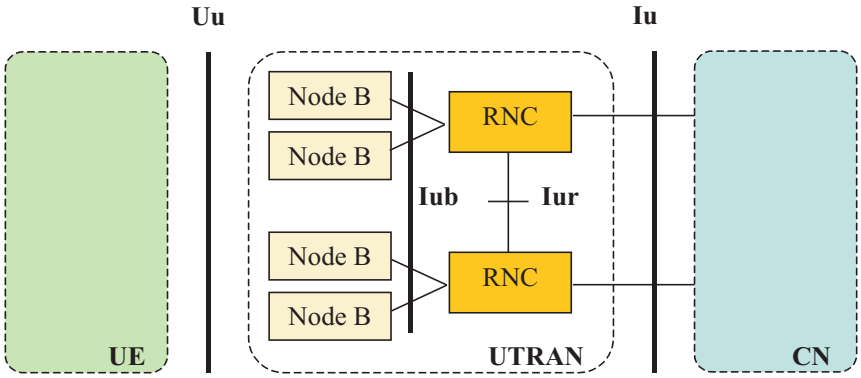

Figure 2.1: UMTS high-level system architecture [Holma04].

The RNC is the network element responsible for the control of the radio resources of UTRAN; it interfaces the CN and also terminates the Radio Resource Control (RRC) protocol, as illustrated in Figure 2.2. The main function of the Node B is to perform the air interface physical layer (L1) processing (channel decoding and de-interleaving, rate adaptation, despreading, etc.). It also performs some basic RRM operations as discussed in Section 2.3.

Figure 2.2 reports an example of the UMTS packet data user and control plane protocol architecture. The physical layer (L1) protocols determine how and with what characteristics data is transferred on the physical channels. In the control plane, the data link layer (L2) contains two sub-layers: The Medium Access Control (MAC) protocol and the Radio Link Control (RLC) protocol. In the user plane and only for services from the packet-switched domain, in addition to MAC and RLC there is the Packet Data Convergence Protocol (PDCP). On the control plane, the network layer (L3) consists of one protocol, namely the RRC protocol, which defines the messages and procedures between the UE and UTRAN. Since the RRC layer handles the main part of the control signalling between the UE and UTRAN, it has a long list of functions to perform [TS25331]. Most of these functions are part of the RRM algorithms.

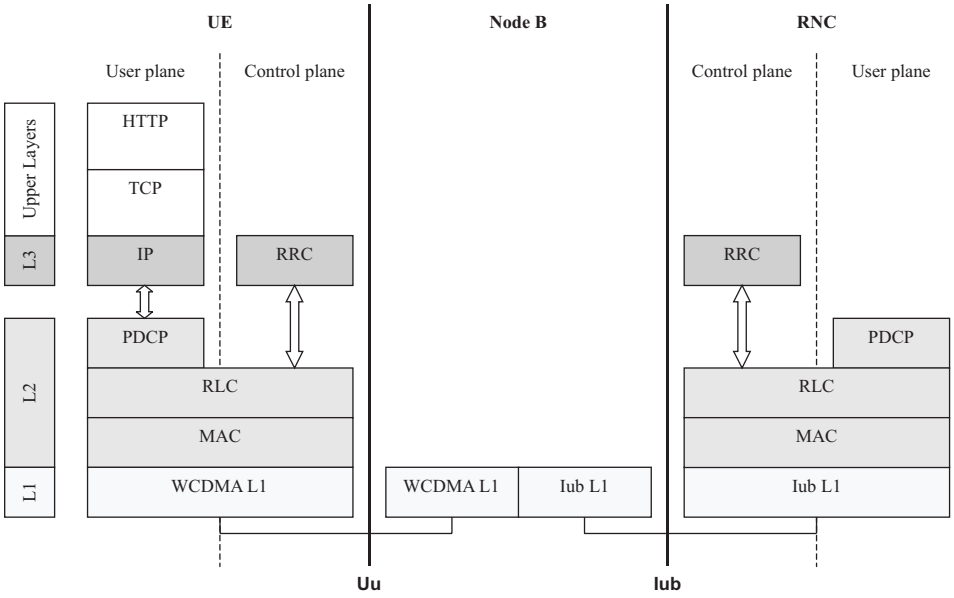

Figure 2.2: Example of UMTS packet data user and control plane protocol stacks; application is HTTP.

A radio bearer (RB) is defined as the service provided by L2 for the transfer of user data between the UE and UTRAN. In relation to the PS functionality, the RRC protocol is responsible for reconfiguring NRT radio bearers, as well as for controlling the UE measurement reporting. In the context of the Release 99 of the 3GPP specifications, these procedures are used to manage the allocation of the available radio resources to the NRT radio bearers, based on information on both network load and users requirements. The packet scheduler functioning in WCDMA uplink is described in more detail in Section 2.4.

2.3 RRM Functions

The RRM functionality consists of a set of algorithms which are used for utilisation of the WCDMA radio interface resources. In the uplink of WCDMA systems, the radio resource to be shared between the users is the total received wideband power at the Node B. Radio resource management is needed to guarantee Quality of Service (QoS), to maintain the planned coverage area, and to maximise the system throughput. RRM can be divided into: Power control (PC), handover control (HC), admission control (AC), load control (LC) and packet scheduler (PS) functionalities. RRM algorithms can be classified according to the network element they are located in. Typical locations of the RRM algorithms in a WCDMA network are shown in Figure 2.3.

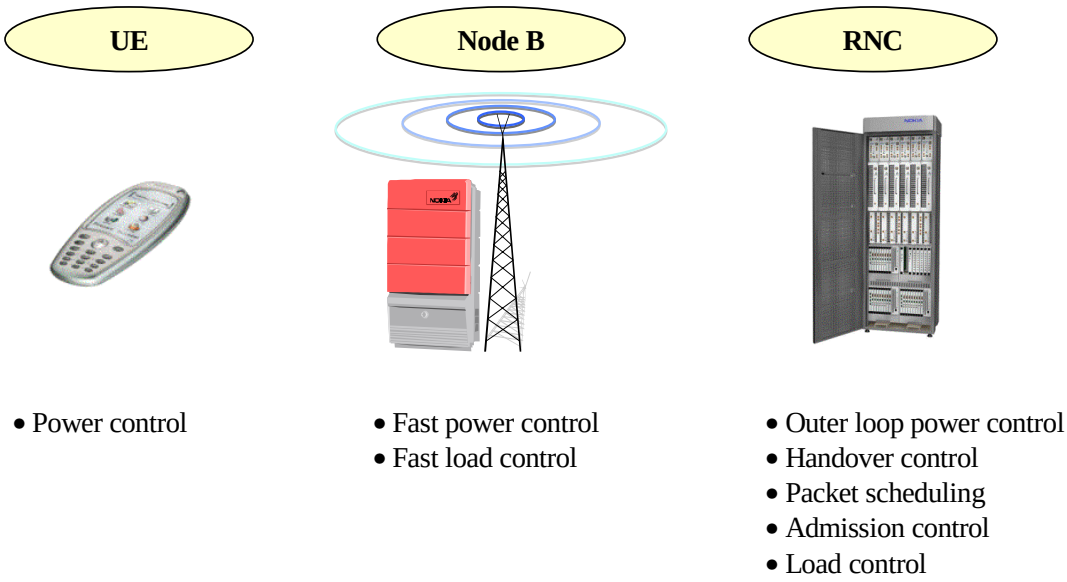

Figure 2.3: Typical location of RRM algorithms in a WCDMA network.

2.3.1 Short Overview of RRM Algorithms

Power control (PC) maintains radio link quality by adjusting the uplink/downlink transmission powers. The quality requirements are maintained with minimum transmission powers to achieve low interference and high capacity. With reference to the uplink direction of transmission, the basic functions of WCDMA power control are:

- *Open loop power control*: is used to set the UE transmission power level on the Random Access Channel (see Section 2.4.1). The transmission power level is set based on an estimation of the path loss in downlink.

- *Fast closed loop power control*: is used to mitigate the so-called near-far problem in the uplink of CDMA systems [Duel95]. In WCDMA, fast closed loop PC is executed at a frequency of 1.5 kHz; it therefore operates faster than any significant change of path loss could possibly happen, and even faster than the dynamics of fast Rayleigh fading for low to moderate mobile speeds. Fast closed loop PC is only performed on dedicated channels (see Section 2.4.1).
- *Outer loop power control*: is needed to keep the level of communication at the required level by setting the target for the fast closed loop PC. It aims at maintaining constant quality, usually defined as a certain target bit error rate (BER) or block error rate (BLER). The frequency of the outer loop power control is typically between 10 and 100 Hz [Holma04].

Handover control (HC) controls the active state mobility of UEs in UTRAN. Handover control preserves the radio link quality and minimises the radio network interference by optimum cell selection in handovers.

Admission Control (AC) decides whether a request to establish an RB is admitted in the Radio Access Network or not. Admission control is used to maintain stability and to achieve high capacity. The AC algorithm is executed during radio bearer setup or reconfiguration.

Load control (LC) continuously updates the load information of cells controlled by the RNC and provides the information to the AC and PS for radio resource controlling purposes. The role of load control is to assure that the system is not overloaded and remains stable.

Packet Scheduler (PS) schedules radio resources for NRT radio bearers. The traffic load of cells determines the scheduled transmission capacity. The PS functionality is introduced and described in more detail in Section 2.4.

2.4 The Packet Scheduler Functionality

As introduced in Chapter 1, 3G systems support both RT and NRT services. The proportion between RT and NRT traffic varies all the time, depending on the momentary traffic conditions. Due to the tight latency and reliability requirements of RT services, the variations of RT traffic cannot be controlled by, for instance, temporarily allocating lower resources to the corresponding radio bearers. The load caused by RT traffic, interference from other cell users and noise together is typically called non-controllable load. The available capacity that is not used for non-controllable load can be used for NRT radio bearers on best effort basis. The load caused by best effort NRT traffic is called controllable load. The PS is a general feature which takes care of scheduling radio resources to NRT radio bearers. Packet scheduling happens periodically, and the scheduled capacity depends on the UE and Node B capabilities, as well as on the availability of the physical radio resources.

The main goal of the PS functionality is to fill the planned load budget by dynamically allocating the instantaneously available radio resources to NRT radio bearers, thereby achieving maximum utilisation of the radio resources.

2.4.1 Channel Type Selection in Uplink

In UTRA the data generated at higher layers is carried over the air interface with transport channels, which are mapped in the physical layer to different physical channels [TS25211]. In uplink, two types of transport channels exist: Dedicated and common channels. The main difference between them is that a common channel is a resource divided between all the users in a cell, whereas a dedicated channel resource is reserved for a single user only. The only

dedicated transport channel is the dedicated channel (DCH). The uplink common channels are the Random Access Channel (RACH) and the Common Packet Channel (CPCH) [Holma04].

An RRC connection is a logical connection between the UE and UTRAN used by two peer entities to support the upper layer exchange of information flows. When the signalling connection exists, there is an RRC connection and the UE is in UTRAN connected mode. The UE leaves the UTRAN connected mode and returns to idle mode when the RRC connection is released or at RRC connection failure. In UTRAN connected mode we can distinguish between different states:

1. The CELL_DCH state is characterised by the allocation of a dedicated transport channel to the corresponding UE.
2. In the CELL_FACH state the UE is enabled to transmit uplink control signals on the RACH, and may be able to transmit data packets on the uplink common channels.
3. Since the UE performs continuous reception on the Forward Access Channel (FACH) [Holma04] in CELL_FACH state, the UE is moved to CELL_PCH (or URA_PCH) state whenever long inactivity is detected in order to reduce the UE power consumption.

In Release 99 WCDMA uplink packet access, traffic volume measurement reports (TVMRs) in the form of RRC messages from the UE to the RNC, and inactivity information detected at the MAC layer in the RNC (see Figure 2.2), are used to determine the transitions between RRC states. The measurement reporting criteria parameters, as well as the measurement quantities and the reporting quantities are set by radio network planning and signalled to the UE using the RRC protocol. Figure 2.4 shows the RRC states and state transitions supported in UTRAN. Refer to [TS25331] for more details on RRC states and state transitions.

One of the tasks of the PS is to decide whether transmission of NRT data has to occur via common or dedicated transport channels, i.e. in CELL_FACH or in CELL_DCH state, respectively.

- An advantage of common channels is the easy resource allocation on the physical layer. No signalling is necessary to setup the channel, therefore channel access is

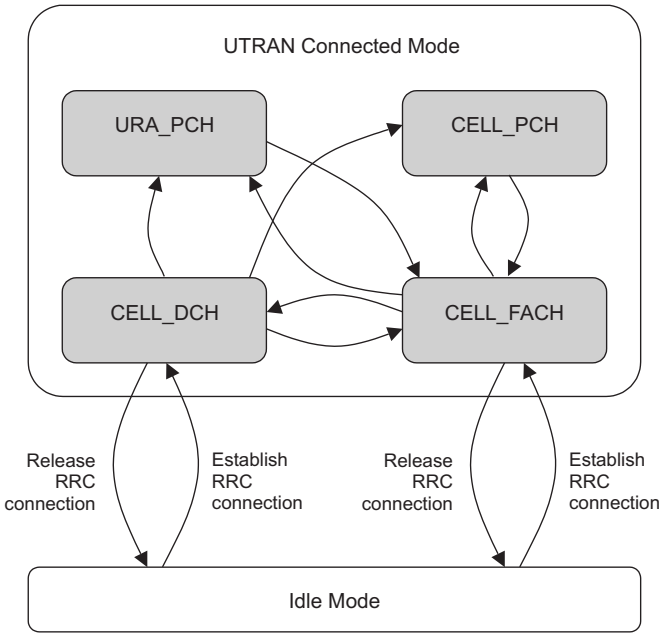

Figure 2.4: RRC states and state transitions in UTRAN [TS25331].

relatively fast. Moreover, compared to dedicated channels, transmitting on common channels reduces the required overhead due to physical layer control signalling.

- On the other hand, the lack of closed loop PC on common channels implies that the transmission power remains constant for the complete transmission time interval (TTI). This leads to a decrease in the spectral efficiency of common channels compared to dedicated channels since, for the same block error rate (BLER), a higher average signal power is needed.

As a consequence, for transmission of small data packets common channels are preferred, whereas for a higher amount of data dedicated channels should be used.

- A transition from CELL_FACH to CELL_DCH state occurs when a dedicated transport channel is established via explicit signalling. A dedicated connection is established if the data in the UE buffer exceeds a threshold value set via apposite RRC signalling from UTRAN to the UE. Otherwise uplink data transmission takes place on uplink common channels, since DCH setup is in general slower compared to packet-data access on common channels.
- A transition from CELL_DCH state to CELL_FACH state can occur either through the expiration of an inactivity timer (to reduce physical channel control overhead when no data has to be transmitted), or via explicit signalling. Moving a UE to CELL_FACH state based on short inactivity can have the drawback of increasing the transmission delay when new data arrives in the UE buffer and a new dedicated connection must be established.

CELL_FACH and CELL_DCH states are the only RRC states in which transmission of user data can occur. In CELL_DCH state, the UE can be allocated a different amount of radio resources. The distribution (or reallocation) of these between users in CELL_DCH state is also a task of the PS. Figure 2.5 shows the RRC states and state transitions limited to the cases in which transmission of user plane data can occur. When in CELL_DCH state the white arrows in Figure 2.5 correspond to the reallocation of dedicated resources ($R_1 \cdots R_N$) to the corresponding NRT user, i.e. data rate upgrade or downgrade.

The scenario considered in this Ph.D. work does not explicitly include the transitions between CELL_FACH and CELL_DCH states. The focus is on packet data transmission on DCH (i.e.

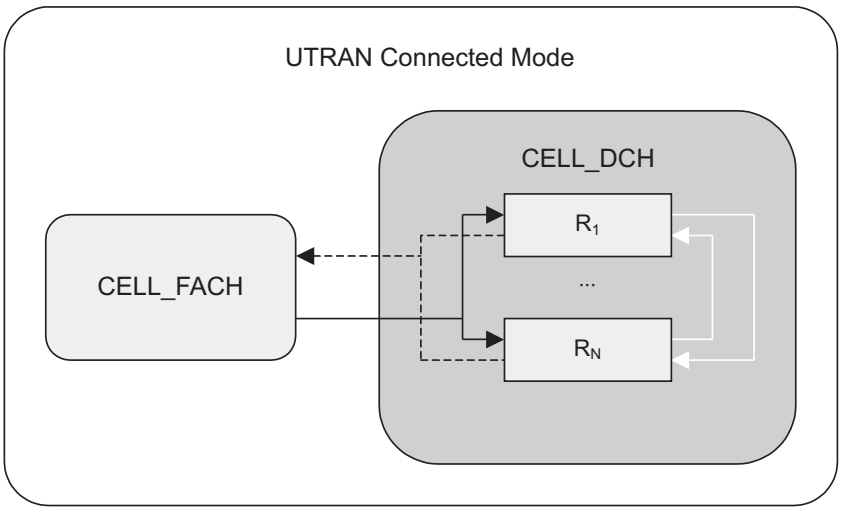

Figure 2.5: RRC states in which transmission of user plane data can occur, including reallocation of radio resources in CELL_DCH state.

in CELL_DCH state), specifically on the way the PS handles the allocation of dedicated resources to NRT users. To this end the principles of packet data scheduling on DCH are detailed in the following section.

2.4.2 Packet Scheduling on DCH

Traffic volume measurement reports are also used in the decision process for the distribution of dedicated resources between NRT radio bearers, e.g. to allocate a higher DCH transmission rate to a packet-data user requiring for additional capacity. L3 RRC signalling needed by PS includes uplink capacity requests, as well as channel and resource allocation procedures, while the MAC protocol sends activity and inactivity indications on a radio bearer basis. Figure 2.6 illustrates the principles of the uplink packet access procedure on DCH according to Release 99 of the 3GPP specifications.

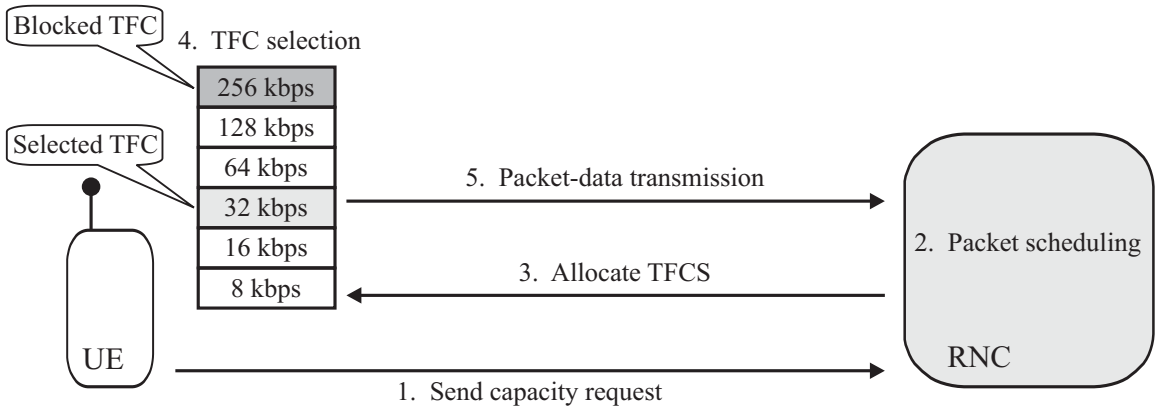

Figure 2.6: Fundamental procedures that take part in the packet scheduling procedure on DCH.

1. UE sends a capacity request (CR) via RRC signalling.
2. Based on the received CRs, inactivity information from MAC layer, and cell load conditions, PS performs reallocation of the available radio resources in uplink.
3. After packet scheduling at the RNC, the Transport Format Combination Set (TFCS) is computed and signalled to the UE via RRC signalling. The TFCS is the set of Transport Format Combinations (TFCs) that can be used by the UE for data transmission in uplink (see Section 2.4.2.3).
4. Depending on the amount of data in the buffer and on the required transmission power, the UE selects the most appropriate TFC between those included in the TFCS.
5. Finally, data is transmitted on the dedicated physical data channel (DPDCH) with the selected TFC.

2.4.2.1 Generating Capacity Requests

A TVMR is usually handled as an uplink CR, although each operator can decide a different mapping from traffic volume reports to uplink capacity requests. For instance, the measurement report can be operated in an event-triggered fashion where a TVMR is sent only if specific conditions are met. In this case, the reception of a TVMR at the RNC can be interpreted as a request for additional radio resources. Alternatively, the UE can be notified to send measurement reports periodically, in which case the PS has to decide whether or not a TVMR has to be translated into a CR.

In the analysis of Release 99 uplink packet access presented in this Ph.D. thesis the assumption is made that UEs send a TVMR only when specific conditions are met. As a consequence, traffic volume measurements received at the RNC PS are always interpreted as requests for additional capacity.

2.4.2.2 Packet Scheduling Procedure at the RNC

In the RNC, the packet scheduler co-operates with other RRM functions like Handover Control (HC), Load Control (LC) and Admission Control (AC).

- LC provides periodical load information to PS on a cell basis.
- PS informs AC and LC of the load caused by NRT radio bearers.
- AC informs PS about new admitted radio bearers, but not yet active.

The packet scheduler operates on a cell basis, though there has to be communication between PS processes for different cells due to the need for Soft Handover (SHO) also for packet data users on dedicated channels. To this end

- PS receives information on SHO status from HC.

The cooperation between the different RRM functions is illustrated in Figure 2.7, which also reports the most relevant information flows between RRM entities with respect to the packet scheduling procedure on DCH.

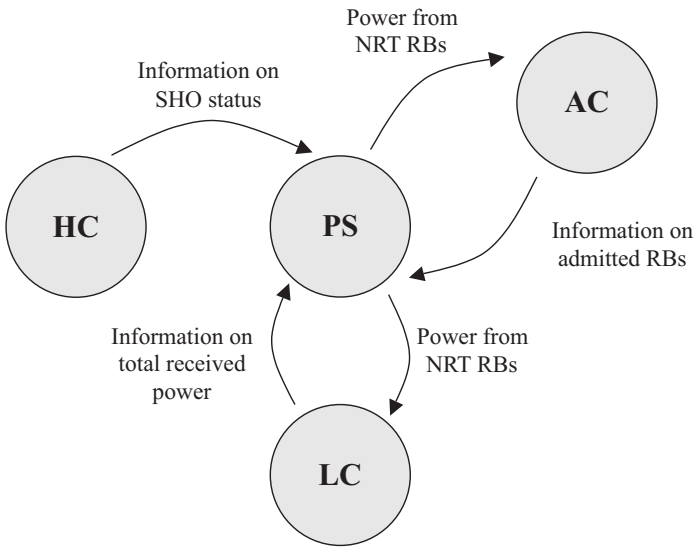

Figure 2.7: Cooperation and information flow between different RRM functions in relation to the packet scheduling procedure on DCH.

The packet scheduler operates periodically, that means, the same actions are repeated within a specific time period. This period is an RNC configuration parameter named scheduling period. The scheduling period is normally the time period between two cell based load information messages received from LC, but also different values can be configured. LC and AC provide periodical load information to PS on a cell basis. The most important are:

- Total received wideband power in uplink (*PrxTotal*), and
- estimated received power of admitted RT and NRT bearers, which are not active yet since establishment phase is ongoing (*PrxRtInactive* and *PrxNrtAdmitted*, respectively).

Packet scheduling is typically based on power measurements performed at the Node B, hence the received power is used as a measure of the load in uplink. The basic idea is that radio network planning sets the uplink load target in a cell (*PrxTarget*) so that stability as well as coverage requirements are respected. The uplink total received interference power (*PrxTotal*) must be maintained below the planned target. Instantaneously, this target can be exceeded due to changes in the interference and propagation conditions. If the system load does exceed a specified load threshold (*PrxThreshold*), an overload situation occurs and load control actions are taken to return the uplink load below the planned target.

Before processing CRs, PS has to calculate the total allowed power for packet scheduling purposes. The total allowed power in uplink direction is *PrxTarget*, which has to be shared between RT and NRT bearers. The packet scheduler calculates the allowed power for uplink packet scheduling on DCH (*PrxAllowed*) as:

$$PrxAllowed = PrxTarget - PrxTotal - PrxRtInactive - PrxNrtAdmitted - PrxNrtInactive \quad (2.1)$$

In (2.1), *PrxNrtInactive* is an estimation of the increase in *PrxTotal* that inactive NRT bearers would cause when they become active, and is directly calculated by PS (see Appendix B). The principle of uplink load distribution in a WCDMA cell is illustrated in Figure 2.8, showing the different factors that contribute to determine the allowed power for scheduling additional DCH resources. In Figure 2.8, *PrxNc* is the power corresponding to the non-controllable load, i.e. the load caused by RT traffic, interference from other cell users and noise, while *PrxNrt* is the received power from NRT radio bearers.

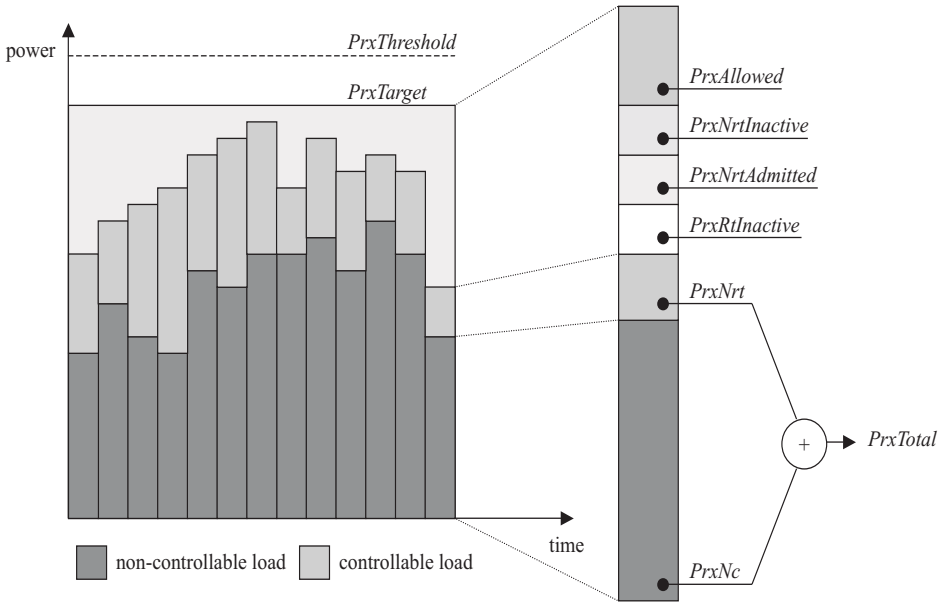

Figure 2.8: Example of uplink load distribution in a WCDMA cell.

Once the allowed power for scheduling is determined, the PS proceeds to allocate additional radio resources to NRT users having issued a CR. To be able to estimate the change in total received power due to radio resource reallocation, the PS has to determine the contribution that each single radio bearer gives to the uplink fractional load. The uplink fractional load η is a function of the total received uplink power and of the background noise power *Pnoise*:

$$\eta = 1 - Pnoise / PrxTotal \quad (2.2)$$

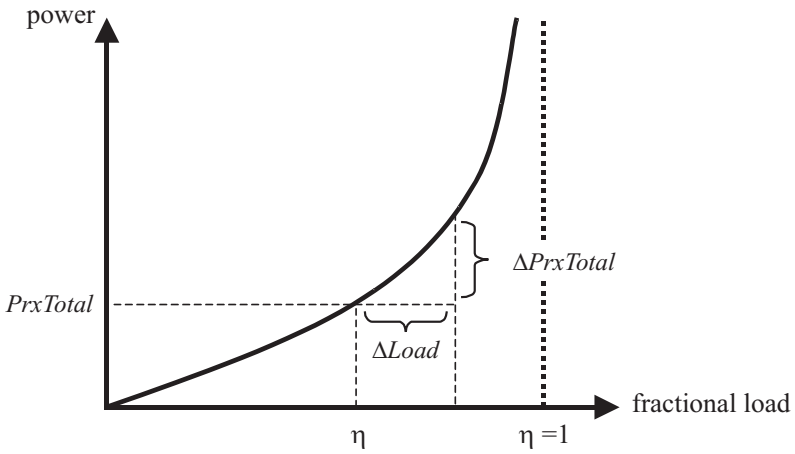

Figure 2.9: Change in total received uplink power (ΔPrxTotal) as a function of the fractional load change (ΔLoad) and of the fractional load (η) in correspondence with the system operation point (PrxTotal).

The combination of all the individual load contributions is used to calculate the total fractional load change (Δ*Load*), which is then mapped into a corresponding variation of the total received power (Δ*PrxTotal*) depending on the system operation point, as illustrated in Figure 2.9.

The method to determine the contribution of each radio bearer to the total change in the fractional load *ΔLoad*, and hence to obtain the change in total received power *ΔPrxTotal*, is described in Appendix B.

To conclude, the flow chart in Figure 2.10 summarises the main steps of the packet scheduling procedure at the RNC. First, the packet scheduler receives information on the total received uplink power *PrxTotal* from LC. If the received power is above a predefined

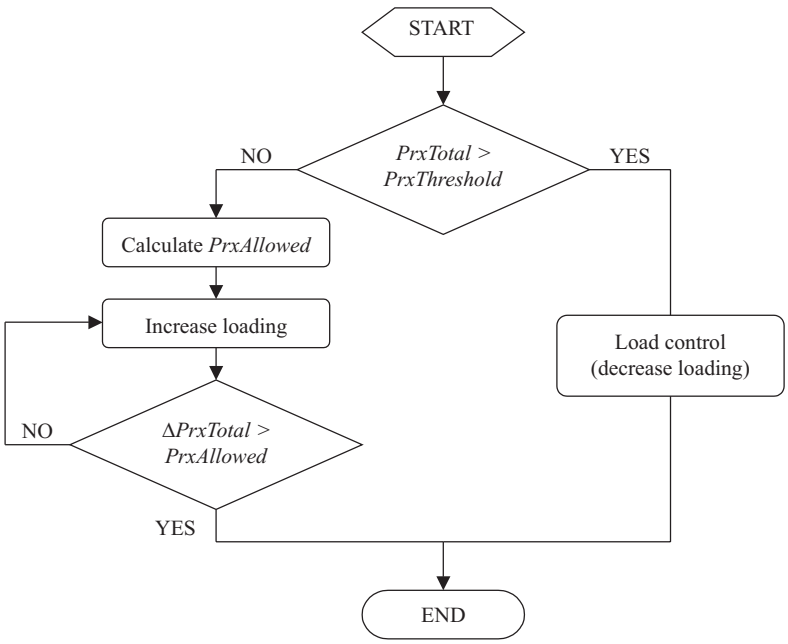

Figure 2.10: Flow chart summarising the main steps during the packet scheduling procedure for dedicated channels at the RNC.

threshold value (*PrxThreshold*), load control is entered and the allocated resources are progressively decreased until the estimated total received power is below the planned target (*PrxTarget*). The packet scheduler can also perform data rate downgrading based on inactivity information on a radio bearer basis. Data rate downgrading (including load control actions) is addressed in more detail in Section 3.3.1.

If the total received power is below the planned target, the PS enters the load increase algorithm. During this phase, the packet scheduler processes the CRs and allocates additional resources until the available power for scheduling (*PrxAllowed*) is exhausted. The load increase algorithm can also be terminated if there are no more capacity requests to be processed.

A simplified example of data rate upgrading in the case with four NRT RBs, two of which issue a CR, is illustrated in Figure 2.11. After having calculated the allowed power for scheduling purposes, the packet scheduler progressively increases the allocated data rate to the users having issued a CR (UE_1 and UE_2). In the upgrading procedure, the packet scheduler distributes the available radio resources between the requesting users on an equal share basis, with the scope of maintaining fairness between them. As a result, in the example of Figure 2.11 the allocated data rate to UE_1 is upgraded from 128 kbps to 256 kbps only after UE_2 has also been granted 128 kbps. Also, the load increase algorithm is terminated because no more power is available for scheduling, i.e. the estimated total received power in uplink (including the contributions from inactive NRT bearers and just admitted bearers) is equal to the planned target *PrxTarget*.

2.4.2.3 TFCS Allocation and TFC Selection at the UE

Based on the cell specific load information from LC and uplink capacity requests from UEs, the packet scheduler produces an appropriate Transport Format Combination Set (TFCS) that is delivered to the MAC layer of the UE via RRC signalling.

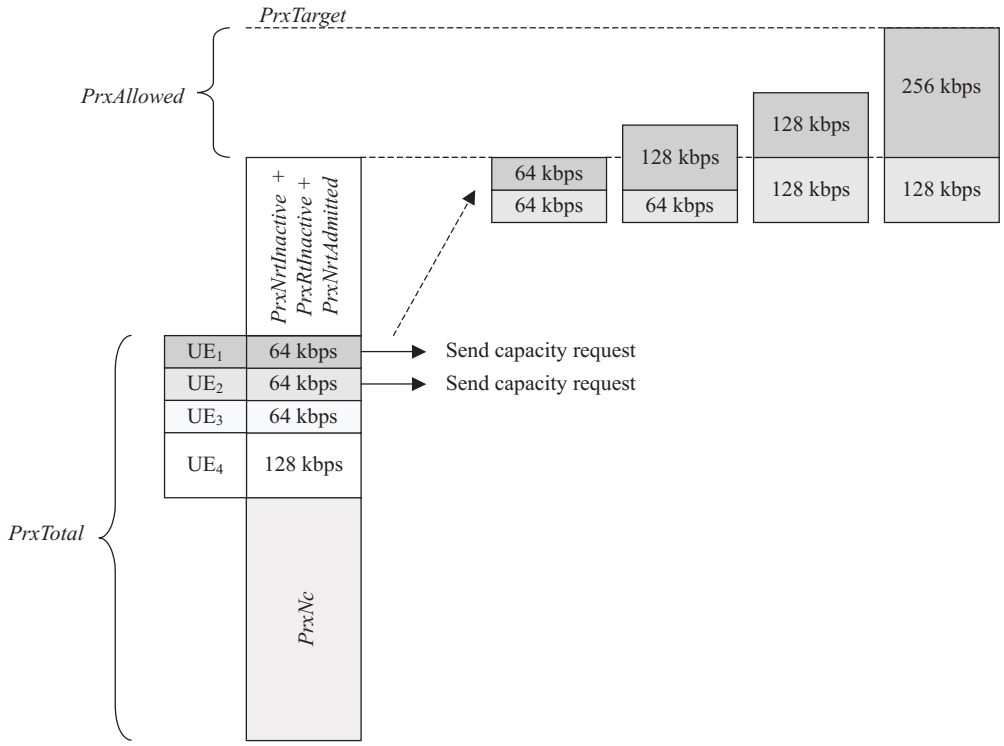

Figure 2.11: Example of load increase algorithm with 4 NRT radio bearers, 2 issuing a capacity request.

- The TFCS is the set of allowed Transport Format Combinations (TFCs) for data transmission on the DPDCH.
- A TFC defines for each of the transport channels multiplexed on the same DPDCH the size and number of Transport Blocks (TBs) that are delivered to L1 every transmission time interval (TTI) [TS25212].

With only one NRT RB per UE a single transport channel is mapped on the DPDCH. In this case a TFC corresponds to a particular data rate for the NRT RB, and the TFCS is simply a set of possible data rates that can be selected for transmission on the DPDCH.

The TFC selection is a MAC function that the UE uses to select a TFC from its current TFCS, whenever it has data to transmit. The TFC is selected based on the need for data rate (i.e. UE buffer contents), the currently available transmission power, the available TFCS as well as the capabilities of the UE. The TFC selection function is more thoroughly described in Section 3.3.2. Further details can be found in [TS25321].

2.5 Summary

This overview chapter has provided an overall description of uplink packet access in Release 99 WCDMA. Some of the topics are only generally introduced and will be more thoroughly described in Chapter 3.

Transmission of user plane data in Release 99 WCDMA uplink can take place on two types of transport channels:

- *Common channels*, and
- ***dedicated channels***.

The focus of the work presented in this Ph.D. thesis is on packet-data transmission on dedicated channels. Release 99 uplink packet access on DCH is essentially based on:

- *Capacity requests* (sent from the UE to the RNC PS),
- ***packet scheduling procedure*** (performed at the RNC), and
- *capacity grants* (sent from the RNC PS to the UE).

During the packet scheduling procedure, and based on measurements of the total received uplink power performed at the Node B, PS allocates dedicated resources to NRT bearers having issued a CR. The packet scheduler can also perform data rate downgrading based on inactivity information on a RB basis. Finally, load control actions can be taken in order to prevent the system from entering an overload situation. In summary, the DCH packet scheduling procedure consists of:

- *Power measurements* (performed at the Node B),
- *data rate upgrading* (based on capacity requests),
- *data rate downgrading* (based on inactivity information), and
- *control of overload situations*.

Chapter 3

Performance of Uplink Packet Access in WCDMA Systems: RNC Packet Scheduler

3.1 Introduction

In this chapter the performance of a basic RNC-located packet scheduler implementation is investigated. As introduced in Chapter 2, the packet scheduler is the entity responsible for allocating the radio resources to NRT radio bearers on a best effort basis. It is therefore responsible for upgrading and downgrading the bitrate allocated to a specific radio bearer depending on the load conditions in the system and on the user requirements, as well as taking into consideration fairness among users.

In the last years the assessment of WCDMA uplink performance for NRT packet services has been considered within several publications. Some of the work presented in literature mainly focuses on admission control strategies such as [Holma99], [Wibe00], and [Outes01]. Other studies address the relation between uplink capacity and coverage in WCDMA uplink; see e.g. [Veer99] and [Hilt03]. In [Fior00], the possibility of adaptively selecting the user bitrate for packet transmission is analysed. However, the main concern is to solve local coverage problems that might happen for mobiles at the cell border, while the core of the packet scheduling functionality is not taken into consideration. The assumption made in all these papers is that once a NRT bearer is admitted and granted a certain bitrate it keeps the allocated resource until the end of the data connection. Differently, some research activities presented in literature have addressed more specifically the problem of packet scheduling for the uplink of WCDMA systems, and consider more dynamic reallocation of the available radio resources between NRT users.

In [Hwan01], a distributed rate control algorithm for throughput maximisation is presented. However, the study is carried out in a single-cell scenario, and without considering any limitation on the UE power capabilities. The simulation approach used in [Vill00] is somehow more consistent since it includes the effect of other-cell interference and imposes a limitation

to the UE power capabilities. Nevertheless, the packet scheduler located in the RNC is assumed to operate under a number of ideal assumptions: First of all, the RNC is assumed to know the status of the RLC buffer of all the mobiles, as well as the path loss between each mobile and each base station receiver in the network. Also, the authors assume that the centralised scheduler operates at the RNC on a radio frame interval (10 ms). This is a rather impractical assumption, since in reality it will require a severe increase in the processing capacity needed at the RNC, in addition to the large signalling overhead required over both the Iub and the radio interface.

The main objective in this chapter is to introduce a reference RNC-located PS and to assess its performance by taking into account both network and user related statistics. The PS is meant to operate in the context of the Release 99 of the 3GPP specifications, although its implementation is not one hundred per cent compliant with the 3GPP standards. The system performance is investigated mainly by means of system level simulations, although a theoretical approach is also presented.

The chapter is organised as follows. First, the issue of estimating the uplink throughput in a WCDMA cell is introduced in Section 3.2. Section 3.3 describes the main simulation assumptions for the considered RNC PS implementation. Simulation results are then presented and discussed in Section 3.4. Section 3.5 presents a discussion on the limitations of an RNC-located packet scheduler. Finally, the concluding remarks are given in Section 3.6.

3.2 Uplink Cell Throughput: a Theoretical Approach

In this section a semi-analytical approach commonly used to estimate the achievable cell throughput in the uplink of WCDMA system is presented. Since the cell throughput can be thought as a stochastic process, the scope is to obtain an estimation that is as close as possible to the expected value of the uplink cell throughput. To this end, an expression for the expected value of the uplink cell throughput on the basis of similar assumptions is also derived, and the level of accuracy of the semi-analytical approach consequently addressed.

3.2.1 The Load Equation

The theoretical uplink throughput of a WCDMA cell is commonly calculated using the so-called load equation [Holma04] [Hilt03], whose derivation is next reported. We first define the E_b/N_0 requirement per receiving antenna for user j (ρ_j) as:

$$\rho_j = \frac{W}{R_j} \cdot \frac{P_j}{P_{total} - P_j} \tag{3.1}$$

In (3.1), W is the WCDMA chip rate, P_j is the received signal power from user j, R_j is the bitrate of user j, and P_{total} is the total received wideband power at the Node B including thermal noise power. Solving for P_j, and defining η_j as the load factor for one connection, gives:

$$P_j = \frac{P_{total}}{\frac{W}{R_j \cdot \rho_j} + 1} = P_{total} \cdot \eta_j \tag{3.2}$$

The total received wideband power at the Node B can be written as:

$$P_{total} = P_{noise} + P_{own} \cdot (1+i) \tag{3.3}$$

In (3.3), i is the other-to-own cell interference ratio, while P_{own} and P_{noise} are the own cell and the background noise power, respectively. Assuming perfect power control, and all the N active users in the cell having the same E_b/N_0 requirement ($\rho_j = \rho \; \forall j \in [1,N]$) and transmitting with the same bitrate R ($\eta_j = \eta \; \forall j \in [1,N]$), the total received own power at the Node B can be written as:

$$P_{own} = \sum_{j=1}^{N} P_j = \sum_{j=1}^{N} P_{total} \cdot \eta_j = N \cdot P_{total} \cdot \eta \tag{3.4}$$

The noise rise NR, defined as the ratio of the total received wideband power to the thermal noise power, can consequently be expressed as in (3.5). The relation between the uplink fractional load η_{UL} and the noise rise is given in (3.6).

$$NR = \frac{P_{total}}{P_{noise}} = \frac{P_{noise} + P_{own} \cdot (1+i)}{P_{noise}} = \left(1 - \frac{N}{\frac{W}{R \cdot \rho} + 1} \cdot (1+i) \right)^{-1} \tag{3.5}$$

$$NR = \frac{1}{1-\eta_{UL}} \tag{3.6}$$

Solving (3.5) for N, the uplink cell throughput T can be finally expressed as in (3.7), where $BLER(\rho)$ is the block error rate in correspondence of the target E_b/N_0 ρ.

$$T = N \cdot R \cdot [1 - BLER(\rho)] = \eta_{UL} \cdot \left(\frac{W}{\rho} + R \right) \cdot \frac{1}{1+i} \cdot [1 - BLER(\rho)] \tag{3.7}$$

The load equation is widely used to make a semi-analytical prediction of the average throughput of a WCDMA cell without going into system level simulations. Under the considered assumptions (perfect power control and all users transmitting with the same bitrate R), (3.7) gives the exact value of the cell throughput given instantaneous values of the other-to-own cell interference ratio i and of the uplink fractional load η_{UL}. The fact is that the load equation is often used for the purpose of predicting cell capacity and planning noise rise in the dimensioning process by substituting into (3.7) the average values of the other-to-own cell interference ratio and of the uplink fractional load [Owen00] [Hilt03]. This approach is particularly of use in classical all-voice-service networks, where typically a high number of users with a low allocated data rate are active in each cell. In such a scenario, the noise rise in the system, the other-to-own cell interference ratio, and the user allocated data rates can be reasonably assumed to be approximately constant. Therefore, the expected values of such quantities can be substituted in (3.7) to estimate the achievable uplink cell throughput. Few examples of uplink cell throughput estimated with (3.7) as a function of the average noise rise and for different values of the average other-to-own cell interference ratio are shown in Figure 3.1. The results are obtained for R equal to 64 kbps and assuming ideal maximal ratio combining (MRC) and 2-branch antenna diversity, with an E_b/N_0 requirement per receiving

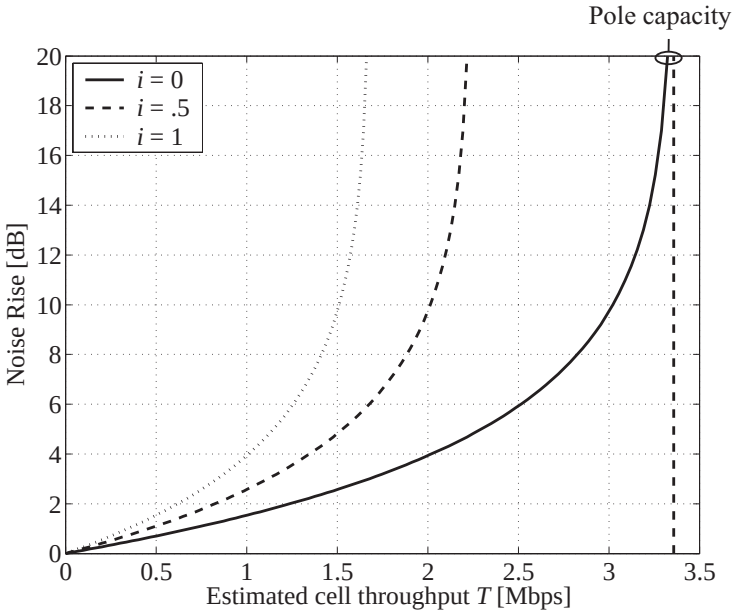

Figure 3.1: Estimated uplink throughput of a WCDMA cell as a function of the noise rise and for different values of the other-to-own cell interference ratio i.

antenna of 0.2 dB for a BLER target of 10% (see Section C.2). Figure 3.1 also plots the system pole capacity, which is defined as the maximum achievable cell throughput when the cell coverage shrinks to zero, i.e. the noise rise tends to infinity [Veer97] (see also definition [A 2.13]).

$$T_{pole} = \left(\frac{W}{\rho} + R \right) \cdot \left[1 - BLER(\rho) \right] \tag{3.8}$$

The pole capacity is independent of the background thermal noise and other-cell interference. Notice that for given values of the noise rise and of the other-to-own cell interference ratio the achievable cell throughput can be much lower than the system pole capacity.

With the introduction of packet data applications the situation changes compared to all-voice-service networks, since system performance starts to be driven also by the characteristics of the offered traffic. For example, the other-to-own cell interference ratio is not only a function of cell environment and antenna pattern [Wack99], but also depends on the burstiness of the generated traffic [Owen00].

In the following section an analytical study is presented that derives the expected value of the uplink throughput of a WCDMA cell under specific assumptions. The main scope is to determine the level of accuracy when estimating the uplink cell throughput by substituting expected values of the uplink load and of the other-to-own cell interference ratio in (3.7).

3.2.2 Expected Value of Uplink Cell Throughput

As introduced in the previous section, the load formula (3.7) gives the exact value of the cell throughput given instantaneous values of the other-to-own cell interference ratio *i* and of the uplink fractional load η_{UL}. On the other hand, from a system performance perspective it is more relevant to evaluate the average cell throughput experienced over a longer time period. The load formula can also be used to predict average cell throughput performance, but in this case an estimation error is made. In order to evaluate the level of accuracy of (3.7), an

expression for the expected value of the uplink cell throughput is here derived. The same assumptions as in the previous section are made, i.e. perfect power control, and all active users having the same E_b/N_0 requirement and transmitting with the same bitrate R. From (3.5), the number of users in a WCDMA cell transmitting at rate R can be written as:

$$N = \left(\frac{W}{R \cdot \rho} + 1\right) \cdot \eta_{UL} \cdot \left(\frac{1}{1+i}\right) \tag{3.9}$$

In (3.9), N, η_{UL} and i are random variables, while W, R and ρ are assumed to be constant. We now define F as:

$$F = \frac{1}{1+i} = \frac{P_{own}}{P_{own} + P_{other}} \tag{3.10}$$

In (3.10), P_{own} and P_{other} are the own-cell and the other-cell power, respectively. By applying the expected value operator $\langle\rangle$ at both sides of equation (3.9), the expected value of the number of users in a WCDMA cell can be written as:

$$\langle N \rangle = \left(\frac{W}{R \cdot \rho} + 1\right) \cdot \langle \eta_{UL} \cdot F \rangle = \left(\frac{W}{R \cdot \rho} + 1\right) \cdot \left[\langle \eta_{UL} \rangle \cdot \langle F \rangle + COV(\eta_{UL}, F)\right] \tag{3.11}$$

From the first part of (3.7), the expected value of the uplink cell throughput can also be derived.

$$\langle T \rangle = R \cdot \langle N \rangle \cdot [1 - BLER(\rho)] \tag{3.12}$$

Finally, substituting $\langle N \rangle$ in (3.12), the expected value of the uplink throughput of a WCDMA cell can be expressed as:

$$\langle T \rangle = \left(\frac{W}{R \cdot \rho} + 1\right) \cdot \left[\langle \eta_{UL} \rangle \cdot \langle F \rangle + COV(\eta_{UL}, F)\right] \cdot [1 - BLER(\rho)] \tag{3.13}$$

First of all it can be noticed that the expected value of the uplink cell throughput does not directly depend on the expected value of the other-to-own cell interference ratio i, but more precisely is a function of the expected value of F (defined in (3.10) as the ratio of the own-cell power to the own-cell power plus other-cell interference). Assuming that the expected values of η_{UL} and F can be accurately estimated, the ratio of the expected value of the cell throughput to the cell throughput derived by substituting $\langle \eta_{UL} \rangle$ and $\langle F \rangle$ into (3.7) is:

$$\frac{\langle T \rangle}{T} = 1 + r(\eta_{UL}, F) \cdot \frac{std(\eta_{UL}) \cdot std(F)}{\langle \eta_{UL} \rangle \cdot \langle F \rangle} \tag{3.14}$$

In (3.14), $r(\eta_{UL}, F)$ is the correlation factor between η_{UL} and F, while *std* stands for standard deviation. In general, η_{UL} includes the impact of own-cell interference, while F includes the effect of other-cell interference. For a given value of $r(\eta_{UL}, F)$, the higher the standard deviation of either η_{UL} or F, the more inaccurate the cell throughput estimation using (3.7). The difference between expected and estimated cell throughput also increases for lower values of $\langle \eta_{UL} \rangle$ and $\langle F \rangle$. Finally, the inaccuracy of the load equation increases with the

	η_{UL}		F	
	Average	Standard deviation	Average	Standard deviation
Traffic-limited scenario	0.43	0.15	0.61	0.25
Interference-limited scenario	0.62	0.05	0.69	0.07

Table 3.1: Estimated average and standard deviation of η_{UL} and F from system level simulations in a traffic-limited and in an interference-limited scenario.

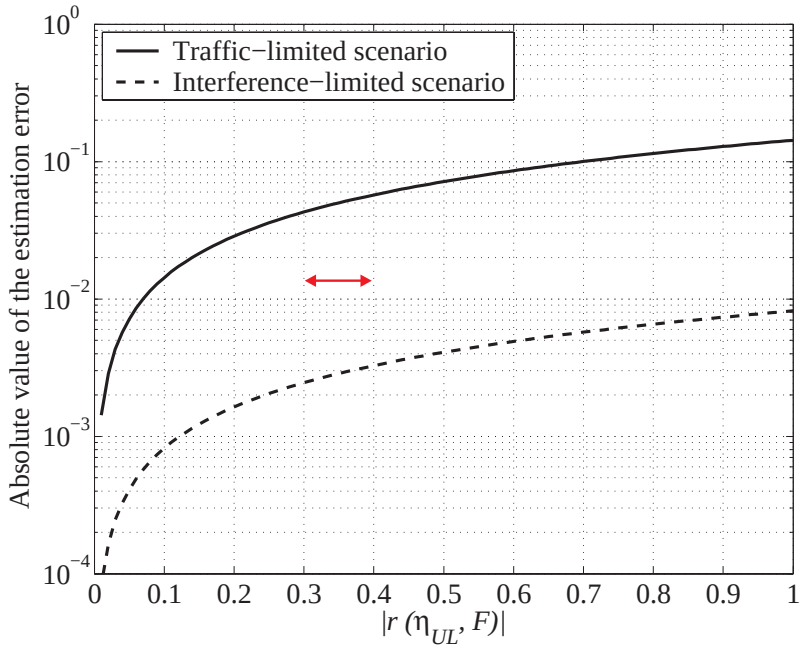

Figure 3.2: Percentage difference between expected and estimated cell throughput for an average uplink load of 75%.

absolute value of the correlation between η_{UL} and F. To theoretically derive the exact value of $r(\eta_{UL}, F)$ is outside of the scope of the presented analysis. However, it can be assumed that the correlation between η_{UL} and F will have some positive value different from zero, since in WCDMA uplink at high load conditions typically correspond low values of the other-to-own cell interference ratio, and vice versa.

Figure 3.2 plots the absolute value of the estimation error as a function of the absolute value of the correlation factor between η_{UL} and F. The expected values and standard deviations of η_{UL} and F to be substituted in (3.14) are reported in Table 3.1, and are obtained from system level simulations assuming two different scenarios:

1. A **traffic-limited** scenario, with a relatively low number of high-data rate users per cell characterised by bursty data transmission, and
2. an **interference-limited** scenario, with a relatively high number of low-data rate users per cell characterised by nearly constant data transmission.

The results are obtained imposing a 5% outage constraint for the uplink load, specifically the probability that the noise rise exceeds 5 dB (corresponding to an uplink fractional load of approximately 68%) is equal to 5% in both simulated scenarios. The traffic-limited scenario is characterised by higher variability and lower average values of both η_{UL} and F compared to the interference-limited case. As a consequence, the method that estimates the uplink cell

throughput by substituting the average values of η_{UL} and F into (3.7) is much more accurate in an interference-limited scenario, where the estimation error is <1% for any value of the correlation factor $r(\eta_{UL}, F)$. The error becomes more significant in the traffic-limited case, however it never exceeds the value of approximately 10%. The difference between traffic-limited and interference-limited scenarios is discussed more in detail in Section 3.4.3.

From the same system level simulations as in Table 3.1, the correlation between η_{UL} and F is estimated between 0.3 and 0.4. In Figure 3.2 it can be observed that in this range the level of accuracy of the load equation for cell throughput prediction is relatively high, especially in the interference-limited scenario. However, to estimate the achievable cell throughput it is necessary to know the values of η_{UL} and F with some precision, which requires the development of more complex simulation models.

3.2.3 Limitations of a Theoretical Approach

In Section 3.2.1 the load formula has been introduced; the load formula is a powerful instrument to predict the achievable system throughput in the uplink of a WCDMA cell. However, some of the underlying assumptions are particularly suitable to all-voice-service networks. Following, the main limitations of a semi-analytical approach are schematically reported.

- The comparison between expected and estimated uplink cell throughput has been presented under the ***assumption of equal and constant bitrate allocation***. This assumption can be quite unrealistic especially for NRT data services scheduled on a best effort basis, services that represent the main target of this Ph.D. thesis.
- The presented theoretical analysis has also assumed ***perfect power control***, i.e. the received E_b/N_0 is always equal to the planned target. Especially in the case of NRT data services with bursty transmissions at high data rates, the effect of non-ideal power control can have a significant impact on the system performance.
- Finally, one of the goals in this chapter is to assess the performance of an RNC-located PS implementation by also taking into consideration the user performance. If for voice services an appropriate level of service can be guaranteed by simply fulfilling the E_b/N_0 requirements [Pinto00], ***with the introduction of data services the picture becomes more complex, and performance indicators such as packet delay, round trip time and average throughput experienced during a packet data session also start playing an important role.***

For all the above-mentioned reasons, the performance of the RNC-located PS scheduler is mainly assessed by means of system level simulations. The semi-analytical model derived in Section 3.2.1 will be used in selected parts of this dissertation mainly to provide a validation of the results obtained from system level simulations (see e.g. Section 3.4.3). Section 3.3 includes a description of the main features related to the implementation of the RNC PS in the system level simulator. A more generic description of the simulation tool is given in Appendix A, while the uplink traffic model used for simulating NRT data users is detailed in Appendix D.

3.3 The RNC-located Packet Scheduler

The principles of packet access on dedicated channels in WCDMA uplink were briefly introduced in Chapter 2, and are further visualised in Figure 3.3. The functioning of the packet access procedure on DCH as it has been implemented for the simulation of the RNC-located PS can be shortly summarised as follows:

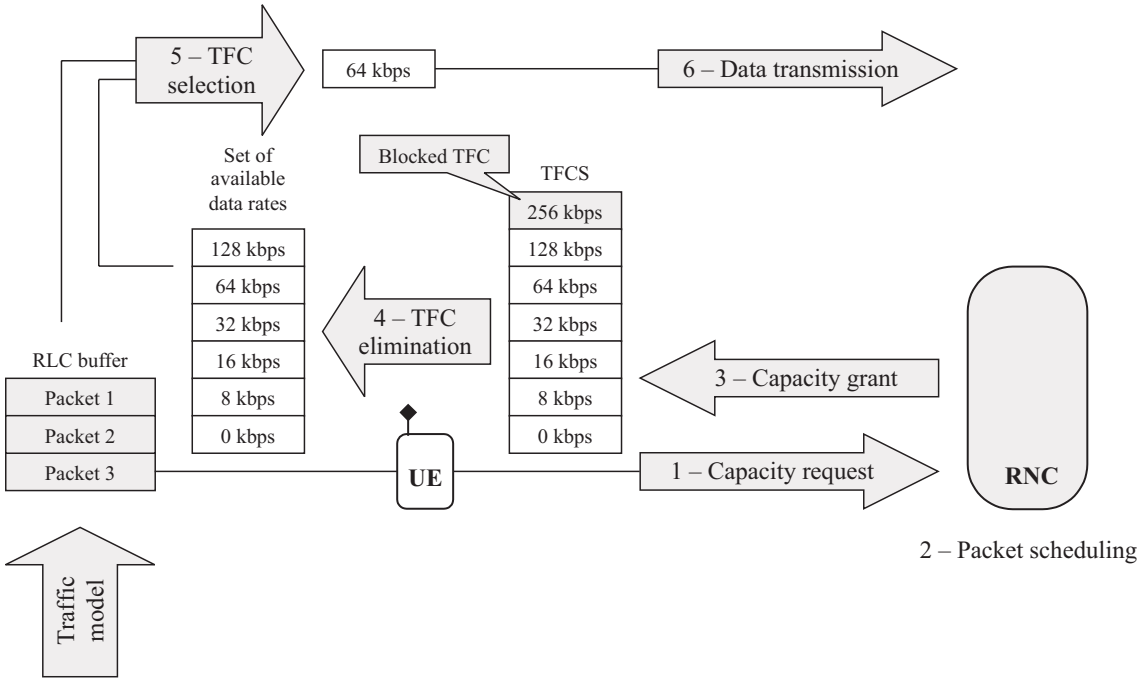

Figure 3.3: Principles of uplink packet access on DCH.

1. Whenever the RLC buffer size exceeds a threshold value pre-set by network planning, the UE sends a Traffic Volume Measurement Report (TVMR).
2. Each report received at the RNC is interpreted as a capacity request and processed in order to grant additional resources to the requesting radio bearers. The PS tries to allocate the users issuing a CR with the highest possible data rate, with respect to the constraint on the received power in uplink, and possibly taking into account fairness issues.
3. The Transport Format Combination Set (TFCS) is then computed and signalled to the corresponding UE. In the presented study, we only consider the case of a single NRT radio bearer per UE, therefore the TFCS is nothing else but a set of available data rates to be used for data transmission in uplink direction.
4. In the UE, a procedure called TFC elimination is also implemented. It consists in the UE autonomously preventing the use of those data rates in the TFCS that require a transmission power exceeding the UE power capabilities.
5. Based on the set of available data rates and on the RLC buffer occupancy, the UE selects the most appropriate transport format combination (64 kbps in the example of Figure 3.3).
6. Finally, the selected bitrate is used for data transmission on the DPDCH.

In the following section, the main functionalities involved in the uplink packet access procedure are described in more detail.

3.3.1 Packet Scheduling: Principles and Implementation

Packet scheduling is run separately and asynchronously for each base station controlled by the RNC. The output of the scheduling process is the maximum data rate the UE is allowed to use for the following scheduling period. The scheduling period is defined as the time interval between two consecutive scheduling actions at each cell specific PS. For UEs in soft handover operation, the maximum allowed data rate corresponds to the lowest among those allocated by all the base stations in the active set. The TFCS to be signalled to the UE is computed as the

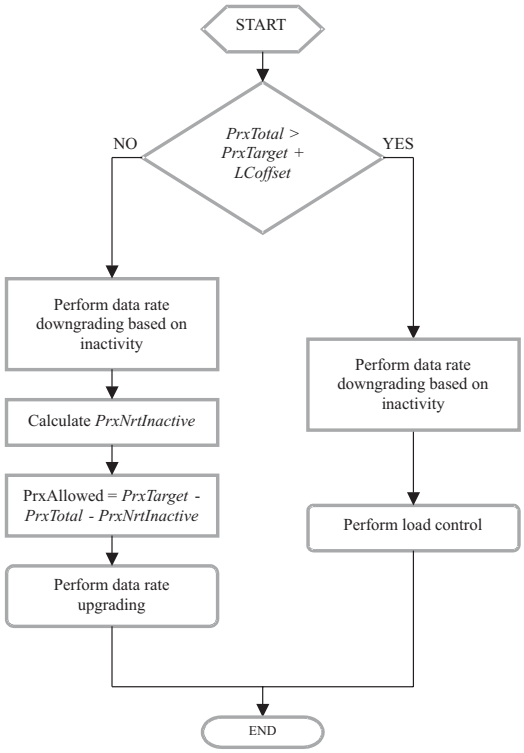

Figure 3.4: Packet scheduling procedure at the RNC PS.

set of all available data rates up to the maximum allowed. In order to avoid excessive signalling, a modification period is also introduced. The modification period is defined as the minimum time period that must elapse between two consecutive TFCS modification messages to a specific NRT radio bearer.

The scheduling algorithm performs both upgrading and downgrading of the users allocated data rates. Downgrading decisions are mainly taken based on inactivity detection, which is carried out by the MAC protocol at the RNC [TS25321]. Moreover, data rate downgrading is also performed whenever the system enters an overload situation. The flow chart in Figure 3.4 illustrates the different phases of the packet scheduling procedure:

1. First, based on the value of *PrxTotal* and on the network planning parameters *PrxTarget* and *LCoffset*, the PS decides whether initiating load control actions or entering the data rate upgrading procedure. *PrxTotal* is the total received wideband power at the Node B averaged over a specified time period. *PrxTotal* is assumed to be available at the RNC PS every scheduling period, this information being exchanged between Node B and RNC via the Node B Application Protocol (NBAP) [TS25433].
2. Next, the PS performs the data rate downgrading procedure based on inactivity information (see Section 3.3.1.2).
3. If the data rate upgrading procedure is initiated, the PS computes the power increase due to NRT radio bearers (*PrxNrtInactive*, see Section 2.4.2.2). Users are included in the calculation of the power from NRT inactive bearers if they have been inactive for a time interval exceeding the averaging period of the total received wideband power at the Node B. Since only NRT RBs are simulated and no admission control is considered, the available power for data rate upgrading is calculated by simplifying (2.1) as

$$PrxAllowed = PrxTarget - PrxTotal - PrxNrtInactive. \tag{3.15}$$

3.3.1.1 Data Rate Upgrading

A general overview of the capacity requests processing performed by the RNC-located PS is given in the example of Figure 2.11 in Chapter 2. The scope of the packet scheduling procedure is to progressively upgrade to the maximum possible data rate all the users issuing a capacity request, with respect to the power constraint set by network planning and maintaining fairness among the users requesting for additional capacity. The PS processes the CRs in ascending order of allocated data rate, i.e. the requests from UEs with lower allocated data rate are handled first. The CR process is terminated whenever one of the following three conditions is met:

1. The available power for packet scheduling is exhausted,
2. the estimated load increase due to modified NRT RBs exceeds the maximum allowed load variation (see Table 3.2), or
3. all the requests are fulfilled, i.e. all UEs issuing a CR are allocated the maximum possible data rate.

The power increase estimator (PIE) and load variation formulas used both in the data rate upgrading procedure and in the computation of received power from NRT inactive users are introduced in Appendix B.

Once the upgrading procedure is terminated, the allocations are signalled to the corresponding UEs and consequently applied. In a real implementation, the RNC applies a random delay to the allocation message for every user in order to avoid overloading of the Iub interface [TS25331]. In the considered implementation, a fixed delay is applied between the scheduling instant at the RNC and the reception of the corresponding allocation message at the UE to allow for the transmission delay (see Table 3.2).

3.3.1.2 Data Rate Downgrading Based on Inactivity

Whenever data packets have not been received from a particular UE for longer than a pre-defined time period, the PS reduces the UE allocated data rate to the minimum allowed. The minimum allowed data rate is a RB specific parameter and is assigned by network planning during the RB establishment phase [TS25331]. In the proposed implementation, a low value of the minimum allowed data rate is considered in order to simulate the switching to CELL_FACH state [TS25321] (see Section 2.4.1). It should be mentioned that in real implementations a UE is moved to CELL_FACH transmission mode when it is inactive for a relatively long time, or even in the case it does not fully utilise the dedicated resources it has been allocated [Holma04]. In the considered implementation, however, neither DCH establishment or release procedures are considered. UEs always keep a DCH connection and are never allocated less than the minimum allowed data rate.

3.3.1.3 Load Control

The considered system level simulator also includes a load control algorithm that is triggered whenever the total received power exceeds the planned target by an amount corresponding to the LC offset. The scope of the load control algorithm is to keep the system in the planned operation region of the load curve, thus avoiding overload situations. The load control functionality is also responsible for guaranteeing the planned coverage. During load control operation the PS performs data rate downgrading according to the same principles as in the data rate upgrading procedure, but this time starting from the user that is allocated the highest data rate. The LC algorithm is exited whenever the received power at the Node B is estimated to be below the planned target.

3.3.1.4 Handling of Capacity Requests

A CR remains in the scheduling queue at the RNC for successive scheduling periods, unless the maximum possible data rate is allocated to the corresponding UE, or the CR has been in the queue for longer than a maximum allowed time period. While a CR is in the queue, the issuing UE is inhibited to send a new request. In the considered RNC PS implementation, a UE sends a CR only if the following three conditions are simultaneously fulfilled:

1. The buffer content exceeds the preset threshold value for traffic volume reporting,
2. the UE is currently allocated less than the maximum possible data rate, and
3. there is currently no request being processed at the RNC PS for the considered UE.

3.3.2 TFC Elimination and TFC Selection at the UE

A TFC elimination algorithm [TR25896] [TS25321] [TR25896] has been implemented in the system level simulator. The main scope of the TFC elimination algorithm is to prevent the UE to run into power limitations, thus corrupting the quality of transmission over the physical channel. In practice, the TFC elimination algorithm consists of inhibiting the use of those data rates in the TFCS that require a transmission power above the maximum at the terminal.

- A TFC is blocked whenever the transmission power required to support the corresponding data rate is estimated above the maximum UE power capabilities for at least *X* slots within the last *Y* transmitted slots. The estimation of the required transmission power is performed through rescaling the current transmission power according to the data rates associated with every TFC.
- A blocked TFC can be recovered if the estimated transmission power needed to support the corresponding data rate does not exceed the maximum UE power capabilities for a period of *Z* consecutive slots.

The specific values of *X*, *Y* and *Z* used in the system level simulator are reported in Table 3.2. Due to notifications between PHY, MAC and RLC layers, as well as reconfiguration of MAC and RLC specific parameters [TR25896] [TS25321], a delay is associated with both the elimination and the recovery of a TFC (see Figure 3.5).

The TFC selection algorithm performs the selection of the most appropriate TFC for data transmission over the DPDCH. The decision is based on the RLC buffer occupancy and on the set of available data rates for transmission. The set of available data rates consists of all the TFCs in the TFCS that are not constrained by the TFC elimination algorithm.

- The TFC selection algorithm selects the minimum TFC in the set of available data rates that minimise the buffer occupancy after TFC selection.

The TFC selection algorithm can be compactly expressed as in (3.17), where *B* is the UE buffer size before TFC selection, {*TFC*} is the set of available data rates, *TTI* is the Transmission Time Interval, and $B_{after}(TFC)$ is the buffer size after transmission with the corresponding TFC, and can be derived as in (3.16).

$$B_{after}(TFC) = \max\{0, B - TFC \cdot TTI\} \tag{3.16}$$

$$TFC_{SEL} = \min\left\{\arg\min_{\{TFC\}}\left\{B_{after}(TFC)\right\}\right\} \tag{3.17}$$

As for the TFC elimination algorithm, a delay is also associated with the TFC selection algorithm. In this case, the delay between the selection of the TFC and the transmission on the DPDCH is mainly due to L1 processing [TR25896]. Figure 3.5 illustrates an example showing the combined functioning of the TFC elimination and of the TFC selection algorithms.

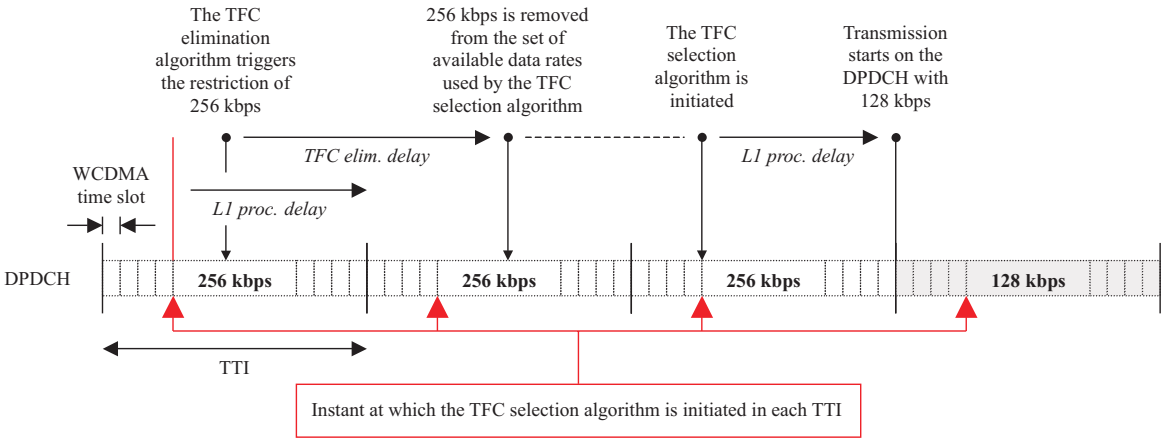

Figure 3.5 Combined functioning of the TFC elimination and TFC selection algorithms.

Whenever the TFC elimination algorithm triggers the blocking of a TFC, the corresponding data rate is removed from the set of available data rates only after the TFC elimination delay has elapsed.

The time elapsing between the initialisation of the TFC selection algorithm and the first time slot of the corresponding TTI is equal to the L1 processing delay. Any change in the set of available data rates occurring after this time instant does not have any effect on the selected TFC for the corresponding TTI.

As a consequence, defining D the time interval between the triggering of either a TFC restriction or a TFC recovery by the TFC elimination algorithm and the instant in which the restriction/recovery is effective, D can be lower and upper bounded as in (3.18).

$$TFC\ elim.\ delay + L1\ proc.\ delay \leq D < TFC\ elim.\ delay + L1\ proc.\ delay + TTI \qquad (3.18)$$

The parameter setup for the TFC elimination and TFC selection algorithms (including TFC elimination and L1 processing delays) is reported together with together relevant parameters in Table 3.2.

3.3.3 Simulation Assumptions

This section includes the main simulation assumptions for the simulation of the RNC PS. More details on the simulation methodology can be found in Appendix A. However, before showing any simulation results, it is worthwhile to mention two main assumptions:

1. First, at the beginning of each simulation a fixed number of users are placed in the network. During the simulation time no users enter or leave the system, and UE generates traffic according to the model described in Appendix D. Therefore, no admission control policy is considered. On the contrary, the focus is entirely on packet scheduling. The average number of users per cell is used as a parameter during the performance assessment of the RNC PS. It is defined as the ratio of the total number of users in the system to the number of cells in the network. Under the specific assumptions, the average number of users per cell is a fixed parameter and does not change during the simulation

Packet Scheduling	Scheduling period			200 ms
	Modification period			600 ms
	NR offset for load control			1 dB
	Power measurement averaging window at the Node B			100 ms
	Maximum allowed load variation (see Section 3.3.1.1)			0.3
	Inactivity downgrading timer			2 s
	Minimum allowed data rate			8 kbps
	Maximum allocated data rate			384 kbps
	TVMR reporting threshold			4 kBytes
	TVMR reporting delay			100 ms
	RNC allocation delay			120 ms
TFC elimination and selection	Maximum UE transmission power			21 dBm
	(*X*, *Y*, *Z*) parameters			(15, 30, 15)
	TFC elimination delay			40 ms
	L1 processing delay			10 ms
Traffic model	Packet Call	Distribution		Exponential
		Mean		5 s
	Reading Time	Distribution		Exponential
		Mean		5 s
	Datagram	Interarrival time	Distribution	Lognormal
			Mean	40 ms
			Standard deviation	38 ms
		Size		1152 Bytes (fixed)
	Resultant average source data rate during packet call periods			≅ 250 kbps
Other parameters	TTI			10 ms
	BLER target			1%
	ARQ process			L2
	L2 retransmission delay			120 ms
	Propagation case			Vehicular A - 3 km/h Clarke's spectrum [Clar68]

Table 3.2: Default parameters for the simulation of the RNC PS.

time. However, the number of users having an active packet call running varies depending on the traffic model characteristics. These users are also defined as active users. For more details see definition [A 2.15] and Appendix D.

2. In the simulations the noise rise (NR) target (i.e. the target value for the total received wideband power at the Node B) is set to obtain a specific *p*% NR outage (see definition [A 2.7]). The scope is to compare the different simulation scenarios under the same load constraint imposed by both stability and coverage requirements.

The parameter setup for the simulation of the RNC-located PS is given in Table 3.2. The parameters related to more standard features such as cell layout, mobility scenario, propagation characteristics, soft handover, power control, etc. are reported in Appendix A. Most of these simulation assumptions are the same as in [TR25896], and are obtained from standardised simulation models in order to allow a fair comparison with previously existing results. The traffic model used for the simulation of NRT data-users is also derived from [TR25896], and its detailed description can be found in Appendix D.

3.4 Performance assessment

This section presents the simulation results for the considered RNC-located PS implementation. Simulations have been run varying the number of users in the system and for different values of the 5% NR outage constraint. First, in Section 3.4.1 the impact of the NR outage constraint on the uplink cell coverage is emphasised. Then, Section 3.4.2 analyses the influence on the system performance of the average number of users per cell. In Section 3.4.3 the cell throughput performance is assessed. In Section 3.4.4 and 3.4.5 the impact on user performance is evaluated, and packet call throughput as well as packet delay statistics presented. Finally, in Section 3.4.6 conclusions are drawn on the relation between uplink cell throughput and user performance.

3.4.1 Impact of the NR Outage Constraint on Cell Coverage

The choice of the NR outage constraint has an impact on both cell throughput and coverage. With a higher NR outage constraint the average uplink load can be increased and the uplink cell throughput consequently enhanced, as it can be directly derived from (3.7) and (3.13). The impact of the NR outage constraint on the achievable cell throughput is analysed more in detail in Section 3.4.3. However, as the NR outage constraint is increased the user with poorer channel conditions start to fall into coverage limitations. The existing trade-off between uplink capacity and coverage in CDMA systems has been thoroughly presented in several books and publications [Holma04] [Veer99]. In this section a simple analysis is presented based on simulation results with different values of the 5% NR outage constraint. Figure 3.6 plots the average per TTI throughput as a function of the average path gain to the strongest Node B. (see definitions [A 2.1] and [A 2.14]).

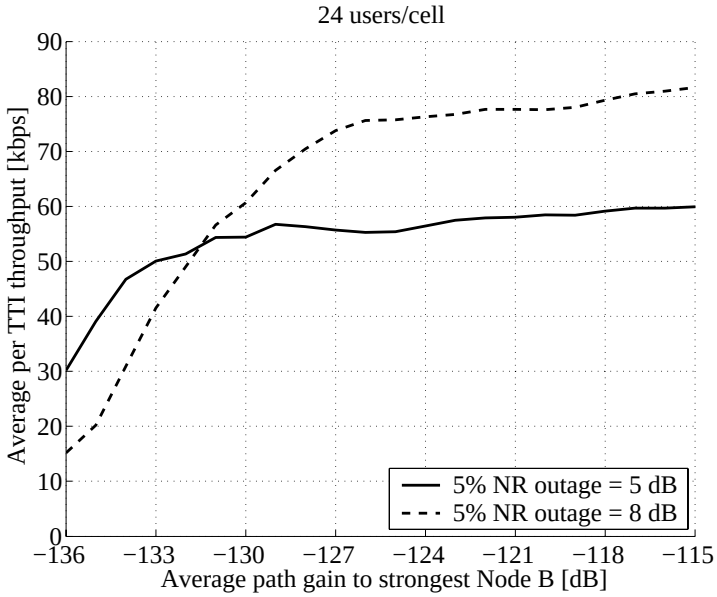

Figure 3.6: Average per TTI throughput as a function of the average path gain to the strongest Node B for two different values of the 5% NR outage constraint and with an average of 24 users per cell.

With a 5% NR outage of 8 dB, users with a higher average path gain experience better throughput performance compared to the case with a 5% NR outage of 5 dB; since a higher uplink load is allowed, users are in general allocated higher data rates. However, with a 5% NR outage of 8 dB a significant throughput loss can be observed for values of the average path gain to the strongest Node B below -133 dB. This effect shows the coverage limitation introduced by increasing the 5% NR outage constraint.

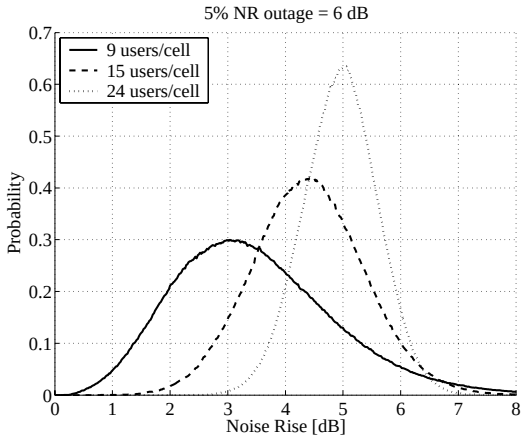

Figure 3.7: Noise rise distribution for different values of the average number of users per cell and for a 5% NR outage of 6 dB.

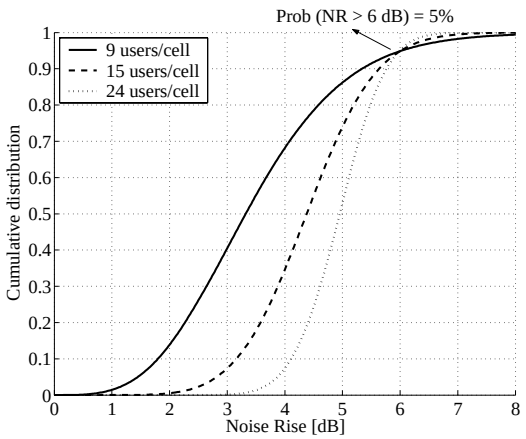

Figure 3.8: CDF of the noise rise for different values of the average number of users per cell. The 5% NR outage is equal to 6 dB in all cases.

3.4.2 Impact of the Average Number of Users per Cell on System Performance

The noise rise distribution is a significant measure of the system load and gives valuable information on the achievable cell throughput in the uplink of WCDMA systems. The noise rise distribution given a specific 5% NR outage constraint strongly depends on the number of packet-data users in each cell. From Figure 3.7 it can be noticed that as the number of users in the system increases, the system can benefit from a reduction in the time variability of the uplink cell load. The required headroom for power scheduling needed to prevent the system from entering unwanted overload conditions consequently decreases. Therefore, the average uplink load to meet the specified NR outage constraint (5% NR outage of 6 dB, see Figure 3.8) can be increased, which directly translates into enhanced cell throughput. The analysis of the cell throughput performance is more specifically addressed in Section 3.4.3.

The reduction of the cell load variations as the average number of users per cell increases can also be explained by observing the distribution of the selected bitrates for data transmission on the DPDCH in Figure 3.9. The higher the number of users in the system, the lower the data rate allocated to each UE. As a consequence, with an average of 9 users per cell every user

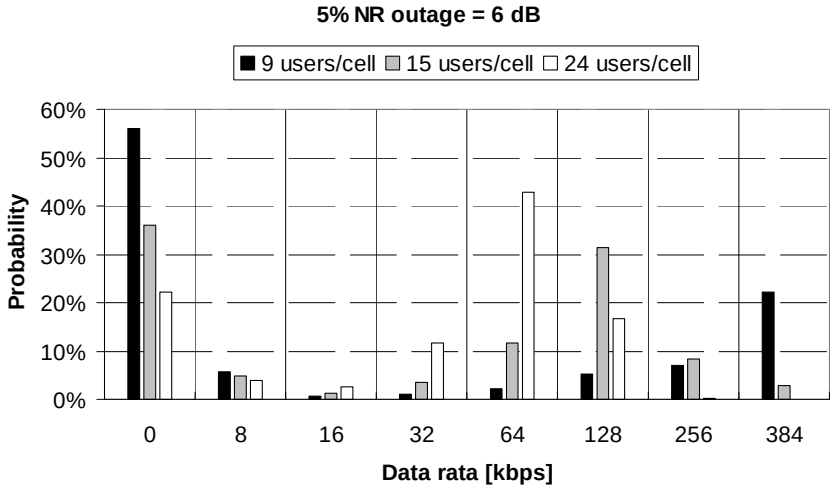

Figure 3.9: Distribution of the selected TFC for data transmission over the DPDCH for different values of the average number of users per cell and for a 5% NR outage of 6 dB.

nearly always selects 384 kbps when he has data to transmit, whereas with 24 users per cell the bitrate more often allocated for data transmission is 64 kbps. As the difference between the data rate allocated by the RNC PS and the average source data rate in the UE buffer increases, data transmission over the DPDCH becomes less bursty. This effect is clear when considering the probability of selecting 0 kbps; in fact, the TFC corresponding to 0 kbps is selected for transmission only when the UE RLC buffer is empty. Since with a higher average number of users per cell the burstiness of data transmission diminishes, the utilisation of the allocated resources increases, and the packet scheduler consequently has more control on the uplink load.

Reducing uncontrolled variations of the uplink cell load has the potential for enhancing the achievable throughput in the uplink of a WCDMA cell. In the presented analysis it has been shown how bursty data transmission on the DPDCH can significantly increase the uplink load variations, thus limiting the maximum achievable system performance. Reducing the burstiness of transmission by allocating relatively lower data rates can provide the RNC PS with a higher control of the uplink load, the main drawback being the significantly decreased user performance. This analysis puts emphasis on the need for a more efficient management of the radio resources that can guarantee a cell throughput improvement and at the same time can provide the users with an acceptable level of service. This issue is introduced in Section 3.5, and more thoroughly addressed in Chapter 4.

3.4.3 Cell Throughput Performance

In order to validate the results obtained from system level simulations, a semi-analytical expression for the estimation of the uplink cell throughput is derived. Differently from (3.7), the expression provided in this section also includes the effect of SHO operation. As in Section 3.2.1, the assumptions of perfect power control and constant and equal bitrate (R) allocation are made. Moreover, users in SHO are assumed to have a lower E_b/N_0 requirement to meet the specified BLER target compared to users connected only to one Node B.

$$\rho_{SHO} = G_{SHO} \cdot \rho \,,\ 0 < G_{SHO} < 1 \tag{3.19}$$

In (3.19), G_{SHO} is the parameter used to model the lower E_b/N_0 requirement per receiving antenna of user in SHO (ρ_{SHO}) compared to the E_b/N_0 requirement per receiving antenna of users not in SHO (ρ). Defining P_{SHO} and P the received power at the Node B from users in SHO and not in SHO, respectively, P_{SHO} and P can be written as (see Section 3.2.1):

$$P_{SHO} = \frac{1}{\frac{W}{\rho_{SHO} \cdot R} + 1} \cdot P_{total} \tag{3.20}$$

$$P = \frac{1}{\frac{W}{\rho \cdot R} + 1} \cdot P_{total} \tag{3.21}$$

In (3.20) and (3.21), P_{total} is the total received wideband power at the Node B. Assuming $W/(\rho R) >> 1$ and $W/(\rho_{SHO} R) >> 1$ (i.e. high processing gain), and introducing the probability of being in SHO operation p_{SHO}, the total received own power can be expressed as:

$$P_{own} = N \cdot p_{SHO} \cdot P_{SHO} + N \cdot (1 - p_{SHO}) \cdot P = \\ = N \cdot P_{total} \cdot R \cdot \rho \cdot \left(\frac{p_{SHO} \cdot (G_{SHO} - 1) + 1}{W} \right) \tag{3.22}$$

In (3.22), N is the total number of users connected to the WCDMA cell. Introducing the uplink fractional load η_{UL}, whose relation to the uplink noise rise is given in (3.6), and solving (3.22) for N gives:

$$N = \eta_{UL} \cdot \frac{W}{\rho R} \cdot \frac{1}{p_{SHO} \cdot (G_{SHO} - 1) + 1} \cdot F \tag{3.23}$$

In (3.23), F is related to the other-to-own cell interference ratio i as in (3.10). Finally, the uplink cell throughput can be calculated as in (3.24), where the throughput due to users in SHO must be scaled so that its contribution is not counted more than once. In this analysis, as well as in the system level simulations, a maximum active set size of 2 is considered, i.e. a user can be simultaneously connected to at most two Node Bs.

$$T = \left[N \cdot (1 - p_{SHO}) \cdot R + \frac{N \cdot p_{SHO} \cdot R}{2} \right] \cdot [1 - BLER(\rho)] = \\ = \eta_{UL} \cdot \frac{W}{\rho} \cdot \frac{1 - p_{SHO}/2}{p_{SHO} \cdot (G_{SHO} - 1) + 1} \cdot F \cdot [1 - BLER(\rho)] \tag{3.24}$$

In Figure 3.10, the average cell throughput both from system level simulations and from (3.24) is plotted as a function of the average number of users per cell. The method to derive the average cell throughput from system level simulations is described in definition [A 2.12]. Results are shown for different values of the 5% NR outage constraint. The scope is to

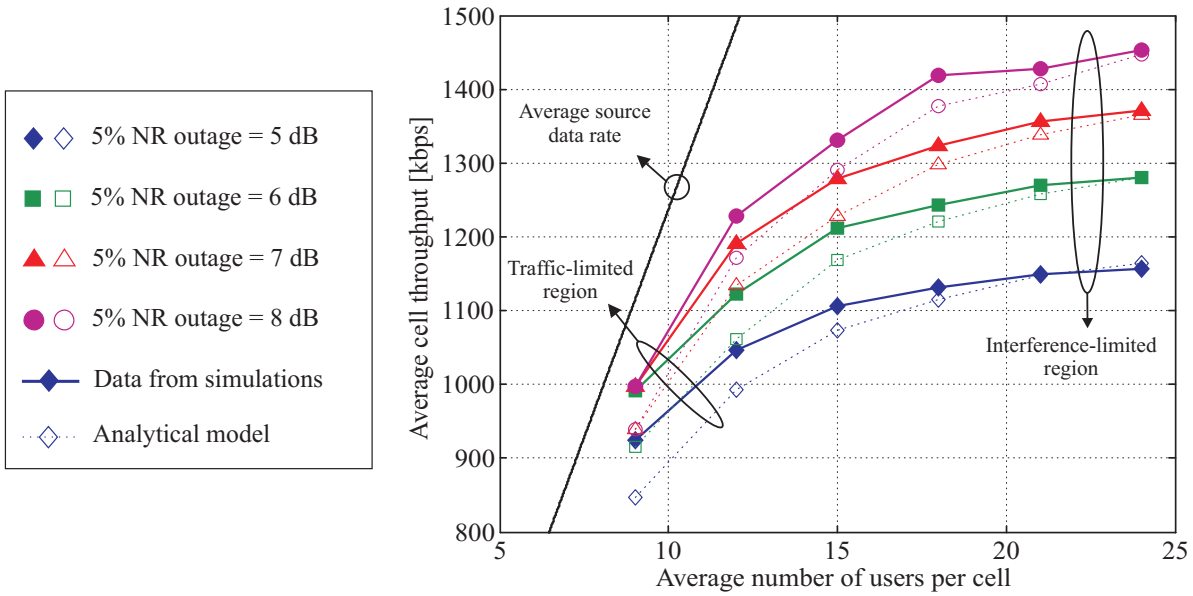

Figure 3.10: Average cell throughput as a function of the average number of users per cell and for different values of the 5% NR outage constraint.

ρ	p_{SHO}	G_{SHO}	$BLER(\rho)$
1.26 (≅1dB)	30%	≅ 0.76 (1.2 dB gain)	1%

Table 3.3: Quantities to be substituted in (3.24) to obtain the semi-analytical cell throughput values plotted in Figure 3.10.

provide a validation of the simulation results by fitting the analytical cell throughput in (3.24) to the experimental data by using output values from the system level simulations. The values of F and η_{UL} to be substituted in (3.24) are obtained from the corresponding system level simulations. The required E_b/N_0 per receiving antenna ρ is derived from Actual Value Interface (AVI) curves assuming a Block Error Rate of 1% (see Appendix C), while the soft handover probability p_{SHO} depends on the mobility scenario and on the SHO settings. Also, an E_b/N_0 requirement reduction of approximately 1.2 dB for users in SHO is assumed [Salo99]. Table 3.3 summarises some of the quantities to be substituted in (3.24) in order to obtain the semi-analytical cell throughput values plotted in Figure 3.10. It can be noticed that the analytical results present a good match with the simulation results, especially in the interference-limited region. The fact that in the traffic-limited region the analytical model tends to underestimate the average cell throughput is due to the higher variability of the uplink fractional load, of the other-to-own cell interference ratio, as well as of the bitrates used for data transmission. In Section 3.2.2, these effects have been shown to have a direct impact on the level of accuracy of the load equation for cell throughput prediction purposes.

In Figure 3.10, the average source data rate is also plotted as a function of the average number of users per cell. The average source data rate in a cell can be approximated assuming a 50% duty cycle and an average input data rate per UE during active periods equal to 250 kbps (see traffic model parameters in Table 3.2). Naming S_{CELL} and N_{CELL} the average source data rate and the average number of users per cell, respectively, S_{CELL} is derived as:

$$S_{CELL} = N_{CELL} \cdot 250 \text{ kbps} \cdot 0.5 \tag{3.25}$$

From Figure 3.10, the cell throughput increases with the 5% NR outage constraint, as well as with the number of packet data users in the system. For low values of the average number of users per cell the system is in the traffic-limited region, i.e. its performance is strongly influenced by the characteristics of the generated traffic. In this region, increasing the number of users in the system causes the uplink cell throughput to significantly improve. For a 5% NR outage of 8 dB, the rise in average cell throughput has approximately the same slope as the increase in average source data rate.

On the other hand, for a high average number of users per cell the system operates in the interference-limited region, i.e. its performance is mainly determined by the constraint imposed on the total received power at the Node B. In this region, the impact on the system performance of different settings of the 5% NR outage constraint is clearly observable. Moreover, since the system is interference-limited, increasing the average number of users in the cell only slightly affects the cell throughput performance.

3.4.4 Packet Call Throughput Performance

Information on the feasible uplink cell throughput does not tell the entire story about the actual opportunity of network operators and content providers to deliver NRT data services to their subscribers. The quality of service that users experience is also an important indicator to be taken into consideration, and the performance of the RNC PS must also be assessed with an eye to the user perspective. Although it might be a hard task to quantify the end-user level

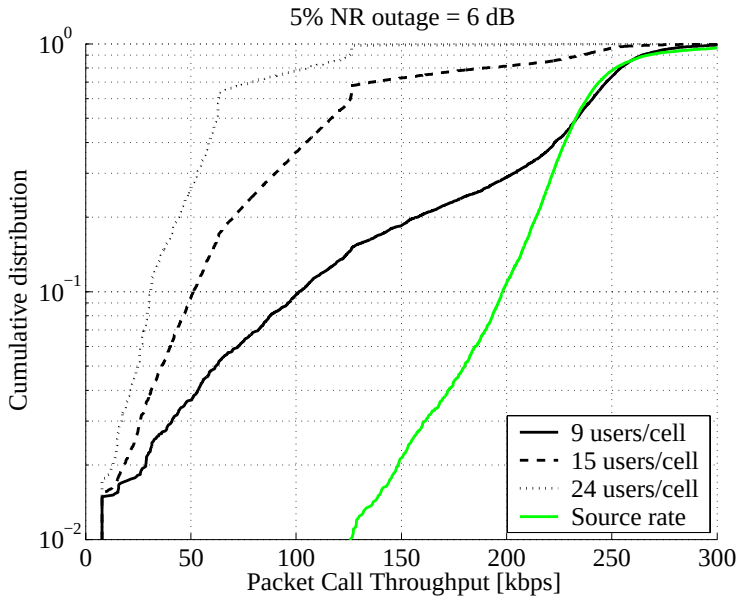

Figure 3.11: Source rate distribution and CDF of the packet call throughput for different values of the average number of users per cell and for a 5% NR outage of 6 dB.

of satisfaction, some engineering measures to evaluate the user performance are introduced. The measure considered in this section is the packet call throughput (PCT), which we define as the average data throughput experienced by a packet-data user during a packet call. See definition [A 2.2] for more details.

Figure 3.11 plots the cumulative distribution functions (CDFs) of the PCT for the same simulation cases of Section 3.4.2, together with the CDF of the source data rate[1]. Results show that increasing the average number of user per cell causes a significant decrease in the PCT performance. The performance reduction is particularly clear at the medium to high levels of the CDF, where the PCT performance is mainly determined by the amount of available resources to be shared between all the active users. At lower levels of the CDF, the PCT performance is largely influenced by the initial allocation of the minimum allowed data rate of 8 kbps (see Table 3.2). I.e., very short packet data sessions generally experience low throughput independently from the amount of available radio resources because they simply do not have the time to recover from the initial allocation of a very low data rate.

Also, for high values of the average number of users per cell the CDF of the packet call throughput presents abrupt changes of slope in correspondence with the available data rates for transmission. This is due to the effect of the packet scheduling policy, where users that are granted a relatively high data rate are never downgraded unless long inactivity is detected, or load control actions are taken. As a consequence, these users experience a higher PCT performance than users allocated with lower data rates.

Finally, with an average of 9 users per cell nearly all the active UEs are allocated the maximum possible data rate (see Figure 3.9). In this case the packet call throughput CDF is smoother than with higher values of the average number of users per cell, and above the 40% level it practically coincides with the CDF of the source data rate. That means, approximately 60% of the packet calls experience an average throughput that is almost equal to the average source data rate during the corresponding packet-data session.

[1] The CDF of the source data rate is obtained from a set of packet calls different from those used to obtain the empirical CDFs also plotted in Figure 3.11.

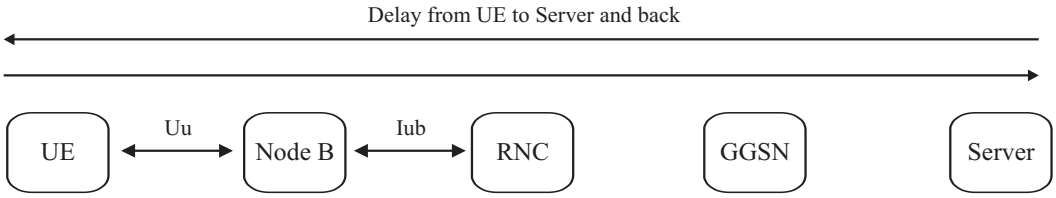

Figure 3.13: Round trip time definition [Holma04].

3.4.5 Packet Delay Performance

The packet call throughput is a measure of the average throughput experienced by a user during a packet connection. This information is quite valuable for services where the level of satisfaction of each user is mainly determined by the average transmission rate. Examples of such services could be file upload using FTP and e-mail upload with large file attachments. On the other hand, the packet delay (see definition [A 2.9]) has a major impact on the performance of interactive type of services such as web browsing and gaming.

Although a strong correlation between packet delay and packet call throughput exists, these two user performance indicators are conceptually different. Information on the packet delay is particularly useful when considering its impact on the round trip time (RTT), which in WCDMA is defined as the delay of a small packet travelling from the UE to a server behind the Gateway GPRS Support Node (GGSN) and back [Holma04]. The round trip time concept is illustrated in Figure 3.13. In mobile networks like UMTS the delay is higher than in fixed IP networks, and as a consequence the RTT is longer when a TCP connection is established over the WCDMA air interface. A shorter RTT gives a benefit in the response time, which is especially advantageous for TCP slow start and for interactive services with small packets like gaming.

In Figure 3.12 it is evident how, as the average number of users per cell increases, the experienced packet delay considerably grows. This is because the delay curves plotted in Figure 3.12 also include buffering delay at the UE side. In the traffic model implemented in

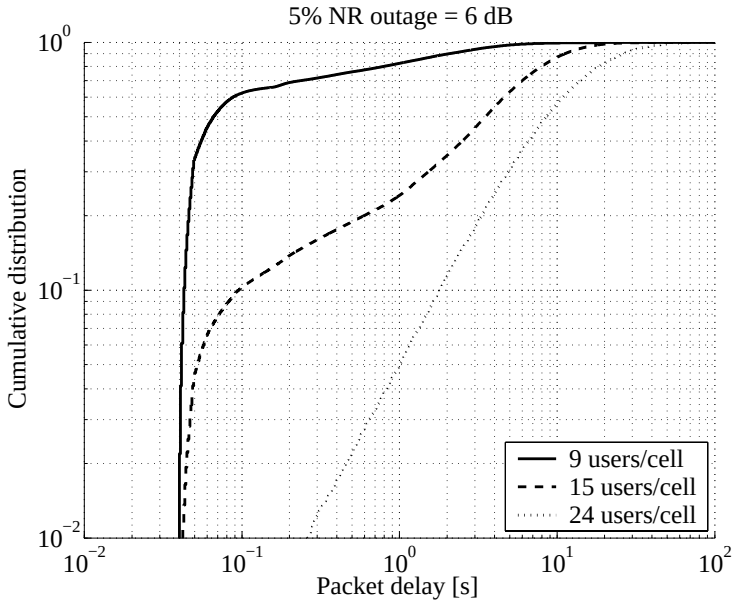

Figure 3.12: CDF of the packet delay for different values of the average number of users per cell and for a 5% NR outage of 6 dB.

the system level simulator (see Appendix D), data is continuously generated in the UE RLC buffer during a packet data call independently from the data rate allocated by the RNC PS. Therefore, the packet delay experienced by users allocated with a transmission rate lower than the average source data rate grows as the size of the RLC buffer increases. In real applications using TCP as transmission protocol, the TCP flow control functionality limits the number of data packets passed to RLC so to adapt to the transmission rate experienced over the air interface. Basically, the TCP congestion window determines the maximum number of data packets that can be delivered to the lower layers and for which TCP acknowledgement is still awaited. If a timeout event occurs (i.e. the RTT exceeds a specified value) the size of the TCP congestion window is reduced. On the other end, at the application level it is of marginal importance whether the delay due to a low allocated data rate on the air interface is seen as RLC buffering delay or it is 'artificially' introduced by the flow control functionality of TCP. In this perspective, the packet delay statistics can be used in order to set a constraint on the maximum packet delay that can be tolerated by a specific application.

3.4.6 Relation between Cell Throughput and User Performance

In Sections 3.4.3, 3.4.4 and 3.4.5 the cell throughput and user performance with the RNC PS has been separately investigated. In general, it has been shown that a high cell throughput can be achieved in uplink at the cost of reducing the level of service experienced by the users. In the present section the relation existing between the achievable cell throughput and the user performance is analysed more in detail. To this end, two new user performance indicators are introduced: The *p*% packet call throughput (PCT) outage and the *p*% packet delay outage (see definitions [A 2.4] and [A 2.10], respectively).

From Figure 3.14, without any restriction on the minimum guaranteed user performance, the achievable cell throughput is in the range between 1.15 and 1.45 Mbps, depending on the NR outage constraint. However, if a 10% PCT outage of 64 kbps is required, the cell throughput loss compared to not having any minimum requirement is approximately 10-15%. Similar conclusions can be drawn for the 5% PCT outage and the 5% and 1% packet delay outage in Figure 3.15, Figure 3.16 and Figure 3.17, respectively.

Alternatively, we can define a minimum packet call throughput or a maximum packet delay requirement for which a user making use of a specific packet data service can be considered satisfied. Information on the achievable cell throughput can be derived based on the level of satisfaction that the network operator wants to achieve.

Figure 3.18 and Figure 3.19 plot the average cell throughput as a function of the probability of experiencing a packet call throughput lower than 64 kbps and a packet delay bigger than 2

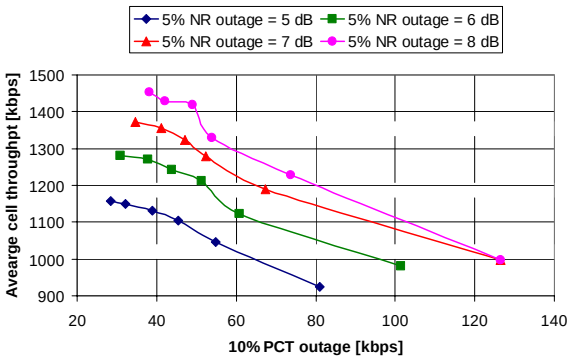

Figure 3.14: Average cell throughput as a function of the 10% PCT outage.

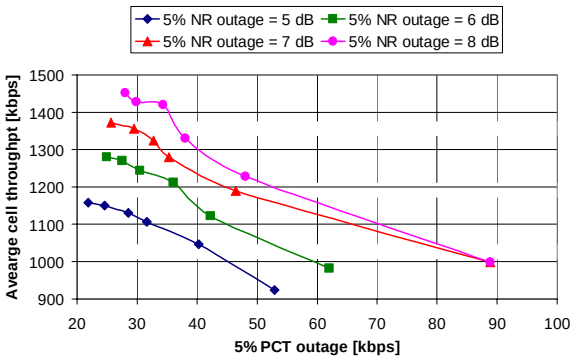

Figure 3.15: Average cell throughput as a function of the 5% PCT outage.

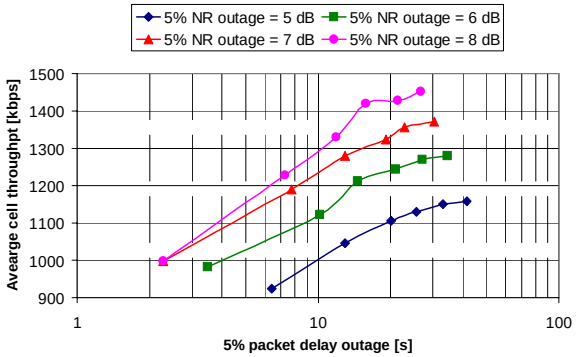

Figure 3.16: Average cell throughput as a function of the 5% packet delay outage.

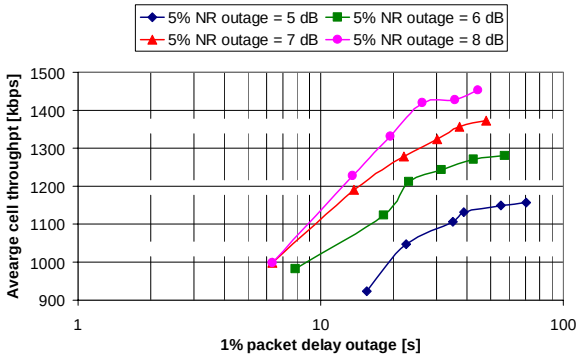

Figure 3.17: Average cell throughput as a function of the 1% packet delay outage.

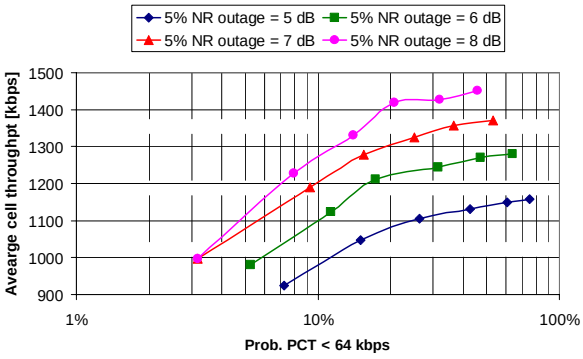

Figure 3.18: Average cell throughput as a function of the probability that the PCT < 64 kbps.

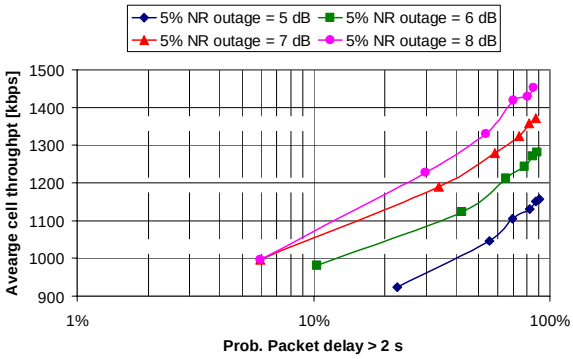

Figure 3.19: Average cell throughput as a function of the probability that the packet delay > 2 s.

seconds, respectively. For instance, for a 5% NR outage of 6 dB the achievable cell throughput is around 1.1 Mbps if at least 90% of the packet calls are required to have a data throughput of 64 kbps. The cell throughput can be increases up to approximately 1.25 Mbps (with an equivalent 14% cell throughput gain) if the network operator can tolerate 35% of the packet data sessions experiencing a throughput below the minimum PCT requirement.[2]

Finally, it should be noticed that the figures reported in this section are essentially different ways of presenting the same results. Here the scope was to generate some cell throughput versus QoS curves for the RNC PS under specific conditions for the generated traffic. As previously introduced, the QoS is a quite abstract concept and it is difficult to define an engineering measure that exactly quantifies the level of satisfaction of the end-user. Therefore, different ways to define a constraint on the minimum guaranteed user performance have been introduced and the achievable cell throughput in uplink presented as a function of the different user performance constraints.

3.5 Limitations of the Release 99 RNC-located Packet Scheduler

In this chapter a specific implementation of the RNC PS functionality has been introduced and its performance assessed. It has been shown that an inherent trade-off exists between maximisation of uplink cell throughput and user performance. If the traffic offered by users in the system is bursty and requires the allocation of relatively high data rates, the main drawback of an RNC PS implementation is its incapability of rapidly reallocating the radio

[2] Notice that under the considered assumptions for the offered data traffic requiring a maximum packet delay of 2 s is much more spectrally inefficient than requiring a minimum packet call throughput of 64 kbps.

resources according to the actual needs of the users in the system. So, once a user has been allocated a high data rate, the assigned radio resources are released only after expiring of an inactivity timer. At this point in a real implementation the user is moved to CELL_FACH state (see Section 2.4.1). Due to the fairly long time required to successively setup a new dedicated connection (approximately 900 ms, see [Holma04]), the inactivity timer for switching to CELL_FACH state cannot be arbitrary reduced without significantly impacting the user performance. It should be kept in mind that in our implementation of the RNC PS the switching to CELL_FACH state is modelled by downgrading users to the minimum allowed data rate (see Section 3.3.1.2).

If the overall objective is to guarantee an acceptable level of service, only a few packet data users should be admitted in the system, and consequently allocated with the required radio resources. The disadvantage of such an approach is that the UEs are more or less constantly allocated with a high data rate, and the utilisation of the allocated radio resources is low due to the burstiness of the generated traffic, thus limiting the maximum achievable cell throughput in uplink.

On the other hand, if the objective is to maximise cell throughput many packet-data users can be admitted in the system. Users are allocated with relatively low data rates and transmit on the physical channel nearly at constant rate. This leads to a reduction in the variations of uplink load and other cell interference, with a corresponding benefit in terms of cell throughput. Obviously, the main drawback is the poor QoS experienced by the users.

An intuitive solution to solve this problem is to make data rate modifications more dynamic so to adapt the allocation of radio resources to the typically bursty nature of NRT traffic. The impact of the radio resource allocation on the trade-off between spectral efficiency and user performance is illustrated with a simplified example in Figure 3.20. Increasing the incidence of the PS functionality might be difficult to accomplish while keeping the PS at the RNC. There are two main reasons why the RNC PS implementation is not particularly suitable for fast packet scheduling operation:

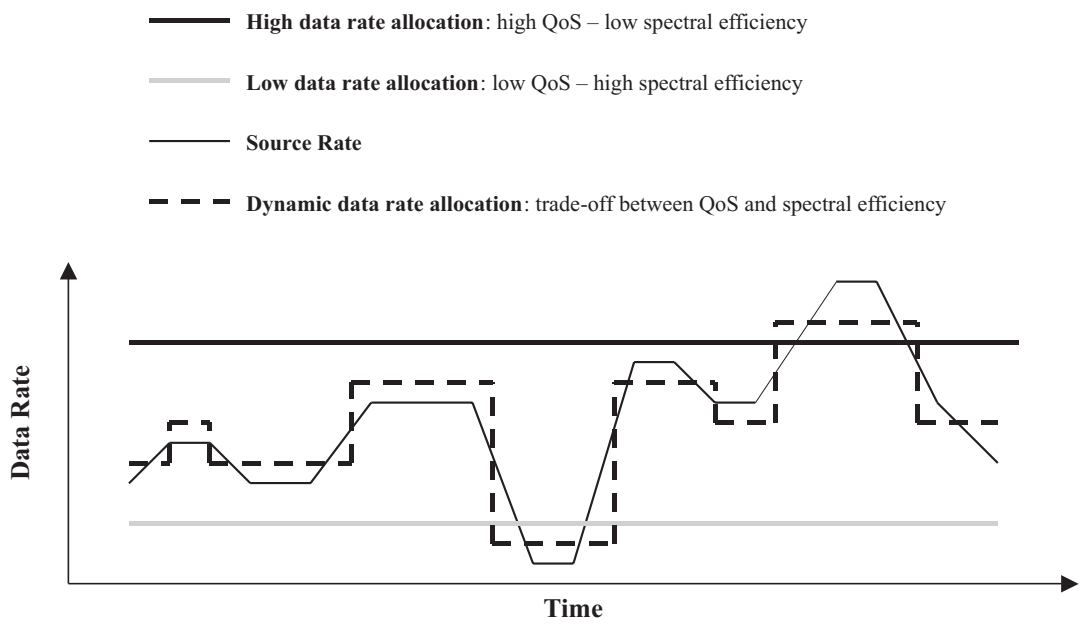

Figure 3.20: Impact of the radio resource allocation principle on the trade-off between QoS and spectral efficiency.

- The first reason is that frequent packet scheduling operation necessitates more processing capacity at the RNC, and at the same time the signalling overhead over the Iub interface significantly increases.
- The second reason is related to the quite significant delay associated with the issuing of a CR from a UE to the RNC PS, and with the reporting of a TFCS modification message from the RNC PS to the UE. This clearly limits the possibility to perform fast reallocation of the radio resources based on the momentary user requirements.

Especially this last issue is the main limiting factor for faster operation of an RNC-located PS. In this perspective architectural changes are necessary, namely the packet scheduler functionality needs to be moved from the RNC to the Node B. Chapter 4 specifically addresses this and other issues concerning the deployment of a fast packet scheduler that operates at a higher incidence compared to the RNC PS implementation presented in this chapter.

3.6 Summary

In the present chapter the problem of assessing the achievable throughput in the uplink of a WCDMA cell has been introduced by means of a theoretical analysis. However, with the introduction of packet-data services a semi-analytical approach becomes rather ineffective, mainly due to the complexity of setting a minimum constraint for the user performance in the load equation formula (3.7). Therefore, a simulation tool for the assessment of both cell throughput and user performance has been introduced. Results have shown that the achievable cell throughput in uplink is mainly determined by:

- The particular setting of the NR outage constraint, and
- the level of burstiness of data transmission over the physical channel.

Without imposing any constraint on the minimum guaranteed user performance, the uplink cell throughput in a macro-cell environment with low user mobility, two-way SHO operation and 2-branch antenna diversity is estimated between 1.15 and 1.45 Mbps, depending on the specific NR outage constraint. The higher the NR outage constraint, the higher the cell throughput, but at the same time uplink coverage is reduced. As soon as user performance constraints are introduced, the achievable cell throughput decreases. Different constraints were introduced to include a minimum guaranteed user performance taking into consideration both packet call throughput and packet delay statistics. For a NR outage constraint of 6 dB and requiring at most 10% of the packet data session to experience a throughput lower than 64 kbps, the cell throughput loss compared to the case with no minimum PCT requirements is in the order of 10-15%.

To achieve maximum utilisation of the radio resources, thus enhancing system throughput without degrading the experienced user performance, the functionality to allocate the radio resources to NRT users needs to be fast and dynamic. The RNC-located PS implementation introduced in this chapter presents some major limitations for the deployment of fast packet scheduling operation. Therefore, the packet scheduler functionality needs to be moved from the RNC to the Node B. In this way, not only the allocation of radio resources can be performed faster due to the reduced allocation delay, but data rate modifications can also be done more frequently without requiring additional processing capacity at the RNC, and the allocation of additional resources on the Iub interface.

Chapter 4

Enhanced Uplink: L1 Retransmission Schemes and Fast Node B Scheduling

4.1 Introduction

The main outcome of the analysis presented in Chapter 3 is that there is an inherent trade-off between system and user performance in the uplink of WCDMA systems. In particular, an RNC PS implementation has been proven to be rather inefficient for NRT data services characterised by bursty traffic profiles, and requiring relatively high transmission rates and short transmission delays. In this perspective, a study item on uplink enhancements for dedicated transport channels has started in September 2002 within the 3GPP. The goal was to investigate enhancements that could be applied to the current WCDMA specifications in order to improve the performance of uplink dedicated transport channels, with focus on data services like gaming, video streaming, image and video-clip upload, P2P applications, etc.

In [TR25896], several candidate approaches aiming at improved WCDMA uplink performance on dedicated channels have been proposed. The work presented in this chapter mainly focuses on two among the techniques considered for enhanced DCH (E-DCH) performance: (i) L1 retransmission schemes, and (ii) fast Node B packet scheduling.

Both techniques have already been shown to give a significant improvement in the downlink evolution of WCDMA packet-data systems, namely High Speed Downlink Packet Access (HSDPA) [Kold03], and for this reason have also been considered for enhanced uplink performance. Though, some fundamental differences exist between uplink and downlink transmission that must be carefully considered when assessing the potential benefit from such techniques for enhanced uplink packet access.

4.1.1 Hybrid ARQ Schemes

A major concern in data communication systems is how to control transmission errors so that error-free data can be delivered. There are two basic categories of error-control schemes for

data communications: (i) automatic repeat request (ARQ) schemes, and (ii) forward error correction (FEC) schemes [Lin84].

ARQ – These error-control schemes make use of error-detecting codes. Whenever an error is detected, the receiver discards the erroneously received word and requests a retransmission of the same codeword via a feedback channel. ARQ schemes are widely used because they are simple and provide high system reliability. The main drawback is that the throughput rapidly falls with increasing channel error rate.

FEC – In a FEC error-control system, an error correcting code is used for combating transmission errors. The throughput of the system is constant and depends on the specific code used by the system. Since no retransmission is required, it is much harder to achieve high system reliability with FEC schemes than it is with ARQ schemes.

To overcome the drawbacks of ARQ and FEC schemes, Hybrid ARQ (HARQ) schemes incorporate both FEC and retransmission to offer the potential for better performance. HARQ schemes can be classified into three different categories [Malk01]:

1. **Type I HARQ** –In these schemes, the receiver discards the packet upon erroneous reception and asks for an entirely new retransmission. Retransmissions take place until the packet is correctly received or until a pre-set number of retransmissions have taken place.
2. **Type II HARQ** – These schemes are also called incremental redundancy (IR) ARQ schemes. With type II HARQ, a packet that needs to be retransmitted is not discarded, but is combined with some incremental redundancy bits provided by the transmitter for subsequent decoding.
3. **Type III HARQ** – These schemes are equivalent to type II HARQ schemes, but in this case each retransmission is self-decodable. I.e., the transmitted packet may be combined with the previous versions if available, but each version contains all the information necessary for a correct reception of the data. A special case of type III HARQ schemes is chase combining (CC) [Chase85]. With CC the erroneous packet is stored at the receiver and combined with the retransmitted packet, which is a replica of the coded data packet transmitted in the first place. This can be considered as incremental redundancy in the form of repetition code.

The different categories of HARQ schemes are illustrated in Figure 4.1. In the presented study

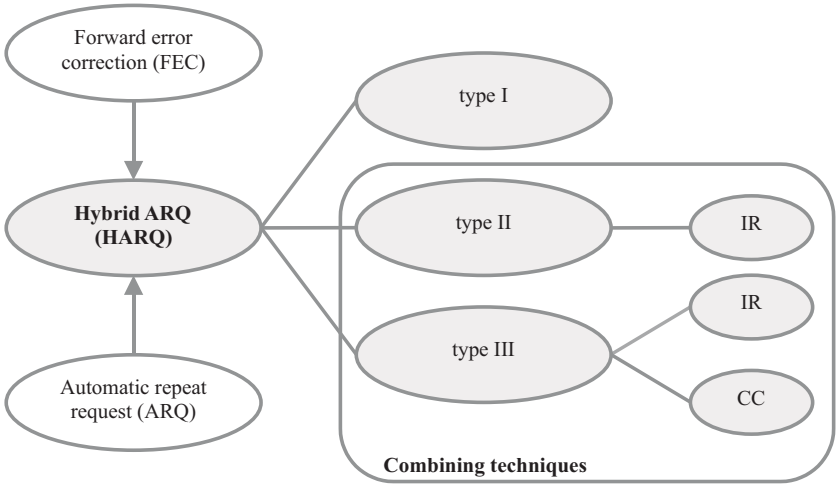

Figure 4.1: Different categories of error-control schemes in data communication systems.

no differentiation is made between type II and type III strategies, and the term type II HARQ is used throughout this chapter to more generally indicate all types of combining techniques.

HARQ schemes have been introduced since the early sixties [Lin84]. In more recent years, advanced physical layer retransmission employing soft combining gain, incremental redundancy and low retransmission delay has been investigated as one of the central features of HSDPA [Fred02] [Peng02]. Type-I HARQ schemes are best suited for communication systems in which a fairly constant level of noise and interference is expected on the channel, whereas CC and IR schemes are more appropriate for channels with a non-stationary bit error rate [Lin84]. In HSDPA, which does not make use of power control, combining techniques have been proven to provide significant gain compared to type-I HARQ strategies [Lin84]. In [Rait98] it is shown that the performance of data transmission on dedicated transport channels can also be improved when combining techniques are deployed together with fast power control, especially for high user mobility. However, the presented analysis is only based on link level simulations, and more importantly only considers downlink transmission on dedicated transport channels. In the uplink of CDMA systems power control is known to be an important feature since the system has to cope with the so-called near-far problem [Duel95]. Hence, in uplink the deployment of CC and IR techniques might not provide the same performance increase as in downlink. However, since the entity controlling the retransmissions is moved to the Node B, L1 retransmission schemes can still benefit from reduced retransmission delays compared to L2-based ARQ strategies. The reduced retransmission delays allow operating the physical channel at somewhat higher error probability, thus increasing the spectral efficiency in the system (see Section 4.2.1). One of the main goals of the analysis presented in this chapter is to estimate the impact from the delay improvement provided by fast L1 retransmission schemes on the uplink throughput of a WCDMA cell.

4.1.2 Node B Uplink Scheduling

Data scheduling in wireless networks is a widely studied topic due to the expected growth of high-speed wireless data services in 3G systems. Due to the asymmetric nature of many services requiring higher downlink capacity, most of the previous research on data scheduling has focused on the downlink direction of transmission. However, some increase in uplink traffic is also expected due to the growth of services that require high data rates on the uplink. These considerations have resulted in some research on the subject of uplink scheduling, see e.g. [Rama98], [Kuma03], [Uluk00], [Jänt03], [Oh03], and [Samp95]. Although formulated in different ways and addressing different specific problems, the general goal of these papers is to define an optimum (or sub-optimum) power and rate allocation scheme that maximises throughput, with or without respect to some fairness constraints. All the proposed solutions assume that the WCDMA system operates with a TDM overlay, so that simultaneous rate and time scheduling is performed. On the other hand, these schemes bring about some practical concerns that are not so easy to quantify but are expected to have great impact on system performance and cost. All these issues are further discussed and more properly addressed in Chapter 5, where more advanced scheduling techniques for the enhancement of WCDMA uplink transmission are considered.

As regards uplink radio resource allocation, the main objective of the work presented in this chapter is to estimate the performance improvement that a radio resource allocation scheme located in the Node B can provide compared to an allocation scheme situated in the RNC. In [Outes01] it is shown that for what concerns admission control, a centralised multi-cell scheme located in the RNC is able to provide a significant benefit compared to a single-cell approach. The situation might be different when considering the PS functionality, whose main task is

the reallocation of radio resources among NRT users that have already been admitted in the system. In this sense, the main drawback of an RNC-located PS is the significant scheduling delays associated, which can be reduced by moving the PS functionality to the Node B. An analysis of RNC versus Node B scheduling has been addressed in [Pi03] for the CDMA2000 1x EV-DV standard. However, the main focus of this paper is on the performance of a multi-layer cooperative radio resource management scheme, and the used approach is also based on a CDMA scheme that operates with a TDM overlay. Recently, an overview of enhanced uplink performance has been presented in [Ghosh04], where both Node B-controlled rate scheduling and Node B-controlled time and rate scheduling are investigated. The authors show that Node B PS operation can provide up to 50% cell throughput gain compared to a PS implementation according to the Release 99 of the 3GPP specifications. Nevertheless, the presented results mainly focus on physical layer performance, whereas cell throughput numbers are obtained under the assumption of full buffer at the UEs (neither traffic modelling nor user performance issues are taken into consideration).

To conclude:

1. All the results presented in this chapter assume a Node B-located PS based on code division multiplexing (CDM), i.e. no time scheduling is considered. This approach corresponds to what [TR25896] and [Ghosh04] define 'Node B rate scheduling', where all uplink transmissions occur in parallel but at a low enough rate such that the target received power at the Node B is not exceeded.
2. Moreover, a specific constraint on the Node B scheduling interval is considered in order to limit the number of allocation messages between the Node B and the UEs.

These assumptions represent the main difference with respect to most of previous research on the subject of uplink scheduling in 3G systems. They have been introduced to evaluate the feasible enhancements for uplink performance under more severe restrictions, mainly dictated by complexity and cost issues.

The chapter is organised as follows: Section 4.2 gives an overview of the potential benefits from L1 retransmission schemes and fast Node B packet scheduling operation. It also introduces architectural issues, increased system complexity, as well as practical implementation problems when both these techniques are introduced. Sections 4.3 and 4.4 discuss more in detail the implementation in the system level simulator of L1 retransmission schemes and of Node B scheduling, respectively. Section 4.3 also includes a theoretical analysis to study the impact of L1 retransmission protocols both on delay and cell throughput performance, whereas Section 4.4 gives a thorough description of the proposed Node B scheduling algorithm. Simulation results are then presented and commented in Section 4.6. Finally, the concluding remarks are given in Section 4.7.

4.2 Basic Concepts and Complexity Issues

The potential benefit from both L1 retransmission protocols and fast Node B packet scheduling comes at the price of increased system complexity. In practice, some of the network functionalities that in the Release 99 UTRAN architecture are located in the RNC are now split between the RNC and the Node B. Sections 4.2.1 and 4.2.2 introduce the basic concepts lying behind L1 retransmission schemes and fast Node B scheduling, respectively, and also give a general overview of the complexity issue possibly related to their implementation in real systems.

4.2.1 L1 Retransmission Schemes

Node B-controlled L1 retransmission schemes rely on fast retransmission of erroneously received data frames to reduce the number of RLC retransmissions, specifically the associated delays. The physical channel can be operated with somewhat higher error probability for the same overall delay performance, which leads to an increase in the system spectral efficiency, and consequently in the maximum achievable cell throughput. The relation between reduced retransmission delay and improved spectral efficiency is illustrated in Figure 4.2. Depending on the delay requirements of the particular NRT service and on the reduction in the retransmission delay, the block error rate at which the physical channel is operated can be increased maintaining the overall delay performance for the considered service, thus reducing the corresponding E_b/N_0 requirement. At this point we introduce the effective E_b/N_0 to meet a specific block error rate target *BLER* defined as [Holma04]:

$$\rho_{eff}(BLER) = \frac{\rho(BLER)}{1 - BLER} \tag{4.1}$$

In (4.1),ρ (*BLER*) is the required E_b/N_0 to meet the specified BLER target *BLER*. From (3.7) and (4.1), it is clear how the effective E_b/N_0 is inversely proportional to the average cell throughput *T*. Depending on the propagation and mobility environment, there exist an optimum *BLER* in correspondence of which the effective E_b/N_0 is minimised, and the achievable cell throughput consequently maximised (T_{MAX}.) Reducing the retransmission delay has therefore the potential for increasing the cell throughput performance.

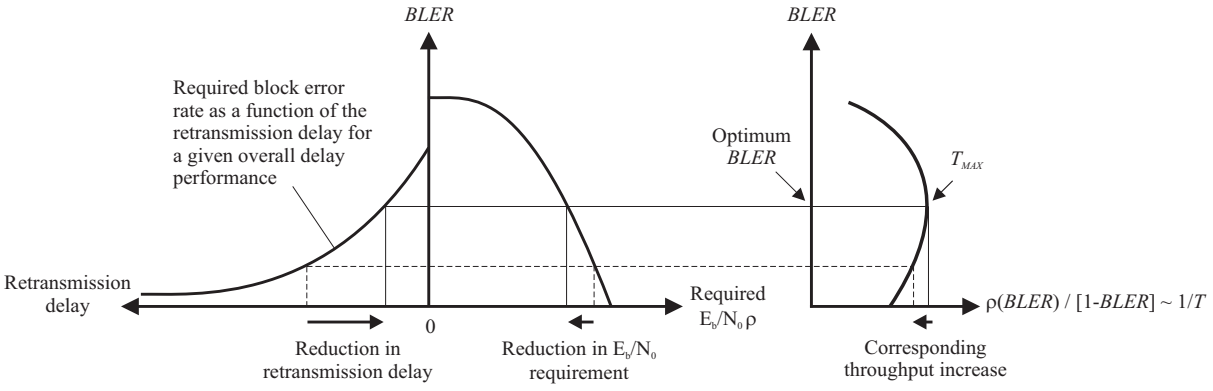

Figure 4.2: Relation between reduced retransmission delay and improved spectral efficiency.

Combining techniques such as chase combining and incremental redundancy can further improve the performance of Node B-controlled L1 retransmission schemes [Fred02]. The fast L1 HARQ retransmission concept is illustrated in Figure 4.3, and compared to a L2 RNC-located retransmission scheme. Clearly, L1 retransmissions reduce the round trip delay between the transmission of a data frame in uplink and the reception of the corresponding positive or negative acknowledgement message in downlink. Notice in Figure 4.3 that the L2 retransmission protocol controlled by RLC is operational also when L1 retransmission schemes are introduced. But in this case, a L2 retransmission only occurs when the maximum number of L1 transmissions is achieved and the corresponding data packet is still not correctly decoded at the Node B.

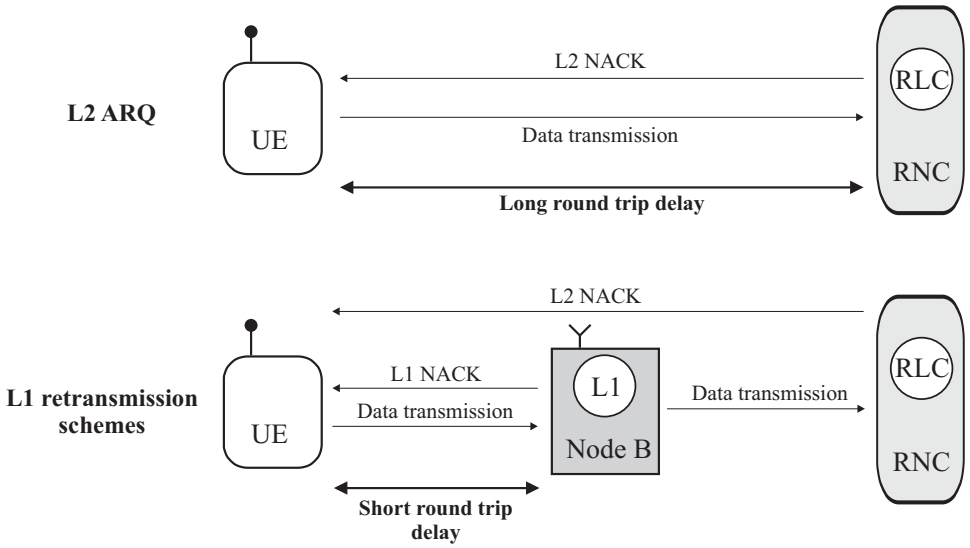

Figure 4.3: L1 Node B-controlled retransmission schemes vs. L2 RNC-located retransmission schemes.

4.2.1.1 N-channel Stop-and-Wait Protocol

L1 retransmission schemes are based on an N-channel stop-and-wait (SAW) protocol [TR25896], whose fundamentals are illustrated in Figure 4.4. When a UE sends a data frame on the DPDCH using a particular SAW channel, it must awaits for a positive or negative acknowledgement from the Node B before either a new transmission or the retransmission of an erroneously received data packet can take place on the same SAW channel. In order to avoid idle periods due to pending ACK/NACK messages from the Node B, the N-channel SAW protocol makes use of N parallel channels. The required number of SAW channels depends on the implementation of the signalling channels, as well as on the processing times required both at the Node B and at the UE. In Figure 4.4, a 3-channel SAW scheme is assumed, where T_{ACK} is the time required to transmit a NACK/ACK message from the Node B to the UE and depends on the downlink signalling channel implementation. The number of SAW channels is a crucial parameter since it determines the buffer requirements for the implementation of combining techniques, but more importantly because it directly affects the required processing time at the Node B.

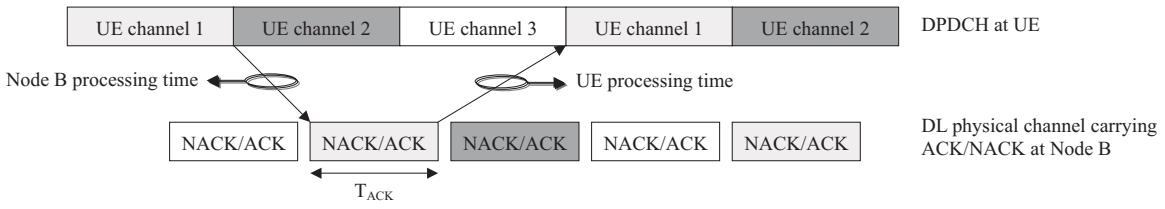

Figure 4.4: Fundamentals of the N-channel stop-and-wait protocol, N = 3.

4.2.1.2 Signalling to Support L1 Retransmission Schemes

In order to support L1 retransmission schemes, some additional exchange of information is required between the UE and the Node B compared to Release 99. In addition to the ACK/NACK messages in downlink direction, the user is also required to send some information on a TTI basis. The amount of additional signalling requirements mainly depends on:

- The particular HARQ scheme to be implemented (type-I, IR or CC), and
- the reordering of data frames that might be delivered in wrong order due to some transport blocks requiring more retransmission than others.

More details on the signalling between Node B and UE needed to introduce L1 retransmission schemes can be found in [TR25896].

4.2.1.3 L1 Retransmission Schemes and SHO

L1 retransmission schemes also present some drawback when the UE is in SHO operation. The major problem is related to the reliability of NACK/ACK messages received from the different Node Bs in the active set. Since NACK/ACK messages are independent from Node B to Node B, they cannot be combined in the UE receiver. Moreover, the UE does not necessarily allocate rake fingers to all Node Bs in the active set if some of the Node B signals are not strong enough. This implies that, at least instantaneously, some of the ACK/NACK messages are unreliable or even cannot be received by the UE.

4.2.1.4 Buffering Requirements

At last, the implementation of L1 retransmission schemes require increased buffering requirements especially at the Node B. The idea behind HARQ combining techniques is to buffer TTIs that were not received correctly, and then combine the buffered data with retransmissions. The soft buffer dimensioning at the Node B depends on:

- The type of combining technique adopted (CC or IR),
- the number of channels of the SAW scheme, and
- the number of UEs that can be simultaneously served by one Node B.

Additional buffering at the Node B is required because of the reordering of data frames that might be received in wrong order [TR25896].

4.2.2 Fast Node B Packet Scheduling

As previously discussed, the long scheduling delays associated with the transmission of capacity requests from the UE to the RNC and the transmission of capacity grants from the RNC to the UE represent the main disadvantage of an RNC PS implementation. To reduce such delays, Node B scheduling is needed, thus providing the system with two main advantages:

- With fast Node B PS operation, which allows faster adaptation to interference variations, tighter control of the total received uplink power is possible. The required power headroom to meet the specified NR outage criteria can consequently be reduced, thus leading to increased cell throughput performance.
- With Node B packet scheduling, the radio resources can be reallocated to NRT users more frequently. Fast reallocation of the radio resources has the potential for adapting to the traffic variations based on the instantaneous requirements of the users, thus improving the experienced user performance.

Therefore, fast Node B PS operation has the potential for enhancing both cell throughput and user performance.

A schematic draw of the Node B PS concept is illustrated in Figure 4.5, also showing a comparison with a basic RNC PS implementation. The reduced allocation delays due to the PS functionality being moved from the RNC to the Node B allow performing more dynamic radio resource allocation so to rapidly adapt to both traffic and interference variations. In

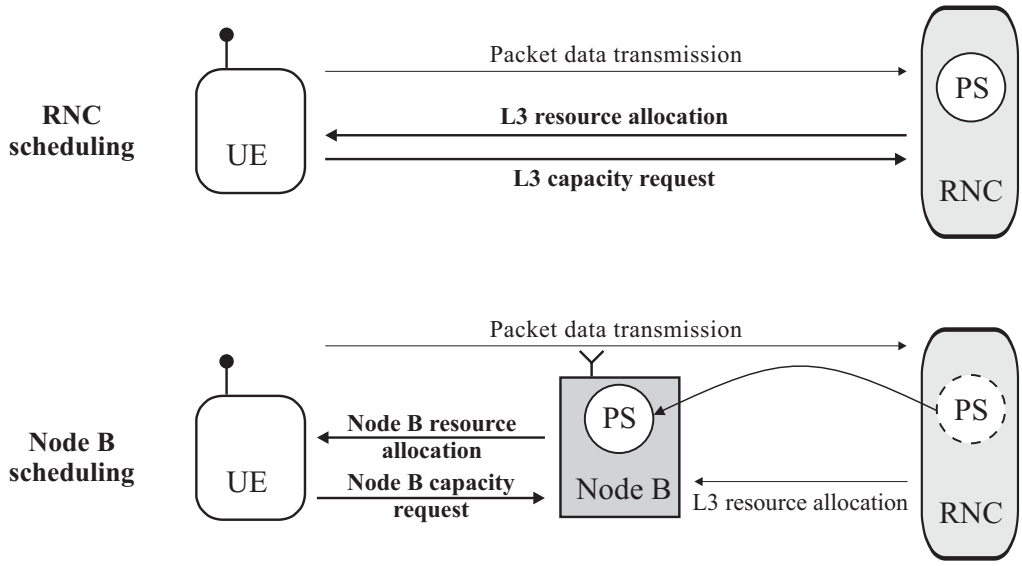

Figure 4.5: PS functional split between RNC and Node B with fast Node B packet scheduling.

reality, the Node B PS is supposed to coexist and cooperate with the RNC PS functionality. Similarly to a basic RNC PS implementation, the Transport Format Combination Set (TFCS) is signalled between RNC and the UE via the Node B. In addition to the TFCS, a new TFC subset named 'Node B controlled TFC subset' is introduced and signalled from the Node B to the UE using appositely defined Node B allocation messages. Any TFC in the 'Node B controlled TFC subset' can be selected by the UE, provided there is sufficient data available and the TFC is not in blocked state [TS25321]. The 'Node B controlled TFC subset' relates to the Transport Format Combination Set (TFCS) and minimum set defined in [TS25331] so that:

$$\text{“Minimum Set”} \subseteq \text{“Node B controlled TFC subset”} \subseteq \text{TFCS} \tag{4.2}$$

In Figure 4.6, the different subsets and their relation are illustrated. The data rate corresponding to the maximum TFC in the minimum set is equivalent to the minimum allowed data rate introduced in Section 3.3.1.2.

4.2.2.1 Additional Complexity with Node B PS

From the assumption that only rate scheduling is considered, the additional complexity by introducing fast Node B PS operation is mainly related to two issues:

1. The first is the interaction between RNC TFC control and Node B TFC control. As previously discussed, the new Node B and the earlier RNC scheduling concepts must cooperate in order to require minimum changes in the current specifications, as well as guarantee backward compatibility.
2. The second issue concerns the definition of the proper uplink and downlink L1 signalling required for supporting Node B TFC control. Downlink signalling is necessary to command the UE to update the Node B controlled TFC subset, whereas uplink signalling is typically required to indicate to the Node B that the UE has data to transmit. Additional information may be provided by the UE: The amount of data in its transmission buffer, an indication of the UE power margin, or other data utilised for scheduling.

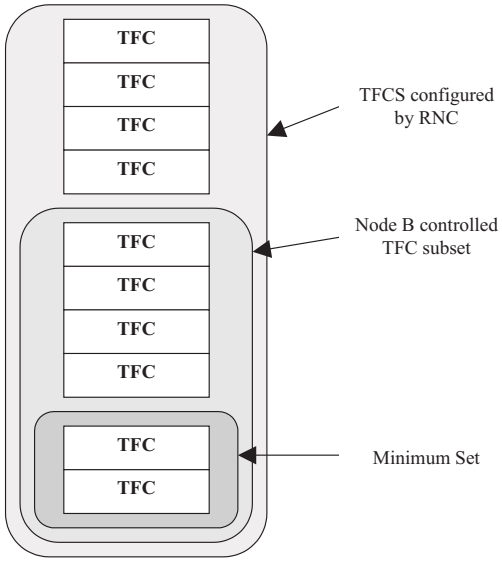

Figure 4.6: Illustration of different sets of TFCs with Node B scheduling operation [TR25896].

4.2.2.2 Node B Scheduling of Users in SHO

As for L1 retransmission schemes, SHO operation also presents some potential drawbacks in the case of Node B PS operation, where each Node B included in the active set for one UE independently performs resource allocation. Two main solutions are discussed in [TR25896]:

1. In the first case the Node B controlling either the best downlink or the best uplink cell is identified as the only scheduling entity. Although this solution is easy to implement, it presents the disadvantage that scheduling a user in SHO only taking into account one cell can lead to unexpected variations of the total received uplink power at other cells in the active set.
2. In the second case all Node Bs in the UE active set are identified as valid scheduling entities. Since UEs in SHO receive TFC control messages from all Node Bs in the active set, the system has better control on the interference level received at all cells in the active set. This solution also has one main drawback: As for the detection of ACK/NACK messages for L1 HARQ schemes, since TFC control messages are received independently from Node B to Node B they cannot be combined in the UE receiver. Therefore, from time to time Node B TFC control messages might be unreliable.

4.3 L1 Retransmission Schemes

4.3.1 Theoretical Analysis

In this section, an analytical approach is presented that estimates the cell throughput improvement provided by L1 retransmission protocols and consider the impact that such retransmission schemes have on the delay performance. With respect to the used retransmission scheme, three different scenarios are considered all along this section:

L2 ARQ – The first scenario corresponds to the Release 99 DCH implementation. The system relies on the RLC retransmission protocol located in the RNC and does not utilise any kind of combining technique.

L1 HARQ type-I – This second scenario corresponds to the case in which an additional entity handling the ARQ process is located in the Node B. A maximum number of L1 retransmissions is defined. If this number is reached and the transmitted data frame is still not

correctly decoded, the physical layer retransmission procedure is terminated. The correct delivery of the data is then assured by the L2 retransmission mechanism. Also in this second scenario no combining technique is deployed.

L1 HARQ type-II – The third scenario is the same as the previous one, but in this case combining techniques are introduced along with fast Node B L1 retransmission protocols. Since for low values of the effective code rate CC and IR performs similarly [Fred02], no differentiation is made between the two combining techniques. Notice that with L1 HARQ type-II we also refer to type III strategies.

4.3.1.1 Considerations on Cell Throughput

For the cell throughput analysis, two propagation environments have been selected, namely ITU Vehicular A channel profile at 3 and 50 km/h [TR25896]. For the two propagation scenarios, the block error probability is plotted in Figure 4.7 as a function of the per TTI average received E_b/N_0. The results have been obtained using the Actual Value Interface (AVI) method described in [Hämä97] for packet data services at 64 kbps with 10 ms TTI, and include the effect of fast closed loop power control. AVI tables constructed from extensive link level simulations are used to map a value of the per TTI average received E_b/N_0 to the corresponding block error probability (see Appendix C).

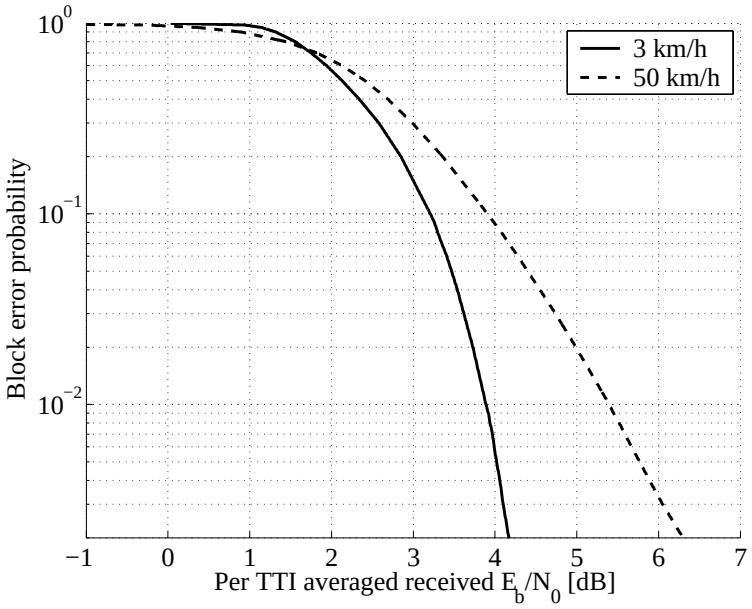

Figure 4.7: Block error probability as a function of the average E_b/N_0 for Vehicular A channel profile at 3 and 50 km/h, packet data services at 64 kbps, 10 ms TTI.

Following, three definitions are introduced that are used in the presented analysis.

1. The target block error rate ($BLER_{target}$) corresponds to the value used in the outer loop power control algorithm [Samp97]. The required E_b/N_0 ρ to meet a specific BLER target can be straightforwardly derived from AVI tables as:

$$\rho(BLER_{target}) = \text{AVI}^{-1}(BLER_{target}) \tag{4.3}$$

2. Similarly, the block error probability (*BLEP*) given a specific per TTI average received E_b/N_0 ρ is derived from AVI tables as:

$$BLEP(\rho) = \mathrm{AVI}(\rho) \tag{4.4}$$

3. Finally, the block error rate (*BLER*) is defined as the ratio of the erroneously received data frames to the total number of transmitted frames over an arbitrarily long time period.

Let us assume perfect power control (the per TTI average received E_b/N_0 is always equal to the required E_b/N_0 to meet the specified BLER target), and neglect combining techniques. In this case the block error probability at each transmission equals the BLER target, and so does the block error rate. The situation is different with CC and IR techniques, where due to soft combining of information received at different transmission instants the block error probability after combining decreases with the number of transmissions although the per TTI average received E_b/N_0 remains constant. In this case the derivation of the block error rate is not straightforward.

Based on the analysis presented in Section 3.2.1, and by simplifying (3.1) under the assumption that $W/R_j\rho_j >> 1$, the received E_b/N_0 for user j given a specific BLER target can be written as:

$$\rho_j(BLER_{target}) = \frac{W}{R_j} \cdot \frac{P_j}{P_{total}} \tag{4.5}$$

In (4.5), W is the chip rate, P_j is the received signal power from user j, R_j is the bitrate of user j, and P_{total} is the total received wideband power including thermal noise power at the base station. Following the same procedure as in Section 3.2.1 the uplink cell throughput T in (3.7) can be rewritten as:

$$T = \eta_{UL} \cdot \frac{W}{1+i} \cdot \frac{1 - BLER(BLER_{target})}{\rho(BLER_{target})} \tag{4.6}$$

In (4.6), η_{UL} is the uplink fractional load, i is other-to-own cell interference ratio, and $BLER(BLER_{target})$ is the block error rate in correspondence of a specific BLER target. We now reintroduce the effective E_b/N_0 to meet a specific BLER target defined in (4.1) as:

$$\rho_{eff}(BLER_{target}) = \frac{\rho(BLER_{target})}{1 - BLER(BLER_{target})} \tag{4.7}$$

From (4.7) and (4.6), it can be seen how the effective E_b/N_0 can be used as a measure to estimate the difference in achievable cell throughput when operating the channel at different error probabilities, or alternatively when applying different HARQ strategies.

HARQ type-I – In (4.7), the E_b/N_0 in correspondence of a specific BLER target can be derived from AVI tables as in (4.3). As previously discussed, for type-I HARQ schemes, the block error rate in correspondence of a specific BLER target corresponds to the BLER target itself.

$$BLER(BLER_{target})^{type-I} = BLER_{target} \tag{4.8}$$

HARQ type-II – The situation is different in the case of type-II HARQ schemes, where the block error probability is equal to the BLER target only at the first transmission. The soft

combining is modelled by summing the received E_b/N_0 at different transmission instants. A combining loss L_{comb} is also considered every time the E_b/N_0 is added to the accumulated E_b/N_0 from the previous n transmissions ($\rho_{acc,n}$). In (4.9), M is the maximum number of L1 transmissions for which soft information can be accumulated at the receiving entity, and it depends on the buffering capability at the Node B.

$$\rho_{acc,n}(BLER_{target}) = \begin{cases} \rho(BLER_{target}) & n = 1 \\ \dfrac{\rho_{acc,n-1}(BLER_{target}) + \rho(BLER_{target})}{L_{comb}} & 1 < n \le M \end{cases} \tag{4.9}$$

The combining loss typically depends on whether CC or IR is employed, as well as on the effective code rate used in the encoding process [Fred02]. For the sake of simplicity, the value of L_{comb} is kept constant and equal to 1.05 (approximately 0.2 dB) [Fred02]. Besides this loss, combining techniques in uplink also suffer from the effect of the physical control channel overhead. This additional loss, which depends on the DPDCH/DPCCH power ratio, is neglected in the presented analysis. This issue is discussed in more detail in Appendix C, Section C.4.

With type-II HARQ schemes, the block error probability at the n^{th} transmission ($BLEP_n$) can be calculated by mapping the value of $\rho_{acc,n}$ using AVI tables.

$$BLEP_n(BLER_{target}) = \mathrm{AVI}(\rho_{acc,n}(BLER_{target})) \tag{4.10}$$

Under these assumptions, the block error rate in correspondence of a specific BLER target to be used in (4.7) in the case of type-II HARQ schemes can be derived as:

$$BLER(BLER_{target})^{type-II} = \frac{\sum_{i=1}^{M}\prod_{j=1}^{i} BLEP_j(BLER_{target})}{1 + \sum_{i=1}^{M-1}\prod_{j=1}^{i} BLEP_j(BLER_{target})} \tag{4.11}$$

Finally, Figure 4.8 plots the effective E_b/N_0 as a function of the BLER target in the case of type-I and type-II HARQ schemes, for Vehicular A channel profile at both 3 km/h and 50 km/h, and for a maximum number of L1 transmissions M equal to 5. The spectral efficiency gain from operating the physical channel at an error probability of 10% instead of 1% is in the order of 0.25 dB (≅6% cell throughput increase) for 3 km/h, and it is approximately 1 dB (≅25% cell throughput increase) for 50 km/h. Due to the deficiency of fast closed loop power control with high user mobility, at 50 km/h it is quite spectral inefficient to keep the block error rate at first transmission at a value as low as 1%. For this reason, the gain from operating the physical channel at 10% error probability is more significant for a higher mobile speed.

For both propagation scenarios, type-II HARQ schemes provide a significant gain over type-I strategies only for values of the BLER target at first transmission above 20-30%. However, with type-II HARQ schemes the gain compared to the maximum achievable cell throughput (corresponding to the lowest effective E_b/N_0) using type-I schemes is not very significant. As a consequence, type-II HARQ schemes are not expected to provide the same cell throughput increase in the uplink of WCDMA systems as in HSDPA [Malk01]. As anticipated in Section 4.1.1, the reason is that in WCDMA uplink HARQ schemes operate together with fast closed

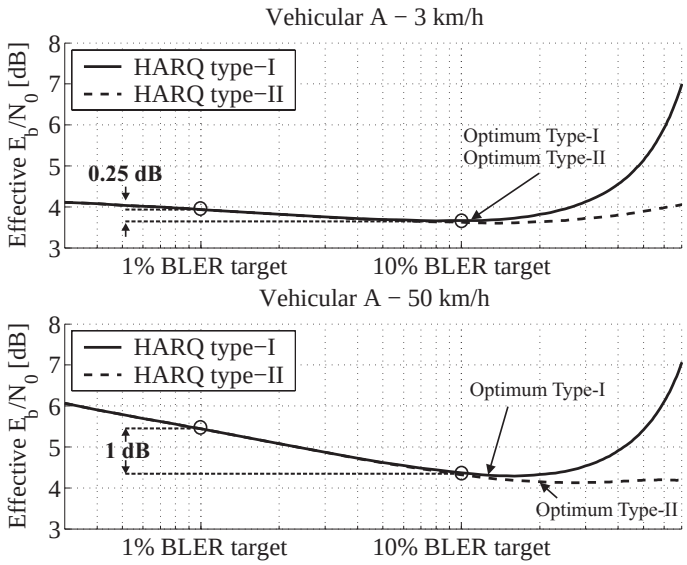

Figure 4.8: Effective E_b/N_0 as function of the BLER target with type-I and type-II HARQ schemes, both for 3 km/h and 50 km/h.

loop power control; since both HARQ and power control are link adaptation mechanisms, the gains they provide cannot be added to each other when both techniques are applied.

4.3.1.2 Delay Analysis

Following, a simple analysis is presented to estimate the average time needed to correctly transmit a data frame in the uplink of a WCDMA system. The three scenarios introduced at the beginning of Section 4.3.1 are considered.

L2 ARQ – In this case the system relies on a L2 retransmission mechanism located in the RNC. Assuming perfect PC, the block error probability at each transmission is equal to the target block error rate. The data frame transmission delays are reported in Table 4.1, together with the transmission number at which the data frame is correctly received and the corresponding probability.

Transmission number	Delay	Probability
1^{st}	$K + TTI$	$(1 - BLEP)$
2^{nd}	$K + DE + 2 \cdot TTI$	$BLEP \cdot (1 - BLEP)$
…	…	…
n^{th}	$K + n \cdot DE + (n+1) \cdot TTI$	$BLEP^{\,n} \cdot (1 - BLEP)$

Table 4.1: Data frame transmission delays for different values of the required number of transmissions and corresponding probabilities.

In Table 4.1, *TTI* is the radio frame length, *BLEP* is the block error probability at every transmission instant and equals the BLER target, and *DE* is the retransmission delay associated with the transmission of a L2 NACK message from the RNC to the UE. Furthermore, *K* is a constant that includes the aggregate processing delays at the UE, at the Node B and at the RNC, plus the delay due to transmission over the Iub interface (see Table 4.2). The average transmission delay of a data frame can be derived summing the elements in the second column of Table 4.1, each one weighted with its corresponding probability.

$$D_{L2\,ARQ} = K + (1 - BLEP)\sum_{n=0}^{\infty} BLEP^n \cdot [(n+1)\cdot TTI + n\cdot DE] \tag{4.12}$$

Keeping in mind that in this case $BLEP = BLER_{target}$, (4.12) can be simplified as:

$$D_{L2\,ARQ} = K + \frac{TTI + BLER_{target}\cdot DE}{1 - BLER_{target}} \tag{4.13}$$

L1 HARQ type-I – In this case *dE* is also introduced as the delay associated with the L1 retransmission protocol located in the Node B. Since no combining techniques are deployed, also in this scenario the block error probability at each transmission instant is equal to the target block error rate. Following the same procedure as before, the average uplink transmission delay with L1 HARQ type-I schemes can be expressed as:

$$D_{type\text{-}I} = K + (1 - BLEP)\sum_{n=0}^{\infty} BLEP^{nM}\left\{\sum_{i=0}^{M-1}[(nM + i + 1)\cdot TTI + (nM - n + i)\cdot dE + n\cdot DE]\cdot BLEP^i\right\} \tag{4.14}$$

In (4.14), *M* is the maximum number of L1 transmissions. Let us also define:

$$F2 = BLEP^M \tag{4.15}$$

$$d2 = (1 - BLEP)\sum_{i=0}^{M-1}[(i+1)\cdot TTI + i\cdot dE]\cdot BLEP^i \tag{4.16}$$

Then, the average transmission delay in (4.14) can be written in a more compact form.

$$D_{type\text{-}I} = K + \frac{F2\cdot[M\cdot TTI + (M-1)\cdot dE + DE] + d2}{(1 - F2)} \tag{4.17}$$

In (4.15) and (4.16), $BLEP = BLER_{target}$.

L1 HARQ type-II – Soft combining is introduced along with L1 retransmission protocols. As already mentioned in Section 4.3.1.1, in this case the block error probability *BLEP* is different at different transmission instants, and equals the target block error rate $BLER_{target}$ only at the first transmission. The following definitions are introduced:

$$a_n = \begin{cases} 1 - BLEP_1 = 1 - BLER_{target} & n = 0 \\ \left(\prod_{i=1}^{n} BLEP_i\right)\cdot(1 - BLEP_{n+1}) & 1 \le n \le M-1 \end{cases} \tag{4.18}$$

$$F3 = \prod_{i=1}^{M} BLEP_i \tag{4.19}$$

Then, the average delay for the transmission of one data frame in the case of L1 HARQ type-II schemes can be expressed as:

$$D_{type\text{-}II} = K + \sum_{n=0}^{\infty} F3^n \sum_{i=0}^{M-1} a_i \cdot [(nM + i + 1) \cdot TTI + (nM - n + i) \cdot dE + n \cdot DE] \quad (4.20)$$

Equation (4.20) can be simplified to the following form:

$$D_{type\text{-}II} = K + \frac{\left(\sum_{i=0}^{M-1} a_i\right) \cdot F3 \cdot [M \cdot TTI + (M - 1) \cdot dE + DE] + d3 \cdot (1 - F3)}{(1 - F3)^2} \quad (4.21)$$

In (4.21), *d3* is defined as:

$$d3 = \sum_{i=0}^{M-1} a_i \cdot [(i + 1) \cdot TTI + i \cdot dE] \quad (4.22)$$

The values of the block error probability at different transmission time instants to be substituted in (4.18) and (4.19) are obtained from AVI tables as described in Section 4.3.1.1.

The values of the parameters used in the delay analysis are stated in Table 4.2, while Table 4.3 reports the average uplink transmission delay of one data frame for the three different scenarios, and for a BLER target at first transmission of 1%, 10% and 20%.

TTI	10 ms
DE **(L2 retransmission delay)**	120 ms
dE **(L1 retransmission delay)**	40 ms
K **(UE delay + Node B delay + Iub delay + RNC delay)**	60 ms
M **(Maximum number of L1 transmissions)**	5

Table 4.2: Parameter setup for the delay analysis.

	BLER target		
	1%	**10%**	**20%**
L2 ARQ	72 ms	88 ms	110 ms
L1 HARQ type-I	71 ms	76 ms	83 ms
L1 HARQ type-II	71 ms	75 ms	80 ms

Table 4.3: Average transmission delay of one data frame.

The theoretical results show that with L1 Node B-controlled retransmission protocols the BLER target can be increased from 1% to approximately 10%-20%, without any significant degradation in the average delay performance compared to an L2-controlled retransmission mechanism. We should emphasise, however, that the average delay for the transmission of one data frame is not sufficient to entirely characterise the user delay performance.

To overcome this limitation, an investigation is presented that more comprehensively evaluates the user delay performance in the uplink of a WCDMA system. The analysis considers the time needed to successfully upload a fixed-size file given a specific allocated data rate on the DPDCH, and for different retransmission strategies and values of the BLER at first transmission. The presented investigation includes the effect of TCP slow start, which is illustrated in Figure 4.9. The UE first transmits a number of packets depending on the initial size of the congestion window. For each TCP acknowledgement message received from the network side the user sends two additional packets, which determines the congestion window

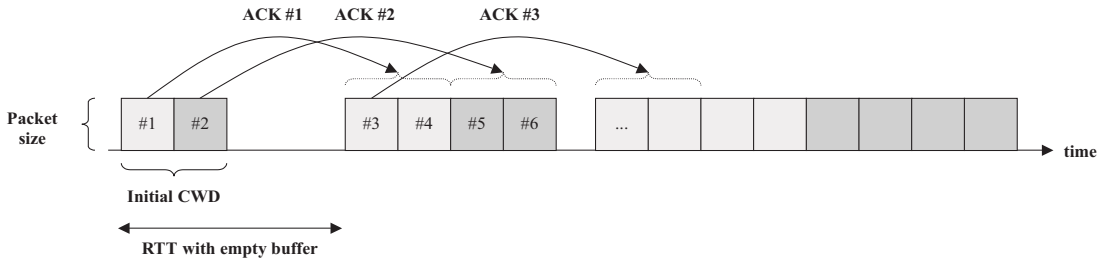

Figure 4.9: Basic functioning of the TCP slow start.

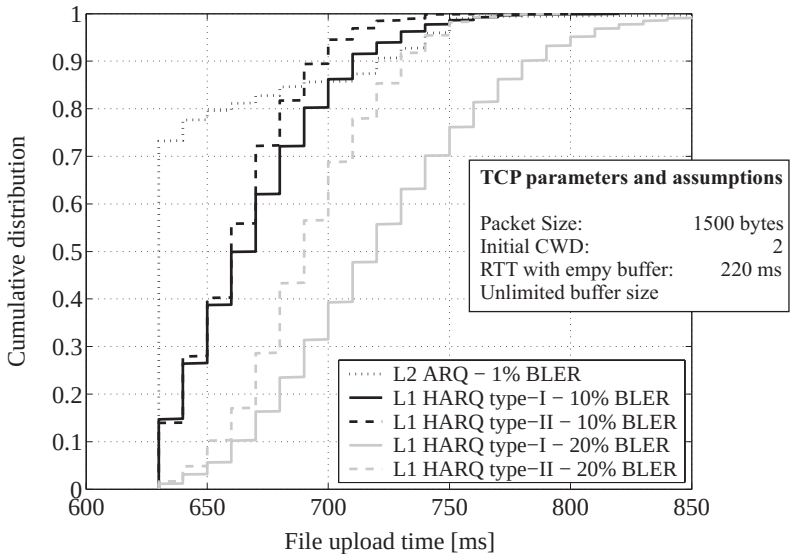

Figure 4.10: CDFs of the upload time of a 10 kBytes file with constant bit rate allocation of 256 kbps, for different HARQ schemes and for different values of the BLER target at first transmission.

to exponentially grow. The value of the round trip time with empty buffer depends on the packet size, on the allocated data rate in uplink, on the delay introduced by the core network, as well as on the transmission delay of a 40 bytes TCP acknowledgement in downlink direction. The considered TCP model does not include the effect of TCP timeout and congestion control.

When evaluating the delay performance with type-II HARQ schemes, the block error probability at the second transmission is assumed equal to zero; i.e., a maximum of two transmissions is needed to correctly receive each data frame. Figure 4.10 reports the cumulative distribution functions of the upload time of a 10 kBytes file assuming a constant bitrate allocation of 256 kbps. The most relevant TCP parameters and assumptions are also reported in Figure 4.10.[3]

L1 HARQ schemes contribute to cut off the tail of the upload time distribution even when the BLER target is increased above 1%. Especially for 20% BLER target, type-II HARQ schemes provide a relevant gain over type-I strategies. Notice that the file upload time is always higher than 630 ms, which corresponds to the case where no retransmissions occur. The value of the minimum upload time depends on the particular TCP settings, on the file size, and on the allocated data rate, but is independent of the target block error rate and HARQ scheme.

In conclusion, using a fairly simple approach the presented analysis has verified that with fast L1 retransmission protocols the BLER target can be increased from 1% to approximately 10%

[3] Jeroen Wigard has provided great part of the code used for the generation of these results.

without degrading the user delay performance. In this case the cell throughput gain due to the improved spectral efficiency is expected to be between 6% and 25%, depending on the mobility scenario. If type-II HARQ schemes are introduced, the BLER target could be further increased to around 20%. However, results in Section 4.3.1.1 have shown that increasing the BLER target from 10% to 20% gives a marginal spectral efficiency gain, and only in the case of high user mobility (50 km/h).

4.4 Fast Node B Packet Scheduling

In this section a radio resource allocation algorithm for NRT bearers is proposed, which is then deployed in the context of fast Node B packet scheduling operation. The main idea behind fast Node B scheduling is to allow the system to be more in control of the total received uplink power. This is achieved by faster and more dynamic reallocation of the radio resources, which are performed by also taking into consideration the actual needs of each mobile user. Hence, we assume a traffic model to include the effect of time-variable users' requirements (see Appendix D).

One of the problems with RNC packet scheduling is the high variability in the air interface load from allocating high data rates. The characteristic discontinuity of NRT traffic must be handled by setting aside a margin in the scheduling power budget. This margin is used to allow for those packet data users who are connected, but inactive and therefore cannot be included in the measurements of uplink load. The dimensioning of this margin somehow relies on the stabilisation of received power as a result of the randomness in packet data traffic, and with very conservative settings for low duty cycle traffic it will create high variability in uplink noise rise and reserve a disproportionate amount of uplink resources, thus limiting the achievable cell throughput.

Although there are some possibilities for improved packet scheduling within the RNC, to get more control over the uplink packet access, a new approach with faster and more accurate scheduling must be considered. Specifically, there is the need to introduce a concept where part of the scheduling is done at the Node B (to make it faster), and with algorithms which track the utilisation of allocated data rates (to make it more accurate).

4.4.1 Node B Packet Scheduling Algorithm

The proposed Node B scheduling algorithm is based on a method that avoids explicit signalling of rate requests from the UE to the Node B. In this way not only the signalling overhead is reduced, but also the delay associated with the allocation of new resources is somewhat decreased. In practice, the Node B scheduling algorithm is defined based on an observation derived at the Node B and updated for every connected UE on a TTI basis. This observation is named Resource Utilisation Factor (RUF). It is a counter bringing information on the number of last consecutive transmissions (data frames) with either selected data rate equal to zero (negative value) or selected data rate corresponding to the maximum allocated TFC at the Node B (positive value). If the selected data rate is both different from zero and from the maximum allocated data rate at the Node B, the RUF counter is reset to zero. Information on the selected data rate is assumed to be available from the uplink TFCI field, transmitted every TTI on the DPCCH [Holma04].

Figure 4.11 reports an example of RUF calculation assuming a maximum allocated data rate of 128 kbps (TFC_{MAX}). The RUF is initially assumed equal to 2. At time instant *n* the UE transmits with 128 kbps and the RUF counter is therefore increased. Next, the UE transmit with 64 kbps and the RUF is reset to zero. In the next two transmissions the UE does not transmit any data and the RUF counter is progressively decreased. When the users start

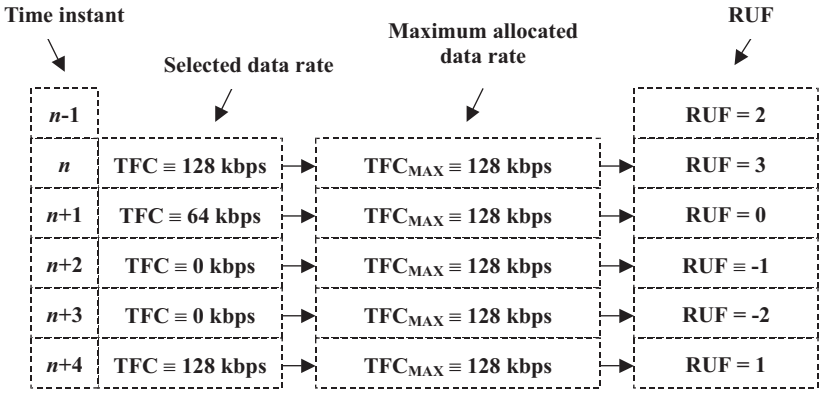

Figure 4.11: Example of RUF calculation with maximum allocated data rate of 128 kbps and RUF initially equal to 2.

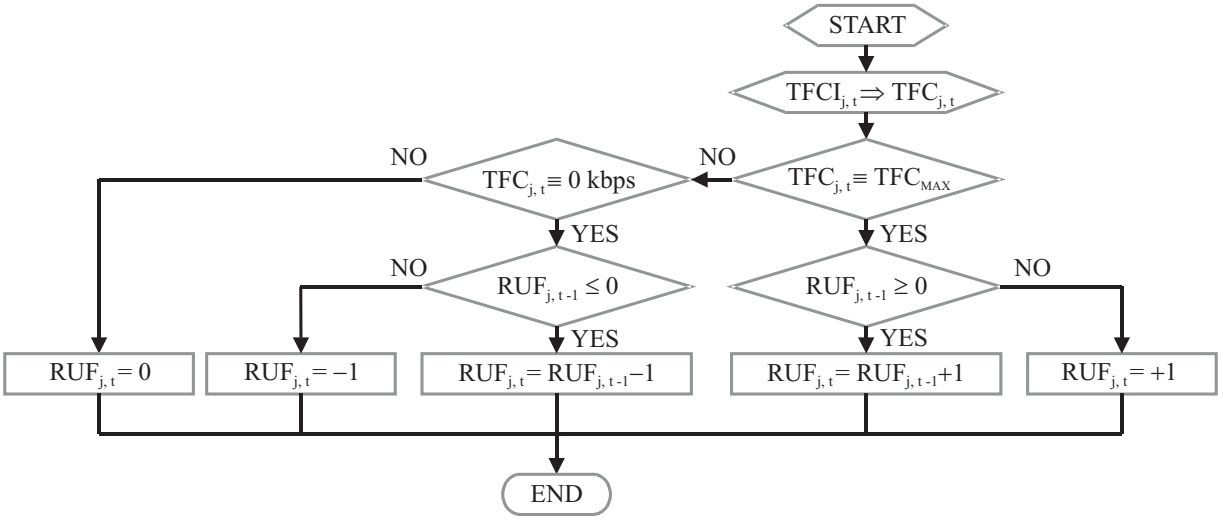

Figure 4.12: Calculation of RUF at the Node B based on TFCI and maximum scheduled TFC (TFC_{MAX}).

transmitting with data rate equal to the maximum allocated, the RUF is set to 1. The flow chart in Figure 4.12 more generally illustrates how the Node B updates the RUF counter for user *j* at each time interval *t* ($RUF_{t,j}$).

The idea behind the proposed algorithm is to keep track of the utilisation of the allocated data rates for each connected UE, and then to relocate the radio resources from users with low utilisation to users with high utilisation.

Hence, during the scheduling procedure the PS first divides the UEs connected to the corresponding Node B into four groups: $DOWN_{MIN}$, $DOWN_{ONE}$, *UP* and *KEEP*. The decision rules for the considered Node B scheduling algorithm are illustrated Figure 4.13:

$DOWN_{MIN}$ – In order to reduce the data rate allocated to inactive users, thus improving utilisation of the allocated radio resources, users are downgraded to the minimum allowed data rate when $RUF \leq -T_{DOWN}$.

$DOWN_{ONE}$ – In order not to allocate data rates higher than the one the UE can support, UEs with $-T_{DOWN} < RUF \leq 0$ are also downgraded but using a downgrading step of one (e.g., from 256 kbps to 128 kbps). For users in SHO, this downgrading criterion also guarantee that the allocated data rates from different Node Bs in the active set will eventually converge to the same value (see Section 4.5.2).

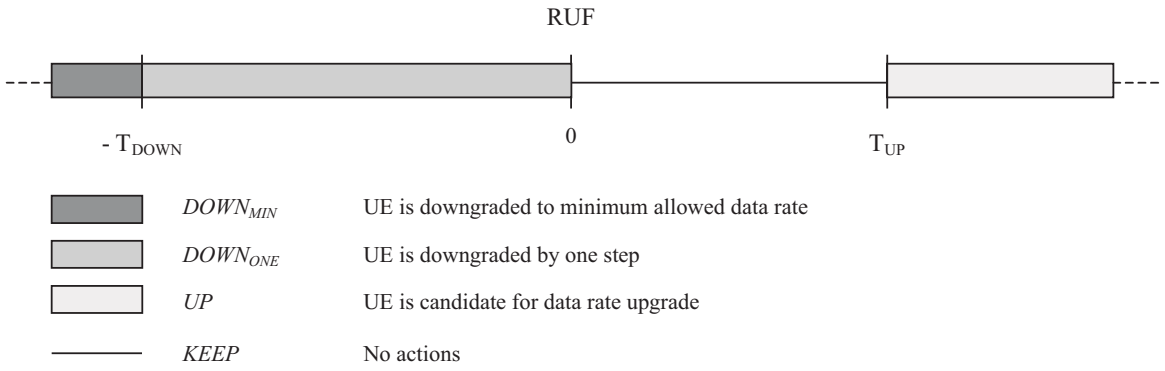

Figure 4.13: Decision rules for UEs partitioning at the Node B PS.

UP – Since users with high utilisation of the allocated resources are likely to need additional capacity, a UE is selected as a candidate for data rate upgrade if RUF ≥ T_{UP}. During the upgrading procedure, UEs are progressively upgraded up to the maximum possible data rate, subject to the constraint of available power and fairness among users. As for the RNC PS, higher priority is given to users that are temporarily allocated lower data rates.

KEEP — No actions are taken for this class of UEs (except in overload conditions).

The task sequence performed by the Node B PS is similar as for the RNC PS (see Section 3.3.1). First the downgrade actions are carried out. Then the candidates for data rate increase are upgraded. In the upgrading procedure, a PIE (see Appendix B) is used to estimate the noise rise after each data rate allocation. If the estimated noise rise exceeds the planned target, the data rate upgrade is not allowed. The load control algorithm is performed exactly as for the RNC PS (see Section 3.3.1.3).

4.5 Assumptions and Implementation in System Level Simulator

In this section the main assumptions for the implementation in the system level simulator of both L1 retransmission schemes and fast Node B packet scheduling are discussed.

4.5.1 L1 Retransmission Schemes

With respect to some of the complexity issues introduced in Section 4.2.1, the modelling of L1 HARQ schemes is based on the following simplifications/assumptions:

1. Signalling is not simulated, and consequently signalling overhead is not included.
2. No signalling errors of L1 ACK/NACK messages are considered, i.e. UEs always correctly receive L1 ACK/NACK messages from all Node Bs in the active set
3. For what concerns transmission of transport blocks on the physical channel:
   - Multiplexing of more transport channels on the same physical channel is not considered. Every simulated UE is only carrying one NRT RB over a dedicated logical channel, which is consequently mapped to one and only one transport channel.
   - All the MAC PDUs delivered from MAC to PHY during a TTI [TS25321] are mapped into a single transport block, which is assumed to be attached the CRC and passed through L1 processing. Only one TB per TTI is sent, and therefore the retransmission protocol controlled by the Node B is assumed to operate on a TTI basis. A maximum number of L1 retransmissions is defined. If after this number of retransmissions the

data frame is still not correctly decoded, the system relies on the RLC retransmission protocol.

4. Regarding the implementation of type II HARQ schemes, the available resources for uplink transmission might change between first and successive transmissions due to resource reallocation, or to TFC elimination [TS25321]. We assume that soft combining is always possible even when the available resources have changed.

   - In the case of CC, where a one to one correspondence between data bits and channel bits is required for different transmissions of the same data frame, we assume the transmitter will adjust the output power depending on the available radio resources to keep the same frame format.
   - If IR is used, we assume that the transmitter will select different IR versions depending on the available radio resources.

   In any case a single model is used for the implementation of combining techniques. The model used is rather simple: Soft combining is implemented by recursively summing the average received E_b/N_0 at different transmission instants, allowing for a fixed combination loss L_{comb} (see Section 4.3.1). The E_b/N_0 for each transmission is calculated assuming a processing gain corresponding to the data rate used at first transmission, and a transmission power depending on the temporarily available radio resources. In this way, if the available resources change between a first transmission and a retransmission, the received E_b/N_0 is scaled correspondingly. Hence, defining ρ_n as the received E_b/N_0 at time instant n, the cumulative E_b/N_0 after n transmissions $\rho_{cum,\,n}$ is calculated as:

$$\rho_{cum,n} = \begin{cases} \rho_n & n = 1 \\ \dfrac{\rho_{cum,n-1} + \rho_n}{L_{comb}} & 1 < n \le M \end{cases} \tag{4.23}$$

5. For users in SHO operation, it might happen that during the L1 retransmission procedure the active set for a particular user changes. In this situation, we assume that the accumulated soft information during previous transmissions is not available at the new Node B in the active set. The newly added Node B is assumed to operate as in the case of a first transmission. If IR is deployed, the assumption made is that each redundancy version is self-decodable.
6. Finally, with combining techniques the function of the outer loop power control (OLPC) is to keep the block error rate at the first transmission as close as possible to the BLER target. Therefore, OLPC is performed only when a first transmission occurs.

4.5.2 Node B Packet Scheduling

For what concerns the implementation of the fast Node B PS functionality in the system level simulator, the following assumptions are made:

1. The Node B is assumed to be in control of the total received uplink power, i.e. all the uplink resources are given to the Node B PS. With reference to Figure 4.6, this corresponds to the assumption that the TFCS allocated by the RNC PS always equals the set of all supportable data rates at the UE. An example is given in Figure 4.14; the 'Node B controlled TFC subset' is lower bounded by the minimum set (i.e. the minimum allowed data rate) and upper bounded by the maximum possible data rate.

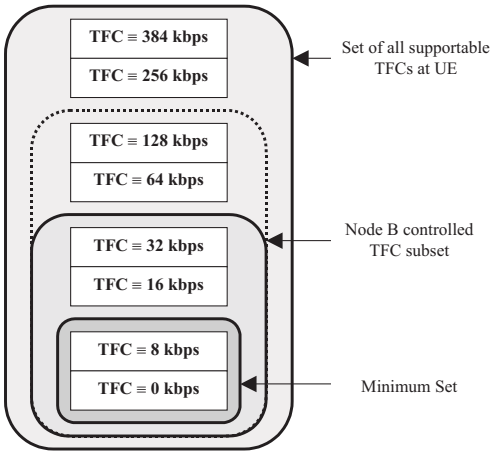

Figure 4.14: Example of Node B PS functioning in the system level simulator.

2. Regarding signalling issues:
   - The proposed algorithm avoids explicit signalling of CRs in uplink direction.
   - Downlink signalling is not modelled, and signalling overhead is consequently not taken into account.
3. For what concerns scheduling users in SHO, the solution implemented in the system level simulator correspond to solution 2 in Section 4.2.2.2:
   - A user in SHO receive TFC control messages from all Node Bs in the active set and computes the maximum allocated data rate as the minimum between those allocated by all the Node Bs in the active set. This is done in order to respect the constraint on the total received uplink power at all the Node Bs in the active set.
   - No signalling errors are simulated, i.e. a UE always correctly receives TFC control messages from all the Node Bs in the active set.

   With these assumptions, when in SHO operation it can happen that the data rate allocated by one of the Node Bs in the active set is not utilised by the user because other Node Bs have not granted the same resources. This might cause some kind of inefficiency in the allocation strategy. It is also to avoid this waste of resources that the proposed algorithm performs data rate downgrade with one step for those UEs that are not fully utilising the allocated radio resources (see Section 4.4.1). This guarantees that the allocated data rates by all the Node Bs in the active set will eventually converge to the same value, which is determined by the most restrictive radio resource allocation. Figure 4.15 illustrates an example of the functioning of the proposed scheduling algorithm during SHO operation. A user in SHO operation is initially allocated 128 kbps at both Node Bs in the active set. At a certain scheduling instant, *Node* B_2 can allocate 384 kbps, while *Node* B_1 cannot. The user therefore continues transmission at 128 kbps. In the following scheduling periods *Node* B_2 detects that the user in not fully utilising the allocated resources and perform data rate downgrading. Eventually, the data rate allocated by both Node Bs in the active set is equal to 128 kbps, thus avoiding potential waste of radio resources at *Node* B_2.

   To conclude, under the considered assumptions only three reasons can cause the UE to select a data rate lower than the maximum allocated by the Node B PS:

   - The UE has not enough data in its buffer,
   - the UE cannot support the allocated data rate due to transmit power limitations, or

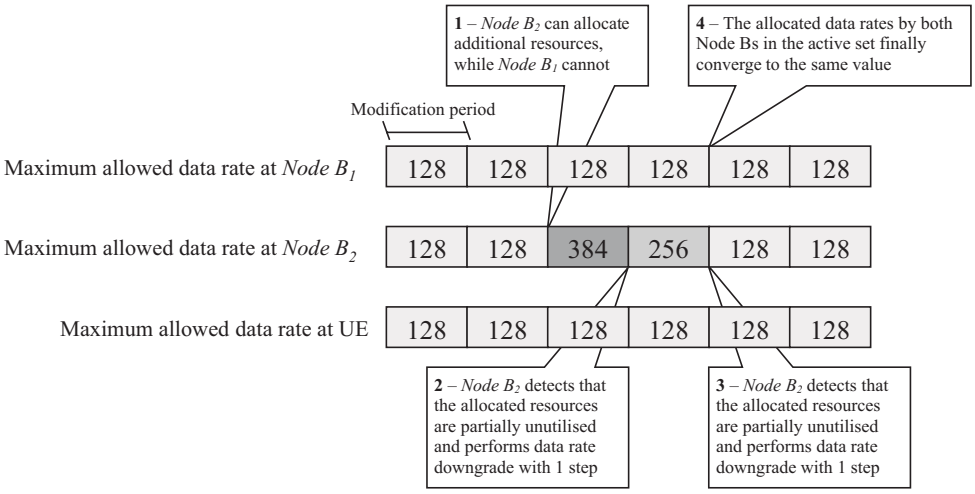

Figure 4.15: Example of Node B PS functioning in SHO.

- the UE is in SHO and other Node Bs in the active set have not granted the same radio resources.

In any of these cases, the proposed scheduling algorithm is designed in order to rapidly respond by opportunely reallocating the available radio resources.

4.6 Performance Assessment

In this section system level simulation results are presented and commented. The main objective is to assess the cell throughput performance enhancement that fast Node B packet scheduling and L1 retransmission schemes can provide in the uplink of WCDMA systems. The section is divided into two main subsections: First in Section 4.6.1 the focus is on the functioning of the proposed Node B scheduling algorithm, while in Section 4.6.2 the performance gain by jointly deploying fast L1 retransmission protocols and fast Node B scheduling is addressed. Results are obtained under specific outage constraints for both uplink load and user performance. In any case, the used traffic model is the same as introduced in Chapter 3, with parameters given in Table 3.2. See Appendix D for more details.

4.6.1 Comparison between RNC and Node B PS

In this section the performance of the proposed Node B scheduling algorithm is compared to that of the RNC PS implementation introduced in Chapter 3. In order to focus on the PS performance, L1 HARQ type-I schemes are introduced for both scheduling scenarios. In this first analysis, no soft combining of information received at different transmission instants of the same data frame is performed. The idea is to compare the two scheduling strategies when operating the physical channel at the same error probability, thus focusing on the efficiency of the resource allocation algorithm more than on the spectral efficiency gain that derives from operating at a higher BLER target. Therefore, the parameter setup for the RNC PS scenario is the same as in Table 3.2, with the exception of the BLER target that is set to 10% due to the introduction of fast L1 retransmission schemes.

Table 4.4 and Table 4.5 report the most relevant parameters for the simulation of the Node B PS and of the RNC PS, respectively. With Node B scheduling the allocation delay is significantly reduced and the PS can operate at a higher frequency, i.e. the time interval between two consecutive scheduling instants is reduced. Relying on faster data rate upgrading when additional radio resources are needed, the proposed scheduling algorithm can also

Packet Scheduling	Packet scheduling period	100 ms
	Modification period	100 ms
	Noise Rise target	Adjusted to get a specific 5% noise rise outage
	Noise Rise Offset (for Load Control)	+1 dB
	Minimum allowed data rate	8 kbps
	Maximum scheduled data rate	384 kbps
	Upgrading Threshold (T_{UP})	5 (5 frames = 50 ms)
	Downgrading Threshold (T_{DOWN})	10 (10 frames = 100 ms)
	Node B allocation delay	40 ms
Retransmissions	Retransmission scheme	L1 HARQ type-I
	L2 retransmission delay	120 ms
	L1 retransmission delay	40 ms
	BLER target	10%
	Maximum number of L1 transmissions	5
Propagation	Channel profile	Vehicular A
	Mobile speed	3 km/h

Table 4.4: Parameter setup for simulation of Node B scheduling.

Packet Scheduling	Packet scheduling period	200 ms
	Modification period	600 ms
	Noise Rise target	Adjusted to get a specific 5% noise rise outage
	Noise Rise Offset (for Load Control)	+1 dB
	Minimum allowed data rate	8 kbps
	Maximum scheduled data rate	384 kbps
	Inactivity Timer - after having been inactive for this time period, a UE is downgraded to the minimum allowed data rate	2 s
	Reporting threshold - UEs send a capacity request if the amount of data in their buffer exceeds this threshold	32 kbits
	RNC allocation delay	100 ms
Retransmissions	Retransmission scheme	L1 HARQ type-I
	L2 retransmission delay	120 ms
	L1 retransmission delay	40 ms
	BLER target	10%
	Maximum number of L1 transmissions	5
Propagation	Channel profile	Vehicular A
	Mobile speed	3 km/h

Table 4.5: Parameter setup for simulation of RNC scheduling.

perform data rate downgrading based on short inactivity, as well as on the utilisation of the allocated resources (see Section 4.4.1). All the results presented in this section are obtained for Vehicular A channel profile at 3 km/h. More general simulation parameters are reported in Table A.1 in Appendix A.

Next, the performance of the proposed Node B PS algorithm is separately investigated for a traffic-limited and an interference-limited scenario. Refer to Sections 3.2.2 and 3.4.3 for the distinction between traffic-limited and interference-limited scenarios.

4.6.1.1 Traffic-Limited Scenario

As illustrated in Figure 4.16, the Node B packet scheduler clearly improves the utilisation of the allocated radio resources with a relatively low number of users in the system, especially for high data rates. Although the overall probability of selecting 384 kbps is reduced (from 25% to 21%), due to a better redistribution of the available resources the probability of being

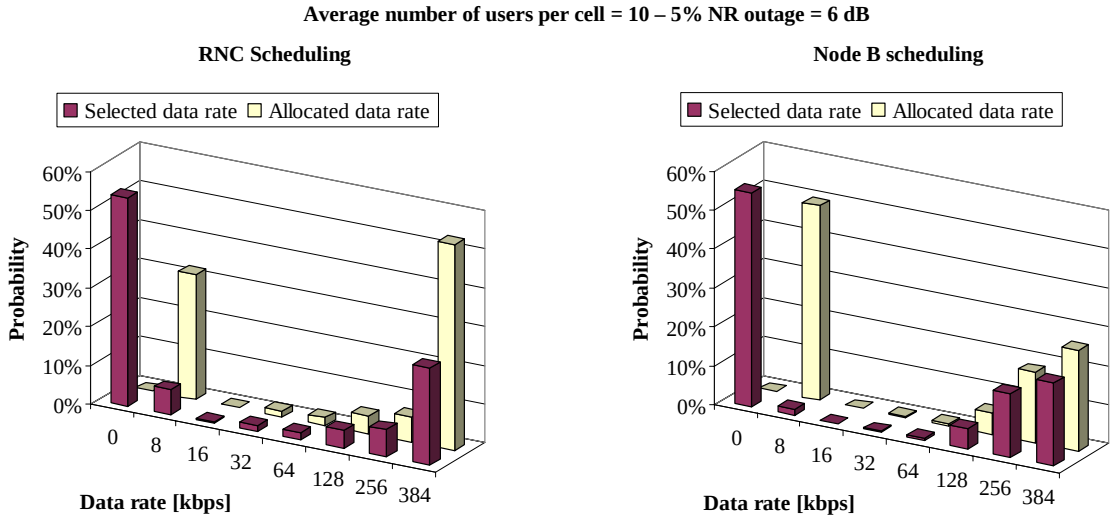

Figure 4.16: PDFs of the selected and allocated data rates with RNC and Node B scheduling, for an average of 10 users per cell and a 5% NR outage of 6 dB.

allocated 256 kbps increases (from 7% to 16%). In this perspective, it is important to notice that the average input data rate during a packet data session with the selected traffic model is approximately 250 kbps (see Table 3.2). As a consequence, the allocation of 384 kbps sometimes results in a waste of radio resources, which is avoided with the proposed Node B scheduling algorithm.

In a traffic-limited scenario the improved radio resource utilisation contributes to a significant enhancement of the PCT performance. Figure 4.17 plots the CDFs of the packet call throughput for both RNC and Node B scheduling. The ability of the Node B scheduling algorithm to track the utilisation of the allocated data rates and, based on such observations, to reallocate the radio resources reflects in a considerable PCT performance improvement, especially at the low levels of the CDF. The 10% PCT outage gain provided by Node B scheduling in a traffic-limited scenario is approximately 35%.

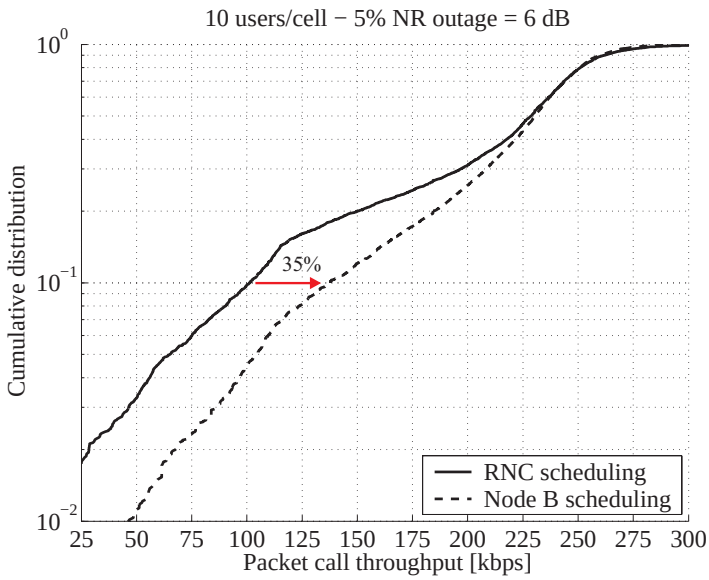

Figure 4.17: CDFs of the packet call throughput with RNC and Node B scheduling, for an average of 10 users per cell and a 5% NR outage of 6 dB.

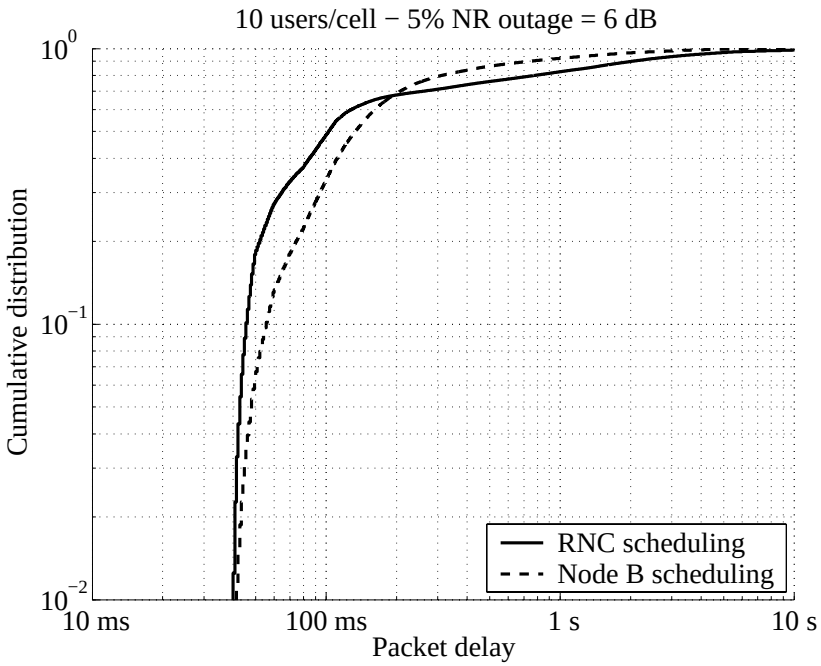

Figure 4.18: CDFs of the packet delay with RNC and Node B scheduling, for an average of 10 users per cell and a 5% NR outage of 6 dB.

The improved fairness with fast Node B scheduling can also be observed by analysing the packet delay statistics in Figure 4.18. With RNC packet scheduling, the user allocated data rate is not downgraded although the utilisation of the allocated resources is low. Hence, users that are allocated high data rates retain such resources for a relatively long time period, thus experiencing a lower packet delay compared to the case of Node B packet scheduling. As a drawback, users that are allocated low data rates do not benefit from an efficient reallocation of the radio resources, thus experiencing significantly higher transmission delays. RNC scheduling guarantees better performance for values of the packet delay below 200 ms. However, the gain never exceeds more than a few tens of milliseconds. Quite the opposite, Node B scheduling contributes to significantly reduce the tail of the packet delay distribution. With Node B scheduling, 90% of the data packets are received in less than 700 ms, while with RNC scheduling the same outage is in correspondence of a delay of 2 s.

4.6.1.2 Interference-Limited Scenario

In this section the performance of the Node B PS algorithm is investigated for a relatively higher average number of users per cell. The focus in this case is on the capability of fast Node B scheduling to more efficiently control the total received power in uplink.

In an interference-limited scenario, due to the increased number of users in the system, high data rates are hardly ever allocated. This can be clearly observed in Figure 4.19, which plots the PDFs of the selected and allocated data rate for both RNC and Node B scheduling for an average of 20 users per cell. As a result, the average source data rate per UE is significantly higher than the most commonly allocated data rate, which in this case is 128 kbps. Though Node B scheduling is shown to still improve the utilisation of allocated data rates (especially 128 kbps), the improvement compared to RNC scheduling is not as remarkable as in Figure 4.16.

In any case, from the data rate histograms no information can be extracted on the capability of the Node B PS to keep the noise rise as close as possible to the planned target. For further clarifications, Figure 4.20 plots the PDFs of the noise rise in the system for the same

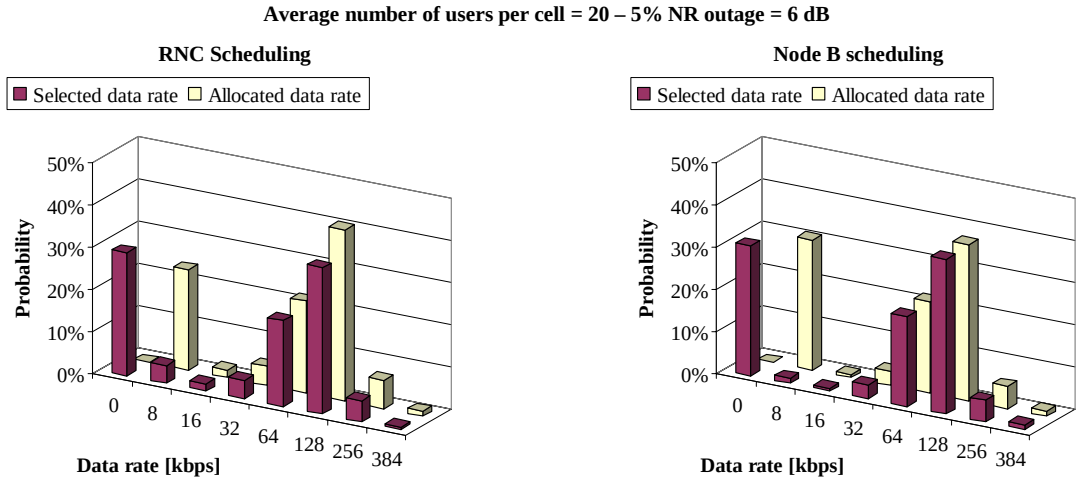

Figure 4.19: PDFs of the selected and allocated data rates with RNC and Node B scheduling, for an average of 20 users per cell and a 5% NR outage of 6 dB.

simulation scenarios as in Figure 4.19. Both distributions have a 5% NR outage equal to 6 dB, as it can be observed from the corresponding CDFs plotted in Figure 4.21. Fast Node B packet scheduling allows the system to more efficiently control the total received uplink power compared to RNC scheduling, and the required power headroom to prevent the system from entering an overload condition is consequently reduced. Hence, the average uplink load to meet the specified NR outage constraint can be increased, and the cell throughput consequently improved.

4.6.1.3 Cell Throughput and PCT Performance Improvement with Node B PS

In this section results are shown considering a wider range for the average number of users per cell. During system level simulations both cell throughput and packet call throughput statistics are collected. The average cell throughput is used as a measure of the system spectral efficiency, while the 10% PCT outage is used to evaluate the user performance.

Figure 4.22 and Figure 4.23 plot the average cell throughput and the 10% PCT outage, respectively, as a function of the average number of users per cell for both RNC and Node B scheduling. Node B scheduling provides a cell throughput improvement compared to RNC scheduling between 6% and 9%, almost independently from the average number of users per cell, while the 10% PCT improvement is more significant with a low number of users in the

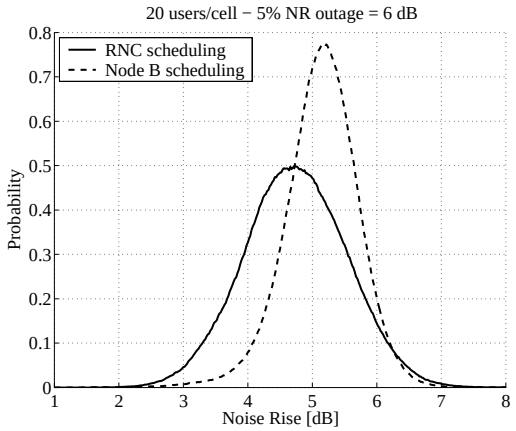

Figure 4.20: Noise rise distribution for RNC and Node B scheduling, an average of 20 users per cell and a 5% NR outage of 6 dB.

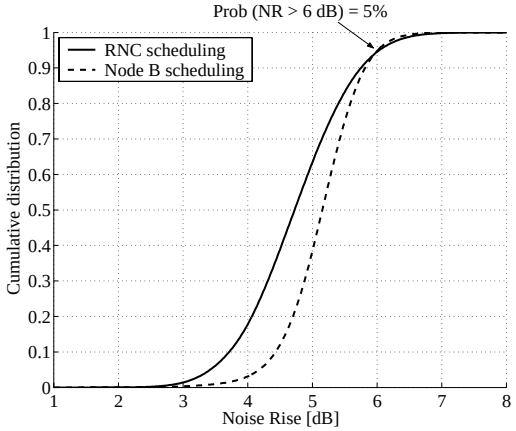

Figure 4.21: CDF of the noise rise for RNC and Node B scheduling, an average of 20 users per cell and a 5% NR outage of 6 dB.

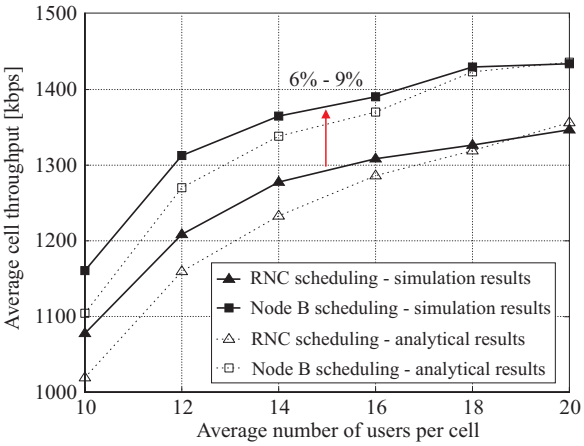

Figure 4.22: Average cell throughput vs. average number of users per cell for both RNC and Node B scheduling and a 5% NR outage of 6 dB.

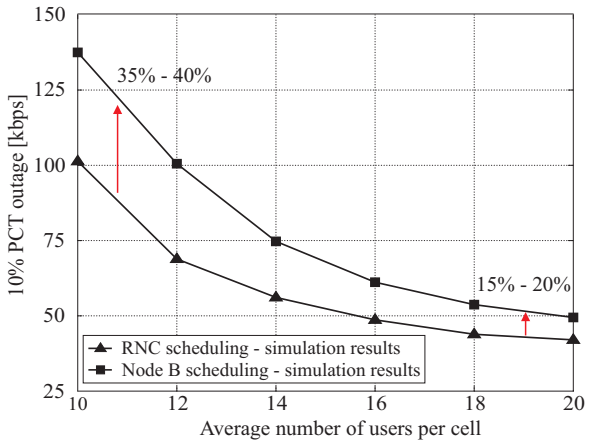

Figure 4.23: 10% PCT outage vs. average number of users per cell for both RNC and Node B scheduling and a 5% NR outage of 6 dB.

system. In this case data transmission is bursty due to the allocation of high data rates, and the Node B scheduling algorithm can take advantage of its capability of reallocating the radio resources based on the utilisation of the allocated data rates. This leads to a 10% PCT outage gain compared to RNC scheduling around 35%-40%. As soon as the number of users in the system is increased, data transmission during 'on' periods of the traffic model duty cycle (see Appendix D) becomes less bursty. Node B scheduling can still take advantage of data rate downgrading due to short inactivity to reduce the required headroom to meet the specified NR constraint, thus increasing the cell throughput. However, the impact from Node B scheduling on the PCT performance is less significant than in a traffic-limited scenario, and the 10% PCT outage gain over RNC scheduling is about 15%-20%.

In Figure 4.22 the analytical cell throughput from (3.24) is compared to the results from system level simulations. The method and parameters used to generate the analytical results are the same as reported in Section 3.4.3, with the exception of the block error rate (BLER), which is increased from 1% to 10%, and the corresponding required E_b/N_0 per receiving antenna ($\rho \cong 1.05$). Once again it can be observed how the analytical results based on the load equation (3.24) fit with the experimental data especially in the interference-limited region.

Finally, Figure 4.24 plots the average cell throughput as a function of the 10% PCT outage for both RNC and Node B scheduling. Node B scheduling can be deployed to either increase the

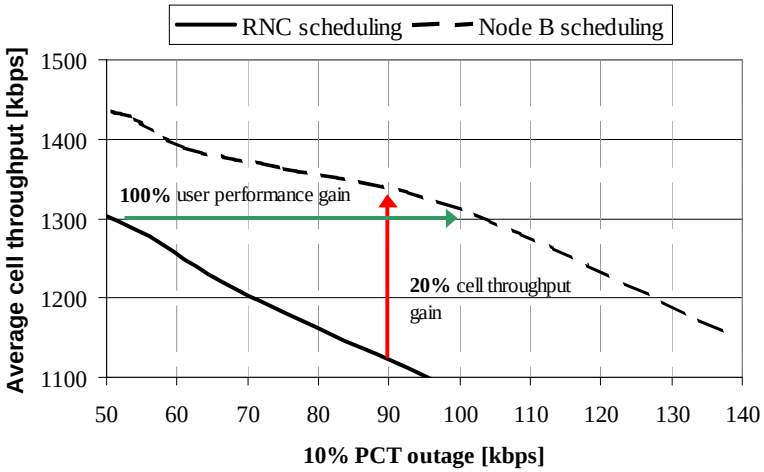

Figure 4.24: Average cell throughput as a function of the 10% PCT outage for both RNC and Node B scheduling and a 5% NR outage of 6 dB.

Scenario No	Retransmission scheme	Packet scheduling	BLER target (at first transmission)
1	L2 ARQ	RNC	1%
2	L1 HARQ type I	RNC	10%
3	L1 HARQ type I	Node B	10%
4	L1 HARQ type II	Node B	10%
5	L1 HARQ type I	Node B	20%
6	L1 HARQ type II	Node B	20%

Table 4.6: Simulation scenarios for the performance assessment of combined L1 retransmission schemes and fast Node B PS.

cell throughout given a specific constraint on the minimum guaranteed user performance, to improve the user experienced QoS while maintaining the overall system performance, or in principle to enhance both QoS and spectral efficiency (see Figure 1.3 in Chapter 1). For a 10% PCT outage of 90 kbps, the cell throughput gain from Node B scheduling over RNC scheduling is about 20%. For a cell load of 1.3 Mbps, the 10% PCT outage increases from approximately 50 kbps with RNC scheduling to more than 100 kbps with Node B scheduling.

4.6.2 Combined Gain from L1 Retransmission Schemes and Node B PS

In this section, the combined gain provided in the uplink of WCDMA systems by jointly deploying fast L1 retransmission schemes and fast Node B scheduling is estimated. To this end, six different simulation scenarios are introduced in Table 4.6, each one characterised by a particular retransmission scheme, a specific scheduling algorithm (and PS location), and a target block error rate (at first transmission for type II HARQ schemes).

The reference case (scenario No 1) corresponds to a system where both the PS functionality and the entity controlling the retransmission of erroneously received data frames are located in the RNC. Therefore, the BLER target for this reference scenario is assumed to be 1%. When considering uplink enhancements, we first introduce L1 HARQ type-I schemes while the PS is still located in the RNC (scenario No 2). The error probability at which the physical channel is operated is consequently increased from 1% to 10%. Next, the proposed Node B scheduling algorithm is introduced and the PS functionality consequently moved from the RNC to the Node B (Scenario No 3). Finally, HARQ type-II schemes are introduced by performing soft combining of information received at different transmission instants of the same data frame (Scenario No 4). Notice that for the simulation scenarios assuming both fast Node B scheduling and L1 HARQ schemes, a BLER target at first transmission of 20% is also considered (Scenarios No 5 and No 6).

For the different simulation cases of Table 4.6, the average cell throughput given a 5% NR outage of 6 dB is plotted in Figure 4.25 and Figure 4.26 for Vehicular A channel profile at 3 and 50 km/h, respectively. In the simulations, the number of users in the system has been adjusted to get the same 10% PCT outage of 64 kbps. In this way the different simulation scenarios can be compared under the same load conditions, and under the same outage constraint for the PCT performance.

Moving the entity controlling the retransmission protocol from the RNC (RNC – 1%) to the Node B (RNC – 10%) leads to a cell throughput gain of about 10% for 3 km/h. The gain is as large as 30% for Vehicular A channel profile at 50 km/h. The obtained results are confirmed by the gain numbers obtained in the theoretical analysis of Section 4.3.1.1. The higher cell throughput increase for a UE speed of 50 km/h can be explained by the higher spectral efficiency gain when reducing the BLER target from 1% to 10% (see Figure 4.7). This is

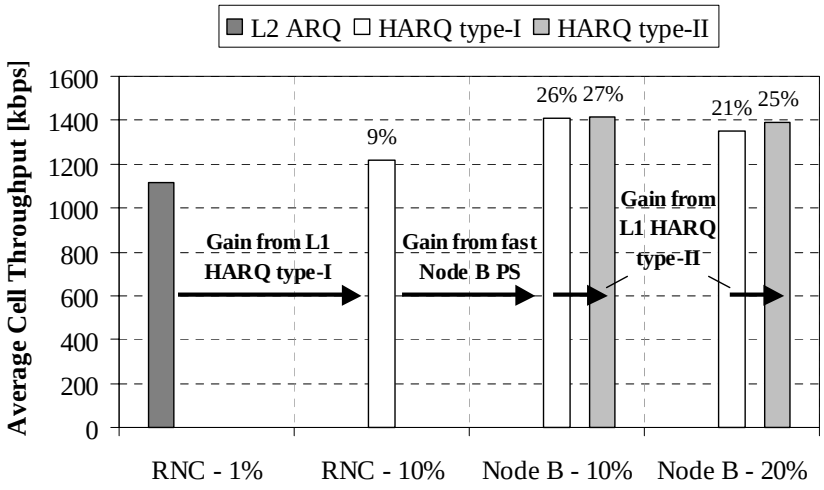

Figure 4.25: Average cell throughput for different retransmission schemes and PS scenarios for Vehicular A channel profile at 3 km/h, 5% NR outage of 6 dB and 10% PCT outage of 64 kbps.

mainly due to the fact that the accuracy of fast power control typically gets worse with increasing speed.

Relocating the PS to the Node B and deploying the proposed scheduling algorithm guarantees an additional increase in cell throughput of about 15%. More precisely, the gain numbers when comparing the Node B PS at 10% BLER target to the RNC PS at 10% BLER target are 16% and 14% for 3 and 50 km/h, respectively. Finally, for both mobility scenarios HARQ type-II schemes provide only a marginal cell throughput gain (< 4%) over type-I strategies, as anticipated in Section 4.3.1.1.

In conclusion, the joint deployment of fast Node B packet scheduling and L1 retransmission schemes can provide a cell throughput improvement in the uplink of WCDMA systems between 25% and 60%, depending on the mobility scenario. It is important to notice that such gain numbers are somehow depending on the assumptions made for the traffic model, as well as on the selected values for the noise rise and 10% PCT outage constraints.

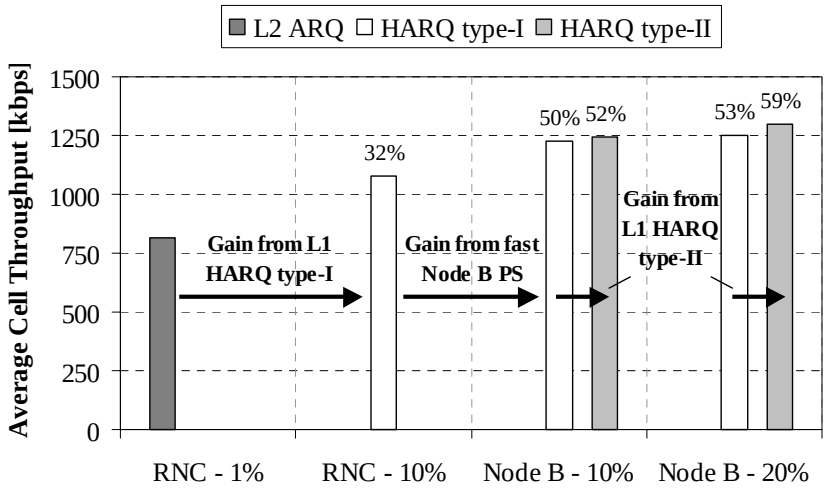

Figure 4.26: Average cell throughput for different retransmission schemes and PS scenarios for Vehicular A channel profile at 50 km/h, 5% NR outage of 6 dB and 10% PCT outage of 64 kbps.

4.7 Summary

In this chapter the potential benefit from L1 retransmission schemes and fast Node B PS operation has been discussed and simulation results presented. After having reviewed complexity and architectural issues, the model used to implement both these features in the system level simulator has been presented. In the case of L1 retransmission schemes, a theoretical analysis has also been developed.

L1 retransmission schemes – With Node B-controlled L1 retransmission schemes the error probability at which the physical channel is operated can be somewhat increased compared to the case in which the entity controlling the retransmission protocol is located in the RNC. A theoretical analysis and a simplified simulation model for the calculation of the upload time of a fixed-size file have been used to estimate that with fast L1 retransmission schemes the BLER target at first transmission can be increased from 1% to approximately 10%-20% without any significant decrease in the user delay performance. The resulting spectral efficiency gain translates into a cell throughput increase of about 10% and 30% for Vehicular A channel profile at 3 km/h and 50 km/h, respectively. The reason for a bigger spectral efficiency gain in the case of higher mobility is that the accuracy of fast power control decreases as the speed increases. HARQ type-II schemes (which perform soft combining of information received at different transmission instants of the same data frame) provide only a marginal gain over type-I strategies when the BLER target is below 20%. The user delay performance gain from HARQ type II schemes is on the other hand quite significant as soon as the BLER target is further increased. However, due to the presence of fast power control, a minor spectral efficiency gain can be achieved when increasing the BLER target to values above 20%, and only in the case of high user mobility.

Fast Node B packet scheduling – For what concerns fast Node B PS operation, a distinction has been done between a traffic-limited and an interference-limited scenario. In the first case, allocation of high data rates is a likely event and the level of burstiness of data transmission on the physical channel is relatively high. Under these circumstances, the fast Node B scheduler can perform fast reallocation of the radio resources based on the level of utilisation of the allocated data rates. The higher efficiency thus achieved provides a cell throughput increase compared to an RNC PS implementation, and more significantly a considerable improvement of the user performance. In an interference-limited scenario, data transmission during packet calls occurs at an almost constant rate due to the allocation of relatively low data rates. The Node B scheduling algorithm can still take advantage of fast downgrading based on short inactivity to more efficiently control the total received uplink power; the power headroom needed for preventing the system from entering overload conditions can be reduced, and the cell throughput consequently increased. However, the PCT performance gain over RNC scheduling reduces compared to the traffic-limited scenario.

Finally, the cell throughput performance has been evaluated for the same 10% PCT outage constraint; namely, 90% of the packet calls were required to experience an average data throughput of at least 64 kbps. Under these assumptions, the estimated cell throughput increase provided by jointly deploying L1 retransmission schemes and fast Node B PS is estimated in the range between 25% and 60%, depending on the mobility scenario and on the BLER target at first transmission.

Chapter 5

Combined Time and Code Division Scheduling for WCDMA Uplink

5.1 Introduction

In the previous chapter the impact from fast and dynamic radio resource allocation on the uplink performance of WCDMA systems has been investigated. Results have shown that for NRT applications characterised by bursty data transmission both cell throughput and PCT performance can be improved by deploying a dynamic allocation strategy that more rapidly redistributes the radio resources between the users. The scheduling decisions are taken at the Node B, allowing a reduction of the delay associated with the resource allocation process and a more frequent PS operation to rapidly adapt to both traffic and interference variations.

In this chapter, more advanced Node B-located scheduling techniques for WCDMA uplink enhancement are considered, techniques which make use of fast Node B PS operation on a per TTI basis. The main idea is to introduce in WCDMA uplink packet access a scheduling principle based on combined time division multiplexing (TDM) and code division multiplexing (CDM), which allows scheduling users for transmission on DCH when experiencing favourable channel conditions.

Two of the first papers to address the issue of channel-state dependent packet scheduling in wireless networks are [Knopp95] and [Bhag96]. Channel-dependent scheduling can significantly improve the utilisation of the wireless channel, and hence the system capacity; see, among the others, [Liu01], [Berg01], [Lin02], and [Berg04a]. The work presented in these papers concentrates on estimating the theoretical gain achievable when the time-varying characteristics of the wireless channel are exploited by means of ‘opportunistic’ transmission scheduling. For what specifically concerns WCDMA systems, research on the beneficial effects of channel-dependent scheduling has been related mainly to the development of HSDPA. Together with link adaptation based on adaptive modulation and coding and L1 HARQ schemes, channel-dependent scheduling represents one of the core features of HSDPA

[Kold03]. A thorough performance evaluation of different scheduling strategies for HSDPA is presented in [Ameg03], showing that channel-dependent resource allocation can provide a significant gain in the downlink of 3G systems.

From the HSDPA experience, time scheduling based on channel state information has also been considered for the enhancement of uplink packet access. This has resulted in some research on the subject of uplink scheduling, although less compared to the literature on downlink scheduling.

The problem of optimal power and rate allocation in the context of a single-cell CDMA uplink system is presented in [Samp95]. The power and rate assignment issue is here formulated as a constrained optimisation problem, where the objective functions used are minimum power and maximum rate. The former reduces interference seen by other cells, the latter attempts to achieve maximum throughput. In [Rama98], the authors introduce time scheduling for delay tolerant users, so that only a limited number of them are transmitting information at any given time instant. It is shown that this hybrid CDM/TDM solution affords a better throughput while imposing the same average power requirements as conventional transmission. In [Uluk00], the problem is formulated as in [Samp95], but the study is extended to a multi-cell scenario, and also considers time scheduling of users on the uplink. The main conclusion is that, in nearly all cases, the solution to the optimisation problem is to allocate the full cell capacity to the highest-path-gain user in each cell, and nothing to other users. The approach of maximising the rate sum, as used in these papers, is of advantage to users with high path gain to the receiver, and mostly at the expense of users in unfavourable channel conditions. The fairness issue is addressed in [Jänt01] and [Kuma03], where the main focus is on maximising system throughput under instantaneous transmit power limitations and with respect to some fairness constraints. In both papers the authors arrive at roughly similar conclusions: It is advantageous on the uplink to schedule ‘strong’ users one-at-a-time (TDM approach), and ‘weak’ users several at a time (CDM approach).

Although formulated in different ways, the overall goal of these previous studies has been to define an optimum (or sub-optimum) power and rate allocation scheme that maximises throughput with or without fairness constraints. The main focus is on the scheduling gain achievable when a combined TDM and CDM approach is used, compared to a pure CDM solution. The impact that time scheduling has on the time variability of both uplink load and other-to-own cell interference is often ignored, as well as the interaction between time scheduling and fast closed loop power control. Taking also into account these and other issues, the main objective of the work presented in this chapter is to assess the uplink performance of a WCDMA system that deploys combined time and code division scheduling. In order to include the effects of non-ideal power control and possibly of high variability in other-cell interference, the performance of the proposed scheduling schemes is mainly evaluated by means of system level simulations.

The chapter is organised as follows: First, Section 5.2 introduces the expected advantages and disadvantages of time division scheduling in WCDMA uplink, and discusses the additional complexity that systems deploying such techniques would require. Although the concept of time scheduling for enhanced DCH performance is directly inherited from HSDPA, some fundamental differences exist between downlink and uplink transmission, which are also addressed in this first section. The main simulation assumptions and the proposed advanced scheduling algorithms are then introduced in Section 5.3. Simulation results are presented and discussed in Section 5.4. Finally, the concluding remarks are given in Section 5.4.5.

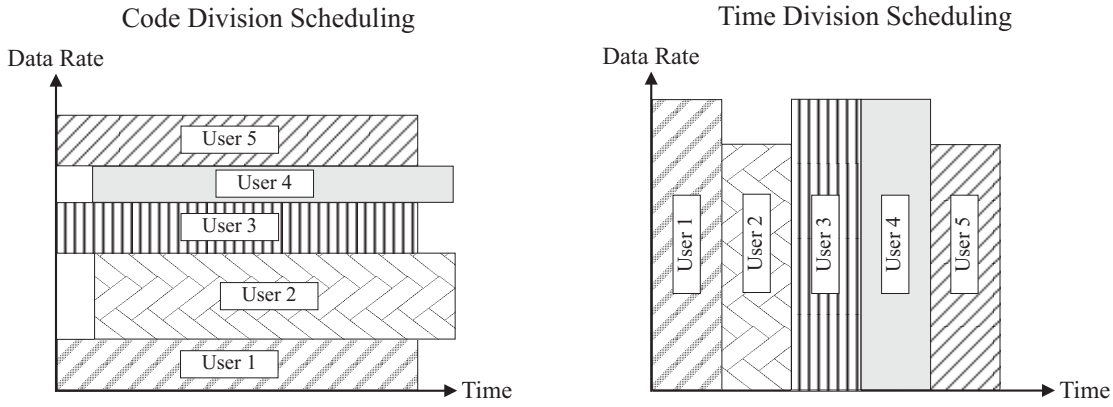

Figure 5.1: Code and time division scheduling principles [Holma04].

5.2 Time and Code Division Scheduling: Concept and Implications

The packet scheduling function shares the available air interface capacity between packet users. The PS can decide the allocated data rates and the length of the allocation. In WCDMA this can be done in two ways, in a code or time division manner. The principles of code and time division scheduling are illustrated in Figure 5.1. In the code division approach a relatively large number of users can have a low data rate channel available simultaneously; when the number of users requiring capacity increases, the data rate that can be allocated to a single user consequently decreases. As an alternative, with time division scheduling the capacity is given to one user or only a few users at each moment of time. Thus, a user can have a relatively high data rate but can use it only for a limited period of time. When the number of users increases in the time division approach, the time elapsing between two consecutive transmissions from the same user increases.

Section 5.2.1 discusses some of the main differences existing between uplink and downlink transmissions. The main objective is to underline which features can be inherited from HSDPA in order to enhance packet data transmission in the uplink of WCDMA systems, and which cannot. Section 5.2.2 gives an overview of the expected advantages and disadvantages of time division scheduling compared to code division scheduling, also including potential complexity issues related to practical implementation.

5.2.1 Differences between Downlink and Uplink WCDMA Evolution

In HSDPA two fundamental features of WCDMA, namely variable spreading factor (VSF) and fast power control are deactivated and their function replaced by adaptive modulation and coding (AMC), short packet size, and fast L1 HARQ schemes. To substitute the functionality of fast power control and VSF, the modulation, coding, and multi-code part of HSDPA must be designed to cover the dynamic range in correspondence with the channel quality variations experienced at the UE (including fast as well as distance-dependent variations). The available dynamic range with HSDPA is in the range between 20 dB (single-code transmission) and 32 dB (multi-code transmission) [Kold03]. Primarily to increase the link adaptation rate and the efficiency of AMC, the radio frame duration is reduced from normally 10 or 20 ms down to a fixed duration of 2 ms. To achieve low delays in the link control, the MAC functionality for HSDPA, containing the HSDPA PS, is moved from the RNC to the Node B. The high scheduling rate thus achieved, combined with the large AMC dynamic range available with the HSDPA concept, makes it possible to conduct packet scheduling according to the radio channel conditions as well as the amount of data to be transmitted to the different users.

Though allocation of radio resources to more than one user at a time is a possibility, the HSDPA PS typically tries to schedule one user at a time, thus maximising the multi-user diversity gain.

If the HSDPA concept is symmetrically reversed so to be applied in uplink transmission, the following holds true:

1. Scheduled users are transmitting with constant power, and
2. link adaptation is performed based on AMC, i.e. the most appropriate modulation scheme and coding rate are selected based on the instantaneous quality of the channel.

Under these assumptions, some fundamental differences between uplink and downlink transmission must be carefully considered:

- *Limited multi-user diversity gain*

First of all, the UE transmission power capabilities are considerably lower compared to the power available at the Node B for downlink transmission. Hence, especially in macro-cell scenarios, the radio resources available in uplink can hardly be allocated to one user at a time, but must be shared among a set of users. This means, the multi-user diversity gain cannot be fully exploited in uplink packet data access as in HSDPA. Differently, in micro-cell environments it might be possible to instantaneously allocate the full uplink capacity to a single user.

- *Intra-cell interference adds complexity to the AMC mechanism*

When more users are scheduled at the same time in uplink their received signals at the Node B are not orthogonal as in downlink. This means, link adaptation has also to cope with the effect of intra-cell interference, which makes even more complicated to perform AMC efficiently. The presence of intra-cell interference also requires the link adaptation method in uplink to deal with the near-far problem [Duel95]. The near-far problem cannot be avoided simply by using AMC, but needs a mechanism to control the UE transmission power. Differently from HSDPA, with the introduction of time division scheduling in the uplink of WCDMA systems power control cannot be completely deactivated and replaced with AMC.

- *The location of the sources of interference in uplink varies*

Even neglecting UE power limitations and assuming one-at-a-time scheduling also in uplink, link adaptation based on AMC still has one main drawback. The fact is that the sources of interference in uplink are the UEs, and more specifically the scheduled UEs when time scheduling is deployed. Since the location of the scheduled UEs may vary from TTI to TTI, abrupt changes in other-cell interference can be expected from one radio frame to the next. This represents a problem since the efficiency of AMC strongly depends on the reliability of channel quality estimations performed at the Node B. To better understand this issue, two simplified examples for downlink and uplink transmissions are reported in Figure 5.2 and Figure 5.3, respectively.

In the HSDPA scenario illustrated in Figure 5.2, the interference seen by UE_1 due to *Node* B_2 is weakly dependent on the specific user scheduled by *Node* B_2. Fast link adaptation relies on channel quality reports from UE_1 to *Node* B_1. If the scheduling can be performed sufficiently fast compared to the time variability of the propagation channel (mainly dependent on the user speed), channel quality reports allow UE_1 to be scheduled for transmission with the most appropriate modulation scheme and coding rate.

In the corresponding uplink scenario of Figure 5.3, the SINR experienced by UE_1 at *Node* B_1 is strongly influenced by the location of the user simultaneously scheduled in the cell

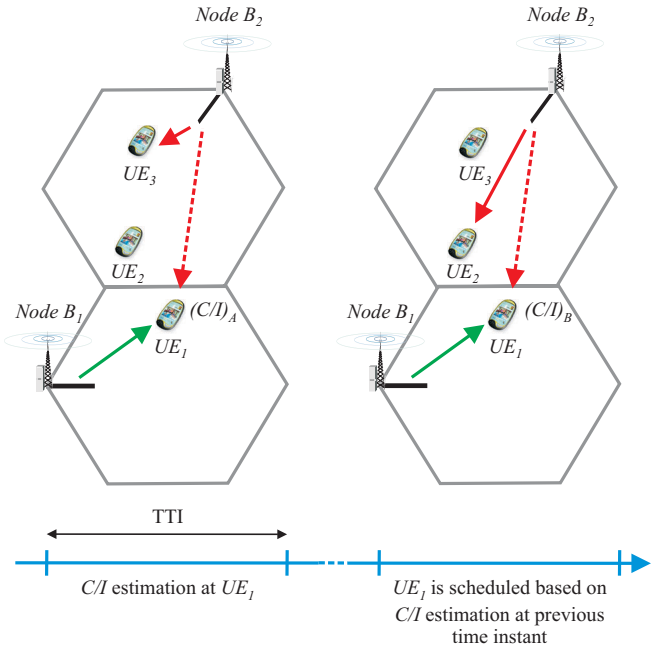

Figure 5.2: Simplified downlink scenario with time division scheduling and AMC based on channel quality estimations performed at the UE.

controlled by *Node* B_2. Therefore, no matter how fast link adaptation can be performed, the interference conditions can vary significantly from the time in which the channel quality is estimated and the instant in which, based on this estimation, UE_1 is scheduled for transmission with specific modulation scheme and coding rate. This clearly limits the potential benefit of uplink link adaptation based on AMC.

As it is described in more detail in Section 5.2.2, these abrupt variations of other-cell interference also represent a problem for link adaptation based on fast power control, though power control is expected to be more robust than AMC since it operates on a WCDMA slot

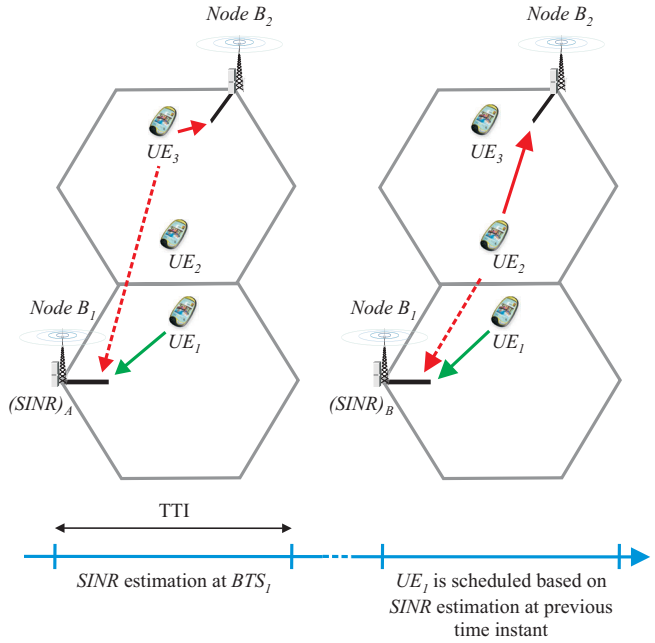

Figure 5.3: Simplified uplink scenario with time division scheduling and AMC based on channel quality estimations performed at the Node B.

basis, and can utilise different values of the power control step in order to more rapidly converge to the desired E_b/N_0. Besides, as previously discussed, some kind of power control is needed in the uplink to cope with the near-far problem.

In principle it would be possible to combine power control with higher order modulation schemes so as to increase the users' peak data rates, and consequently the multi-user diversity gain achievable with time division scheduling (see Section 5.2.2.1). However, higher order modulation schemes and multicode transmission increase the peak-to-average ratio (PAR) of transmission power, and hence reduce the efficiency of the terminal power amplifier [Outes04]. This contributes further to the UE power capabilities as a limiting factor. The effect of multi-code transmission is shortly introduced in Chapter 6, where the allocation of peak data rates up to 768 kbps is considered. Higher order modulation schemes are not considered in this Ph.D. thesis.

Based on these considerations, AMC is not seen as being a feasible solution for link adaptation in uplink. For the advanced scheduling techniques based on time division scheduling presented in this chapter, the two following assumptions are made:

- Link adaptation is based on fast closed loop PC, and
- time scheduling based on channel quality information is made possible by means of fast VSF.

A more detailed description of the proposed scheduling concept is given in Section 5.3.

5.2.2 Time Division Scheduling: Advantages and Disadvantages

5.2.2.1 Advantages

The possibility to perform time scheduling on DCH allows the Node B PS to schedule for transmission users that experience favourable channel conditions. The available resources at Node B (received power) are allocated to a limited set of users, while data transmission from other users can be 'switched off' and delayed until they experience more advantageous radio conditions. In this way, the transmission power of the scheduled users can be lowered relatively to their data rate. As a result, the interference generated to other cells can be reduced and the spectral efficiency increased. The multi-user diversity gain, which results in a reduction of inter-cell interference, is dependent on the number of users that must be simultaneously scheduled in order to fully utilise the cell capacity: The lower the number of users simultaneously scheduled, the higher the multi-user diversity gain. The main advantage of introducing time scheduling on DCH in the uplink of WCDMA systems can be summarised as follows:

- *Time division scheduling allows channel-dependent allocation of radio resources so that inter-cell interference can be reduced, and cell throughput increased.*

Another advantage of time division scheduling compared to code division scheduling is that scheduled users transmit at a higher instantaneous data rate. In this way, for a fixed noise rise value, each scheduled user contributes more to the total received uplink power at the Node B. As a result, the same user experiences less interference from other users in the own cell compared to the case where all active users continuously transmit with a relatively lower instantaneous data rate. Therefore:

- *Allocation of higher instantaneous data rates results in a reduction of intra-cell interference for a fixed value of the total received uplink power.*

Next, a simplified example is presented that tries to analyse in more detail the advantages of introducing time scheduling on DCH in the uplink of WCDMA systems. The example is

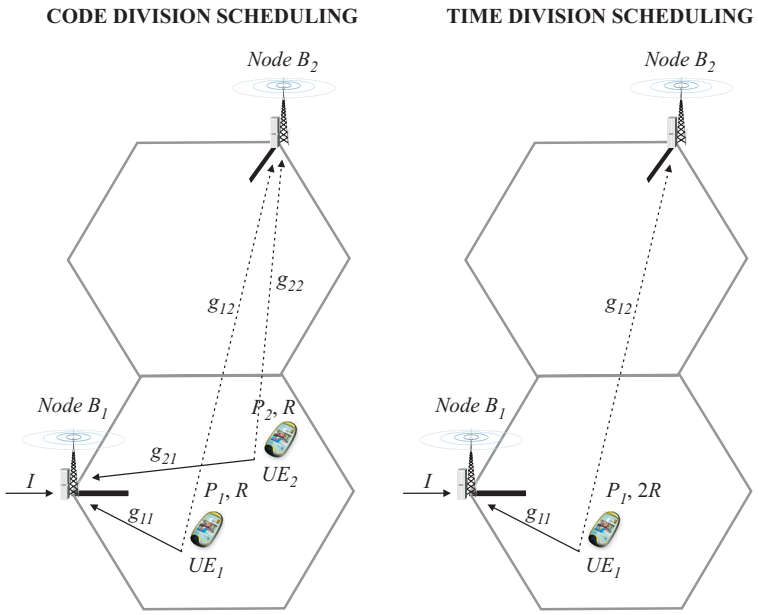

Figure 5.4: Simplified example comparing the different scenarios with code and time division scheduling.

visualised in Figure 5.4. The first scenario corresponds to the case of code division scheduling: UE_1 and UE_2 simultaneously transmit with data rate R and with transmission powers equal to P_1 and P_2, respectively. The second scenario refers to the case of time division scheduling, where at a specific time instant only UE_1 is scheduled for transmission with an instantaneous data rate that is twice the one allocated in the case of code division scheduling ($2R$). In both scenarios, g_{ij} is the path gain between UE_i and *Node* B_j, and I is the additional interference at *Node* B_1 due to thermal noise and other-cell interference. Assuming perfect power control and the same required E_b/N_0 (ρ) for both users, the following system of equations can be written in the case of code division scheduling.

$$\begin{cases} \dfrac{P_1 \cdot g_{11}}{P_2 \cdot g_{21} + I} \cdot \dfrac{W}{R} = \rho \\ \dfrac{P_2 \cdot g_{21}}{P_1 \cdot g_{11} + I} \cdot \dfrac{W}{R} = \rho \end{cases} \tag{5.1}$$

In (5.1), W is the WCDMA chip rate. Solving the system of equations in (5.1), the transmission powers of UE_1 and UE_2 can be derived.

$$P_1 = \frac{\rho \cdot I}{g_{11} \cdot \left(\dfrac{W}{R} - \rho \right)}; \; P_2 = \frac{\rho \cdot I}{g_{21} \cdot \left(\dfrac{W}{R} - \rho \right)} \tag{5.2}$$

The amount of inter-cell interference caused by UE_1 and UE_2 to *Node* B_2 in the case of code division scheduling can be written as:

$$ICI_{code} = P_1 \cdot g_{12} + P_2 \cdot g_{22} \tag{5.3}$$

Substituting in (5.3) the power values in (5.2), the following expression is obtained.

$$ICI_{code} = \frac{\rho \cdot I}{\frac{W}{R} - \rho} \cdot \left(\frac{g_{12}}{g_{11}} + \frac{g_{22}}{g_{211}} \right) \tag{5.4}$$

The same approach can be used in the case of time division scheduling, where only *UE₁* is scheduled for transmission with data rate equal to 2*R*. At this point it should be noticed that in practice high data rates have different E_b/N_0 requirements compared to lower data rates, mainly because of the increased multipath interference and the reduced DPCCH/DPDCH power ratio (see Appendix C). Anyway, these are opposite effects and it is reasonable to assume the same required E_b/N_0 ρ when the selected data rate for transmission is increased from *R* to 2*R*. At last, assuming the same amount of noise power and other-cell interference at *Node B₁*, the transmission power required at *UE₁* can be written as:

$$P_1 = \frac{2R \cdot \rho \cdot I}{W \cdot g_{11}} \tag{5.5}$$

In this case, the amount of inter-cell interference towards *Node B₂* is:

$$ICI_{time} = P_1 \cdot g_{12} = \frac{2R \cdot \rho \cdot I}{W} \cdot \frac{g_{12}}{g_{11}} \tag{5.6}$$

Finally, while the same cell throughput is achieved at *Node B₁* (2*R*), the ratio of the interference generated at *Node B₂* in the case of code division scheduling to the amount of interference caused in the case of time division scheduling can be derived.

$$\frac{ICI_{code}}{ICI_{time}} = \left[\frac{W}{W - R\rho} \right] \cdot \left[\left(1 + \frac{g_{11}}{g_{21}} \cdot \frac{g_{22}}{g_{12}} \right) \Big/ 2 \right] \tag{5.7}$$

In (5.7), the effect on the interference generated at *Node B₂* when time scheduling is deployed compared to code division scheduling can be separated into two different contributions, which can be related to the two advantages of time division scheduling previously discussed.

1. The first term in square brackets shows that inter-cell interference can be reduced if high data rates are momentarily allocated. With time division scheduling the scheduled users (*UE₁*) experience less intra-cell interference by contributing more to the total received power at the Node B compared to the case of code division scheduling. As a result, for a given E_b/N_0 requirement, the transmission power per information bit is somewhat reduced, which consequently turns into a reduction of inter-cell interference.
2. The second term in square brackets in (5.7) shows that performing time scheduling of users in favourable channel conditions can reduce the inter-cell interference while achieving the same cell throughput. Due to fast as well as slow fading, the channel gain (g_{11}) between the best user (*UE₁*) and the serving Node B (*Node B₁*) can be several dB higher compared to the channel gain (g_{21}) between the user with the worst channel conditions (*UE₂*) and the same Node B. Allocating all the uplink radio resources to the best user can result in a significant decrease in inter-cell interference compared to the case of code division scheduling. The reduction of inter-cell interference also depends on the difference in the path gains (g_{12} and g_{22}) between the two considered users and the interfered Node B (*Node B₂*). In general, the probability that the ratio g_{22}/g_{12} is higher than

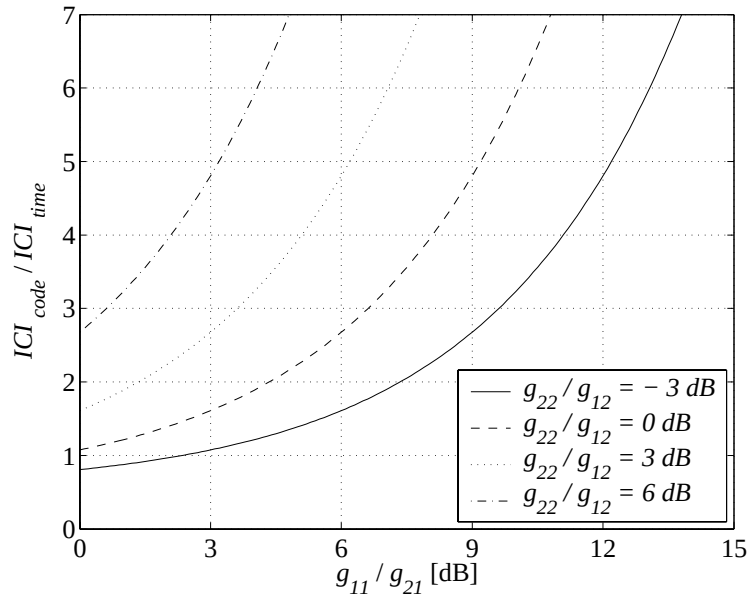

Figure 5.5: Ratio of the interference generated to Node B_2 in the case of code division scheduling to the amount of interference caused in the case of time division scheduling, as a function of g_{12}/g_{21} and for different values of g_{22}/g_{12} (see Figure 5.4).

one is bigger than 50% if UE_2 has a larger average path gain to *Node* B_2 than UE_1, and vice versa. However, no further investigations on the ratio between g_{22} and g_{12} are made.

Figure 5.5 plots the ratio of the interference generated to *Node* B_2 in the case of code division scheduling to the amount of interference caused in the case of time division scheduling. The value reported on the x-axis is a logarithmic measure of the difference in the path gain to *Node* B_1 between the user in most favourable channel conditions (UE_1) and the user in worst channel conditions (UE_2). The different curves are obtained for different values of the ratio g_{22}/g_{12}, for W that equals the WCDMA chip rate (3.84 Mcps), for a date rate R =128 kbps, and for an E_b/N_0 requirement ρ = 2.09 (≈ 3.2 dB). Notice that this simplified example does not include the effect of increased signalling overhead needed to perform time division scheduling.

For example, assuming that UE_1 and UE_2 have the same path gain to the interfered Node B (g_{22}/g_{12} =0 dB), with time division scheduling the inter-cell interference can be decreased by a factor of 2.67 if the scheduled user has a path gain to the serving Node B that is 6 dB higher than the other UE. If the difference in channel gain is 9 dB, the inter-cell interference is almost 5 times less than in the case of code division scheduling.

The discussed scenario is of course just a simplified example used to clarify why time scheduling based on channel-state information and with the momentary allocation of high data rates can provide a cell throughput increase in the uplink of WCDMA systems. More detailed results based on extensive system level simulations are presented and discussed in Section 5.4.

Other advantages of time division scheduling compared to code division scheduling are:

- *High data rates have lower E_b/N_0 requirements*.

High data rates typically require less energy per transmitted bit for a given BLER performance. The main reason why the required E_b/N_0 depends on the data rate is that the DPCCH is needed to keep the physical layer connection running and it contains, among other

things, reference symbols for channel estimation. The E_b/N_0 performance depends on the accuracy of the channel estimation, therefore the more power that can be allocated for the DPCCH, the better the channel estimation. On the other hand, DPCCH is only overhead and its power should be minimised. For high data rates, the power of DPCCH is higher, thus enabling more accurate channel estimation, and the overhead of DPCCH is still small compared to lower data rates [Holma04]. Both these factors improve E_b/N_0 performance, hence time division scheduling can benefit from lower E_b/N_0 requirements compared to code division scheduling. For more information on this issue, refer to Appendix C.

- *High data rates have the potential for improving user delay performance.*

Since the instantaneous transmission rate is higher with the time division approach, the experienced transmission delay over the air interface is in general shorter than with code division scheduling, especially when considering short packet calls. The delay performance improvement due to high peak data rates becomes less significant as soon as the size of the packet call increases.

- *Time scheduling on a TTI basis allows allocating radio resources based on near instantaneous buffer information.*

With the introduction of time division scheduling, scheduling decisions are taken at the Node B once every TTI. Provided that some information on the UE buffer occupancy is exchanged between users and PS beforehand, the Node B PS can perform resource allocation based on near instantaneous buffer information. This can improve radio resource utilisation, thus increasing the achievable cell throughput, as well as enhance the user performance by allocating radio resources 'on demand'.

5.2.2.2 Disadvantages

The introduction of time division scheduling in the uplink of WCDMA also presents some disadvantages:

- *Time division scheduling in the uplink of WCDMA has potential coverage problems.*

With time division scheduling users are scheduled in time with a temporary transmission data rate that is higher than in the case of code division scheduling. At network planning, given a particular area coverage probability for a specific data rate (e.g. 95% cell area coverage for 64 kbps), the corresponding coverage probability for a higher data rate (e.g. 384 kbps) is lower. As a result, users at the cell edge cannot be temporarily allocated high data rates. This clearly limits the potential gain from time division scheduling.

- *Time division scheduling in uplink is likely to increase the time variability of inter-cell interference; as a consequence, the required headroom for power scheduling given specific noise rise outage constraints increases.*

This problem is related to one of the issues introduced in Section 5.2.1, where it was discussed how with time scheduling the location of the sources of uplink interference might continuously change from one scheduling period to the next. This can cause abrupt changes in the interference generated to other cells, thus deteriorating the performance of the link adaptation mechanism based on fast power control, and increasing the required power headroom that the PS needs to meet the specified NR outage criteria. As previously discussed, the multi-user diversity gain from channel-dependent scheduling depends on the number of users that can be simultaneously scheduled to utilise the cell capacity. At the same time, the fewer users simultaneously scheduled for transmission, the higher the expected time variability of inter-cell interference. One of the main goals in this chapter is to evaluate which

is the combined effect of these two opposite trends when time division scheduling is introduced in the uplink of WCDMA systems.

5.2.2.3 Complexity and Practical Implementation Issues

In addition to these inherent disadvantages, the introduction of time scheduling in the uplink of real systems brings about some practical concerns not so easily quantified but with a possible major impact on system performance and cost.

- *Frame synchronisation*

In order to time schedule users for uplink transmission on DCH, uplink frame synchronisation is required. This issue is illustrated using a simplified example in Figure 5.6. In WCDMA uplink, the timing between uplink radio frames is derived from the corresponding downlink DCH timing by an apposite time offset $T_{DL\text{-}UL}$ [Holma04]. Since downlink DCH transmission is frame asynchronous, so is the uplink DCH transmission. In order to achieve uplink frame synchronisation, thus allowing time division scheduling on DCH, some timing information must be signalled from the network side to the UEs. Moreover, a timer needs to be run at each UE (T_1, T_2 and T_3) so that the DCH timing information can be opportunely corrected. This has a direct impact on the mobile terminal complexity and cost.

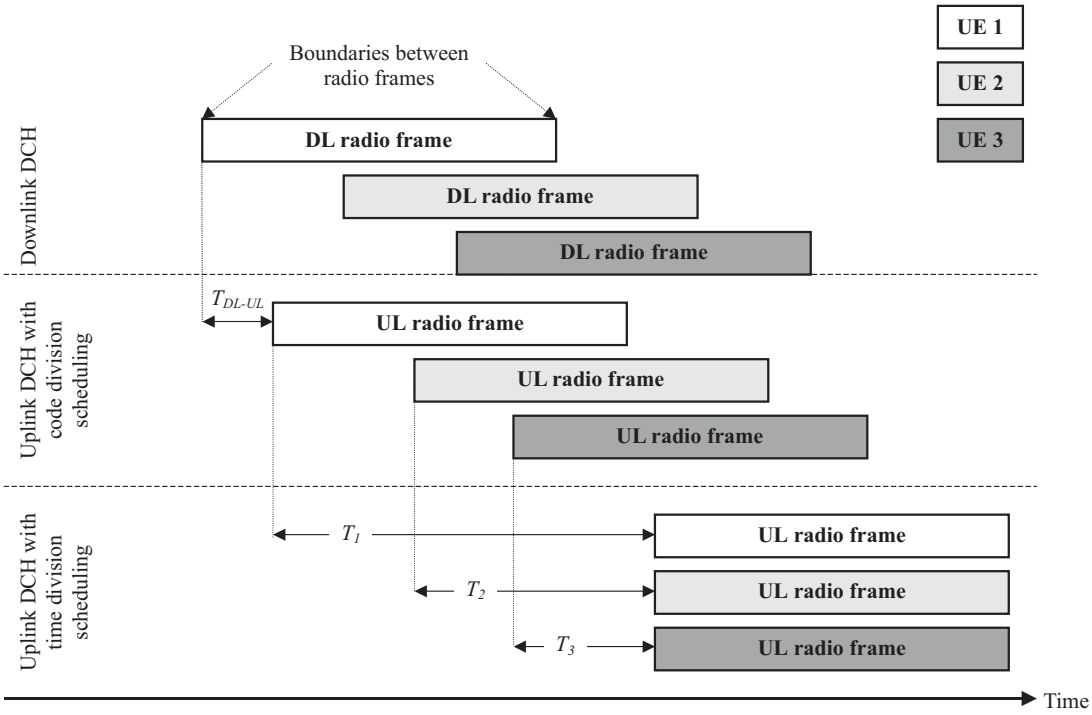

Figure 5.6: Uplink frame synchronisation with time division scheduling concept in uplink DCH.

- *Increased signalling overhead*

Time scheduling on a TTI basis require a significant signalling overhead both in uplink (UEs must send information on their buffer occupancy and possibly some additional information to perform channel-dependent scheduling) and in downlink (Node B must signal every TTI which users are scheduled for transmission and at which rate). The required signalling overhead is more significant if a 2 ms frame size is used in order to better exploit the characteristics of the fading channels in the scheduling procedure, and to achieve better delay performance by reducing both transmission and processing delays.

- *Measurement accuracy at the Node B*

Another practical problem of time scheduling is related to measurements accuracy at the Node B, where instantaneous and accurate measurements of the received power must be available in order to keep the uplink load as close as possible to the planned target. In traditional CDMA systems, measurements of the received uplink power are collected over a relatively long period of time so that the effect of measurement errors can be averaged out. In contrast, time scheduling requires nearly instantaneous power measurements since the total received uplink power is now redistributed between the users every TTI. As a consequence, the accuracy of power increase estimations in the case of time division scheduling is likely to be more affected by measurements errors than traditional code division schedulers, which typically operate at a higher scheduling rate (≥100 ms).

- *Errors when setting the transmission power to be used at the beginning of one frame*

A change of output power is required whenever the TFC, and thereby the data rate, is changed from one TTI to the next. The power step due to a change in TFC is calculated in the UE so that the power transmitted on the DPCCH follows the inner loop power control. The accuracy in determining the power step decreases as the step size increases [TS25101]. Since time scheduling requires the users to continuously switch from no data transmission to data transmission with high instantaneous data rate, this can introduce significant uncertainty in the selection of the transmission power to be used at the beginning of each TTI. This issue mostly concerns transmission with 2 ms TTI, where only 3 power control commands are available to recover from an inaccurate setting of the transmission power at the beginning of each TTI. Nevertheless, L1 HARQ schemes can mitigate this problem by adding robustness to the link adaptation method based on fast closed loop power control.

Table 5.1 summarises the most important advantages and the disadvantages from introducing time division scheduling in the uplink of WCDMA systems.

Advantages	Disadvantages
▪ Channel-dependent scheduling ▪ High data rates have the potential for reducing the intra-cell interference for a fixed value of the total received uplink power ▪ High data rates have lower E_b/N_0 requirements ▪ Radio resource allocation based on near instantaneous buffer information ▪ Reduced transmission delay for short packet calls	▪ Increased time variability of inter-cell interference ▪ Limited UE power capabilities ▪ Uncertainty in the selection of the transmission power to be used at the beginning of each TTI ▪ Increased signalling overhead ▪ Frame synchronisation ▪ Coverage problem ▪ Measurement errors at the Node B

Table 5.1: Advantages and disadvantages of time division scheduling compared to a more traditional code division concept.

5.3 Simulation Assumptions

To recapitulate what introduced in Section 5.2, the main advantage of time division scheduling is the possibility to perform channel-dependent radio resource allocation, while the major disadvantage is the expected increase in the time variability of other-cell interference.

In order to focus on these two key aspects, the results presented in this chapter are based on some fundamental simplifications:

- *Information on the UE buffer state (empty/non-empty) is instantaneously available at the Node B on a per TTI basis.*

The buffer state indicates whether the UE transmission buffer is empty or non-empty. In practice it would be needed to signal from the UE to the Node B PS any change of the buffer state. This information is assumed to be available at the Node B PS instantaneously on a per TTI basis (scheduling rate). Due to the minimal signalling overhead required, it might not be impractical to have the UE buffer state available at the Node B PS with relatively low delays.

- *Accurate knowledge about the transmit power of each UE being served by the Node B on a per TTI basis, including accurate setting of the UE transmit power when the data rate changes*.

Information on the UE transmission power is needed at the Node B to perform channel-dependent scheduling, as well as not to allocate the users with a data rate they cannot support due to TFC elimination (see Section 5.3.2). In reality, information on the UE transmission power cannot be determined accurately by the UE, and cannot practically be signalled every TTI; hence, channel-dependent scheduling would need to rely on less frequent signalling to estimate the transmit power at every scheduling instant. The problem of accurately estimating the transmission power of each user served by the considered Node B has been neglected, and the Node B is assumed to know with precision the UE transmission power at a TTI resolution.

- *Accurate measurements of the received SINR are instantaneously available at the Node B PS on a per TTI basis*.

Information on the received SINR is used together with information on the UE transmission power to perform channel-dependent scheduling (see Section 5.3.2). Measurements of the received SINR are already used for fast power control operation. The assumption is made that these measurements are instantaneously available at the Node B PS on a per TTI basis. No measurement errors are considered.

- *Accurate estimates of the total average wideband received power at the Node B are instantaneously available at the PS on a per TTI basis*.

Due to measurement errors, to estimate accurately the total received wideband power over the short TTI interval is practically unfeasible, whereas the fact that the measurement are done at the Node B suggests that there should be no major problem in having the information available at Node B PS without delays. The simulation assumptions do no take into account the effect of any inaccuracy in the measurement of the average received power.

- *Delays associated with resource allocation are modelled generically*.

In the modelling, packet scheduling is implemented so to account for an allocation delay between the scheduling decisions at the Node B and the application of the allocated data rates by the scheduled UEs on the uplink DPDCH. It allows for the processing delay at the Node B, the time needed to signal the allocation, as well as for the processing delay at the UE.

Figure 5.7 illustrates the scheduling delay principle. It also specifies which information is available at the Node B PS, as well as the relation between the time at which such information is collected and the scheduling instant. In addition to the quantities previously introduced (buffer state, transmission power, SINR, and average received power at Node B), information on the UE selected data rate is also available at the Node B PS. This information is easily accessible from the TFCI field transmitted on the DPCCH [Holma04].

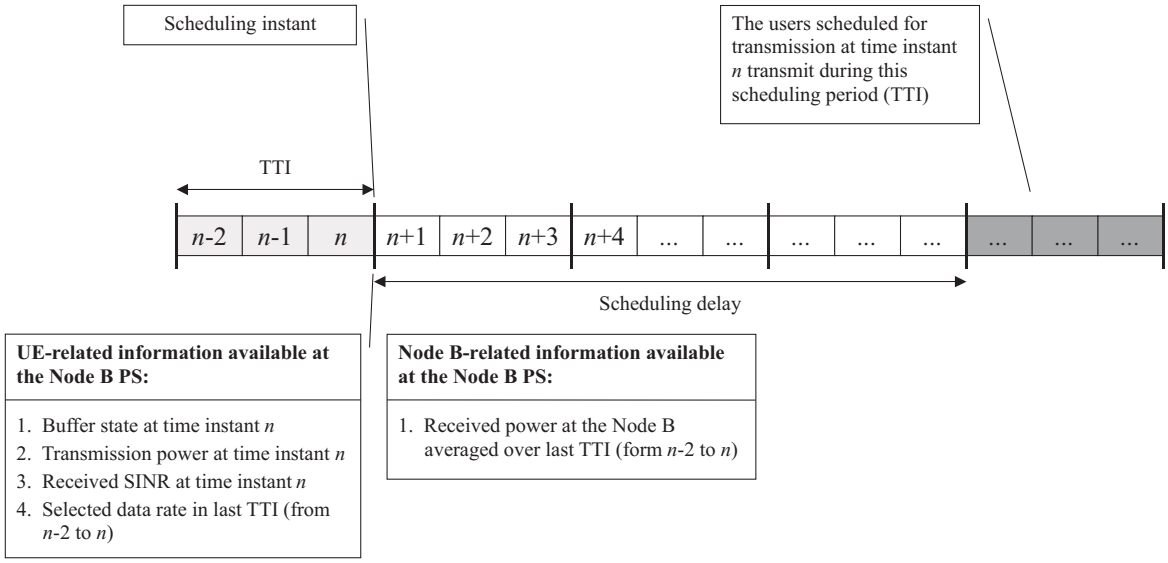

Figure 5.7: Scheduling delay, available information for scheduling and relation between the time at which this information is collected and the scheduling instant.

Moreover, the model used for the simulation of time division scheduling on DCH relies on two main assumptions:

- *Uplink transmissions within a single cell are fully synchronised*.

All uplink transmissions from several users within a single cell are TTI aligned, which implies that there is no overlap between transmissions from different users in different scheduling intervals.

- *The influence of signalling overhead has not been considered*.

The implications for the downlink of the scheduling related signalling are not considered. Similarly, the implications for the uplink signalling are also neglected, including here the effect on the uplink cell throughput.

5.3.1 Scheduling Principle

Based on these simplifications and assumptions, three algorithms for combined time and code division scheduling are proposed. All the considered scheduling algorithms operate at a scheduling rate of one TTI, and the common steps to all of them can be summarised as follows:

1. From the users that are currently served in the considered cell, the scheduler constructs a queue based on information about the UE buffer state. A user is included to the scheduling queue only if its buffer is non-empty.
2. The scheduling queue thus obtained is then ordered according to the particular scheduling policy (see Section 5.3.2).
3. Based on this rank, the Node B PS schedules the total amount of available power (up to the planned target) starting from the first user in the scheduling queue. The increase in the total received power due to each allocation is estimated by applying the same PIE used for the code division schedulers described in Chapter 3 and Chapter 4 (see Appendix B).
   a. The PS always tries to allocate the maximum supportable data rate at the UE. To this end, the PS must have information about the UE transmission power in order not to

allocate the users with data rates they cannot support due to transmission power limitations.

b. If there is not enough power available for scheduling, lower data rates than the maximum supportable can also be allocated. Though, a minimum allocated data rate is defined and no lower allocation is allowed.

c. A user is considered as scheduled irrespective of the allocated data rate. Hence, the Node B PS does not increase the scheduling priority of users scheduled with lower data rates.

The different steps of the scheduling procedure are illustrated in Figure 5.8, showing an example of the PS functioning in the case of combined time and code division scheduling. At the first scheduling instant only 2 out of 4 users having data in their buffers are scheduled for transmission; one is allocated 384 kbps (UE_2) and one 256 kbps (UE_3), the reason being the limited power available for scheduling. At the following scheduling instant UE_2 has no longer data to transmit, while new data has arrived in the buffer of UE_1. In the example a simple round robin scheduling strategy is assumed, therefore the 2 users who previously were not scheduled despite they had data to transmit (UE_4 and UE_6) have now higher priority. Notice that the priority of UE_3 is not increased after the first allocation, although the user was allocated only 256 kbps. In this way, the adopted resource allocation strategy can be temporarily unfair. At one scheduling instant, as more and more users are scheduled for

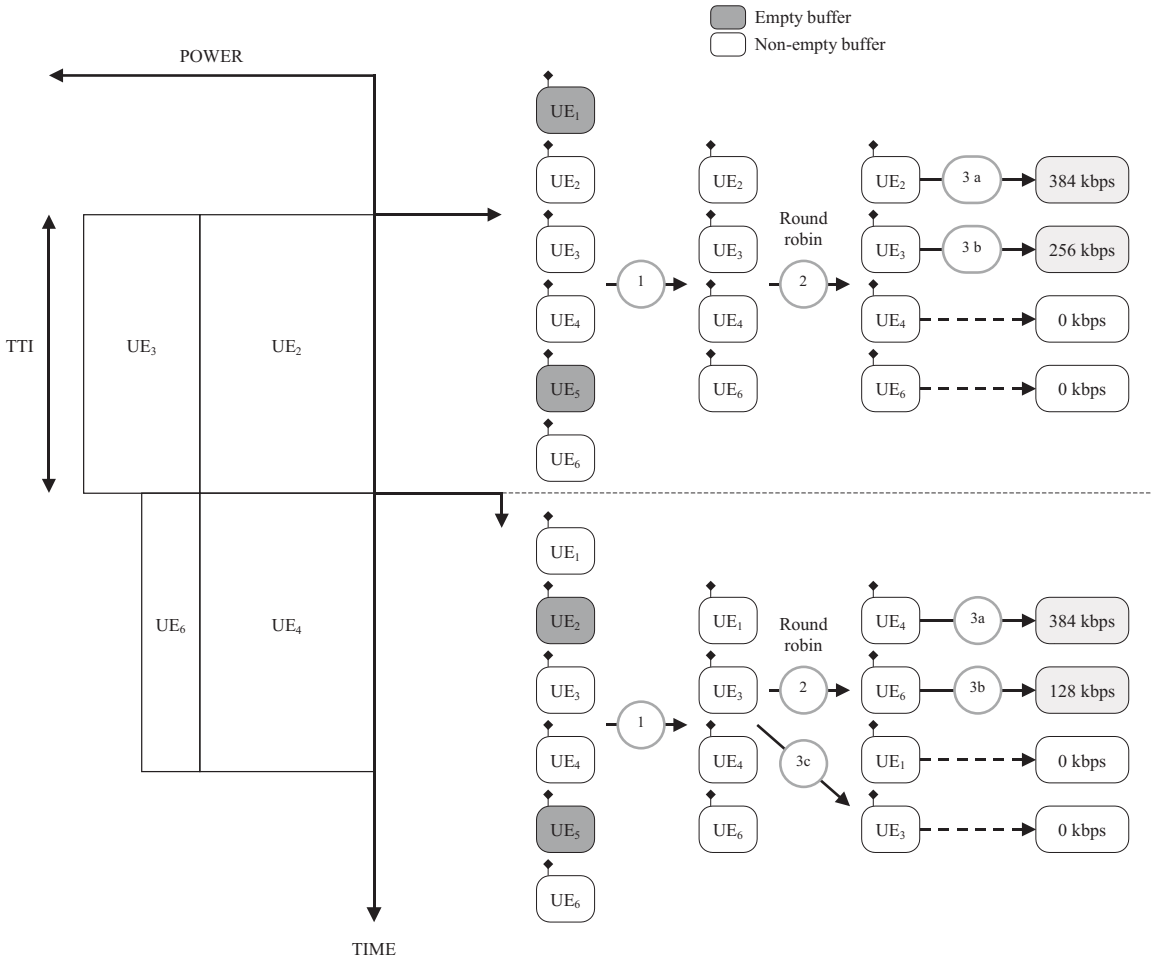

Figure 5.8: Example of the functioning of the packet scheduler based on time division scheduling in the case of round-robin allocation strategy. The numbers in the circles refer to the numbered items in the text explanation.

transmission, the available power for scheduling decreases. In the example of Figure 5.8, UE_3 and UE_6 are allocated only 128 kbps and 256 kbps, respectively. Though it is quite unlikely that the same user will end up with the lowest allocation the next time is being scheduled, a 'minimum allocated data rate to scheduled users'[4] is defined; instead of allocating a user with a very low data rate and moving him to the back of the scheduling queue, no resources are allocated and the user remains at the top of the queue. In this way the same user will likely be allocated with the maximum supportable data rate at the next scheduling instant.

5.3.2 Scheduling Algorithms

Next, three algorithms based on combined time and code division scheduling are described. A scheduler is defined 'fair resource' if on average it allocates the same amount of resources to all active users. In the uplink of WCDMA systems the resource to be shared is the total received wideband power at the Node B. As a consequence, a fair resource scheduler, on average, allocates the same amount of received power to different users; since fast power control is assumed, the implication is that users are granted the same average throughput performance. Hence, the terms 'fair resource' and 'fair throughput' can in this case be used interchangeably.

5.3.2.1 Blind Fair Throughput (BFT)

Users in the scheduler queue are time scheduled for transmission on DCH in a round robin fashion. This scheduling policy is based solely on UE buffer state information (empty/non-empty). The scheduler is 'blind' because it does not take into account channel-state information, and 'fair throughput' because it provides the users with the same channel access probability.

5.3.2.2 Maximise Transmit Power Efficiency (MTPE)

This scheduling strategy allocates uplink resources to those users that are estimated to experience the most favourable channel conditions with the scope to minimise the interference generated to neighbouring cells. This type of scheduler does not consider fairness issues and for this reason can be considered the uplink counterpart of the HSDPA maximum C/I scheduler [Kold03]. In order to perform channel-dependent scheduling of radio resources, we introduce the *Uplink Channel Quality Indicator* (*UCQI*). The *UCQI* for user *k* at time instant *n* (see Figure 5.7) is derived as:

$$UCQI_k[n] = \frac{R_k[n]}{TxPw_k[n]} \cdot SINR_k[n] \tag{5.8}$$

In (5.8), $TxPw_k[n]$, $R_k[n]$ and $SINR_k[n]$ are the transmission power, the transmission rate, and the received SINR of user *k* at time instant *n*, respectively. The quality measure defined in (5.8) is directly proportional to the achievable transmission rate per transmission power unit of user *k* at time instant *n*. The users in the scheduling queue are scheduled for transmission in descending order of the *UCQI* parameter. I.e., the MTPE algorithm prioritises users that can support the largest transmission rate for a given amount of transmission power. The MTPE scheduling rules resemble closely to the greedy rate packing algorithm proposed in [Berg04b].

5.3.2.3 Channel-State Aware Fair Throughput (CSAFT)

This scheduler is designed to offer a trade-off between user fairness and maximisation of cell throughput. Together with the instantaneous achievable transmission rate per transmission

[4] The simulation results presented in Section 5.4 assume a 'minimum allocated data rate to scheduled users' of 128 kbps.

power unit $UCQI_k[n]$, the Node B keeps track of the average value of $UCQI_k$ over a specified time period. The Node B then computes the *Relative UCQI* (*RUCQI*) as the ratio of the instantaneous *UCQI* to the average *UCQI*:

$$RUCQI_k[n] = \frac{UCQI_k[n]}{\langle UCQI_k \rangle} \tag{5.9}$$

In (5.9), the operator $\langle\rangle$ refers to time average[5]. The CSAFT scheduler prioritises users that experience constructive fading in relation to their average channel quality. As a consequence, it can be considered the uplink counterpart of the HSDPA Fast Fair Throughput scheduler presented in [Ameg03], and based on the concept introduced in [Barr02].

Figure 5.9 illustrates an example of the functioning of the three different scheduling algorithms in the case with only two simultaneously active users per cell. The BFT and the CSAFT are fair resource schedulers since they allocate the same amount of resources to each user for an equal amount of time. However, the CSAFT algorithm utilises information on both instantaneous and average channel quality to perform intelligent allocation of the radio resources. The MTPE is not a fair scheduler since it more often schedules for transmission users that in average experience better channel conditions.

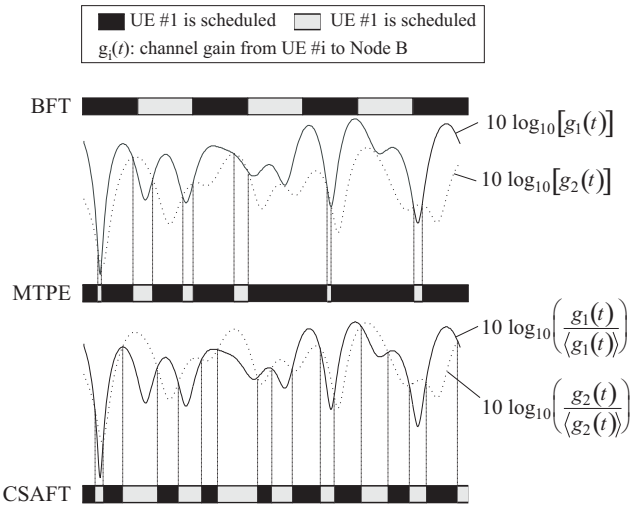

Figure 5.9: An example of the functioning of the three algorithms based on time division scheduling with only two users per cell simultaneously active.

5.3.3 Scenarios for System Level Simulations

In Section 5.4 the cell throughput and PCT performance with time and code division scheduling is compared to the performance of the reference RNC scheduler described in Chapter 3 and to the Node B code division scheduler introduced in Chapter 4. As for the Node B code division scheduler, the time and code division schedulers assume L1 HARQ type-II retransmission schemes, modelled as in Section 4.5.1. Soft handover functionality is also included, but in the case of combined time and code division scheduling only the serving Node B is allowed to perform scheduling decisions whenever a user is in SHO operation.

Refer to Table 3.2 and Table 4.4 for the parameter setup with RNC and Node B code division scheduling, respectively. More general parameters used in the system level simulations can be

[5] The simulation results presented in Section 5.4 assume an averaging period of 200 ms.

found in Appendix A. For convenience, Table 5.2 reports a comparison between the most relevant parameters for the simulation of the reference RNC code division (CD) PS, the Node B CD PS, and the Node B schedulers based on combined time and code division scheduling. In all the cases, the traffic model used is the same as in Chapter 3 and Chapter 4 (see Appendix D). Simulation results presented in Section 5.4 are obtained for both Vehicular A and Pedestrian A channel profiles at 3 km/h. The cell plan and propagation parameters for these two propagation scenarios are reported in Appendix A, while the corresponding AVI tables can be found in Appendix C.

		Scheduler		
		RNC - CD	Node B - CD	Time & Code
Packet Scheduling	Scheduling period	200 ms	100 ms	2 ms
	Modification period	600 ms	100 ms	2ms
	Scheduling delay	120 ms	40 ms	6 ms
	Maximum scheduled data rate	384 kbps	384 kbps	384 kbps
	TTI	10 ms	10 ms	2 ms
Retransmissions	Retransmission scheme	L2 ARQ	L1 HARQ type-II	L1 HARQ type-II
	Maximum number of L1 retransmissions	-	5	5
	BLER target (at 1st transmission)	1%	10%	10%

Table 5.2: Most relevant parameters for the simulation of the RNC code division scheduler, of the Node B code division scheduler and of the combined time and code division schedulers.

For what concerns the mapping between link and system level simulations, it should be mentioned that the AVI tables in Appendix C have been obtained assuming packet-switched services at 64 kbps, and for a TTI of 10 ms. Nevertheless, in the system level simulations they are used independently of the selected data rate. As a consequence, the following effects are not taken into account in the generated results:

- Due to the decreased DPCCH overhead, higher data rates have better E_b/N_0 performance compared to lower data rates.
- Since the autocorrelation properties of the spreading codes are not ideal, multipath components typically interfere with each other. If the processing gain is large, the inter-path interference term is negligible, but the higher the data rate the more clearly inter-path interference affects the E_b/N_0 performance.

These two are however opposing effects, and the overall impact on system level performance (especially on relative gain numbers between different scheduling strategies) is expected to be minimum. See Appendix C for details.

Moreover, AVI tables generated assuming 10 ms TTI are used in the case of 2 ms TTI size. This leads us to the following considerations:

- The size of the code block at the input of the turbo coder typically affects the physical layer performance. The higher the number of information bits, the better the performance of the turbo coder. However, for a code block size of approximately 400-500 bits the maximum coding gain is achieved, and further increasing the block size does not improve the turbo coder performance. Therefore the decrease in the performance of the turbo coder with 2 ms TTI can be considered negligible for data

rates above 200-250 kbps, which are most likely to be allocated with combined time and code division scheduling.

- With 2 ms TTI the interleaving gain is also reduced compared to 10 ms TTI, which is expected to have some impact on the physical layer performance. However, the results presented in this chapter only assume low mobility users (3 km/h). At this speed the coherence time of the fading channel is much larger than both 2 ms and 10 ms, and the interleaving gain from 10 ms TTI compared to 2 ms TTI can be assumed negligible.

Further issues on the use of AVI tables with 2 ms TTI are addressed in Appendix C.

Finally, based on these remarks, it is fairly reasonable to assume that the E_b/N_0 requirements are independent of the selected data rate and of the TTI size. Despite introducing some inaccuracy in the generation of absolute performance numbers, this underlying assumption allows focusing on the gain from packet scheduling when deploying the combined time and code division concept in the uplink of WCDMA systems.

5.4 Performance Evaluation

As for the previous chapters, first the performance of the proposed schedulers is separately analysed for a traffic-limited and an interference-limited scenario. Then, simulation results are obtained for different values of the average number of users per cell in order to emphasise the relation between cell throughput and PCT performance with combined time and code division scheduling. Finally, cell throughput results are compared when imposing a specific 10% PCT outage constraint. All the results presented and discussed in this section are obtained assuming a 5% NR outage constraint of 6 dB.

5.4.1 Interference-limited Scenario

For the case of an interference-limited system, Figure 5.10 plots the average cell throughput, the average packet call throughput (PCT) and the 10% PCT outage for the different scheduling scenarios introduced in Table 5.2. The gain numbers reported in Figure 5.10 are relative to the performance of the reference RNC CD scheduler.

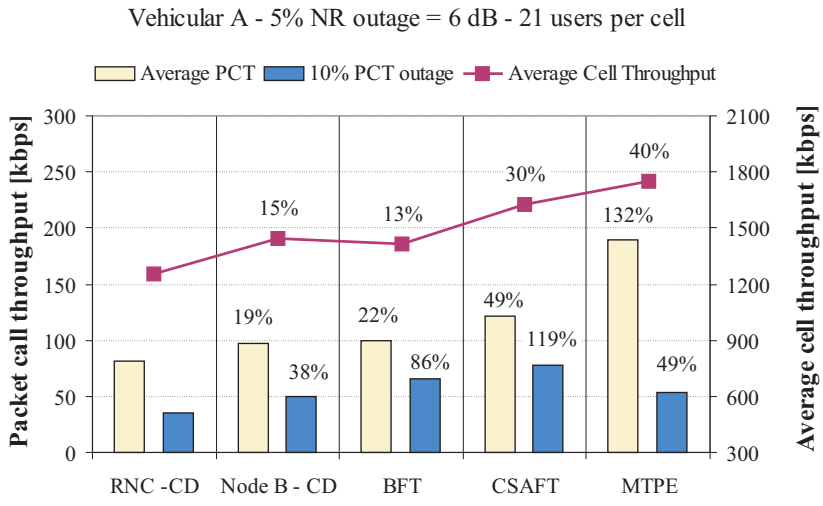

Figure 5.10: Average cell throughput, average PCT and 10% PCT outage for different scheduling scenarios and for an average of 21 users per cell.

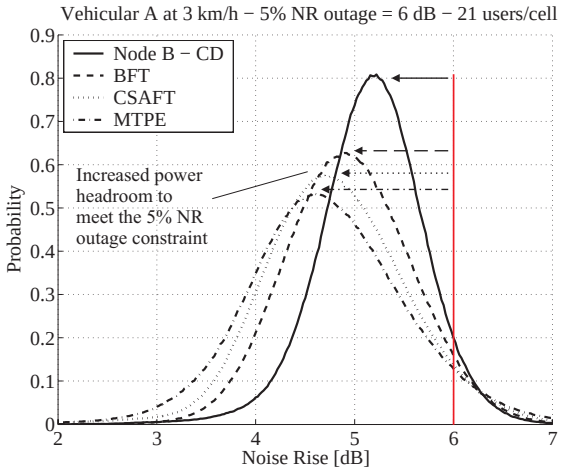

Figure 5.11: PDFs of the noise rise in the system for different scheduling scenarios.

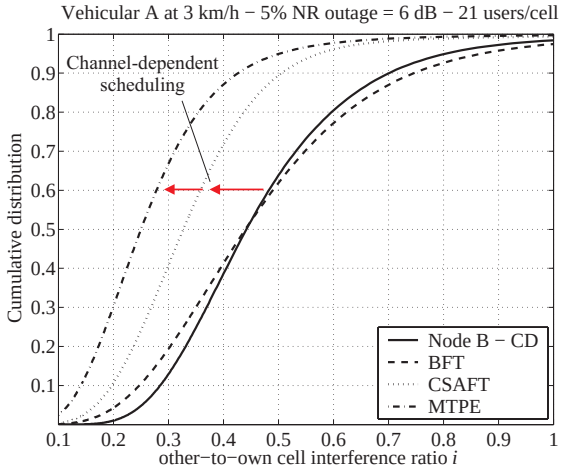

Figure 5.12: CDFs of the other-to-own cell interference ratio i for different scheduling scenarios.

The BFT algorithm is proven not provide any significant cell throughput gain compared to the Node B CD scheduler. The main reason is that the increased power headroom to meet the specified NR outage criteria (see Figure 5.11) is not balanced by any reduction in the interference generated to other cells (see Figure 5.12). In Figure 5.11 the power headroom to meet the specified NR outage criteria is shown to generally increase with combined time and code division scheduling. However, with the channel-dependent schedulers (CSAFT and MTPE) the reduction of the power headroom is compensated by a significant decrease of the interference generated to other cells, as illustrated in Figure 5.12. As a consequence, effectively the total cell throughput increases compared to Node B CD scheduling. While the MTPE algorithm maximises cell throughput at the cost of a low degree of fairness between the users, the CSAFT scheduler offers an appealing trade-off between cell throughput maximisation and fairness between users, significantly reducing the difference between average and 10% outage PCT performance (see Figure 5.10).

The different behaviour of the combined time and code division schedulers is clearly illustrated in Figure 5.13 and Figure 5.14. Figure 5.13 plots the CDF of the normalised packet call throughput (mean normalisation). The MTPE scheduler is an unfair scheduler, hence the probability of experiencing a packet call throughput lower than the average performance is relatively high. On the contrary, the BFT and the CSAFT are fair schedulers, as a consequence the distribution of the packet call throughput does not deviate much compared to the average value. The different fairness behaviour of the proposed time division schedulers can be better observed in Figure 5.14; for high values of the average path gain to the strongest Node B the average per TTI throughput with the MTPE scheduler is about 250 kbps, value that corresponds to the average source data rate and depends on the traffic model parameter setup (see Table 3.2). As soon as the average path gain to the strongest Node B is lower than approximately -105 dB, the average per TTI throughput with the MTPE scheduler starts to drop, and reaches approximately 10 kbps for an average path gain of -130 dB. The fair behaviour of the CSAFT and the BFT schedulers is evident by observing the constant throughput they guarantee almost independently from the average path gain to the strongest Node B. Only when the average path gain is below approximately -127 dB, the CSAFT and the BFT schedulers start to suffer from coverage limitations. Compared to the CSAFT, the MTPE scheduler can guarantee about 120% more throughput for high values of the average path gain to the strongest Node B, but at the same time users in unfavourable conditions can suffer from a performance loss up to 80%. Finally, the ability of the CSAFT scheduler to

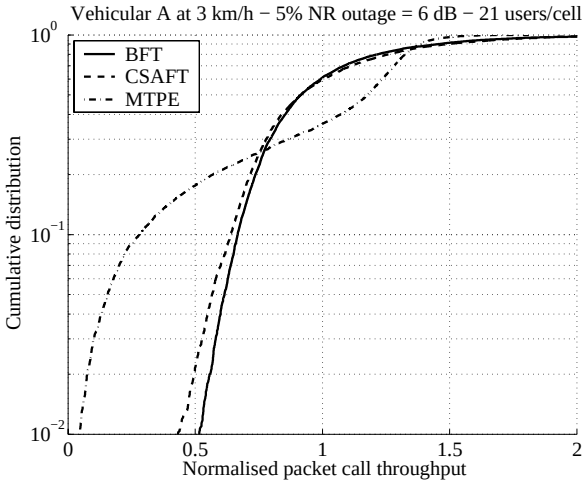

Figure 5.13: CDF of the normalised packet call throughput for the different time division schedulers.

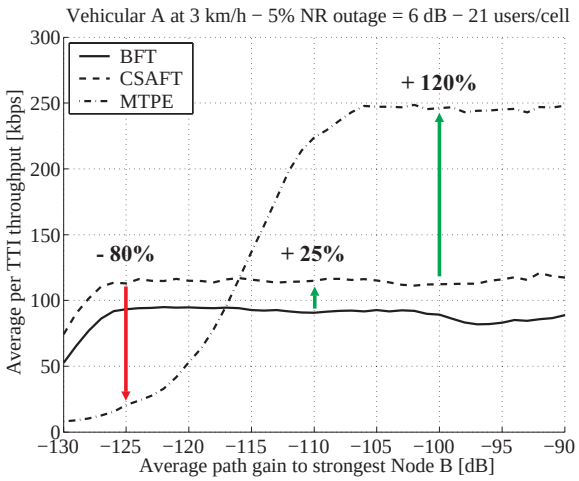

Figure 5.14: Average per TTI throughput for the different time division schedulers as a function of the average path gain to the strongest Node B.

perform channel-dependent scheduling provides a 25% gain over the entire average path gain range compared to the BFT scheduler.

The fast variability of uplink load introduced with combined time and code division scheduling can be observed in Figure 5.15 and Figure 5.16, which plot the autocorrelation functions of the noise rise and of the average per TTI E_b/N_0. The time traces used to compute these autocorrelation functions are obtained from a reference Node B for the noise rise, and from a reference UE for the average per TTI E_b/N_0. Compared to the Node B CD scheduler, the time division schedulers introduce fast and uncorrelated variations in the NR on a per TTI basis, and consequently a similar effect to the received E_b/N_0. As a general observation, the channel-dependent schedulers show better correlation properties compared to the BFT scheduler. This can be explained by the fact that the CSAFT and MTPE algorithms prioritise users experiencing favourable channel conditions. In a low mobility scenario, if a user is scheduled for transmission in one TTI there is a high probability that he will be scheduled also in the next scheduling period, thus reducing the fast variations caused in the total received power at the Node B. Quite the opposite happens with the BFT scheduler where, due

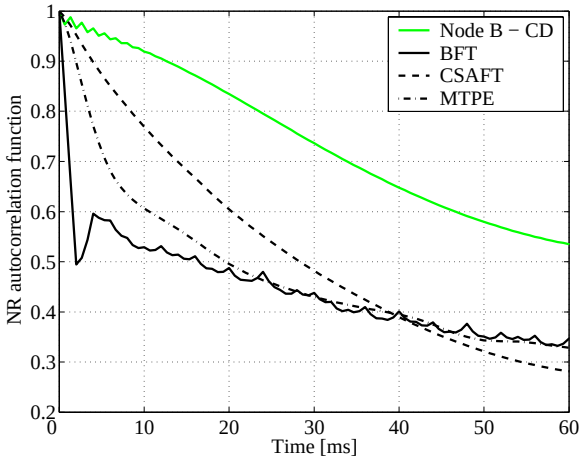

Figure 5.15: Autocorrelation of the instantaneous NR for the different time division schedulers and for the Node B CD scheduler.

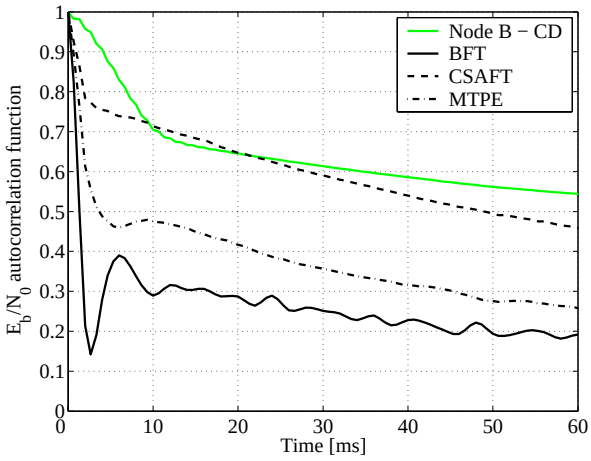

Figure 5.16: Autocorrelation of the per TTI E_b/N_0 for the different time division schedulers and for the Node B CD scheduler.

to the round robin allocation policy, a user scheduled for transmission in one TTI will likely not be scheduled in the next one.

In Figure 5.15 it can be observed that the correlation of the noise rise is higher for the CSAFT scheduler than for the MTPE scheduler, the reason being that with the CSAFT users are typically scheduled for transmission when 'at the top of a fade', i.e. when the time variability of their fading channel is minimum. This results in a reduction of the fast variability of uplink received power, which also explains why the correlation properties of the per TTI E_b/N_0 in the case of the CSAFT scheduler are close to those of the Node B CD scheduler. In Figure 5.16, it can be seen how the fast variations introduced with time division scheduling are likely to influence the performance of the link adaptation mechanism based on fast power control especially for the BFT scheduler.

The fast variations introduced with time division scheduling can in part explain the increased power headroom to meet the specified NR outage criteria compared to the Node B CD scheduler (see Figure 5.11). Another explanation is that time division scheduling significantly changes the idea lying behind the power scheduling procedure compared to traditional code division schedulers.

Code Division Scheduling – With code division scheduling the main goal is to adapt the radio resource allocation to the varying propagation and traffic conditions so as to keep the uplink load as close as possible to the planned target. In this perspective, in Chapter 4 the Node B CD scheduler has been shown to improve the performance of an RNC-based scheduler by making data rate modifications more dynamic and dependent on the actual utilisation of the allocated radio resources. Based on average measurements of the total received uplink power, the power scheduler performs relatively small modifications of the allocated radio resources, and the system then evolves towards a new operating point.

Time Division Scheduling – With time division scheduling the rate at which the radio resource are reallocated to NRT users considerably increases compared to traditional code division schedulers, and at the same time the extent of the modifications to the allocated resources is significantly increased. As a consequence, the capability of the power-based code division schedulers to keep the uplink load close to the planned target is partially lost. The effect is a decrease of the average noise rise when specific NR outage criteria are defined.

5.4.2 Traffic-Limited Scenario

In a traffic-limited scenario the gain from channel-dependent scheduling (CSAFT and MTPE) in terms of both cell throughput and average packet call throughput generally decreases compared to an interference-limited scenario (see Figure 5.17 and Figure 5.10). With only a few users per cell the multi-user diversity in the system reduces, hence the gain achievable with channel-dependent scheduling decreases. In principle, with a very low number of users in the network the MTPE and CSAFT converge to BFT performance, and the only gain left is from faster scheduling operation based on near, instantaneous buffer-state information, and from the allocation of high peak data rates. Short packet data sessions particularly benefit from the allocation of high peak data rates based on near instantaneous buffer information, which explains the quite significant gain in 10% PCT outage performance with combined time and code division schedulers in a traffic-limited scenario.

5.4.3 Cell Throughput vs. PCT Performance

To illustrate the relation between uplink cell throughput and the level of satisfaction of the users in the network, Figure 5.18 plots the probability of experiencing a packet call

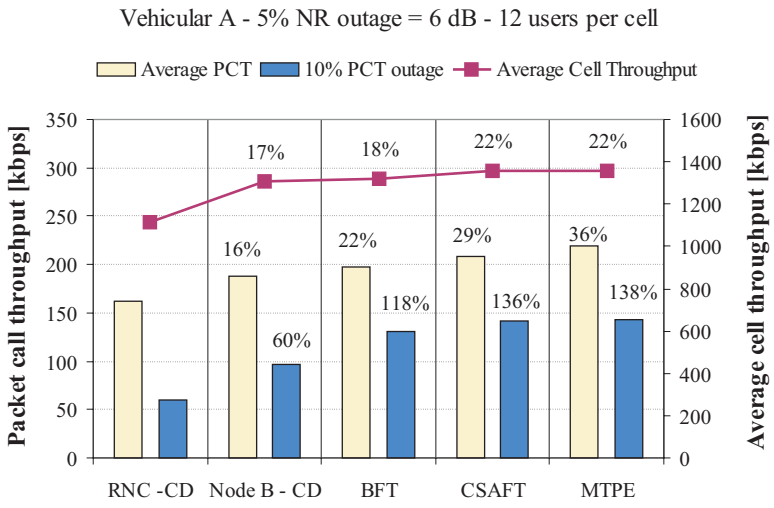

Figure 5.17: Average cell throughput, average PCT and 10% PCT outage for different scheduling scenarios and for an average of 12 users per cell.

throughput (PCT) lower than 64 kbps as a function of the average cell throughput for the combined time and code division schedulers, and for the Node B CD scheduler.

In the presented comparison, the CSAFT scheduler outperforms all the other scheduling algorithms and provides the highest cell throughput given a probability of experiencing a PCT lower than 64 kbps in the range between 1% and 10%. The tighter the PCT outage constraint, the higher the gain from CSAFT scheduling over the Node B CD and the MTPE schedulers. Given a 2% probability of experiencing a PCT lower than 64 kbps, the CSAFT can achieve a cell throughput gain of 30%, 18% and 14% compared to the Node B CD, the MTPE and the BFT schedulers, respectively. Notice that for low values of the probability of experiencing a PCT lower than 64 kbps, the BFT algorithm outperforms both the Node B CD and the MTPE schedulers. However, when the PCT outage constraint is relaxed further, the BFT is not able to achieve higher cell throughput, and for a probability of experiencing a PCT lower than 64

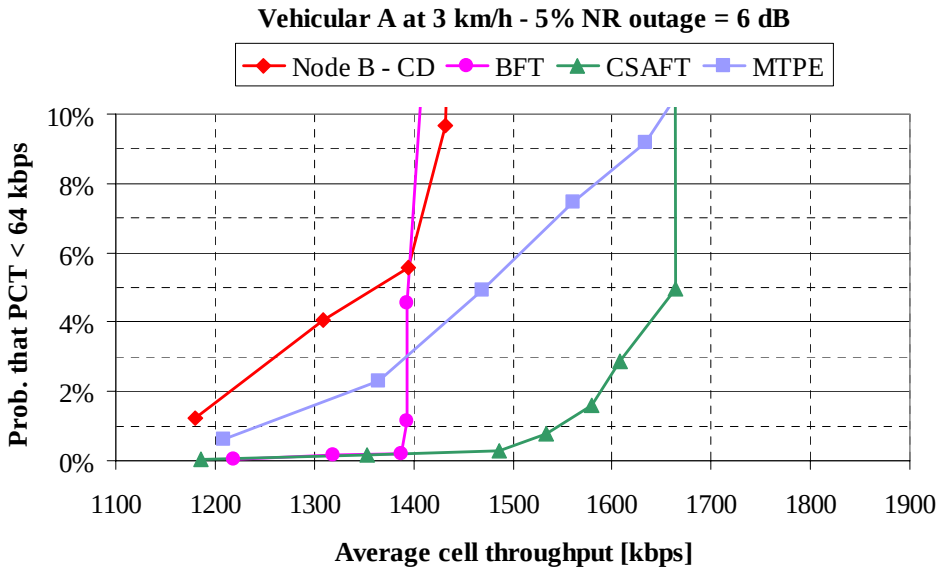

Figure 5.18: Probability of experiencing a packet call throughput < 64 kbps as a function of the average cell throughput for different scheduling scenarios, Vehicular A channel profile at 3 km/h, and 5% NR outage of 6 dB.

	Scheduler	Average cell throughput [kbps]	Gain relative to the RNC - CD scheduler	Gain relative to the Node B - CD scheduler
Code division schedulers	RNC - CD	1093.8	-	-
	Node B - CD	1410.3	29%	-
Time & code division schedulers	BFT	1409.5	29%	0%
	CSAFT	1653.8	51%	17%
	MTPE	1640.0	50%	16%

Table 5.3: Average cell throughput and relative gain numbers for different scheduling scenarios with Vehicular A channel profile at 3 km/h, 10% PCT outage of 64 kbps, and 5% NR outage of 6 dB.

kbps above 5% it is shown to be the worst performing scheduling strategy. Moreover, as more and more unsatisfied users are allowed in the network, the cell throughput performance of the MTPE scheduler get closer to the achievable cell throughput with CSAFT scheduling.

5.4.4 Cell Throughput Performance Given a Specific PCT outage Constraint

In this section, the different scheduling concepts are compared under the same 10% PCT outage constraint. Simulations have been run while adjusting the number of users in the system so to obtain the same 10% PCT outage of 64 kbps for all the considered scheduling scenarios. Table 5.3 reports the average cell throughput for a 5% NR outage of 6 dB, a 10% PCT outage of 64 kbps and for Vehicular A channel profile at 3 km/h.

When imposing a specific outage constraint on the PCT performance, the CSAFT algorithm takes advantage of its capability to make a fair distribution of the radio resources between the users, while still exploiting instantaneous channel-state information. It achieves the maximum cell throughput performance, with a 51% gain over the RNC scheduler. The corresponding cell throughput increase compared to the Node B CD scheduler is 17%. Despite the additional complexity introduced (see Section 5.2.2.3), the BFT algorithm does not provide any relevant gain compared to the Node B CD scheduler.

The same results are reported in Table 5.4, but for a Pedestrian A channel profile at low mobile speed. Also in this propagation environment the CSAFT is confirmed as the most performing algorithm, with a cell throughput increase of 78% and 29% with respect to the RNC CD and the Node B CD schedulers, respectively. Due to the lower inherent diversity in the Pedestrian A channel profile, the gain from channel-dependent scheduling is higher compared to Vehicular A. For the same reason, the impact of time scheduling on the time variability of uplink load is more significant with Pedestrian A channel profile, thus the BFT algorithm presents a slight performance decrease compared to the Node B CD scheduler.

	Scheduler	Average cell throughput [kbps]	Gain relative to the RNC - CD scheduler	Gain relative to the Node B - CD scheduler
Code division schedulers	RNC - CD	1065.6	-	-
	Node B - CD	1468.9	38%	-
Time & code division schedulers	BFT	1392.9	31%	-5%
	CSAFT	1893.7	78%	29%
	MTPE	1822.9	71%	24%

Table 5.4: Average cell throughput and relative gain numbers for different scheduling scenarios with Pedestrian A channel profile at 3 km/h, 10% PCT outage of 64 kbps, and 5% NR outage of 6 dB.

5.4.5 Discussion on the Impact of Non-Ideal Channel Quality Estimation, Increased User Mobility and Signalling Overhead

In this last section simulation results are introduced that show the impact of non-ideal channel quality estimation on the performance of the CSAFT scheduling strategy. Moreover, a discussion on the effect of the increased signalling overhead with channel-dependent radio resource allocation based on combined time and code division scheduling is presented, with focus on the potential impact on uplink capacity.

The proper functioning of the Node B CSAFT scheduler is based on accurate estimations of the uplink channel quality. Channel quality estimations are performed using (5.8), i.e. every TTI the Node B PS needs to have knowledge of: (i) the received SINR on the DPCCH, (ii) the data rate used for transmission on the DPDCH, and (iii) the corresponding UE transmission power. While the DPCCH SINR is already measured at the Node B on a time slot basis to execute fast closed loop PC, and the DPDCH data rate can be derived from the TFCI field transmitted on the DPCCH, information on the UE transmission power needs to be signalled from the UE to the PS. Provided that this information can be signalled in the uplink on a TTI basis (similarly to CQI reporting in HSDPA [Kold03]), a major drawback is still represented by the fact that the transmission power cannot be measured at the UE with absolute precision [TS25101]. Therefore, the assumption is made that the information on the UE transmission power used at the PS to estimate the channel quality is corrupted with a lognormal distributed error to allow for measurement inaccuracy.

$$10 \cdot \log_{10}\left(TxPw_k^{\,UCQI}[n]\right) = 10 \cdot \log_{10}(TxPw_k[n]) + \sigma \tag{5.10}$$

In (5.10), $TxPw_k[n]$ is the transmission power of user k at time instant n (see Figure 5.7), $TxPw_k^{\,UCQI}[n]$ is the corresponding information used for channel quality estimation at the PS, and σ is a normal distributed random variable with zero mean and specified standard deviation. The cell throughput gain with CSAFT scheduling compared to both RNC CD and Node B CD scheduling given specific outage constraints on the noise rise and on the packet call throughput is plotted in Figure 5.19 as a function of the standard deviation of σ. As

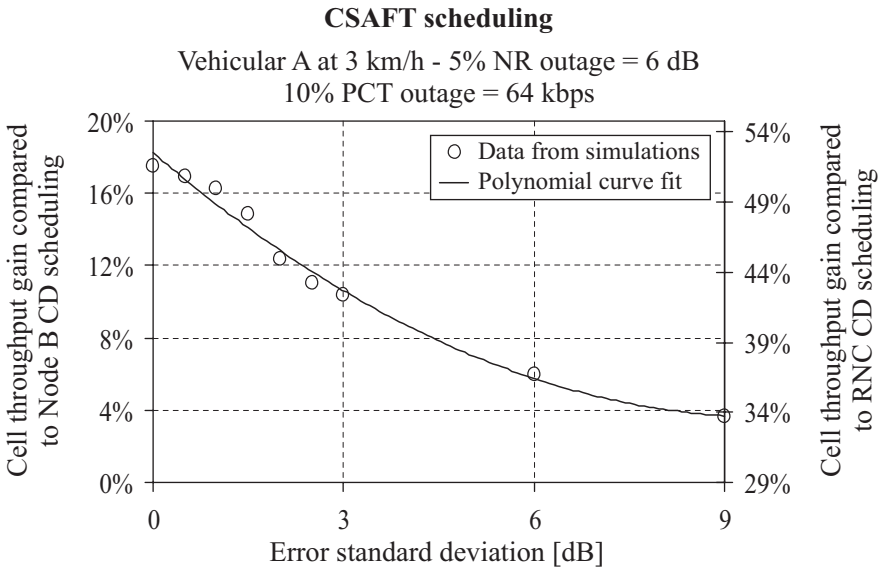

Figure 5.19:.Cell throughput gain from CSAFT scheduling compared to both RNC CD and Node B CD scheduling as a function of the standard deviation of the UE transmission power measurement error.

expected, the gain from channel-dependent scheduling reduces as the error standard deviation increases, although the gain is still quite significant for values of the error standard deviation below 3 dB (which is a good approximation of the measurement accuracy specified by the 3GPP [TS25101]).

Apart from measurement inaccuracy at the UE, channel-dependent scheduling can potentially suffer from increased user mobility, in which case CSAFT converges to BFT performance. Moreover, to make information on the UE transmission power available at the Node B PS additional signalling is required from the UE to the Node B on a TTI basis. The increased signalling overhead to perform channel-dependent scheduling has therefore a direct impact on the uplink cell throughput performance. In real implementation of WCDMA networks all these practical issues are expected to somewhat reduce the gain from CSAFT scheduling compared to Node B CD scheduling, which on the other hand can be implemented with limited complexity and necessitates less signalling overhead. For all these reasons, in Release 6 of the 3GPP specifications code division scheduling techniques are currently preferred to combined time and code division strategies for the enhancement of uplink packet access [TR25896].

5.5 Summary

In this chapter a new scheduling concept for WCDMA uplink based on combined time and code division scheduling has been introduced. Inherently, time division scheduling on a TTI basis has both advantages and disadvantages compared to traditional code division scheduling, and also introduces additional complexity. The main advantage of time division scheduling is that users can be scheduled for transmission with high instantaneous data rates and when experiencing favourable channel conditions, thus reducing the interference generated to other cells and consequently with an increase in uplink spectral efficiency. The performance of three different algorithms based on combined time and code division scheduling has been assessed by means of system level simulations which allow to include the impact of time scheduling on the time variability of both uplink load and other-cell interference, on fast power control performance, etc. Moreover, two of the proposed algorithms make use of an appositely defined uplink channel quality indicator to exploit channel-state information during the scheduling procedure. Despite of an inherent increase in the power headroom required to meet the specified NR outage criteria, channel-dependent scheduling is able to provide a significant performance increase compared to traditional code division schedulers.

An unfair scheduler (MTPE) that always allocates the uplink radio resources to the users with best channel conditions achieves the maximum cell throughput. On the other hand, a fair throughput scheduler (CSAFT) that still makes use of channel-state information in the scheduling procedure can guarantee an attractive trade-off between throughput maximisation and fairness between users. Under specific assumptions for the traffic model and for the number of users in the network, the MTPE scheduler can provide approximately 120% (from 115 to 250 kbps) more throughput to users in favourable channel conditions compared to the CSAFT strategy, with a corresponding performance loss of about 450% (from 115 to 20 kbps) for unfortunate users.

As an illustration of the trade-off between cell throughput maximisation and fairness between users, the CSAFT algorithm has been shown as the most performing scheduling strategy when a specific PCT outage constraint is considered. For a 5% NR outage of 6 dB and a 10% PCT outage of 64 kbps, the CSAFT scheduler provides a cell throughput increase of about 50% in a macro-cell environment at low mobile speed compared to a reference RNC-located PS. The

gain is as large as 78% in a micro-cell environment at low mobile speed. The gain numbers respectively reduce to 17% and 29% when compared to the performance of the Node B code division scheduler introduced in Chapter 4.

Despite the complexity and practical implementation issues discussed in Sections 5.2.2.3 and 5.4.5, the proposed time and code division schedulers can guarantee an enhancement in both cell throughput and packet call throughput performance compared to traditional code division scheduling. Especially the CSAFT scheduler is promising a quite significant improvement by increasing the uplink spectral efficiency while maintaining the QoS requirements.

Chapter 6

Performance of High Data Rates, 4 Rx Antenna Diversity and Interference Cancellation in WCDMA Uplink

6.1 Introduction

Among the emerging technologies aimed at improving the spectral efficiency of 3G systems, two of the most promising solutions are antenna arrays and multi-user detection (MUD) [Verdu00]. These techniques are particularly suitable for enhanced uplink performance since the additional complexity they require is concentrated at the receiver side. Both antenna arrays and MUD can be deployed to improve cell capacity and/or coverage. To this end, they can represent a flexible solution for network operators in the transition between early implementation of WCDMA networks, where uplink coverage will be the main limiting factor, and later extensions, where uplink capacity becomes an issue due to the introduction of more demanding uplink services.

6.1.1 Antenna Arrays

Concerning the deployment of antenna arrays at the base station receiver, the basic choice is whether to maximise diversity or antenna gain. In [Ylit00], a performance evaluation of different antenna array approaches for WCDMA uplink is presented. It is shown how the diversity and beamforming concepts perform similarly with a small number of antennas per sector, while the conventional beamforming approach starts to overcome the diversity techniques with a large number of antennas and low azimuth spread. However, diversity techniques are shown to perform better in low mobility environments since longer averaging periods can be applied for better channel estimates. Concerning diversity techniques, this

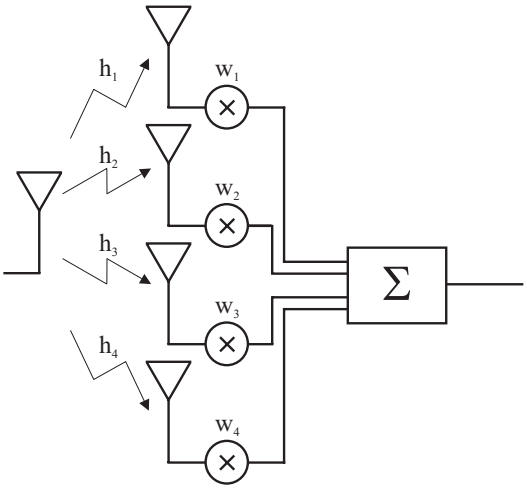

Figure 6.1: Receiver structure with 4-branch antenna diversity.

paper also compares maximal ratio combining (MRC) with interference rejection combining (IRC), and shows that the gain from IRC is modest in CDMA due to closed loop power control which drives the operation point in a normally loaded network to a level in which the interference to noise ratio is small. Some diversity techniques for WCDMA uplink have been presented and their performance investigated in [Tiir03]. The main conclusion of this paper is that doubling the number of receiving antennas is much more effective than introducing the second transmitting antenna at the terminal. Finally, in [Holma01] the performance of uplink 4-branch antenna diversity is studied by means of both link level simulations and field measurements; results show that 4-branch reception gives a coverage gain compared to 2-branch receiver diversity between 3 and 4 dB, depending on the propagation environment. Figure 6.1 illustrates an example of the receiver structure with 4-branch antenna diversity.

6.1.2 Multi-User Detection

Although multiple access interference (MAI) is often approximated as additive white Gaussian noise (AWGN) [Proak95], in reality it consists of distinctly received signals of CDMA users. As a consequence, multiple access interference possesses some structure and can be taken into consideration in the receiver. Verdú was able to demonstrate that CDMA is not inherently interference-limited, but rather limited by the conventional matched filter receiver [Verdu98]. However, the optimal multi-user detector in [Verdu86] presents a major drawback: Its implementation complexity is an exponential function of the number of users, and as a consequence it is not feasible for most practical CDMA receivers. This has led to a large number of publications on suboptimal multi-user receivers. Authors in [Duel95] and [Mosh96] present a survey of MUD for CDMA communication systems, while a more detailed simulation comparison between the most common MUD receivers for cellular CDMA is given in [Bueh00]. One way to perform MUD is through interference cancellation (IC): The basic principle underlying IC is the creation at the receiver of separate estimates of the MAI contributed by each user in order to subtract some or all of the MAI seen by each user. Figure 6.2 depicts the simplified structure of a single-stage parallel interference cancellation receiver for two users [Holma04].

The impact of IC techniques on the capacity of CDMA uplink has been more in detailed addressed in [Hämä96] and [Meng03] for parallel and successive interference cancellation, respectively. However, both papers estimate the capacity gain from IC for a given outage probability, i.e. the probability that the SINR is lower than a specified target. More comprehensive user performance metrics are not considered, and traffic model issues are also neglected. Moreover, the results are obtained by means of Monte Carlo simulations. In [Meng03], the effect of fast fading is also not included.

6.1.3 Combined Performance of Antenna Arrays and MUD

The combined performance of adaptive antennas and multi-user detection for WCDMA uplink is investigated in [Hern00], showing a considerable performance improvement over the single antenna receiver with a matched filter. In [Dahl00], the authors also consider the case in which no directional information of the impinging waves is exploited for the demodulation in

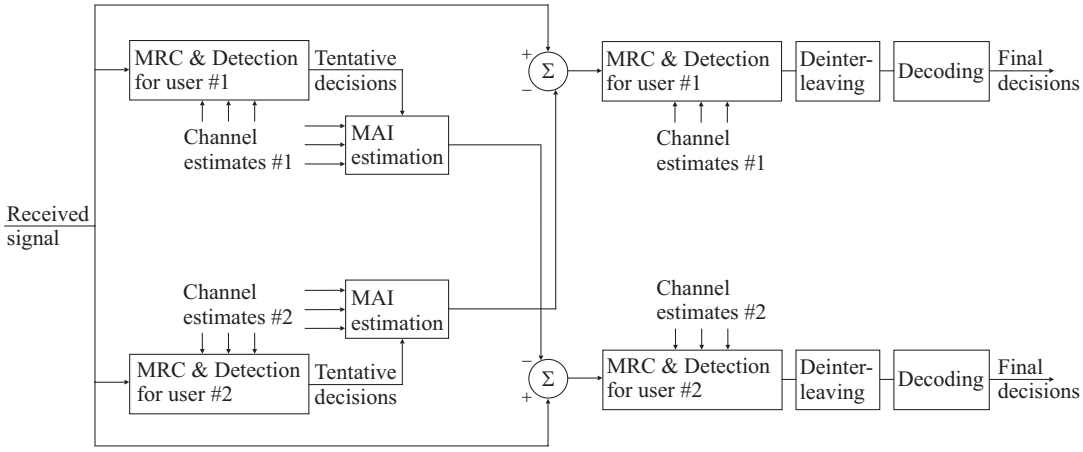

Figure 6.2: Parallel interference cancellation receiver for two users [Holma04].

uplink, thus essentially reducing the smart antenna approach to a space diversity scheme. For channel environments with a large angular spread, the space diversity schemes with IC are shown to represent an attractive solution in terms of e.g. complexity and robustness against calibration errors of the antenna array.

6.1.4 Objective

For what concerns MUD, the objective of this last chapter is to investigate the impact that IC techniques have on both cell throughput and packet call throughput performance in the uplink of WCDMA systems. In particular, the focus is on the performance enhancement achievable when IC techniques are combined with the advanced packet scheduling strategies introduced in the previous chapters. To evaluate the various methods used to perform interference cancellation is out of the scope of the presented analysis. To this end, results are obtained for different values of the MUD efficiency as defined in [Hämä96], but independently of the specific IC technique that provides such efficiency.

Moreover, based on the conclusions in [Dahl00] discussed in Section 6.1.3, we specifically consider a space diversity configuration with 4 receiving antennas (see Figure 6.1), i.e. no conventional beamforming techniques are investigated.

The chapter is organised as follows: First, in Section 6.2 the impact on uplink packet access performance from the allocation of peak data rates up to 768 kbps is investigated. To focus on the benefit from the allocation of high data rates, the system is initially assumed to operate with the same basic features as in previous chapters, i.e. 2-branch antenna diversity and conventional matched filter receiver. Then, in Section 6.3 the performance enhancement provided by 4-branch antenna diversity and IC techniques is investigated. Results are shown and discussed for both code division and combined time and code division scheduling. Concerning the cell throughput gain from multi-user detection, a theoretical analysis is also presented, and semi-analytical results compared to the outcome from system level simulations. Finally, the concluding remarks are given in Section 6.4.

6.2 Allocation of Peak Data Rates up to 768 kbps

In this section, the impact from the allocation of data rates as high as 768 kbps on the cell throughput and packet call throughput performance of WCDMA uplink is investigated. On the uplink physical channel the user data rate of 768 kbps is achieved using multi-code transmission, in particular simultaneously transmitting on two DPDCHs (see Figure C.1 in Appendix C). In general, with multi-code transmission the peak-to-average ratio (PAR)

performance of the power amplifier is decreased [Outes04]. However, results in [Rata02] show that with two DPDCHs the performance decrease compared to single-code transmission is marginal due to the fact that both DPDCHs use the same channelisation code (see Figure C.1). Therefore, the PAR issue for data transmission at 768 kbps is neglected in the presented analysis.

In the following sections, the effect of high data rate allocations is investigated for both code division and time division scheduling. Based on the results in Chapter 5, the best performing scheduling strategies in the case of code division and combined time and code division scheduling are selected for performance evaluation, namely the Node B CD PS introduced in Chapter 4, and the CSAFT scheduler introduced in Section 5.3.2.3, respectively.

6.2.1 Code Division Scheduling: the Node B CD Scheduler

6.2.1.1 Traffic Modelling

With code division scheduling users are simultaneously scheduled for transmission, and at a given time instant are likely to be allocated the same data rate due to the fair resource approach used by the Node B CD scheduler. With code division scheduling the allocation of peak data rates higher than 384 kbps makes sense only when data traffic in the UE buffer is instantaneously generated at a rate higher than 384 kbps. As a consequence, in order to investigate the impact from the allocation of data rates as high as 768 kbps on the performance of the Node B CD PS, a new parameter setup for the traffic model is introduced. This new model is referred to as modified traffic model so to distinguish it from the default traffic model used in previous chapters (see Appendix D). For convenience, the parameter setup for both the default and the modified traffic models is reported in Table 6.1.

				Default	**Modified**
Packet Call	Distribution of packet call period	Exponential	Mean	5 s	5 s
	Distribution of reading time	Exponential	Mean	5 s	5 s
Datagram	Distribution of inter-arrival time between datagrams	Log-Normal	Mean	40 ms	50 ms
			Standard deviation	38 ms	47 ms
	Size (Fixed)			1152 bytes	3000 bytes
Resultant average source rate during packet call periods				≅ 250 kbps	≅ 495 kbps

Table 6.1: Parameters setup for the modified and the default traffic models.

6.2.1.2 Simulation Results

The results presented in this section have been obtained assuming Node B CD scheduling, the modified traffic model, and basic system features such as 2-branch antenna diversity and conventional matched filter receiver. The propagation scenario is macro-cellular with Vehicular A channel profile and a user speed of 3 km/h. The cell throughput and PCT performance with peak data rates up to 768 kbps is compared to the case in which the maximum data rate allocated by the PS is 384 kbps.

With basic system features and for the considered propagation and mobility scenario, the maximum achievable throughput in the uplink of a WCDMA cell with the Node B CD PS ranges around 1.15 and 1.5 Mbps, depending on whether the system is operating in a traffic-limited or in an interference-limited region. The allocation of 768 kbps with code division scheduling only makes sense for a low average number of users per cell, i.e. in the traffic-limited region. In principle, with more than 3-4 NRT users simultaneously transmitting and a

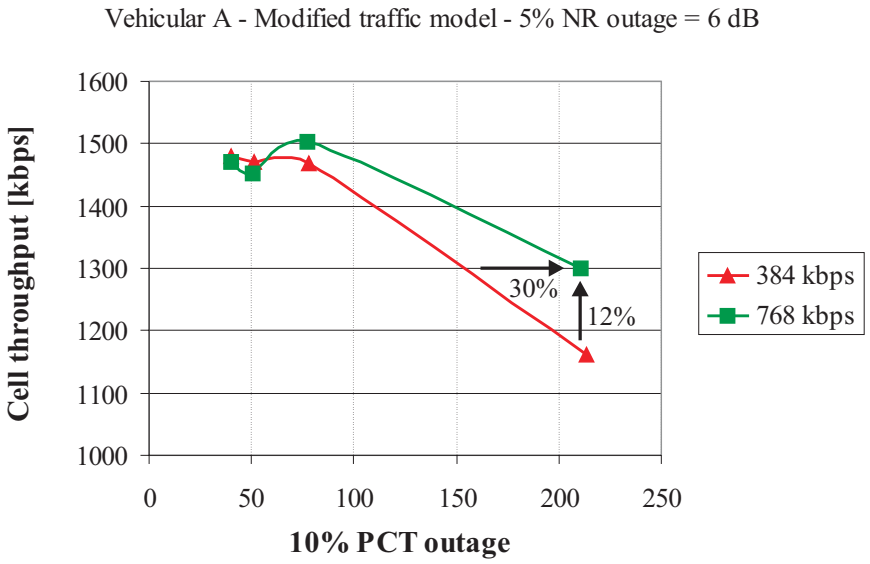

Figure 6.3: Average cell throughput as a function of the 10% PCT outage for the Node B CD scheduler with both 384 and 768 kbps as maximum scheduled data rate.

fair resource allocation policy, the allocation of 768 kbps is not possible. The simulation results in Figure 6.3 show that a peak data rate of 768 kbps compared to 384 kbps can enhance the 10% PCT outage by 30% in the traffic-limited region; the corresponding cell throughput increase is about 12%. However, as soon as the number of users in the network is increased and the scenario becomes interference-limited, no difference can be observed between 768 kbps and 384 kbps as maximum scheduled data rate.

Due to the code-division fair-resource scheduling approach, the probability of being allocated (and therefore selecting) high data rates depends on the number of users in the network, as illustrated in Figure 6.4 and Figure 6.5.

Traffic-Limited scenario: With an average of 6 users per cell the availability of transmission rates higher than 384 kbps is actually exploited, with a probability of selecting 768 kbps close to 20%. With only 384 kbps as maximum supportable data rate the cell throughput and packet call throughput performance is constrained by the limited UE capabilities. This leads to an increased PCT performance when 768 kbps is introduced, and to an equivalent cell throughput enhancement (see Figure 6.3).

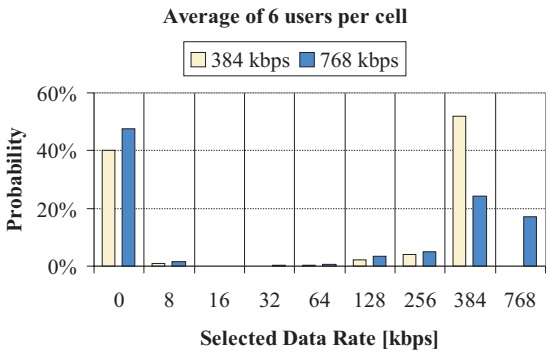

Figure 6.4: Distribution of the selected data rate for an average of 6 users per cell and maximum scheduled data rate of both 384 kbps and 768 kbps.

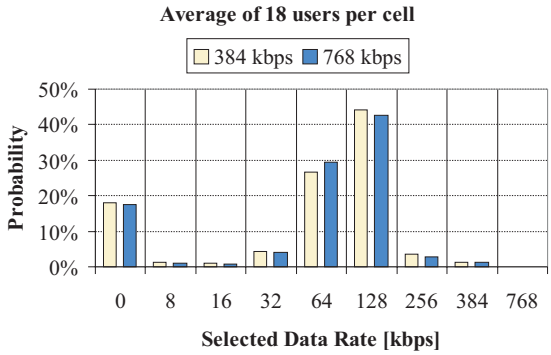

Figure 6.5: Distribution of the selected data rate for an average of 18 users per cell and maximum scheduled data rate of both 384 kbps and 768 kbps.

Interference-Limited scenario: With an average of 18 users per cell, the available uplink resources must be shared between several NRT users that simultaneously transmit on DCH. In this case the availability of 768 kbps makes no difference, since such a high data rate is in practice never allocated by the Node B CD PS. From a cell throughput perspective, there is not much to gain in a highly loaded network from the allocation of peak data rates higher than 384 kbps.[6]

The impact on the PCT performance from the allocation of 768 kbps can be better observed in Figure 6.6, which together with the CDFs of the PCT also plots the distribution of the average source data rate during a packet call for the modified traffic model introduced in Table 6.1.

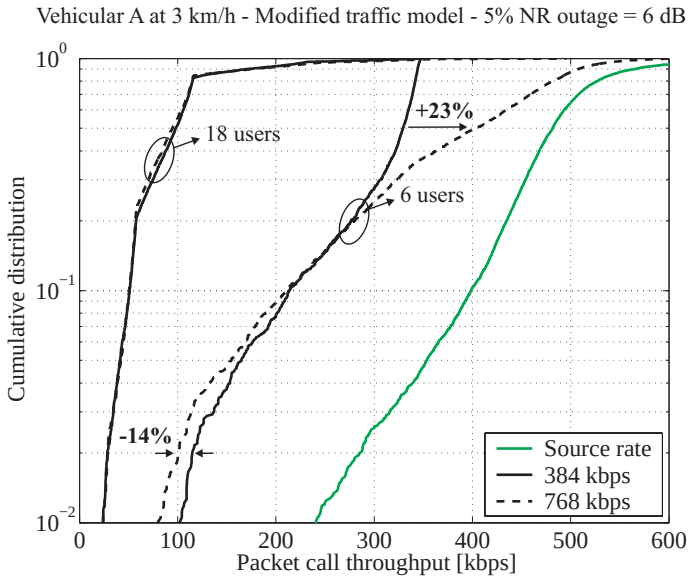

Figure 6.6: Source rate distribution for the modified traffic model and CDF of the PCT for Node B CD scheduling, an average of both 6 and 18 users per cell, and a maximum scheduled data rate of both 384 kbps and 768 kbps.

Peak data rates up to 768 kbps in the case with an average of 6 users per cell cause a slight PCT performance decrease at the low levels of the CDF. The fact is that the allocation of 768 kbps prevents other users from being allocated with high instantaneous data rates. But for the same reason, the packet call throughput experienced by the users transmitting with 768 kbps is much higher than in the case in which only 384 kbps is allocated. This leads to a significant PCT performance increase at the medium to high levels of the CDF. With an average of 18 users per cell, no difference in the packet call throughput distribution is observable between 384 kbps and 768 kbps as maximum scheduled data rate.

6.2.2 Combined Time and Code Division Scheduling: CSAFT Scheduler

With combined time and code division scheduling, at a given time instant, the available uplink resources are shared between a limited set of users transmitting at a relatively high data rate, while the rest of the users do not transmit any data. In such a scenario the allocation of instantaneous data rates higher than 384 kbps can increase the multi-user diversity in the system independently from the average source data rate of the generated traffic. The higher

[6] Notice that with 768 kbps as maximum allocated data rate and an average of 6 users per cell the probability of selecting 0 kbps is in the order of 50%; with code division scheduling users only select 0 kbps when their transmission buffer is empty. Therefore, with an average of 6 users per cell the average number of users having data to transmit is approximately 6·0.5 = 3.

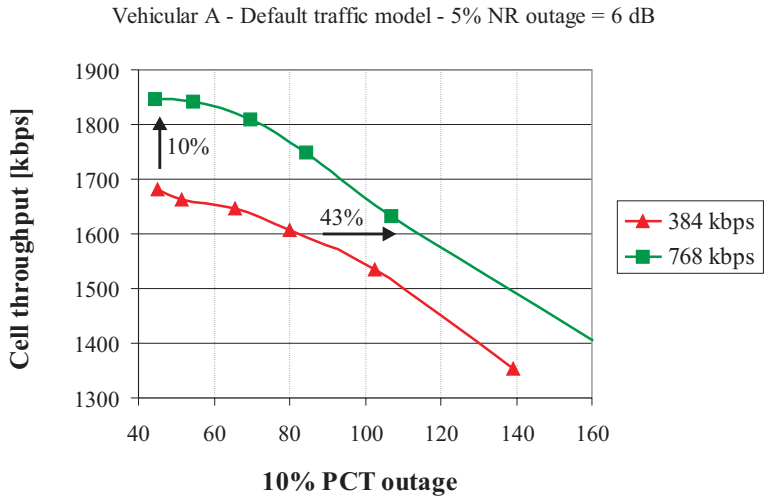

Figure 6.7: Average cell throughput as a function of the 10% PCT outage for the CSAFT scheduler with both 384 and 768 kbps as maximum scheduled data rate.

the peak data rate, the lower the number of users to be scheduled for utilising the full cell capacity, the higher the multi-user diversity gain from channel-dependent scheduling (see Section 5.2.2). Therefore, for the performance evaluation of the CSAFT scheduler with peak data rates of 768 kbps, the default traffic model is assumed (see parameter setup in Table 6.1). The functioning of the allocation strategy is the same as described in Sections 5.3.1 and 5.3.2.3, and with scheduling parameters given in Table 5.2. Only, the maximum scheduled data rate is now 768 kbps.

With the CSAFT scheduler, the increased multi-user diversity due to higher peak data rates provides an increase in both cell throughput and packet call throughput performance, as illustrated in Figure 6.7. Since the multi-user diversity clearly increases with the number of users in the system, the gain from 768 kbps is shown to be more significant in an interference-limited scenario, i.e. for lower values of the 10% PCT outage. The cell throughput gain from 768 kbps is about 10%, while given an average cell throughput of 1.6 Mbps, the 10% PCT outage can be increased from 80 kbps to approximately 115 kbps.

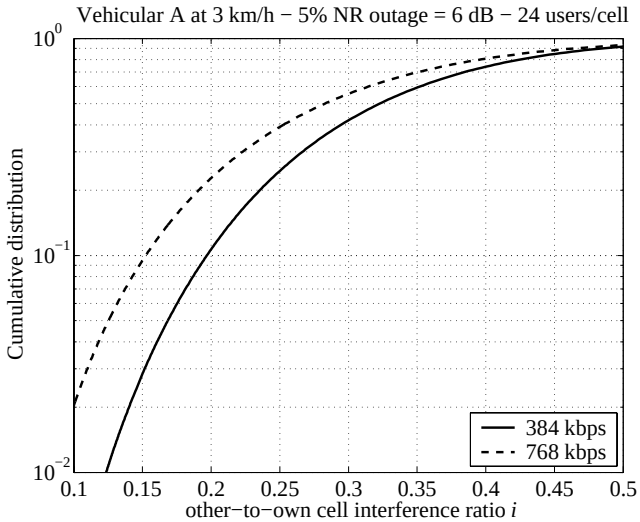

Figure 6.8: CDF of the other-to-own cell interference ratio i for the CSAFT scheduler, an average of 24 users per cell, and a maximum scheduled data rate of both 384 kbps and 768 kbps.

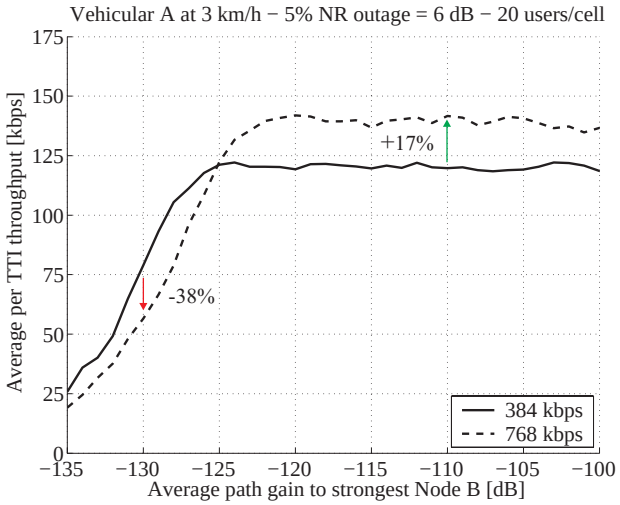

Figure 6.9: Average per TTI throughput as a function of the average path gain to the strongest Node B for the CSAFT scheduler and an average of 20 users per cell.

The higher multi-user diversity with a peak data rate of 768 kbps can be observed by looking at the distribution of the other-to-own interference ratio in Figure 6.8. With higher peak data rates the number of users simultaneously scheduled for transmission can be reduced, thus allowing the scheduling algorithm to better exploit the characteristics of the fading channels. In this way the interference generated to other cells is reduced

The impact on the performance of the CSAFT time division scheduler from the allocation of 768 kbps compared to a peak data rate of 384 kbps is also illustrated in Figure 6.9, which plots the average per TTI throughput as a function of the average path gain to the strongest Node B.

The increased multi-user diversity provides an average per TTI throughput increase as long as the data rate of 768 kbps can be supported at the UE. For values of the average path gain to the strongest Node B below -120 dB, the pert TTI throughput with 768 kbps gets closer to that with 384 kbps. This is because users in poor channel conditions cannot support 768 kbps due to their limited power capabilities. As the average path gain to the strongest Node B reduces further, the performance with 768 kbps even presents a loss compared to 384 kbps. The fact is that the CSAFT is a fair throughput scheduler subject to the condition that users, when scheduled, transmit with the same data rate. With 768 kbps as maximum scheduled data rate users are scheduled for transmission less often than with 384 kbps, but typically can transmit twice as much data when scheduled. For low values of the average path gain to the strongest Node B (where users can only support lower data rates), being less frequently scheduled for transmission results in a reduction in the experienced per TTI throughput. This drawback can be avoided by allowing users with restricted TFCs to be scheduled for transmission more often than users that can support the maximum scheduled data rate. On the other hand, the improved fairness performance of this approach is likely to slightly reduce the multi-user diversity available in the system.

Finally, the cell throughput gain from the CSAFT scheduler with the allocation of 768 kbps is assessed for a given PCT outage constraint (10% PCT outage = 64 kbps). Results are reported in Table 6.2 for both Vehicular A and Pedestrian A channel profiles at 3 km/h. The table also reports the results for the reference RNC scheduler, the Node B CD scheduler, and the CSAFT scheduler with maximum scheduled data rate equal to 384 kbps (see results in Section 5.4.4). The increased multi-user diversity with peak data rates up to 768 kbps results in a

	Scheduler	Average cell throughput [kbps]	Gain relative to the RNC - CD scheduler	Gain relative to the Node B - CD scheduler
Vehicular A	RNC - CD	1093.8	-	-
	Node B - CD	1410.3	29%	-
	CSAFT – 384 kbps	1653.8	51%	17%
	CSAFT – 768 kbps	1824.1	67%	29%
Pedestrian A	RNC - CD	1065.6	-	-
	Node B - CD	1468.9	38%	-
	CSAFT – 384 kbps	1893.7	78%	29%
	CSAFT – 768 kbps	2059.8	93%	40%

Table 6.2: Average cell throughput for different scheduling scenarios for both Pedestrian A and Vehicular A channel profile at 3 km/h, and for a 10% PCT outage of 64 kbps.

significant cell throughput enhancement. The gain relative to the reference RNC PS scenario compared to the case with 384 kbps as maximum scheduled data rate increases from 51% to 67% in a macro-cell environment, from 78% to 93% in a pedestrian micro-cell environment.

6.3 4-branch Antenna Diversity and Interference Cancellation

In this section the impact on cell throughput and PCT performance from 4-branch antenna diversity and IC techniques is evaluated. First, the two techniques are separately introduced and the assumptions for their implementation in the system level simulator presented. For IC techniques, a theoretical analysis is also introduced. Simulation results are first shown for a traffic-limited scenario in order to investigate the impact from the allocation of 768 kbps on the performance of a system that deploys 4-branch antenna diversity and IC. Next, the cell throughput and packet call throughput performance with 4-branch antenna diversity and IC is evaluated in an interference-limited scenario. Finally, the cell throughput given a specific PCT outage constraint is derived.

6.3.1 4-Branch Antenna Diversity

The model used to implement 4-branch antenna diversity in the system level simulator assumes ideal maximal ratio combining (MRC). MRC involves co-phasing and amplitude weighted sum of the received signals at the different branches. The general assumption is that the signal components at the Rake receiver can be summed coherently, while the noise components are combined incoherently. When all the antenna elements are uncorrelated, the resulting SINR γ after ideal MRC can be written as in (6.1), where $\gamma_{i,j}$ is the SINR at the j^{th} finger of the i^{th} antenna, and M is the number of Rake fingers for receiving antenna [Jakes74].

$$\gamma = \sum_{i=1}^{4} \sum_{j=1}^{M} \gamma_{i,j} \tag{6.1}$$

Since the channel estimate is obtained from the pilot symbols on the DPCCH, in practice coherent combining is only possible on the DPDCH. As a consequence, the channel estimates tend to deteriorate as the number of diversity branches increases since the SINR per antenna decreases. This leads to a loss that must be deducted from the ideal MRC gain with 4-branch antenna diversity. This loss is not considered in the presented study. Results in [Holma01] show that in a macro-cell environment with low user mobility and a user data rate of 144 kbps, the loss from 2-branch to 4-branch antenna diversity due to the decreased SINR on the DPCCH is in the order of 0.5 dB. I.e., the gain numbers presented in this chapter for 4-branch

antenna diversity compared to 2-branch diversity must be reduced by a factor of approximately 10%.

6.3.2 Interference Cancellation

Assuming a conventional matched filter receiver, the SINR of user m at the i^{th} antenna ($\gamma_{m,i}$) can be written as:

$$\gamma_{m,i} = \frac{p_{m,i}}{p_{total,i} - p_{m,i}} \tag{6.2}$$

In (6.2), $p_{m,i}$ is the received power from user m at the i^{th} antenna, while $p_{total,,i}$ is the total received power at the i^{th} antenna and is the sum of the own-cell power ($p_{own,i}$), the other-cell power ($p_{other,i}$), and the background noise power (P_{noise}).

In the uplink of CDMA systems interference cancellation is effective only towards intra-cell interference. Defining the efficiency of the IC receiver β (also referred to as MUD efficiency) as the ratio between the equivalent intra-cell interference after and before interference cancellation [Hämä96] [Hage04], the SINR of user m at the i^{th} antenna in the case with interference cancellation can be modelled as:

$$\gamma_{m,i} = \frac{p_{m,i}}{(p_{own,i} - p_{m,i}) \cdot (1-\beta) + p_{other,i} + P_{noise}} \tag{6.3}$$

If β in (6.3) is set equal to zero, then (6.3) reduces to (6.2). The approach used to allow for interference cancellation in the simulation assumptions is equivalent to the one used in both [Hämä96] and [Hage04]. In reality the efficiency of the interference cancellation receiver depends on the specific receiver implementation, as well as on a number of factors such as: Propagation environment, number of simultaneously transmitting users, E_b/N_0 target [Meng03], effective coding rate, DPDCH/DPCCH power ratio [Hage04], etc. In the presented analysis the system and user performance enhancement with IC is evaluated for two different values of β, namely β=0.3 (30% MUD efficiency) and β=0.7 (70% MUD efficiency). The idea is to give a lower and upper bound for the range of the achievable gain with low and high complexity IC receivers, respectively. A MUD efficiency of 30% is close to the efficiency of IC receivers that can be implemented at the base station with an acceptable level of complexity [Hage04]. An efficiency of 70% represents the performance of near-optimum multistage detectors [Hämä96], but is hardly feasible for practical implementation.

6.3.2.1 Theoretical Analysis

In this section a theoretical analysis is presented that tries to estimate the cell throughput gain from interference cancellation in the uplink of WCDMA systems. From (6.3), the required E_b/N_0 per receiving antenna for user j (ρ_j) in the case with a MUD receiver at the Node B can be written as:

$$\rho_j = \frac{W}{R_j} \cdot \frac{P_j}{(P_{own} - P_j) \cdot (1-\beta) + P_{other} + P_{noise}}. \tag{6.4}$$

In (6.4), W is the WCDMA chip rate (3.84 Mcps), R_j is the selected data rate for transmission by user j, P_j is the total received power per receiving antenna from user j, P_{own} is the total received own-cell power per receiving antenna, P_{other} is the total received other-cell power per

receiving antenna, P_{noise} is the background noise power per receiving antenna, and β is the efficiency of the IC receiver. Introducing the other-to-own cell interference ratio i ($P_{other} = P_{own} \cdot i$) and solving (6.4) for P_j gives:

$$P_j = \frac{P_{own} \cdot (1 - \beta + i) + P_{noise}}{\frac{W}{\rho_j R_j} + 1 - \beta} \tag{6.5}$$

Assuming perfect power control, the same E_b/N_0 requirement for all users in the system ($\rho_j = \rho \ \forall \ j$), and all active users transmitting with the same data rate R ($R_j = R \ \forall \ j$), all users are consequently received with the same power level P ($P_j = P \ \forall \ j$). Then, the total received own power per receiving antenna can be written as:

$$P_{own} = N \cdot P = \frac{N \cdot P_{noise}}{\frac{W}{\rho R} + (1 - \beta) - N \cdot (1 - \beta + i)} \tag{6.6}$$

In (6.6), N is the total number of users in the cell. The noise rise (defined as the ratio of the total received wideband power to the background noise power) can be written as:

$$NR = \frac{P_{noise} + P_{own} \cdot (1 + i)}{P_{noise}} = 1 + \frac{N \cdot (1 + i)}{\frac{W}{\rho R} + (1 - \beta) - N \cdot (1 - \beta + i)} \tag{6.7}$$

The relation between the uplink fractional load η_{UL} and the noise rise is given in (6.8) (see Section 3.2.1).

$$NR = \frac{1}{1 - \eta_{UL}} \tag{6.8}$$

Finally, substituting (6.8) in (6.7) and solving for N, the average number of users transmitting at rate R that can be supported in a WCDMA cell for a given uplink fractional load η_{UL} with MUD efficiency β can be expressed as:

$$N = \eta_{UL} \cdot \left[\frac{G_p}{\rho} + (1 - \beta) \right] \cdot \frac{1}{1 + i - \beta \cdot \eta_{UL}} \tag{6.9}$$

In (6.9), G_p is the processing gain defined as the ratio of the WCDMA chip rate W to the data rate R. For β equal to zero, (6.9) reduces to the uplink cell throughput estimation with conventional matched filter receiver (see Section 3.2.1); hence, the cell throughput gain from interference cancellation can be written as:

$$G = \frac{N}{N_{\beta=0}} = \left[\frac{G_p / \rho + (1 - \beta)}{G_p / \rho + 1} \right] \cdot \left[\frac{1 + i}{1 + i - \beta \cdot \eta_{UL}} \right] \tag{6.10}$$

The second term in square brackets in (6.10) shows that the gain from IC mainly depends on three factors:

- The MUD efficiency β,
- the other-to-own cell interference ratio i, and
- the uplink fractional load η_{UL}.

Clearly, the cell throughput gain increases with the MUD efficiency, as well as it decreases with i since interference cancellation is only effective towards intra-cell interference. However, it is shown how the impact of the MUD efficiency on the cell throughput gain is scaled by the uplink fractional load η_{UL}. The reason for this is that the gain from multi-user detection clearly increases with the amount of interference to be cancelled. The theoretical results derived in e.g. [Hämä96] and [Hage04] concentrate on the pole capacity (see definition [A 2.13]) gain from IC, which corresponds to assuming η_{UL} = 1 in (6.10). The presented analysis shows that the cell throughput gain from IC given a certain value of the other-to-own cell interference is always smaller than the corresponding pole capacity gain, and depends on the MUD efficiency β as well as on the amount of total received power at the base station receiver.

The first term between square brackets in (6.10) indicates that the gain from IC expressed by the second term must be opportunely reduced since the received power from the desired user cannot be included in the amount of interference to be cancelled. However, for $G_p/\rho >>1$ the first term in square brackets in (6.10) tends to 1 even for very high values of the MUD efficiency β[7]. Assuming a selected data rate equal to 768 kbps (G_p=5), the impact on the cell throughput gain from the first term in square brackets in (6.10) ranges around 5-10%. For data rates lower than 768 kbps, the impact on the cell throughput gain becomes less relevant and can be neglected.

Bearing in mind this effect due to allocation of instantaneous data rates as high as 768 kbps, the capacity gain from interference cancellation can be simplified by taking into consideration only the second term in (6.10).

$$G \cong \frac{1+i}{1+i-\beta \cdot \eta_{UL}} \tag{6.11}$$

As previously analysed, the cell throughput gain decreases with i, since only intra-cell interference can be cancelled, whereas the impact of the MUD efficiency β is scaled by the uplink fractional load η_{UL}. Figure 6.10 and Figure 6.11 plot the theoretical cell throughput gain from IC for a MUD efficiency of 30% and 70%, respectively, as a function of the uplink fractional load $\eta_{UL,}$ and for different values of the other-to-own cell interference ratio i. It can be noticed that for a fully loaded isolated cell (η_{UL}=1, i=0) the theoretical capacity gain is 42% for a MUD efficiency of 30%, and approximately 230% for a MUD efficiency of 70%. However, assuming a cell load around 75% (corresponding to a noise rise of 6 dB) and an other-to-own cell interference ratio between 0.4 and 0.6 (which from previous simulation results appears as a reasonable range to consider), the cell throughput gain from IC significantly reduces to approximately 18% and 55% for a MUD efficiency of 30% and 70%, respectively.

[7] Notice that ρ is the required E_b/N_0 per receiving antenna, and therefore reduces as the number of antennas increases. For a required E_b/N_0 of 3.2 dB (10% BLER for Vehicular A channel profile at 3 km/h, see Figure C.2) and assuming ideal MRC at the base station receiver, the required E_b/N_0 per antenna with 4-branch antenna diversity is approximately -2.8 dB (6 dB MRC gain).

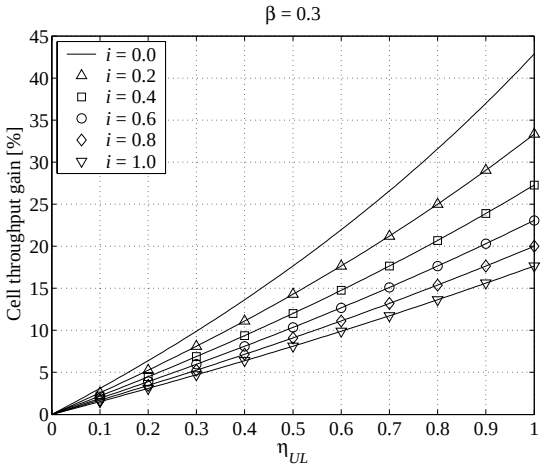

Figure 6.10: Theoretical cell throughput gain from IC as a function of η_{UL}, for β=0.3 and different values of the other-to-own cell interference ratio i.

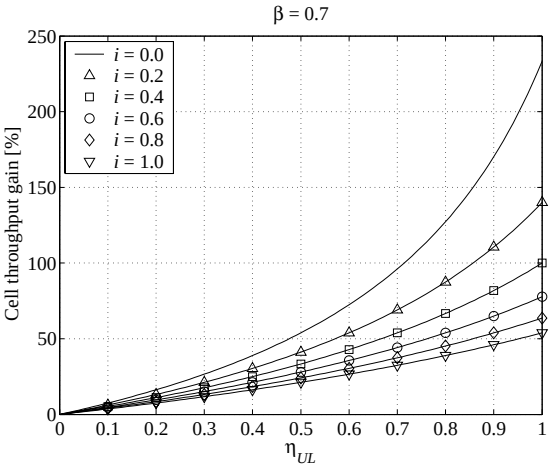

Figure 6.11: Theoretical cell throughput gain from IC as a function of η_{UL}, for β=0.7 and different values of the other-to-own cell interference ratio i.

The presented analysis has shown that the expected cell throughput gain from IC in uplink depends on a number of factors. If the MUD efficiency is a direct consequence of the particular implementation of the IC receiver, the impact of both uplink load and other-to-own cell interference cannot be straightforwardly derived.

1. In Chapter 5 it has been shown that time-division scheduling based on channel-state information can be deployed to reduce the required transmission power per information bit, thus decreasing the other-to-own cell interference ratio. Therefore, a higher gain from IC should be expected with combined time and code division scheduling than with code division scheduling.

2. On the other hand, time division scheduling has also been proven to increase the required power headroom to meet the specified NR outage criteria (see Figure 5.11). As a consequence, given a specific NR outage constraint, the corresponding average NR (and therefore the average uplink fractional load) is lower with combined time and code division scheduling than it is with traditional code division scheduling.

3. Moreover, with time division scheduling scheduled users are likely to transmit with instantaneous high data rates. If 768 kbps is allocated, the first term in square brackets in (6.10) also starts to play a role in determining the actual cell throughput gain.

The different effects on the expected gain from IC with code division and combined time and code division scheduling in the uplink of WCDMA systems are summarised in Table 6.3. However, it cannot be concluded 'a priori' if IC techniques will benefit one scheduling

	Expected impact on IC gain with code division scheduling (+ /–)	Expected impact on IC gain with combined time and code division scheduling (+ /–)
i	–	+
η_{UL}	+	–
G_p/ρ	+	–

Table 6.3: Different effects on the expected cell throughput gain from IC with code division and combined time and code division scheduling.

concept more than another. A simulation-based estimation of the cell throughput gain with IC for both code and time division scheduling is presented in Section 6.3.3.2.

6.3.3 Simulation Results

6.3.3.1 High Data Rate Allocation in a Traffic-Limited Scenario

In this section, the impact on uplink performance from the allocation of 768 kbps is investigated in a system that deploys 4-branch antenna diversity and interference cancellation. A network with an average of 12 users per cell is selected in order to evaluate the cell throughput and PCT performance in a scenario that with the introduction of 4-branch antenna diversity and IC is not inherently interference-limited. For this analysis, only the Node B CD scheduler is considered.

With 2-branch antenna diversity and conventional matched filter receiver the system is interference-limited, in which case the availability of 768 kbps does not provide any improvement since users are in fact never allocated with such a high data rate due to the code-division fair-resource scheduling approach (see Section 6.2.1.2). Introducing 4-branch antenna diversity and IC, the system pole capacity increases due to the improved spectral efficiency. Already with 4-branch antenna diversity and no IC, with 384 kbps as maximum scheduled data rate the planned load budget (5% noise rise outage equal to 6 dB) cannot be fulfilled, as it can be observed in Figure 6.12. In this case the system is not interference-limited, on the contrary its performance is rather constrained by the limited UE capabilities. Peak data rates up to 768 kbps overcome this limitation and allow fulfilling the planned load budget, and the cell throughout consequently increases. Notice in Figure 6.12 that with 4-branch antenna diversity and 70% efficient IC even the allocation of 768 kbps is not sufficient in order to utilise the full cell capacity. In this case the system performance is clearly limited by the amount of traffic generated by the users in the network.

The impact on packet call throughput performance from the allocation of 768 kbps with 4-branch antenna diversity and IC is illustrated in Figure 6.13. As 4-branch antenna diversity and IC techniques are introduced, 768 kbps can provide a significant gain in average PCT performance compared to 384 kbps. Notice that the gain numbers for the 10% PCT outage are

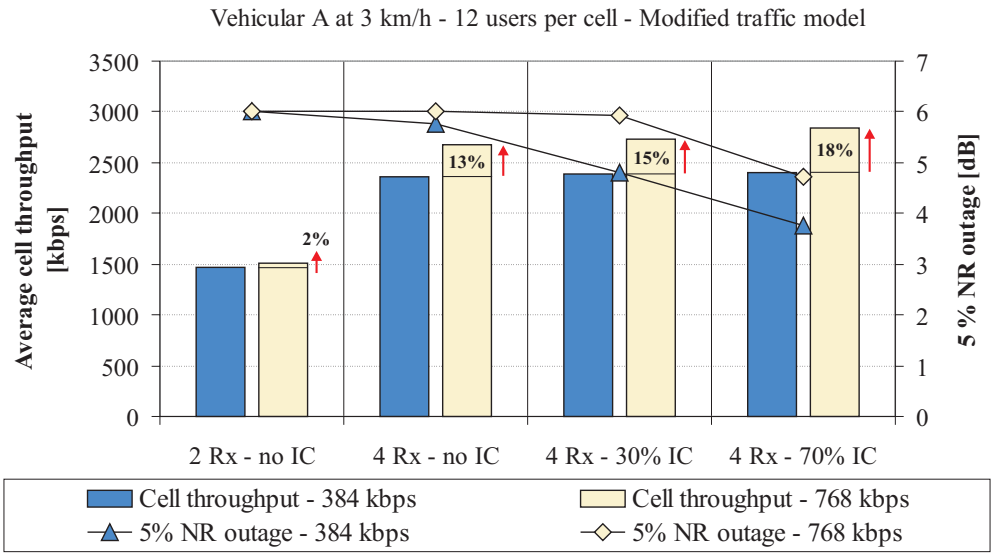

Figure 6.12: Average cell throughput and 5% NR outage for the Node B CD scheduler, and for different antenna diversity and IC scenarios.

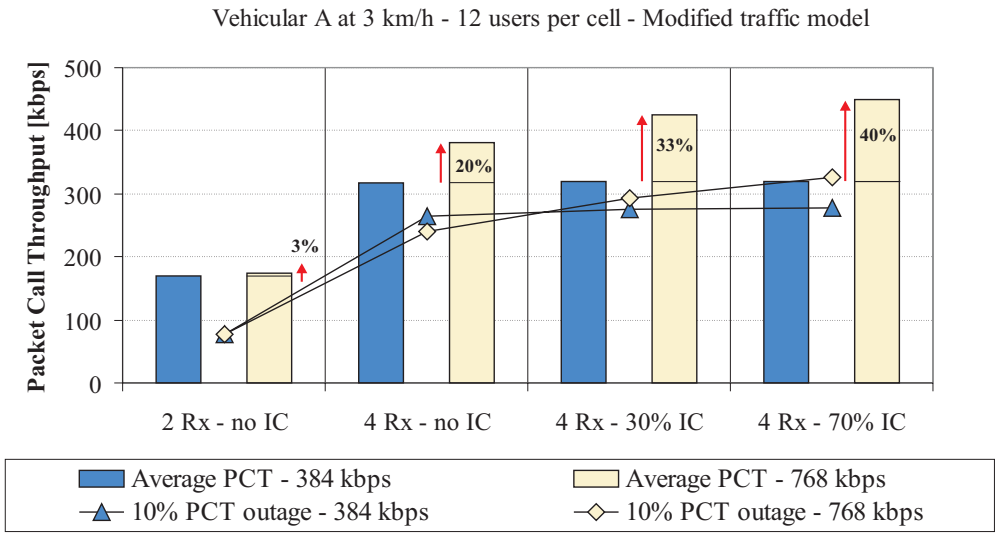

Figure 6.13: Average PCT and 10% PCT outage for the Node B CD scheduler, and for different antenna diversity and IC scenarios.

smaller than for the average PCT, and in some cases even a slight loss is observable when comparing the performance of 768 kbps with that of 384 kbps. The reason is that with the Node B CD PS the allocation to one user of 768 kbps can momentarily prevent other users from being allocated with high transmission rates, thus reducing the fairness characteristics of the scheduler.

From Figure 6.12 and Figure 6.13 it can be seen that with 384 kbps it is not possible to fulfil the planned load budget as soon as the average packet call throughput gets close to the limit imposed by the maximum scheduled data rate (≅350 kbps when transmission errors are also considered). In the case with 768 kbps, the same behaviour is observed whenever the average PCT gets close to the limit imposed by the traffic model (≅450 kbps when errors are also considered, see Table 6.1).

The limit imposed by having a peak data rate of 384 kbps can be better understood observing the distributions of the selected data rate for transmission in Figure 6.14. Already with

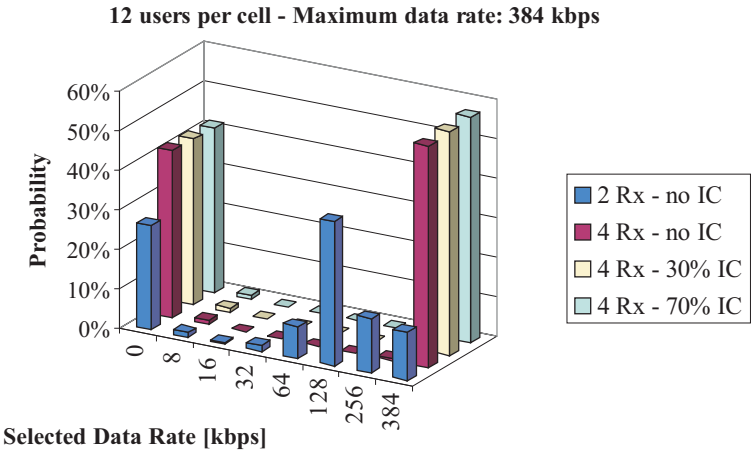

Figure 6.14: Distribution of the selected data rate for a maximum scheduled data rate of 384 kbps and an average of 12 users per cell.

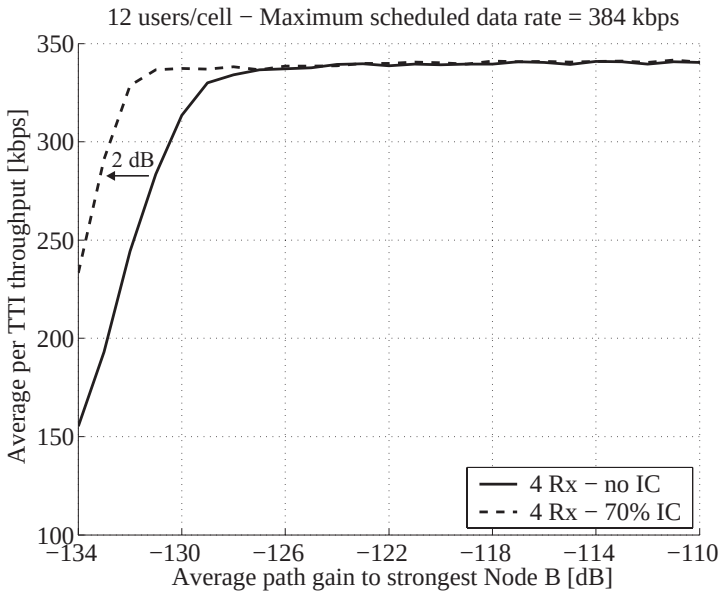

Figure 6.15: Average per TTI throughput as a function of the average path gain to the strongest Node B for the Node B CD scheduler, 4-branch antenna diversity, with and without IC.

4-branch antenna diversity and conventional matched filter receiver, users almost always select 384 kbps when they have data to transmit. As a consequence, neither PCT nor cell throughput improvement can be achieved by introducing IC techniques. In this case the effect of IC is to reduce the corresponding 5% NR outage, thus improving uplink coverage (see Figure 6.12). To illustrate the coverage gain from IC, Figure 6.15 plots the average per TTI throughput as a function of the average path gain to the strongest Node B. It is clear how interference cancellation can provide a coverage gain which reflects the corresponding 2 dB decrease observed for the 5% NR outage (see Figure 6.12).

The effect of high peak data rates on the cell throughput and PCT performance with 4-branch antenna diversity and IC is not considered in the case of combined time and code division scheduling. Except for the increased multi-user diversity with 768 kbps compared to 384 kbps already discussed in Section 6.2.2, approximately the same conclusions as for the Node B CD scheduler can be drawn: In a WCDMA system with a fairly low number of high data rate users, the availability of peak data rates up to 768 kbps is indispensable in order to exploit the full cell capacity with 4-branch antenna diversity and IC. Alternatively, the considered techniques can be deployed to improve uplink coverage.

6.3.3.2 Cell Throughput and PCT Performance with 4-branch Antenna Diversity and IC

Next, the cell throughput and packet call throughput performance enhancement with 4-branch antenna diversity and IC is evaluated for both the Node B CD and the time and code division

Number of receiving antennas	2	4
Average number of users per cell	18	36
Interference Cancellation	No IC	No IC / 30% IC / 70% IC
Maximum scheduled data rate	384 kbps	768 kbps
Traffic model	Default	Modified
5% NR outage	6 dB	6 dB

Table 6.4: Simulation assumptions for 2-branch and 4-branch antenna diversity with and without IC.

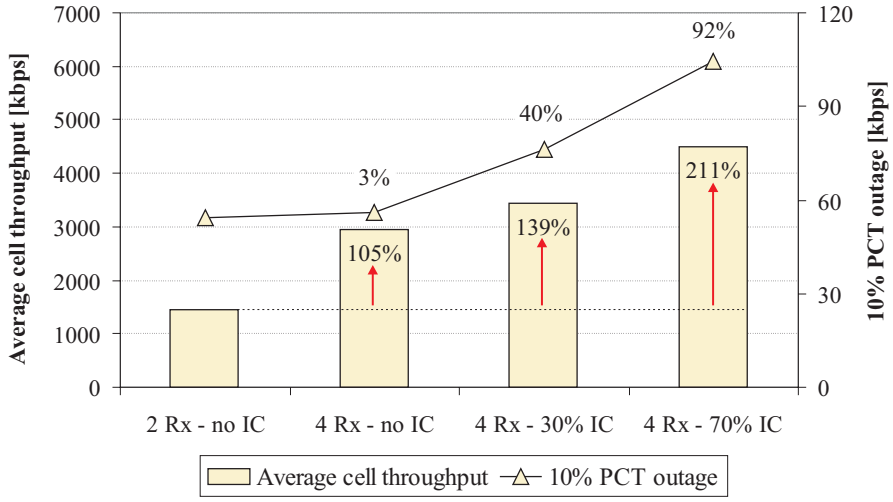

Figure 6.16: Average cell throughput and 10% PCT outage for the Node B CD scheduler with 2 and 4-branch antenna diversity, with and without IC.

CSAFT schedulers. In order to estimate the achievable cell throughput gain, two simulation scenarios that are clearly not traffic-limited, but interference-limited, are selected. The corresponding simulation assumptions are reported in Table 6.4.[8]

6.3.3.2.1 Node B CD Scheduler

With 4-branch antenna diversity a cell throughput increase of about 100% is achieved compared to 2-branch diversity, as illustrated in Figure 6.16. This is in accordance with the implementation of 4-branch antenna diversity in the system level simulator described in Section 6.3.1, where we considered ideal MRC with no channel estimation loss due to the decreased SINR per antenna. Under these assumptions, with 4-branch antenna diversity the required E_b/N_0 per receiving antenna is expected to reduce of approximately 3 dB, which corresponds to a theoretical cell throughput gain of 100%. The fact that the gain from simulations is not much different from the theoretical gain from ideal MRC means that the gain from increased diversity is nearly negligible. This is also in line with expectations, since the degree of diversity is already very high with basic system features: 2-branch antenna diversity, macro-diversity due to SHO operation, and high multipath diversity in the Vehicular A channel.

With 4-branch antenna diversity and no IC, having also doubled the average number of users per cell compared to 2-branch antenna diversity (see Table 6.4), the 10% PCT outage performance is not improved. In the case of code division scheduling, similar packet call throughput performance means similar probability distribution function of the selected data rate; hence, UE transmission power statistics can be compared without being biased by the difference in the selected data rate for transmission. To this end, Figure 6.17 plots the CDF of the UE transmission power for 2-branch and 4-branch antenna diversity with no interference cancellation, and shows approximately the same 3 dB reduction for the UE transmission power as observed for the required E_b/N_0 per receiving antenna.

Finally, from Figure 6.16 it is clear how IC techniques can further enhance both cell throughput and PCT performance. With a MUD efficiency of 30%, the cell throughput gain

[8] Notice that in order for the system to operate in the interference-limited region, the average number of users per cell is doubled when 4-branch antenna diversity is introduced.

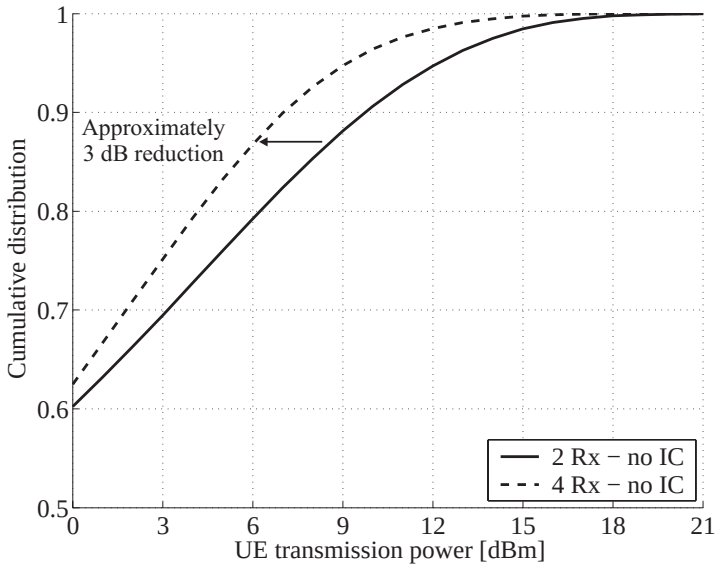

Figure 6.17: CDF of the UE transmission power for the Node B CD scheduler, with 2 and 4-branch antenna diversity and no IC.

over 2-branch antenna diversity and conventional matched filter receiver is 139%, and the corresponding 10% PCT gain is 40%.

6.3.3.2.2 CSAFT Scheduler

In this section, simulation results are presented for the CSAFT combined time and code division scheduler and for the same simulation scenarios as in Section 6.3.3.2.1. With the CSAFT scheduler the gain from 4-branch antenna diversity is slightly higher than 100%, as shown in Figure 6.18. Compared to 2-branch antenna diversity, with 4-branch antenna diversity the maximum scheduled data rate is increased from 384 kbps to 768 kbps (see Table 6.4), and in principle also the uplink cell throughput should increase by a factor of approximately two due to the reduced E_b/N_0 requirement per receiving antenna. But having also doubled the average number of users per cell (from 18 to 36, see Table 6.4), the multi-

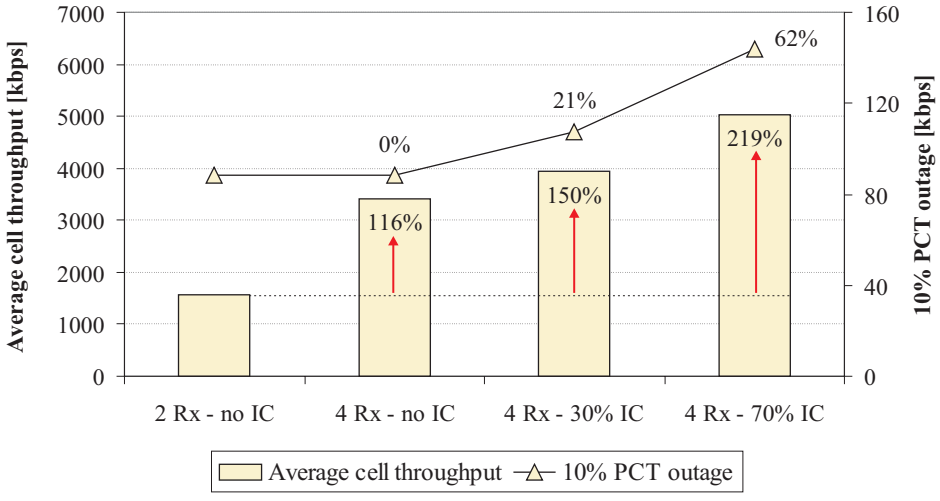

Figure 6.18: Average cell throughput and 10% PCT outage for the CSAFT scheduler, with 2 and 4-branch antenna diversity, with and without IC.

user diversity is somewhat increased. This reflects into an additional cell throughput gain of approximately 16%, to be added to the theoretical 100% gain due to ideal MRC.

The additional cell throughput gain from IC is slightly higher to the gain estimated for the Node B CD scheduler. The overall cell throughput gain from 4-branch antenna diversity and IC compared to the case with 2-branch antenna diversity and conventional matched filter receiver is 150% for a MUD efficiency of 30%. On the other hand, the 10% PCT outage gain when introducing IC is smaller for the CSAFT scheduler than it is for the Node B CD scheduler (see Figure 6.16 and Figure 6.18). Since the CSAFT scheduler allocates resources based on near instantaneous buffer-state information, its fairness characteristics are marginally better than for the Node B CD scheduler, which on the other hand operates at a much slower scheduling rate. In Section 6.2.1.2, the allocation of peak data rates up to 768 kbps has been shown to have a negative effect on the fairness performance of the Node B CD scheduler. The introduction of IC techniques can mitigate this effect by increasing the available resources for transmission in uplink.[9]

Finally, Figure 6.19 plots the CDF of the other-to-own cell interference ratio *i* for the CSAFT scheduler, assuming 4-branch antenna diversity, a maximum scheduled data rate of 768 kbps, and different IC scenarios. Due to the increased pole capacity, with interference cancellation the number of users that must be simultaneously scheduled for transmission with the CSAFT scheduler to fully utilise the cell capacity increases. This results in a reduction of the multi-user diversity, which directly reflects into an increase in other-cell interference. This effect must be considered when the gain from 4-branch antenna diversity and IC is estimated in combination with channel-dependent packet scheduling. If the uplink pole capacity increases, the user peak data rates must be increased in order to maintain the same level of multi-user diversity in the system.

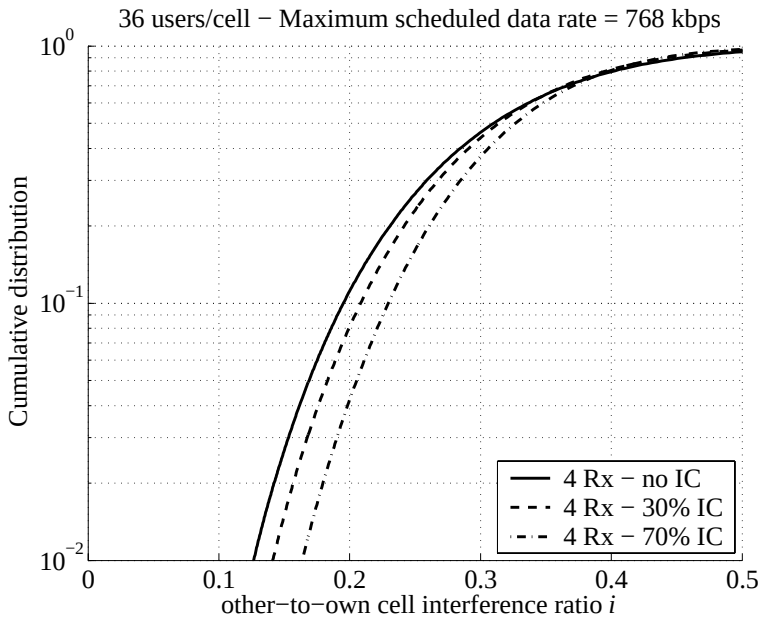

Figure 6.19: CDF of the other-to-own cell interference ratio i for the CSAFT scheduler with 4-branch antenna diversity, and for different IC scenarios.

[9] Notice that, although the 10% PCT outage gain from IC is lower for the CSAFT scheduler, for the same antenna diversity and IC scheme the absolute value of the 10% PCT outage is always higher than with Node B CD scheduling.

6.3.3.2.3 Cell Throughput Performance Given a Specific 10% PCT Outage Constraint

In this last section results are presented for both Node B CD and CSAFT scheduling by imposing specific PCT outage constraints. The main simulation assumptions are reported in Table 6.5. The required 10% PCT outage is set to 64 kbps for 2-branch antenna diversity, and to 128 kbps for 4-branch antenna diversity, mainly to account for the increased user requirements due to the higher source data rates with the modified traffic model.

Number of receiving antennas	2	4
Average number of users per cell	Varied to get the specified 10% PCT outage constraint	Varied to get the specified 10% PCT outage constraint
Interference Cancellation	No IC	No IC / 30% IC / 70% IC
Maximum allocated data rate	384 kbps	768 kbps
Traffic model	Default	Modified
5% NR outage	6 dB	6 dB
10% PCT outage	64 kbps	128 kbps

Table 6.5: Simulation assumptions for the scenarios corresponding to 2 and 4-branch antenna diversity.

Figure 6.20 reports the values of the average cell throughput for the simulation scenarios of Table 6.5. The gain numbers are given relative to a reference RNC scheduling scenario operating at 1% BLER target with L2 ARQ retransmission schemes (see Chapter 3). It can be seen that the overall cell throughput enhancement with fast Node B scheduling, L1 HARQ schemes, 4-branch antenna diversity, 30% efficient IC, and channel-dependent radio resource allocation based on time division scheduling is 253%. This gain is achieved in addition to a 100% increase in the 10% PCT outage performance (see Table 6.5). The overall cell throughput gain in the case of Node B code division scheduling is 208%. In the most optimistic scenario with a MUD efficiency of 70% the cell throughput increase is as big as 364%; however, it has been discussed in Section 6.3.2 how such a high efficiency is in practice unfeasible with an acceptable level of complexity at the base station receiver

For both Node B CD and CSAFT scheduling, the cell throughput gain from 4-branch antenna diversity and IC techniques relative to the basic schedulers performance with 2-branch

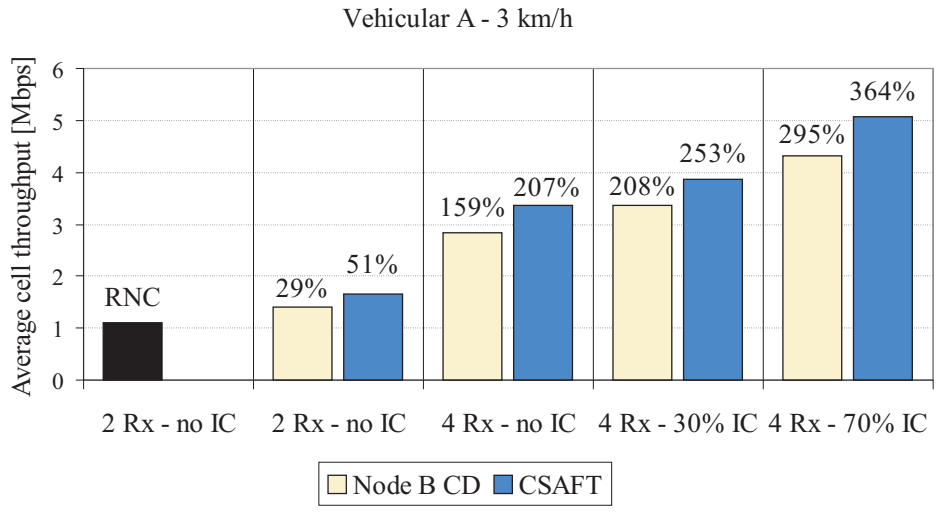

Figure 6.20: Average cell throughput for different antenna diversity and IC scenarios for both the Node B CD and the CSAFT schedulers, and compared to the performance of a reference RNC scheduler.

	Node B CD scheduler		CSAFT scheduler	
	Cell Throughput	Relative gain	Cell Throughput	Relative gain
2 Rx – No IC	1410 kbps	-	1654 kbps	-
4 Rx – No IC	2835 kbps	101%	3359 kbps	103%
4 Rx – 30% IC	3364 kbps	139%	3858 kbps	133%
4 Rx – 70% IC	4325 kbps	207%	5074 kbps	207%

Table 6.6: Average cell throughput and gain numbers relative to the basic scheduler performance with 2-branch antenna diversity and no IC, for both the Node B CD and the CSAFT schedulers.

antenna diversity and conventional matched filter receiver is reported in Table 6.6. Notice that the gain numbers are very similar independently of the scheduling strategy.

Finally, a comparison between the theoretical and the simulation-based estimation of the cell throughput gain from IC is presented in Table 6.7, which reports the semi-analytical gain obtained from (6.10) and the estimated gain by means of system level simulations for different values of the MUD efficiency β, and for both Node B CD and CSAFT scheduling.

The values for the uplink fractional load η_{UL} and for the other-to-own cell interference ratio i to be used in (6.10) are obtained from the corresponding system level simulations. For the Node B CD scheduler, $G_p/\rho = \infty$ corresponds to neglecting the first term in square brackets in (6.10). For the CSAFT time division scheduler, the value of G_p/ρ is obtained assuming a data rate equal to 768 kbps and a required E_b/N_0 per antenna of -2.8 dB. Notice that the gain from IC is approximately the same independently from the considered scheduler, although with the CSAFT scheduler the other-cell interference is reduced, and therefore a higher gain from IC could have been expected. But with time division scheduling users are scheduled for transmission with high peak data rates, and consequently contribute more to the total received power at the Node B. Obviously, the power from the desired user cannot be included in the interference available for cancellation, thus limiting the gain from IC.

	Average NR	η_{UL}	i	G_p/ρ	β	Theoretical gain	Gain from simulations
Node B CD scheduler	5.1 dB	0.69	0.46	∞	0.3	16%	19%
	5.2 dB	0.70	0.45	∞	0.7	51%	53%
CSAFT scheduler	5.0 dB	0.68	0.34	9.53	0.3	15%	15%
	5.2 dB	0.70	0.33	9.53	0.7	48%	51%

Table 6.7: Comparison between semi-analytical and simulation-based estimation of the uplink cell throughput gain with IC, for both the Node B CD and the CSAFT schedulers.

The gain numbers obtained from the system level simulations are very much in accordance with the semi-analytical estimations. The uplink cell throughput gain provided by IC techniques is between 15% and 20% for a MUD efficiency of 30%, and it is about 50% for a MUD efficiency of 70%.

6.4 Summary

In the first part of this chapter the impact on the cell throughput and PCT performance from the allocation of peak data rates higher than 384 kbps has been investigated. It has been shown how with basic system features (2-branch antenna diversity and conventional matched filter receiver) and traditional code division scheduling, the allocation of peak data rates up to 768 kbps makes sense only in a traffic-limited scenario. The situation is different in the case

of channel-dependent radio resource allocation based on time division scheduling, in which case the instantaneous allocation of higher peak data rates allows for a reduction of the number of users simultaneously scheduled for transmission. For the CSAFT scheduler, the additional multi-user diversity gain from the instantaneous allocation of 768 kbps compared to 384 kbps is about 10%; the cell throughput gain relative to a reference RNC scheduler implementation is increased from 51% to 67%, and from 78% to 93% for Vehicular A and Pedestrian A channel profiles at low mobile speed, respectively.

The impact from the allocation of high data rates in the case of code division scheduling has also been studied when introducing advanced system features such as 4-branch antenna diversity and IC. Both these features increase the system spectral efficiency, and consequently the system pole capacity. In a system with a relatively low number of high data rate users per cell, the allocation of 768 kbps is indispensable in order to fully utilise the cell capacity provided by such advanced techniques. Alternatively, 4-branch antenna diversity and IC can be deployed to improve uplink coverage.

A semi-analytical expression for the cell throughput gain from IC has been derived, showing that the gain mainly depends on three factors: The efficiency of the IC receiver, the other-to-own cell interference ratio, and the uplink load. System level simulations have confirmed that besides a 100% cell throughput increase from 4-branch antenna diversity, IC can provide an additional gain between 15% and 20% for a MUD efficiency of 30%. The gain is approximately 50% for a MUD efficiency of 70%, though such a high efficiency is actually unfeasible for practical implementation.

Finally, 4-branch antenna diversity and 30% efficient IC combined with channel-dependent packet scheduling and fast L1 HARQ schemes are able to enhance the uplink throughput of a WCDMA macro-cell with low user mobility from 1.1 Mbps to approximately 3.9 Mbps (≅ 250% gain). This gain is achieved while increasing the 10% PCT outage from 64 kbps to 128 kbps (100% gain).

Chapter 7

Conclusions

This Ph.D. thesis has investigated some potential enhancements for improved uplink packet access in WCDMA systems. In the wide range of 3G packet data services, the focus has been on NRT services, specifically on the background and interactive traffic classes defined in the UMTS standard [Holma04]. This concluding chapter gives a summary of the Ph.D. dissertation and draws the main conclusions from the most relevant topics investigated.

7.1 Performance of the Release 99 RNC PS

Chapter 3 concentrated on evaluating the performance of a system deploying basic features in line with the Release 99 of the 3GPP standards. The packet scheduler is the main functionality responsible for the allocation of the network resources to the NRT users, and with Release 99 it is located in the RNC. For NRT services characterised by bursty data transmission and high data rate requirements, the main drawback of Release 99 uplink packet access is the inability of the RNC-located packet scheduler to rapidly reallocate the radio resources between the NRT users depending on the varying traffic and interference conditions.

In a macro-cell environment with low mobility users the maximum achievable cell throughput with Release 99 uplink packet access is between 1.15 and 1.45 Mbps, depending on the specific constraint imposed on the noise rise in the system. A higher noise rise results in increased cell throughput performance at the cost of reduced uplink coverage. Moreover, for a 5% probability of exceeding a noise rise of 6 dB (≈ 75% cell load) and requiring 90% of the packet data calls to experience an average throughput of at least 64 kbps, the system performance loss compared to the case with no minimum QoS constraints is around 15%.

7.2 Performance of L1 Retransmission Schemes and fast Node B PS

Chapter 4 has addressed the performance evaluation of two of the most important technological improvements for enhanced packet access in uplink WCDMA evolution, namely fast L1 retransmission schemes and fast Node B packet scheduling.

Fast L1 Retransmission Schemes

For a specific NRT service, fast L1 retransmissions allow the uplink to operate with a higher block error rate (BLER) without degrading the overall delay performance, thus enabling transmission with a lower power for a given data rate. The spectral efficiency gain thus obtained directly translates into an increase in uplink cell throughput. The gain in a macro-cell environment from increasing the BLER target at first transmission from 1% to 10%-20% is approximately 10% and 30% for low (3 km/h) and high (50 km/h) user mobility, respectively. The higher gain in high mobility scenarios is due to the deficiency of fast power control when the mobile speed increases. Combining techniques such as chase combining (CC) and incremental redundancy (IR) can further increase the performance of fast L1 retransmission schemes by significantly reducing the experienced delay when the BLER target at first transmission is increased to values above 20%. In this case however, due to the joint deployment of fast power control and combining techniques, only a marginal spectral efficiency gain can be achieved, and limited to the case of high user mobility. As a consequence, CC and IR techniques are not foreseen to provide the same capacity improvement in WCDMA uplink evolution as in HSDPA. However, they can be implemented with minimum complexity compared to type-I HARQ schemes and provide additional robustness to the link adaptation mechanism based on fast power control, especially in high mobility environments. Therefore, it makes sense that CC and IR have already been included in the Release 6 of the 3GPP specifications.

Fast Node B Packet Scheduling

In addition to fast L1 retransmission schemes, fast Node B scheduling also contributes to enhance the uplink performance. Fast Node B scheduling can rapidly react to changes in the interference conditions as well as to variations in the offered traffic from NRT applications. This reduces the variability of the noise rise and gives an opportunity to reduce the headroom reserved in the uplink for overload situations, thus achieving higher user data rates and cell throughput.

To take advantage of fast packet scheduling operation at the Node B, a scheduling algorithm has been designed which at each scheduling instant redistributes the available resources between NRT users based on the utilisation of the allocated data rates. In a few words, the radio resources are ‘taken’ from users with low utilisation and ‘given’ to users with high utilisation. The proposed algorithm also avoids explicit signalling of capacity requests from the users to the Node B packet scheduler, thus minimising the signalling overhead in uplink.

Fast Node B scheduling can allow network operators to increase the user experienced data rate while maintaining the same cell throughput. Assuming type-I HARQ schemes and a cell throughput of 1.3 Mbps, with fast Node B scheduling 90% of the packet-data calls experience an average throughput higher than 100 kbps, while the corresponding value with RNC scheduling is 50 kbps. Alternatively, given specific packet call throughput outage constraints, with Node B scheduling the uplink cell throughput can be increased by approximately 15-20% compared to RNC scheduling.

Combined Performance

Finally, the uplink cell throughput with both L1 retransmission schemes and fast Node B scheduling has been evaluated; in a macro-cell environment the gain compared to the performance of a system operating with Release 99 features is approximately 25% and 60% for low and high user mobility, respectively.

7.3 Performance of Combined Time and Code Division Scheduling

Chapter 5 has introduced a new radio resource allocation concept based on combined time and code division scheduling, with the aim to further enhance the performance of WCDMA uplink packet access. The main idea is to combine the principles of CDMA with a TDM scheme, thus allowing users to be scheduled for transmission on dedicated channels with high peak data rates, and based on near instantaneous buffer state information.

The main advantage of the proposed scheme is the possibility to perform radio resource allocation based on channel-state information, thus reducing the interference generated to other cells. The multi-user diversity gain achievable with combined time and code division scheduling depends on the number of users that must be simultaneously scheduled to utilise the cell capacity; the lower the number of users, the higher the multi-user diversity gain.

In order to exploit the characteristics of the fading channels in the radio resource allocation procedure, packet scheduling must be performed on a per TTI basis. Hence, the allocation of high data rates to a limited set of users is likely to cause abrupt changes in other-cell interference. As a consequence, the variability in the noise rise is expected to increase, and so is the power headroom needed to prevent the system from entering an overload situation. This effect can potentially limit the capacity gain from channel-dependent scheduling.

To assess the performance of combined time and code division scheduling, three algorithms have been introduced: the ‘blind fair throughput’ (BFT) scheduler, the ‘maximise transmit power efficiency’ (MTPE) scheduler and the ‘channel-state aware fair throughput’ (CSAFT) scheduler. While the BFT algorithm does not perform channel-dependent resource allocation, the other schedulers utilise an appositely defined uplink channel quality indicator to exploit channel-state information in the packet scheduling procedure.

With the BFT scheduler, the increased power headroom for overload protection is not balanced by any reduction in the interference generated to other cells. On the other hand, the BFT algorithms can still benefit from the temporary allocation of high peak data rates based on near-instantaneous buffer state information. The aggregate outcome is that the BFT has no advantage, and in some cases becomes even worse compared to the Node B code division scheduler introduced in Chapter 4.

Differently from the BFT allocation strategy, the channel-dependent schedulers are able to exploit information on the instantaneous channel quality thus reducing the interference generated to other cells. The overall effect is a cell throughput and packet call throughput performance increase compared to the Node B code division scheduler of Chapter 4. While the MTPE scheduler maximises cell throughput at the cost of a low degree of fairness between users, the CSAFT algorithm offers an appealing trade-off between users’ fairness and throughput maximisation. Under specific outage constraints for the noise rise and for the packet call throughput, the CSAFT algorithm outperforms the other scheduling strategies; compared to a Release 99 system implementation, it provides a cell throughput increase of 50% and 80% for a macro-cell and a micro-cell environment at low mobile speed, respectively.

7.4 Performance of 768 kbps, 4-Branch Antenna Diversity and IC

Chapter 6 has presented a performance evaluation of three different solutions for the enhancement of uplink performance: Allocation of peak data rates up to 768 kbps, 4-branch antenna diversity and interference cancellation.

768 kbps

The possibility to instantaneously allocate peak data rates as high as 768 kbps has a major potential for enhancing the user experienced data rate. However, in a system that deploys basic features such as 2-branch antenna diversity, conventional matched filter receiver and traditional code division scheduling users can take advantage of the allocation of 768 kbps only when the system is operating in the traffic-limited region, i.e. in case there are only a few high data rate users simultaneously active in one cell.

The situation is different in the case of combined time and code division scheduling, where the instantaneous allocation of 768 kbps allows a reduction of the number of users that must be simultaneously scheduled for transmission in order to utilise the full cell capacity. As a consequence, the multi-user diversity in the system increases. For the CSAFT scheduler introduced in Chapter 5 the multi-user diversity gain from 768 kbps compared to 384 kbps is about 10%. For given outage constraints on both network load and packet call throughput, the gain with CSAFT scheduling and 768 kbps relative to the Release 99 cell throughput performance is 67% and 93% for a macro-cell and a micro-cell environment at low mobile speed, respectively.

4-Branch Antenna Diversity and Interference Cancellation

Among the emerging technologies aiming at increasing the spectral efficiency of 3G systems, two of the most promising solutions are antenna arrays and multi-user detection (MUD).

Concerning the deployment of antenna arrays at the base station, only a space diversity scheme has been considered for performance investigation, mainly due to its advantages in terms of complexity and robustness. The deployment of 4-branch antenna diversity in a macro-cell environment provides a cell throughput increase of about 100% compared to 2-branch antenna diversity. The gain comes from a corresponding reduction of approximately 3 dB in the required E_b/N_0 per receiving antenna. The extra diversity gain with 4-branch antenna diversity is practically negligible, which is also in line with expectations due to the high degree of diversity already available with basic system features (2-branch antenna diversity, macro-diversity due to SHO operation, and multipath diversity in the Vehicular A channel).

The impact on cell throughput performance of interference cancellation techniques has been investigated by means of a semi-analytical approach. The cell throughput gain from IC essentially depends on three factors: The efficiency of the IC receiver, the other-to-own cell interference ratio (since interference cancellation is only effective towards intra-cell interference), and on the uplink load (since the amount of interference that can be cancelled depends on the total received power at the base station receiver). It has been demonstrated that the cell throughput gain with interference cancellation is always smaller than the corresponding pole capacity gain, the pole capacity being defined as the achievable cell throughput when the cell coverage shrinks to zero. System level simulations have validated the semi-analytical results. In a macro-cell environment with low user mobility and for a 5% probability of exceeding a noise rise of 6 dB, the uplink cell throughput gain with a 30% efficient IC receiver (i.e. a receiver able to cancel 30% of the intra-cell interference) is between 15% and 20%. The cell throughput gain can be increased up to approximately 50% if a 70% efficient IC receiver is deployed. However, such high efficiency is unfeasible for practical implementation with an acceptable level of complexity at the receiver.

7.5 Overall Performance Improvement with WCDMA Uplink Evolution

Finally, Figure 7.1 illustrates the overall cell throughput and packet call throughput performance enhancement that can be achieved with WCDMA uplink evolution compared to the Release 99 uplink packet access, and also emphasises the relative gain provided by each one of the enabling technologies. In the most optimistic scenario the average cell throughput in a macro-cell environment with low user mobility can be increased from 1.1 Mbps with basic Release 99 features to approximately 3.9 Mbps. At the same time, the throughput experienced by 90% of the packet calls increases from 64 kbps to 128 kbps.

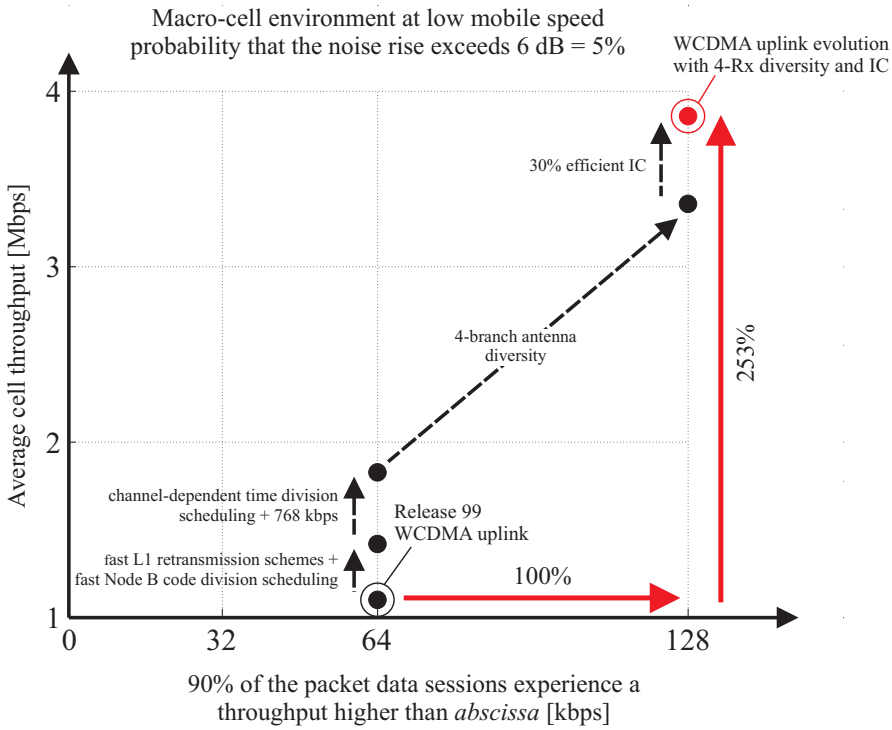

Figure 7.1: Overall cell throughput and packet call throughput performance gain with WCDMA uplink evolution compared to a system operating with basic Release 99 features.

7.6 Future Research

This section addresses proposals for future research activities in relation to some of the issues considered in this Ph.D. thesis.

Perhaps the most relevant topic for further investigations on the performance of WCDMA uplink evolution is traffic modelling. The results presented in this Ph.D. thesis have assumed a single reference traffic model. Its bursty properties and high source data rate made it suitable for studying the performance of enhanced uplink packet access, especially when considering NRT background services. However, other 3G applications characterised by different traffic profiles might have a different impact on the performance evaluation of WCDMA uplink evolution. Moreover, due to the high number of data applications making use of TCP as transport protocol, future research could include in the generated traffic the effect of e.g. TCP slow start, TCP congestion control, and TCP timeouts.

Fast physical layer HARQ schemes can significantly improve the TCP performance and reduce the transmission delays, which might also have a major impact on the performance of

interactive type of services. In presence of data traffic characterised by bursty packet arrivals with more severe delay requirements, fast Node B packet scheduling techniques can provide the system with an attractive feature for a more efficient utilisation of the radio resources. In this case faster and more dynamic packet scheduling operation can significantly improve the system performance, while the benefit from channel-dependent radio resource allocation is expected to reduce due to the lower flexibility allowed by services with tighter delay requirements.

Concerning uplink packet scheduling in 3G systems, an algorithm to be deployed in the context of fast Node B code division scheduling has been introduced. The proposed algorithm has been proven to provide the system with the capability of adapting to both interference and traffic variations by efficiently monitoring the level of utilisation of the allocated resources to NRT users. However, its performance could be improved further by making use of additional information during the packet scheduling procedure. For instance, information on the user buffer occupancy could be utilised to improve the user experienced QoS. Also, information on the UE power margin could be used to allocate users with higher transmission rates when experiencing favourable channel conditions as in the case of channel-dependent scheduling. In this case the scheduler would only be able to exploit the slow fading characteristics of the mobile propagation channel, but still there is the potential for increasing the uplink spectral efficiency.

For what concerns combined time and code division scheduling, future research should be mainly addressed at including some of the complexity issues neglected in this Ph.D. study. The most important among these issues is perhaps the increased signalling overhead, especially the required uplink signalling since it has a direct impact on the achievable cell throughput in uplink. Another issue is the accuracy in the estimation of the uplink channel quality indicator, which is used in determining the priority between users. The proposed method to derive information on the instantaneous uplink channel quality assumes exact information on the UE transmission power available at the Node B packet scheduler on a TTI basis. Since this is in practice not feasible, a robust technique to extract information on the uplink channel quality should be derived, or alternatively the impact of estimation errors should be investigated in more detail. On the other hand, with time and code division scheduling there is also the possibility for advancing the performance of WCDMA uplink packet access: First of all by enabling peak data rate in the order of a few Mbps, thus increasing the multi-user diversity in the system. Second, by developing more sophisticated scheduling priorities that together with the instantaneous channel quality make use of additional information on e.g., the amount of data users have in their buffers.

Bibliography

[Aldi03] N.M. Aldibbiat, M.R. McVeeigh, and T. O'Farrel. *Evaluation of Traffic Mixing in the UTRA for Shadowed and Non-Shadowed Environments*. Proceedings of London Communication Symposium, pp. 177-180, September 2003.

[Ameg03] P. J. Amegeiras. *Packet Scheduling and Quality of Service in HSDPA*. Ph.D. Thesis, Aalborg University (Denmark), October 2003.

[Barr02] G. Barriac, and J. Holtzman. *Introducing Delay Sensitivity into the Proportional Fair Algorithm for CDMA Downlink Scheduling*. Proceedings of the 7th International Symposium on Spread Spectrum Techniques and Applications, Vol. 3, pp. 652-656, September 2002.

[Berg01] F. Berggren, Seong-Lyun Kim, R. Jäntti, and J. Zander. *Joint Power Control and Intracell Scheduling of DS-CDMA Nonreal Time Data*. IEEE Journal on Selected Areas in Communications, Vol. 19, Issue No 10, pp. 1860-1870, October 2001.

[Berg04a] F. Berggren, and R. Jäntti. *Asymptotically Fair Transmission Scheduling Over Fading Channels*. IEEE Transactions on Wireless Communications, Vol. 3, Issue No 1, pp. 326-336, January 2004.

[Berg04b] F. Berggren, and S.-L. Kim. *Energy-Efficient Control of Rate and Power in DS-CDMA Systems*. IEEE Transactions on Wireless Communications, Vol. 3, Issue No 3, pp. 725-733, May 2004.

[Bhag96] P. Bhagwat, P. Bhattacharya, A. Krishna, and S.K. Tripathi. *Enhancing Throughput Over Wireless LANs Using Channel State Dependent Packet Scheduling*. IEEE Proceedings of the INFOCOM '96, Vol.3, pp. 1133-1140, March 1996.

[Bouch00] A. Bouch, A. Kuchinsky, and N.T. Bhatti. *Quality is in the Eye of the Beholder: Meeting Users' Requirements for Internet Quality of Service*. Proceedings of SIGCHI, Conference on Human Factors in Computing Systems, pp. 297-304, April 2000.

[Bueh00] R.M. Buehrer, N.S. Correal-Mendoza, and B.D. Woerner. *A Simulation Comparison of Multiuser Receivers for Cellular CDMA*. IEEE Transactions on Vehicular Technology, Vol. 49, Issue No 4, pp. 1065-1085, July 2000.

[Chase85] D. Chase. *Code Combining: A Maximum-Likelihood Decoding Approach for Combining an Arbitrary Number of Noisy Packets*. IEEE Transactions on Communications, Vol. 33, Issue No 5, pp. 385-393, May 1985.

[Chau99] P. Chaudhury, W. Mohr, and S. Onoe. *The 3GPP Proposal for IMT-2000*. IEEE Communications Magazine, Vol. 37, Issue No 12, pp. 72-81, December 1999.

[Chen99] E.J. Chen, and W.D. Kelton. *Simulation-Based Estimation of Quantiles*. Proceedings of the 31st Conference on Winter Simulation, pp. 428-434, December 1999.

[Clar68] R.H. Clarke. *A Statistical Theory of Mobile-Radio Reception*. Bell Systems Technical Journal, Vol. 47, pp. 957-1000, 1968.

[Dahl00] D. Dahlhaus, and Zhenlan Cheng. *Smart Antenna Concepts with Interference Cancellation for Joint Demodulation in the WCDMA UTRA Uplink*. IEEE Proceedings of the 6th International Symposium on Spread Spectrum Techniques and Applications, Vol.1, pp. 244-248, September 2000.

[Das01] A. Das, F. Khan, A. Sampath, and S. Hsuan-Jung. *Performance of Hybrid ARQ for High Speed Downlink Packet Access in UMTS*. IEEE Proceedings of the 54th Vehicular Technology Conference, Vol. 4, pp. 2133-2137, October 2001.

[Duel95] A. Duel-Hallen, J. Holtzman, and Z. Zvonar. *Multiuser Detection for CDMA Systems*. IEEE Personal Communications, Vol. 2, Issue No 2, pp. 46-58, April 1995.

[Erik01] M. Eriksson, D. Turina, H. Arslan, K. Balachandran, and Jung-Fu Cheng. *System Performance with Higher Level Modulation in the GSM/EDGE Radio Access Network*. IEEE Global Telecommunications Conference GLOBECOM '01, Vol. 5, pp. 3065-3069, November 2001.

[Fior00] A. Fiorini. *Uplink User Bitrate Adaptation of Packet Data Transmission in WCDMA*. The 11th IEEE International Symposium on Personal, Indoor and Mobile Radio Communications (PIMRC), Vol. 2, pp. 1510-1514, September 2000.

[Fosc96] G.J. Foschini. *Layered Space-Time Architecture for Wireless Communication in a Fading Environment When Using Multiple Antennas*. Bell Labs Technical Journal, Vol. 1, Issue No 2, pp. 41-59, Autumn 1996.

[Fred02] F. Frederiksen, and T.E. Kolding. *Performance and Modeling of WCDMA/HASDPA Transmission/H-ARQ Schemes*. IEEE Proceedings of the 56th Vehicular Technology Conference, Vol. 1, pp. 472-476, September 2002.

[Fren01] P. Frenger, S. Parkvall, and E. Dahlman. *Performance Comparison of HARQ with Chase combining and Incremental Redundancy for HSDPA*. IEEE Proceedings of the 54th Vehicular Technology Conference, Vol. 3, pp. 1829-1833, October 2001.

[Furu99] A. Furuskar, S. Mazur, F. Muller, and H. Olofsson. *EDGE: Enhanced Data Rates for GSM and TDMA/136 Evolution*. IEEE Personal Communications, Vol. 6, Issue No 3, pp. 56-66, June 1999.

[Ghosh04] A. Ghosh, R. Love, N. Whinnett, R. Ratasuk, W. Xiao, and R. Kuchibhotla. *Overview of Enhanced Uplink for 3GPP W-CDMA*. IEEE Proceedings of the 59th Vehicular Technology Conference, May 2004.

[Hage04] B. Hagerman, F. Gunnarsson, H. Murai, M. Tadenuma, and J. Karlsson. *WCDMA Uplink Interference Cancellation Performance – Field Measurements and System Simulations*. Nordic Radio Symposium, Session 10 – WCDMA Enhancements. August 2004.

[Hedb01] T. Hedberg, and S. Parkvall. *Evolving WCDMA*. Ericsson Review, Issue No 3, pp. 124-131, 2001. Available at www.ericsson.com.

[Heid81a] P. Heidelberger, and P.D. Welch. *A Spectral Method for Confidence Interval Generation and Run Length Control in Simulations*. Communications of the ACM, Vol. 24, Issue No 4, pp. 233-245, April 1981.

[Heid81b] P. Heidelberger, and P.D. Welch. *Adaptive Spectral Methods for Simulation Output analysis*. IBM Journal of Research and Development, Vol. 25, Issue No 6, pp. 860-876, November 1981.

[Hern00] M.A. Hernandez, G.J.M. Janssen, and R. Prasad. *Uplink Performance Enhancement for WCDMA Systems through Adaptive Antennas and Multiuser Detection*. IEEE Proceedings of the 51st Vehicular Technology Conference, Vol. 1, pp. 571-575, May 2000.

[Hilt03] K. Hiltunen, and M. Karlsson. *A Novel WCDMA Uplink Capacity and Coverage Model Including the Impact of Non-Ideal Fast Power Control and Macro Diversity*. IEEE Proceedings of the 57th Vehicular Technology Conference, Vol. 1, pp. 98-102, April 2003.

[Holma99] H. Holma, and J. Laakso. *Uplink Admission Control and Soft Capacity with MUD in CDMA*. IEEE Proceedings of the 50th Vehicular Technology Conference, Vol. 1, pp. 431-435, September 1999.

[Holma01] H. Holma, and A. Tölli. *Simulated and Measured Performance of 4-Branch Uplink Reception in WCDMA*. IEEE Proceedings of the 53rd Vehicular Technology Conference, Vol. 4, pp. 2640-2644, May 2001.

[Holma04] H. Holma, and A. Toskala. *WCDMA for UMTS: Radio Access for Third Generation Mobile Communications*. Third edition, John Wiley & Sons, 2004.

[Hwan01] Gyung-Ho Hwang, and Dong-Ho Cho. *Distributed Rate Control for Throughput Maximization and QoS Support in WCDMA*. IEEE Proceedings of the 54th Vehicular Technology Conference, Vol. 3, pp. 1721-1725, October 2001.

[Hytö01] T. Hytönen. *Optimal Wrap-Around Network Simulation*. Helsinki University of Technology Report, A432, 2001.

[Hämä96] S. Hämäläinen, H. Holma, and A. Toskala. *Capacity Evaluation of a Cellular CDMA Uplink with Multiuser Detection*. IEEE Proceedings of the 4th International Symposium on Spread Spectrum Techniques and Applications, Vol.1, pp. 339-343, September 1996.

[Hämä97] S. Hämäläinen, P. Slanina, M. Hartman, A. Lappeteläinen, and H. Holma. *A Novel Interface Between Link and System Level Simulations*. Proceedings of the ACTS Mobile Telecommunications Summit, pp. 599-604, October 1997.

[Jakes74] W.C. Jakes. *Microwave Mobile Communications*. IEEE Press, 1974.

[Jänt01] R. Jäntti, and Seong-Lyun Kim. *Transmission Rate Scheduling for the Non-Real Time Data in a Cellular CDMA System*. IEEE Communications Letters, Vol. 5, Issue No 5, pp. 200-202, May 2001.

[Jänt03] R. Jäntti, and D. Zhao. *On Minimum Time Span Scheduling of Non-Real Time Data in Uplink of DS-CDMA Systems*. IEEE Proceedings of the 57th Vehicular Technology Conference, Vol. 3, pp. 1699-1703, April 2003.

[Kim01] D.K. Kim, S.H. Hwang, E.K. Hong, and S.Y. Lee. *Capacity Estimation for an Uplink Synchronised CDMA System with Fast TPC and Two-Antenna Diversity Reception*. IEICE Transactions on Communications, Vol. E84-B, Issue No 8, pp. 2309-2312, August 2001.

[Knopp95] R. Knopp, P.A. Humblet. *Information Capacity and Power Control in Single-Cell Multiuser Communications*. IEEE International Conference on Communications, Vol. 1, pp. 331-335, June 1995.

[Kold03] T.E. Kolding, K.I. Pedersen, J. Wigard, F. Frederiksen, and P.E. Mogensen. *High Speed Downlink Packet Access: WCDMA Evolution*. IEEE Vehicular Technology Society News, Vol. 50, Issue No 1, pp. 4-10, February 2003.

[Kuma03] K. Kumaran, and L. Qian. *Uplink Scheduling in CDMA Packet-Data Systems*. IEEE Proceedings of the INFOCOM 2003, Vol.1, pp. 292-300, April 2003.

[Lin84] Shu Lin, D. Costello, and M. Miller. *Automatic-Repeat-Request Error-Control Schemes*. IEEE Communications Magazine, Vol. 22, Issue No 12, pp. 5-17, December 1984.

[Lin02] Hao Lin, Wei Wu, Yong Ren, and Xiuming Shan. *A Time-Scale Decomposition Approach to Optimize Wireless Packet Resource Allocation and Scheduling*. IEEE Wireless Communications and Networking Conference, Vol. 2, pp. 699-705, March 2002.

[Liu01] X. Liu, E.K.P. Chong, , and N.B. Shroff. *Opportunistic Transmission Scheduling with Resource-Sharing Constraints in Wireless Networks*. IEEE Journal on Selected Areas in Communications, Vol. 19, Issue No 10, pp.2053-2064, October 2001.

[Malk01] E. Malkamäki, D. Mathew, and S. Hämäläinen. *Performance of Hybrid ARQ Techniques for WCDMA High Data Rates*. IEEE Proceedings of the 53rd Vehicular Technology Conference, Vol. 4, pp. 2720-2724, May 2001.

[Mall04] D. Malladi, X. Zhang, J. Damnjanovic, and S. Willenegger. *WCDMA Uplink System Performance*. IEEE Proceedings of the 60th Vehicular Technology Conference, September 2004.

[Mand74] D.M. Mandelbaum. *Adaptive-Feedback Coding Scheme Using Incremental Redundancy*. IEEE Transaction on Information Theory, IT-20, pp. 388-389, May 1974.

[Mason89] R.L. Mason, R.F. Gunst, and J.L. Hess. *Statistical Design and Analysis of Experiments*. John Wiley & Sons, 1989.

[Meng03] Meng Cai, Xi Zhang, Ning Zhou, and S.B. Slimane. *On the Capacity of CDMA with Linear Successive Interference Cancellation*. 5th European Personal Mobile Communications Conference, Conf. Publ. No 492, pp. 362-366, 2003.

[Mosh96] S. Moshavi. *Multi-User Detection for DS-CDMA Communications*. IEEE Communications Magazine, Vol. 34, Issue No 10, pp. 124-136, October 1996.

[NOK02] K. Heiska. *Radio Resource Management*. March 2002. Reproduced by permission of John Wiley & Sons Limited. Available at http://www.mit.jyu.fi/riesta/WCDMA_ACLCPC_001.pdf

[Oh03] Seong-Jun Oh, A.D. Damnjanovic, and A.C.K. Soong. *Information-Theoretic Sum Capacity of Reverse Link CDMA Systems*. IEEE Proceedings of the 57th Vehicular Technology Conference, Vol. 1, pp. 93-97, April 2003.

[Outes01] J. Outes, L. Nielsen, K.I. Pedersen, and P.E. Mogensen. *Multi-Cell Admission Control for UMTS*. IEEE Proceedings of the 53rd Vehicular Technology Conference, Vol. 2, pp. 987-991, May 2001.

[Outes02a] J. Outes, K.I. Pedersen, and P.E. Mogensen. *Performance of Uplink Synchronous WCDMA at Network Level*. IEEE Proceedings of the 55th Vehicular Technology Conference, Vol. 1, pp. 105-109, May 2002.

[Outes02b] J. Outes, K.I. Pedersen, P.E. Mogensen, and T.E. Kolding. *Uplink Synchronous WCDMA Combined with Variable Modulation and Coding*. IEEE Proceedings of the 56th Vehicular Technology Conference, Vol. 1, pp. 482-486, September 2002.

[Outes04] J. Outes. *Uplink Capacity Enhancement in WCDMA*. Ph.D. Thesis, Aalborg University (Denmark), March 2004.

[Owen00] R. Owen, P. Jones, S. Dehgan, and D. Lister. *Uplink WCDMA Capacity and Range as a Function of Inter-to-Intra Cell Interference: Theory and Practice*. IEEE Proceedings of the 51st Vehicular Technology Conference, Vol. 1, pp. 298-302, May 2000.

[Park03] S. Parkvall, E. Englund, P. Malm, T. Hedberg, M. Persson, and J. Peisa. *WCDMA evolved – High-Speed Packet-Data Services*. Ericsson Review, Issue No 2, pp. 56-65, 2003. Available at www.ericsson.com.

[Park04] S. Parkvall, E. Englund, K. W. Helmersson, and M. Samuelsson. *WCDMA Uplink Enhancements for High-Speed Data Access*. IEEE Proceedings of the 60th Vehicular Technology Conference, September 2004.

[Peng02] Xiaoming Peng, F.P.S. Chin, Ying-Chang Liang, and M. Motani. *Performance of Hybrid ARQ Techniques Based on Turbo Codes for High-Speed Packet Transmission*. IEEE Proceedings of the 7th International Symposium on Spread Spectrum Techniques and Applications, Vol. 3, pp. 682-686, September 2002.

[Pi03] Z. Pi, and R.T. Derryberry. *CDMA2000 1x EV-DV Reverse Link System Design*. Wireless Communications and Networking, Vol. 1, pp. 514-519, March 2003.

[Pinto00] H. Bento Pinto, J. Gaspar da Silva, and A. Rodrigues. *Uplink Capacity of the WCDMA FDD Mode in UMTS Networks for Mixed Services*. IEEE Proceedings of the 52nd Vehicular Technology Conference, Vol. 6, pp. 2617-2624, September 2000.

[Proak95] J.G. Prakis. *Digital Communications*. McGraw-Hill, 1995.

[Rait98] M. Raitola, and H. Holma. *Wideband CDMA Packet Data with Hybrid HARQ*. IEEE Proceedings of the 5th International Symposium on Spread Spectrum Techniques and Applications, Vol. 1, pp. 318-322, September 1998.

[Rama98] S. Ramakrishna, and J.M. Holtzman. *A Scheme for Throughput Maximization in a Dual-Class CDMA System*. IEEE Journal on Selected Areas in Communications, Vol.16, Issue No 6, pp. 830-844, August 1998.

[Rami03] J. Ramiro-Moreno. *System Level Performance Analysis of Advanced Antenna Concepts in WCDMA*. Ph.D. Thesis, Aalborg University (Denmark), July 2003.

[Rata02] R. Ratasuk, and A. Ghosh. *Performance Analysis of Time-Multiplexed Services for UMTS W-CDMA Reverse Link*. IEEE Proceedings of the 56th Vehicular Technology Conference, Vol. 3, pp. 1607-1611, September 2002.

[Salo99] O. Salonaho, and J. Laakso. *Flexible Power Allocation for Physical Control Channel in Wideband CDMA*. IEEE Proceedings of the 49th Vehicular Technology Conference, Vol. 2, pp. 1455-1458, May 1999.

[Samp95] A. Sampath, P. Sarath Kumar, and J.M. Holtzman. *Power Control and Resource Management for a Multimedia CDMA Wireless Systems*. The 6th IEEE International Symposium on Personal, Indoor and Mobile Radio Communications (PIMRC), Vol. 1, pp. 21-25, September 1995.

[Samp97] A. Sampath, P. Sarath Kumar, and J.M. Holtzman. *On Setting Reverse Link Target SIR in a CDMA System*. IEEE Proceedings of the 47th Vehicular Technology Conference, Vol. 2, pp. 929-933, May 1997.

[Tiir03] E. Tiirola, and J. Ylitalo. *Performance of a UMTS Uplink MIMO Scheme*. IEEE Proceedings of the 58th Vehicular Technology Conference, Vol. 1, pp. 657-661, October 2003.

[TR25896] 3GPP. Technical Specification Group Radio Access Network. *Feasibility Study for Enhanced Uplink for UTRA FDD*. 3GPP TR 25.896 version 6.0.0, Release 6, March 2004. Available at www.3gpp.org.

[TS25101] 3GPP. Technical Specification Group Radio Access Network. *User Equipment (UE) Radio Transmission and Reception (FDD)*. 3GPP TS 25.101 version 6.5.0, Release 6, September 2004.

[TS25211] 3GPP. Technical Specification Group Radio Access Network. *Physical Channels and Mapping of Transport Channels onto Physical Channels (FDD)*. 3GPP TS 25.211 version 6.2.0, Release 6, September 2004.

[TS25212] 3GPP. Technical Specification Group Radio Access Network. *Multiplexing and Channel Coding (FDD)*. 3GPP TS 25.212 version 6.2.0, Release 6, June 2004

[TS25213] 3GPP. Technical Specification Group Radio Access Network. *Spreading and Modulation (FDD)*. 3GPP TS 25.213 version 6.0.0, Release 6, December 2003.

[TS25214] 3GPP. Technical Specification Group Radio Access Network. *Physical Layer Procedures (FDD)*. 3GPP TS 25.214 version 6.3.0, Release 6, September 2004.

[TS25321] 3GPP. Technical Specification Group Radio Access Network. *Medium Access Control (MAC) Protocol Specification*. 3GPP TS 25.321 version 6.2.0, Release 6, June 2004. Available at www.3gpp.org.

[TS25331] 3GPP. Technical Specification Group Radio Access Network. *Resource Control (RRC) Protocol Specification*. 3GPP TS 25.331 version 6.3.0, Release 6, September 2004. Available at www.3gpp.org.

[TS25433] 3GPP. Technical Specification Group Radio Access Network. *UTRAN Iub Interface NBAP Signalling*. 3GPP TS 25.433 version 6.3.0, Release 6, September 2004.

[Uluk00] S. Ulukus, and L.J. Greenstein. *Throughput Maximization in CDMA Uplinks Using Adaptive Spreading and Power Control*. IEEE Proceedings of the 6th International Symposium on Spread Spectrum Techniques and Applications, Vol. 2, pp. 565-569, September 2000.

[UMTS00] UMTS Forum. UMTS Forum Report No 11. *Enabling UMTS / Third Generation Services and Applications*. October 2000. Available at www.umts-forum.org.

[UMTS03] UMTS Forum. White Paper No 1. *Mobile Evolution: Shaping the Future*. August 2003. Available at www.umts-forum.org.

[UM3003] European Telecommunications Standards Institute, TR 101 112. *Selection Procedures for the Choice of radio Transmission Technologies of the UMTS*. UMTS 30.03 version 3.2.0, April 1998.

[Veer97] V.V. Veeravalli, A. Sendonaris, and N. Jain. *CDMA Coverage, Capacity and Pole Capacity*. IEEE Proceedings of the 47th Vehicular Technology Conference, Vol. 3, pp. 1450-1454, May 1997.

[Veer99] V.V. Veeravalli, and A. Sendonaris. *The Coverage-Capacity Tradeoff in Cellular CDMA Systems*. IEEE Transactions on Vehicular Technology, Vol. 48, Issue No 5, pp. 1443-1450, September 1999.

[Verdu86] S. Verdú. *Minimum Probability of Error for Asynchronous Gaussian Multiple-Access Channels*. IEEE Transactions on Information Theory, Vol. 32, Issue No 1, pp. 85-96, January 1986.

[Verdu98] S. Verdú. *Multi-User Detection*. New York, Cambridge University Press, 1998.

[Verdu00] S. Verdú. *Wireless Bandwidth in the Making*. IEEE Communications Magazine, Vol. 38, Issue No 7, pp. 53-58, July 2000.

[Vill00] E. Villier, P. Legg, S. Barret. *Packet Date Transmission in a W-CDMA Network – Examples of Uplink Scheduling and Performance*. IEEE Proceedings of the 51st Vehicular Technology Conference, Vol. 3, pp. 2449-2453, May 2000.

[Ylit00] J. Ylitalo, and E. Tiirola. *Performance Evaluation of Different Antenna Array Approaches for 3G CDMA Uplink*. IEEE Proceedings of the 51st Vehicular Technology Conference, Vol. 2, pp. 883-887, May 2000.

[Wack99] A. Wacker, J. Laiho-Steffens, K. Sipilä, K. Heiska. *The Impact of the Base Station Sectorisation on WCDMA Radio Network Performance*. IEEE Proceedings of the 50th Vehicular Technology Conference, Vol. 5, pp. 2611-2615, September 1999.

[Wibe00] N. Wiberg, and A. Gioia. *Uplink Packet Access Control in WCDMA*. IEEE Proceedings of the 51st Vehicular Technology Conference, Vol. 3, pp. 2203-2206, May 2000.

[Zand97] J. Zander. *Radio Resource Management in Future Wireless Networks: Requirements and Limitations*. IEEE Communications Magazine, Vol. 35, Issue No 8, pp. 30-36, August 1997.

Appendix A

System Level Simulator and Performance Indicators

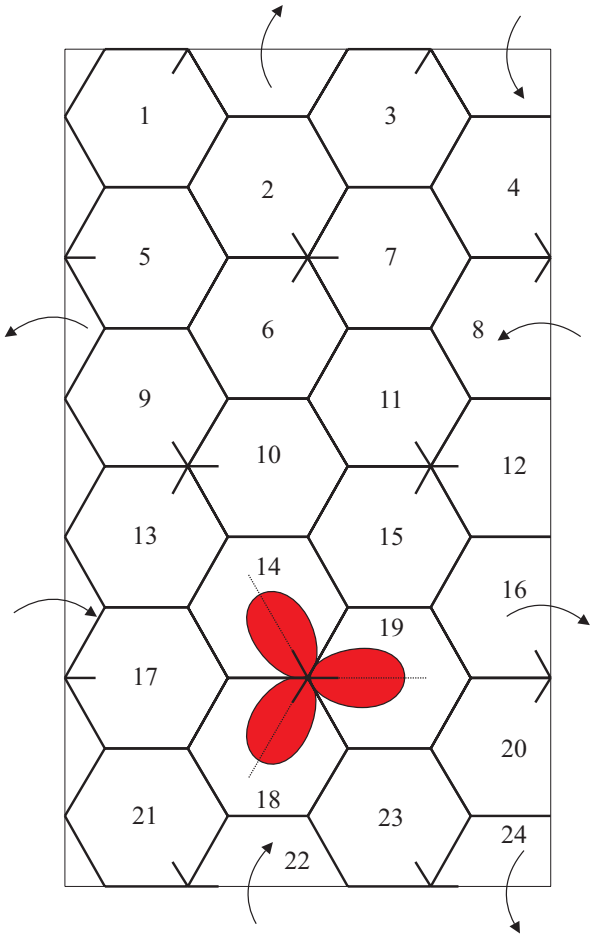

Figure A.1: Simulated network layout with wrap around technique.

This appendix shortly describes the model used in the system level simulator for the performance assessment of WCDMA uplink packet access. It also introduces the definition of some fundamental measures used in this Ph.D. thesis for both network and user performance evaluation, and explains how these measures are derived from system level simulations. Finally, some considerations are made on the level of accuracy of the most relevant among these key performance indicators.

A.1 System Level Simulator

A.1.1 Network Layout

The cell layout is a regular grid comprising 24 cells and 8 sites and includes the wrap around technique described in [Hytö01]. At the beginning of each simulation, users are placed in the network area illustrated in Figure A.1 according to a uniform over area distribution. Users remain in the network for the duration of the simulation and no new users are admitted. The site-to-site distance depends on the propagation scenario, whether it is macro-cell or micro-cell.

A.1.2 Mobility and Propagation

During the simulation, users move around with constant velocity depending on the mobility scenario, and with constant direction assigned to each user during the initialisation phase according to a uniform distribution on the interval [0°, 360°).

The power attenuation between each user and each Node B is modelled according to either the vehicular or the pedestrian test environments in [TR25896], including path loss, large-scale fading (shadowing), and small-scale time-dispersive fading. It also includes the effect of a sectorised antenna pattern.

Two different path loss models are used for the simulation of macro-cell vehicular and a micro-cell pedestrian environment [UM3003]. The shadow fading is modelled according to a lognormal distribution, and is assumed to be uncorrelated between every link connecting a mobile terminal to a Node B. The shadowing model uses a simple decreasing correlation function to model the spatial-correlation properties of the channel [Aldi03]. Small scale fading is modelled by independent Rayleigh processes at each tap of the power delay profile, which is either the ITU Vehicular A or the ITU Pedestrian A [TR25896]. Classical Doppler is included to model the temporal evolution of fading on each tap of the power delay profile. The antenna radiation pattern is obtained from [TR25896]:

$$A(\theta)_{dB} = -\min\left[12\left(\frac{\theta}{\theta_{3dB}}\right), A_m\right] \qquad -180^\circ \le \theta \le 180^\circ \tag{A.1}$$

In (A.1), θ_{3dB} is the 3 dB beam width, A_m is the maximum attenuation, and θ is the azimuth angle of the user relative to the broadside direction of the corresponding sector.

A.1.3 Basic Network Functions

In the default implementation of the system level simulator, the Node B is assumed to deploy 2-branch antenna diversity with ideal Rake processing of the received signals. The model also includes SHO with selection diversity performed at the RNC. If the Node Bs in the active set are located at the same site (see Figure A.1), then ideal MRC is performed at the base station receiver (softer-handover). The SHO status for each simulated user is modified according to the variations in the path loss and in the large-scale fading, the underlying assumption being that fast fading is averaged out during the measurement procedure.

Both inner loop and outer loop power control algorithms are implemented in the system level simulator. Fast closed loop power control is run for each user on a WCDMA slot interval. Neither transmission errors nor transmission delay of power control commands are modelled. Users in SHO increase their transmission power only upon receiving a power up command from all the Node Bs in the active set.

The outer loop power control (OLPC) algorithm deployed in the system level simulator is the one presented in [Samp97]. The algorithm is based on the result of a CRC check of the transmitted data and can be characterised in pseudocode as in Figure A.2. In our implementation, the result of the CRC check is included in the BLER calculation. In Figure A.2, *Eb/N0_target* [*n*] is the target E_b/N_0 at radio frame *n*, *BLER_target* is the target block error rate, and *Step_size* is an algorithm's specific parameter that determines the convergence speed to the desired target, and also defines the overhead caused by the algorithm. The OLPC algorithm is only performed in case data is transmitted on the DPDCH. With HARQ and combining techniques such as CC and IR, the OLPC is only performed at the first transmission of each data frame.

IF CRC check OK
Eb/N0_target [*n*+1] = *Eb/N0_target* [*n*] – *BLER_target* * *Step_size*
ELSE
Eb/N0_target [*n*+1] = *Eb/N0_target* [*n*] + (1-*BLER_target*) * *Step_size*
END

Figure A.2: Pseudocode of the outer loop power control algorithm.

A summary of the most relevant system model parameters for the simulation of both macro-cell and micro-cell environments is reported in Table A.1.

General	Time resolution	WCDMA time slot (0.667 ms)
	Admission control	None (fixed # users)
Cell layout	Grid size (hexagonal)	24 cells – 8 sites with 3 sectors per site (see Figure A.1)
	Grid configuration	Wrap around [Hytö01]
	Site-to-site distance	3232 m (1) – 1040 m (2)
	Receive antennas per cell	2 (uncorrelated ideal MRC)
	Node B antenna gain	14 dBi
	Receiver antenna gain pattern	See (A.1) – $\theta_{3dB} = 70°$, A_m=20 dB
	UE antenna gain	0 dB
Propagation	Path loss [dB] with distance *d* [km]	128.1 + 37.6 log *d* (1) 147.7 + 40 log *d* (2)
	Shadow fading standard deviation	8 dB
	Shadow fading decorrelation distance	100 m
	Power delay profile	ITU Vehicular A (1) – ITU Pedestrian A (2)
	Doppler spectrum	Clarke's spectrum [Clar68]
	Noise level per receive antenna	-102.9 dBm
Soft handover	Maximum active set size	2
	Window add / drop / replace	2 dB / 4 dB / 2dB
	Drop timer	0.05 s
Power control	Fast closed loop PC step size	1 dB for 10 ms TTI, 0.3 dB for 2 ms TTI (see Section C.5)
	Outer loop PC step size	0.3 dB
	Frequency of outer loop PC updates	Once every TTI

Table A.1: Summary of the main system model parameters for the simulation of both macro-cell (1) and micro-cell (2) environments.

A.2 Definition of Performance Indicators

This section outlines some of the most significant indicators used for the performance assessment of WCDMA uplink packet access. Let us first introduce the following definitions:

$n_1^{i,m}$ Is the TTI number in correspondence with the transmission of the first data frame in the m^{th} packet call of user *i*.

$n_2^{i,m}$ Is the TTI number in correspondence with the transmission of the last data frame in the m^{th} packet call of user *i*.

$t_0^{i,m}$ Is the time slot number in correspondence with the arrival at the user buffer of the first data packet of the m^{th} packet call of user *i*.

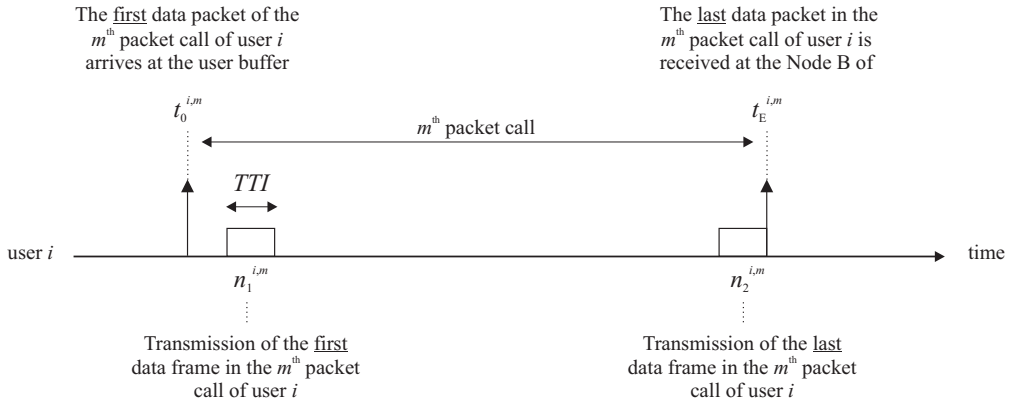

Figure A.3: Timing diagram for the m^{th} packet call of user i.

$t_E^{i,m}$ Is the time slot number in correspondence with the correct reception at the Node B of the last data packets in the m^{th} packet call of user i.

TTI Is the duration of one transmission time interval.

TS Is the duration of a WCDMA time slot.

Figure A.3 illustrates the significance of the introduced definitions. The time resolution for $n_1^{i,m}$ and $n_2^{i,m}$ is one transmission time interval, while the time resolution for $t_0^{i,m}$ and $t_E^{i,m}$ is one WCDMA time slot. That is why there can be a short gap between the arrival of the first data packet in a packet call ($t_0^{i,m}$) and the transmission of the first data frame over the air interface ($n_1^{i,m}$). In general, the indexes n and t are used whether the time resolution is one TTI or one time slot, respectively.

[A 2.1] *Per TTI Throughput*

Let us define $b_i[n]$ as the number of data bits correctly transmitted by user i in transmission time interval n. The per TTI throughput of user i at transmission time interval n is then defined as the ratio of $b_i[n]$ to the duration of the transmission time interval.

$$\lambda_i[n] = \frac{b_i[n]}{TTI} \qquad n \in \bigcup_{m=1}^{M_i} \left[n_1^{i,m}, n_2^{i,m} \right] \tag{A.2}$$

In (A.2), M_i is the total number of packet data sessions completed by user i during the simulation time. Notice that the per TTI throughput is only defined when the user is in an active packet call, i.e. in the 'on' period of the traffic model duty cycle (see Appendix D).

[A 2.2] *Packet Call Throughput*

We define the packet call size as the number of bits generated in the user buffer during a packet call, and the packet call delay as the time interval between the time of arrival of the first data packet ($t_0^{i,m}$) and the instant in which the last data packet is correctly received at the Node B ($t_E^{i,m}$). Then, the packet call throughput is defined as the ratio of the packet call size to the packet call delay. Based on the definitions previously introduced, the packet call throughput for the m^{th} packet data session of user i is defined as:

$$p_i^{\,m} = \frac{\sum b_i[n]}{TS \cdot (t_{\mathrm{E}}^{\,i,m} - t_0^{\,i,m})} \qquad m = 1,\ldots,M_i \tag{A.3}$$

[A 2.3] *Average Packet Call Throughput*

Let us define PCT_1, PCT_2,…, PCT_M the collection of all the packet call throughput values calculated from (A.3) during the entire simulation time, and for all the simulated users.

$$\begin{aligned} &PCT_1, PCT_2, \ldots, PCT_{M_1} = p_1^{\,1}, p_1^{\,2}, \ldots, p_1^{\,M_1} \\ &PCT_{M_1+1}, PCT_{M_1+2}, \ldots, PCT_{M_1+M_2} = p_2^{\,1}, p_2^{\,2}, \ldots, p_2^{\,M_2} \\ &\ldots \\ &PCT_{\sum_{i=1}^{N-1} M_i+1}, PCT_{\sum_{i=1}^{N-1} M_i+2}, \ldots, PCT_{\sum_{i=1}^{N-1} M_i+M_N} = p_N^{\,1}, p_N^{\,2}, \ldots, p_N^{\,M_N} \end{aligned} \tag{A.4}$$

Given N (the total number of simulated users) and M_i (the number of packet calls completed by user i during the simulation time), the total number M of packet call throughput values can be derived as:

$$M = \sum_{i=1}^{N} M_i \tag{A.5}$$

The average packet call throughput is defined as the sample average of the values PCT_1, PCT_2,…, PCT_M.

$$\overline{PCT} = \frac{1}{M} \sum_{i=1}^{M} PCT_i \tag{A.6}$$

[A 2.4] *100·p% Packet Call Throughput Outage*

Let us define Y_1, Y_2,…, Y_M the order statistics of PCT_1, PCT_2,…, PCT_M introduced in definition [A 2.3] (i.e. Y_i is the i^{th} smallest of PCT_1, PCT_2,…, PCT_M).

The 100·p% packet call throughput outage is defined as the sample p percentile of the order statistics Y_1, Y_2,…, Y_M.

$$pct^{\,p} = Y_{\lceil M \cdot p \rceil} \tag{A.7}$$

In (A.7), $\lceil z \rceil$ denotes the integer ceiling of the real number z.

[A 2.5] *Data Bit Energy to Interference Ratio (E_b/N_0)*

In the system level simulator, the data bit energy to interference ratio is calculated for each user on a per time slot basis. At time slot t and for user i, the E_b/N_0 at the a^{th} antenna of the b^{th} Node B is defined as:

$$\rho_{i,a}{}^{b}[t] = \frac{W}{R_i[t]} \cdot \frac{P_{tx}{}^{i}[t] \cdot \left(\underline{\boldsymbol{h}}_{i,a}{}^{b}[t]\right)^{H} \cdot \underline{\boldsymbol{h}}_{i,a}{}^{b}[t]}{\sum_{\substack{j=1 \\ j \neq i}}^{N} P_{tx}{}^{j}[t] \cdot \left(\underline{\boldsymbol{h}}_{j,a}{}^{b}[t]\right)^{H} \cdot \underline{\boldsymbol{h}}_{j,a}{}^{b}[t] + P_{noise}} \tag{A.8}$$

- W is the WCDMA chip rate.
- $R_i[t]$ is the data rate of user i at time slot t.
- $P_{tx}{}^{i}[t]$ is the transmission power of user i at time slot t.
- $\underline{\boldsymbol{h}}_{i,a}{}^{b}[t]$ is the channel impulse response at time slot t between user i and the a^{th} antenna of the b^{th} Node B. It includes the effects of path loss, shadow fading, fast fading, sectorised antenna pattern, and power delay profile depending on the specific channel model.
- $(\underline{\boldsymbol{h}})^{H}$ is the conjugate transpose of vector $\underline{\boldsymbol{h}}$.
- P_{noise} is the background noise power.
- N is the total number of users in the system.

In the case the user does not transmit data on the DPDCH, the E_b/N_0 is calculated assuming a data rate equal to 2 kbps. For more clarifications on this issue, refer to Appendix C.

[A 2.6] *Noise Rise*

The noise rise is defined as the ratio of the total received uplink wideband power to the background noise power. In the system level simulator, the noise rise at the b^{th} Node B at time slot t is derived as:

$$nr_b[t] = \frac{\sum_{a=1}^{A}\left(\sum_{j=1}^{N} P_{tx}{}^{j}[t] \cdot \left(\underline{\boldsymbol{h}}_{j,a}{}^{b}[t]\right)^{H} \cdot \underline{\boldsymbol{h}}_{j,a}{}^{b}[t]\right)}{A \cdot P_{noise}} \tag{A.9}$$

In (A.9), A is the number of receiving antennas at the b^{th} Node B, while the other variables have been introduced in definition [A 2.5].

[A 2.7] *100·p% Noise Rise Outage*

Let us define NR_1, NR_2,…, NR_L the collection of all the noise rise values calculated from (A.9) during the entire simulation time, and for all the Node Bs in the simulated network. The number L of noise rise values depends on the simulation time and on the number of simulated Node Bs (see Table A.1). Let us also introduce Z_1, Z_2,…, Z_L as the order statistics of NR_1, NR_2,…, NR_L (i.e. Z_i is the i^{th} smallest of NR_1, NR_2, … NR_L).

The 100·p% packet call throughput outage is defined as the sample (1-p) percentile of the order statistics Z_1, Z_2,…, Z_L.

$$nr^{p} = Z_{\lceil L \cdot (1-p) \rceil} \tag{A.10}$$

[A 2.8] *Other-to-Own Cell Interference Ratio*

The other-to-own cell interference ratio at one Node B is defined as the ratio of the total received power from users served by the Node B to the total received power from users served by other Node Bs. For the b^{th} Node B at time slot t, the set Ψ of users in the system can be divided into two disjoint subsets ${\Psi_b}^{own}[t]$ and ${\Psi_b}^{other}[t]$:

1. ${\Psi_b}^{own}[t] \cup {\Psi_b}^{other}[t] = \Psi$
2. User $j \in {\Psi_b}^{own}[t]$ if the b^{th} Node B is in the active set of user j at time slot t.
3. User $j \in {\Psi_b}^{other}[t]$ if the b^{th} Node B is not in the active set of user j at time slot t.

The other-to-own cell interference ratio for the b^{th} Node B at time slot t is defined as:

$$i_b[t] = \frac{\sum_{a=1}^{A}\left(\sum_{j\in\Psi_{other}{}^{b}[t]} {P_{tx}}^{j}[t]\cdot\left(\underline{\boldsymbol{h}}_{j,a}{}^{b}[t]\right)^{H}\cdot\underline{\boldsymbol{h}}_{j,a}{}^{b}[t]\right)}{\sum_{a=1}^{A}\left(\sum_{j\in\Psi_{own}{}^{b}[t]} {P_{tx}}^{j}[t]\cdot\left(\underline{\boldsymbol{h}}_{j,a}{}^{b}[t]\right)^{H}\cdot\underline{\boldsymbol{h}}_{j,a}{}^{b}[t]\right)} \qquad \text{(A.11)}$$

The distributions of the other-to-own cell interference ratio i shown in this dissertation include the statistics collected during the entire simulation time, and for all the Node Bs in the simulated network.

[A 2.9] *Packet Delay*

The packet delay is defined as the time interval between the time of arrival of a data packet in the user buffer and the instant in which the last bit of the data packet is correctly received at the Node B.

[A 2.10] *100·p% Packet Delay Outage*

Let us define PD_1, PD_2,…, PD_K the collection of packet delay values (see definition [A 2.9]) assembled during the entire simulation time, and for all the simulated users. The number K of packet delay values depends on the simulation time, on the number N of simulated users, as well as on the characteristics of the generated traffic. Let us also introduce J_1, J_2,…, J_K as the order statistics of PD_1, PD_2,…, PD_K (i.e. J_i is the i^{th} smallest of PD_1, PD_2,…, PD_K).

The 100·p% packet delay outage is defined as the sample (1-p) percentile of the order statistics J_1, J_2,…, J_K.

$$pd^{\,p} = J_{\lceil K\cdot(1-p)\rceil} \qquad \text{(A.12)}$$

[A 2.11] *Cell Throughput*

Let us define the ${\Psi_b}^{active}[t]$ the set of users being in an active packet call at time slot t, and for which the b^{th} Node B is the serving Node B. The serving Node B for a specific user is the Node B characterised by the strongest average path gain (see the definition [A 2.14]).

The instantaneous cell throughput for the b^{th} Node B at time slot t is defined as the sum of the per TTI throughput of all the users in the set $\Psi_b^{active}[t]$.

$$\Omega_b[t] = \sum_{j \in \Psi_b^{active}} \lambda_j[n_t] \tag{A.13}$$

In (A.13), n_t is the TTI number in correspondence of time slot t (see Figure A.3).

[A 2.12] *Average Cell Throughput*

Let us define T_1, T_2,…, T_L the collection of all the cell throughput values calculated from (A.13) during the entire simulation time, and for all the Node Bs in the simulated network. The number L of cell throughput values depends on the simulation time and on the number of simulated Node Bs (see Table A.1).

The average cell throughput is defined as the sample average of the values T_1, T_2,…, T_L.

$$\overline{T} = \frac{1}{L}\sum_{i=1}^{L} T_i \tag{A.14}$$

[A 2.13] *Pole Capacity*

The pole capacity is defined as the expected value of the instantaneous cell throughput as the noise rise tends to infinity. See definitions [A 2.11] and [A 2.6] for instantaneous cell throughput and noise rise, respectively.

[A 2.14] *Average Path Gain*

The average path gain between a user and a Node B at a given time instant is defined as the product between the distance-dependent path loss (including the effects of sectorised antenna pattern and antenna gain) and the lognormal distributed shadowing.

[A 2.15] *Average Number Of Users per Cell*

In this dissertation, the average number of user per cell is used as a parameter for the assessment of both system and user performance. It is defined as the ratio of the total number of users in the system to the number of cells in the network. Since both the number of users in the system and the number of cells in the simulated network are fixed parameters, the average number of users per cell does not change during the simulation time.

A.3 Accuracy of the Most Relevant Performance Indicators

This section deals with the level of accuracy of the simulation-based estimates of the most relevant performance indicators used throughout this Ph.D. thesis, namely:

- The *average cell throughput*,
- the *5% noise rise outage*,
- the *10% packet call throughput outage*, and
- the *average packet call throughput*.

The definition of these performance indicators has been introduced in detail in Section A.2.

The analysis of the level of accuracy of the performance indicators is mainly performed by means of standard statistical methods based on the simulation outputs generated by running approximately one hundred simulations with identical parameter setup, but modifying the seed of the random number generator at the beginning of each simulation.

This section also provides confidence intervals for the steady state average cell throughput and 5% noise rise outage. In this case, the generation of confidence intervals is based on the spectral analysis of time traces of both instantaneous cell throughput and instantaneous noise rise obtained from a single simulation, and only for one reference Node B.

Due to simulation time constraints, only the Node B code division scheduler of Chapter 4 is selected as a test case for the assessment of the level of accuracy of the performance indicators. The investigation is carried out for two simulation scenarios with an average of 11 and 21 users per cell, corresponding to a traffic-limited and an interference-limited scenario, respectively. The idea is to provide an indication of the stability of the performance indicators in two different scenarios characterised by different behaviours of the generated traffic. In a traffic-limited scenario the system is typically less stable, therefore higher variability of the performance indicators is expected. The lower stability in the traffic-limited region allow us to extend the accuracy results obtained for this scenario to the case of combined time and code division scheduling, which is typically characterised by higher variability compared to traditional code division scheduling.

A.3.1 Network-Related Performance Indicators

Figure A.4 and Figure A.5 report the box and whiskers diagrams for the average cell throughput and the 5% noise rise outage, respectively. Both average cell throughput and 5% NR outage are normalised to the sample mean, i.e. the mean value estimated by averaging over the output values from all one hundred simulations. In the box and whisker diagrams, the box is drawn stretching from the lower hinge (defined as the 25% percentile) to the upper hinge (the 75% percentile); the median value is also shown as a line across the box. The length of the box is defined as the inter-quartile range while the whisker on each side of the box extends to the most extreme data value within 1.5 times the inter-quartile range. Data values beyond the ends of the whiskers are marked as outliers [Mason89].

It is seen that the deviation of the network-related performance indicators from their corresponding sample mean never exceeds 3%. Also, the inter-quartile range is always

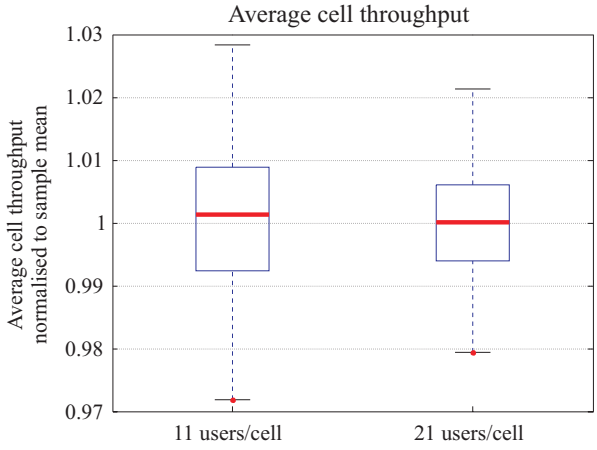

Figure A.4: Box plot of the average cell throughput normalised to the sample mean, for an average of both 11 and 21 users per cell.

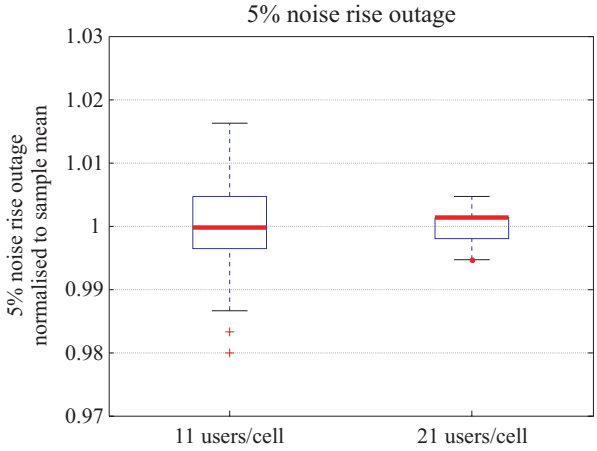

Figure A.5: Box plot of the 5% noise rise outage normalised to the sample mean, for an average of both 11 and 21 users per cell.

smaller than 0.02, i.e. in 50% of the cases the deviation from the sample mean is smaller than 1% Since in an interference-limited scenario the system is more stable due to less variations in the generated traffic, the accuracy of both average cell throughput and 5% NR outage estimates increases with the number of users in the system.[10]

As previously introduced, the level of accuracy of average cell throughput and 5% NR outage estimates can also be investigated through the generation of confidence intervals. In this case, the method used is based on the spectral analysis of time traces from a single simulation output.

A.3.1.1 Average Cell Throughput

For the average cell throughput, the generation of confidence intervals relies on the assumption that the variance of the sample mean of a covariance stationary process is given approximately by $p(0)/M$, where $p(f)$ is the spectral density at frequency f, and M is the sample size [Heid81b].

The method used to derive the estimate $\hat{p}(0)$ of the power spectrum at frequency zero makes use of the periodogram of the time trace of the instantaneous cell throughput for a reference Node B. The details on the method used for the derivation of $\hat{p}(0)$ can be found in [Heid81a].

Once the estimate of the spectral density at frequency zero is obtained, confidence intervals are derived assuming that $(\hat{\omega} - \omega)/(\hat{p}(0)/M)^{1/2}$ has a t-distribution with m degrees of freedom, where ω and $\hat{\omega}$ are the expected value and the sample mean of the covariance stationary sequence of cell throughput values, respectively. The number of degrees of freedom of the t-distribution depends on some specific parameters used for the estimation of $\hat{p}(0)$. See [Heid81a] for details.

Finally, the relative half-width of the confidence interval (defined as the half-width of the confidence interval divided by the point estimate $\hat{\omega}$) is derived as [Heid81a]:

$$\text{relative half-width} = \frac{t_{1-\alpha/2}{}^{m} \cdot (\hat{p}(0)/M)^{1/2}}{\hat{\omega}} \qquad \text{(A.15)}$$

In (A.15), $t_{1-\alpha/2}{}^{m}$ is the $1-\alpha/2$ percentile of the t-distribution with m degrees of freedom, and $1-\alpha$ is defined as the confidence interval. That is, there is a probability of $1-\alpha$ that the calculated confidence interval contains the true mean.

$$\text{Prob}\,(\,|\hat{\omega} - \omega| \le \text{half-width}\,) = 1-\alpha \qquad \text{(A.16)}$$

As already pointed out, both the estimation of the power spectrum at frequency zero and the point estimate $\hat{\omega}$ only make use of a single time trace from one reference Node B. On the other hand, the average cell throughout estimate from one system level simulation is derived taking into consideration all the Node Bs in the simulated network (see definition[A 2.12]). In the considered case, $\hat{p}(0)$ and $\hat{\omega}$ are estimated from a time trace with 20,000 cell throughput samples, while the total number of samples used for estimating the average cell throughput is $M = 20{,}000 \cdot 24 = 480{,}000$.

[10] Notice that with an average of 21 users per cell the median value coincides with the 75% percentile of the normalised 5% NR outage. The reason is that the 5% NR outage is estimated from system level simulations with a resolution of 0.02 dB. In a interference-limited scenario this value is comparable with the variability of the performance indicator itself, thus leading to a loss of resolution in the box plot at the right side of Figure A.5.

	Relative half-width of the corresponding confidence interval	
	11 users/cell	21 users/cell
95% confidence interval	2.1%	0.8%
80% confidence interval	1.3%	0.5%

Table A.2: Relative half-width of the 95% and 80% confidence intervals of the average cell throughput estimate, for an average of both 11 and 21 users per cell.

Table A.2 summarises the results obtained from (A.15) for an average of both 11 and 21 users per cell. The obtained values for the relative half-width confirm a high level of accuracy for the average cell throughput estimator. Notice that the confidence results in Table A.2 present a reasonable match (and the same trend versus number of users) with the standard statistical results reported in the box plots of Figure A.4.

A.3.1.2 5% Noise Rise Outage

For what concerns the 5% noise rise outage, a similar approach is used. In this case the generation of confidence intervals is slightly different since it is related to the estimation of a percentile value. Let us consider the time trace NR_1, NR_2,…, NR_L of noise rise values obtained from one system level simulation, and for one reference Node B. Let us also define the binary process $X_n(x)$ as:

$$X_n(x) = \begin{cases} 1 & \text{if } NR_n \le x \\ 0 & \text{otherwise} \end{cases} \tag{A.17}$$

Then, the relative half-width of the confidence interval for the estimation of the 100·p% percentile of the noise rise distribution can be obtained as [Chen99]:

$$\text{relative half-width} = \frac{(q_{1-\alpha/2} / f_{nr}(nr^{\wedge}_p)) \cdot (p_X{}^{\wedge}(0)/M)^{1/2}}{nr^{\wedge}_p} \tag{A.18}$$

In (A.18):

- $q_{1-\alpha/2}$ is the 1-α/2 percentile of the standard normal distribution,
- 1-α is the confidence interval,
- $f_{nr}(x)$ is the empirical probability density function of the noise rise obtained from the samples NR_1, NR_2,…, NR_L,
- $nr^{\wedge}_p$ is the point estimate of the 100·p% noise rise outage derived from the time trace NR_1, NR_2,…, NR_L,
- M is the total sample size, and
- $p_X{}^{\wedge}(0)$ is the estimation of the power spectrum at zero frequency of the binary process $X_n(nr^{\wedge}_p)$.

The details for the derivation of (A.18) can be found in [Chen99], while $p_X{}^{\wedge}(0)$ is estimated using the same procedure as described in [Heid81a]. The estimation of $p_X{}^{\wedge}(0)$ and $nr^{\wedge}_p$ is based on a noise rise trace with approximately 300,000 samples, while the 5% noise rise outage estimate obtained from one system level simulation is based on a total sample size of M = 300,000·24 = 7,200,000.

	Relative half-width of the corresponding confidence interval	
	11 users/cell	21 users/cell
95% confidence interval	1.0%	0.5%
80% confidence interval	0.7%	0.3%

Table A.3: Relative half-width of the 95% and 80% confidence intervals of the 5% noise rise outage estimate, for an average of both 11 and 21 users per cell.

Table A.3 summarises the results obtained from (A.18) for an average of both 11 and 21 users per cell. Also in this case the generated confidence intervals for the 5% NR outage are very much in accordance with the standard statistical results shown in Figure A.5.

A.3.2 User-Related Performance Indicators

Due to the limited sample size in case of packet call throughput statistics, and hence limited accuracy for spectral estimation, the level of accuracy of the user-related performance indicators is assessed only by means of standard statistical methods.

Figure A.6 and Figure A.7 report the box and whiskers diagrams for the 10% PCT outage and for the average PCT, respectively. Both performance indicators are normalised to their corresponding sample mean, i.e. the mean value estimated by averaging over the output values from all one hundred simulations.

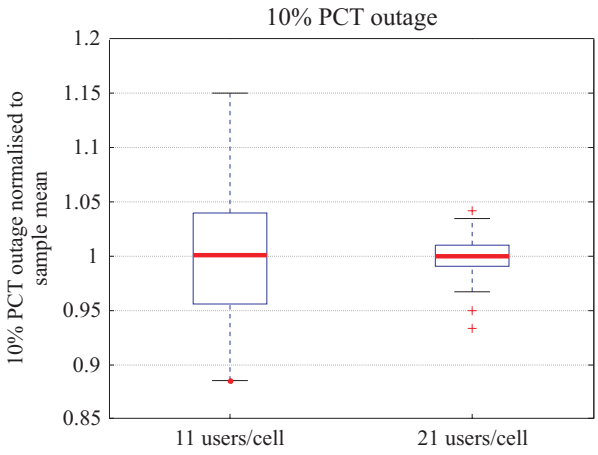

Figure A.6: Box plot of the 10% PCT outage normalised to the sample mean, for an average of both 11 and 21 users per cell.

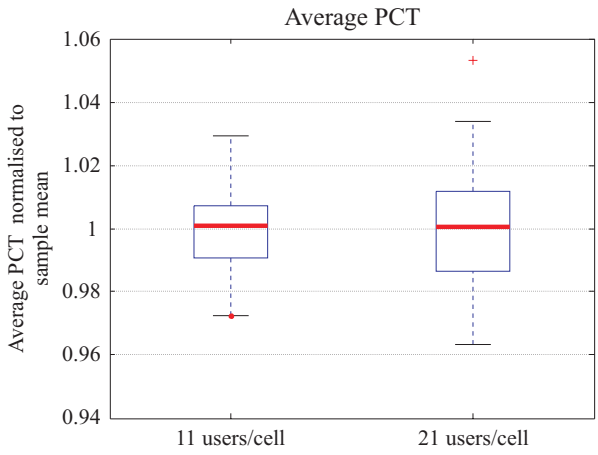

Figure A.7: Box plot of average PCT normalised to the sample mean, for an average of both 11 and 21 users per cell.

It is seen that the variability of the 10% PCT outage estimate is relatively high in the traffic-limited scenario, in which case a maximum deviation from the sample mean of approximately 15% can be observed. However, the inter-quartile range is included in the region between 0.95 and 1.05, i.e. in 50% of cases the error is smaller than 5%. The variability of the 10% PCT outage estimate significantly decreases for a higher number of users in the system. Concerning the average packet call throughput, the deviation from the sample mean is in practice always smaller than 5%.

Appendix B

Power Increase Estimator for Uplink

This appendix provides a general description of the uplink power increase estimator PIE used in the system level simulator. As shortly introduced in Chapter 2, the PIE is used in the packet scheduling procedure to determine the uplink fractional load variation when upgrading the allocated user data rate, and hence to derive an estimate of the change in total received power at the base station receiver. Moreover, the power increase estimator is used to determine the contribution to the total uplink load change from inactive NRT bearers that can potentially start transmission during the next scheduling period. The scope of the power increase estimator is to prevent the system from entering overload conditions, and to guarantee the respect of the planned coverage area. The power increase estimator described in this appendix is also used in the decrease load algorithm for load control purposes (see Figure 2.10).

B.1 Basic Principles

Every packet scheduling period, the packet scheduler (PS) estimates the increase in uplink load caused by any data rate upgrade, and allows the allocation of additional radio resources only if the total receive power is estimated below the planned target, as shown in Figure B.1.

In Figure B.1, *PrxTotal* is the total received power at the base station receiver before entering the packet scheduling procedure. The total change in uplink received power due to the allocation of additional resources to requesting bearers and to the reservation of the granted resources to inactive NRT bearers is denoted as $\Delta PrxTotal$. *PrxTarget* is the total planned received power, while the relation between the uplink fractional load η_{UL} and the noise rise (see definition [A 2.6]) is given in (3.6). The difference ΔL between the uplink fractional load after and before packet scheduling can be estimated by summing the single contributions from each bearer being allocated additional radio resources, and from each inactive bearer being reserved its currently allocated radio resources.

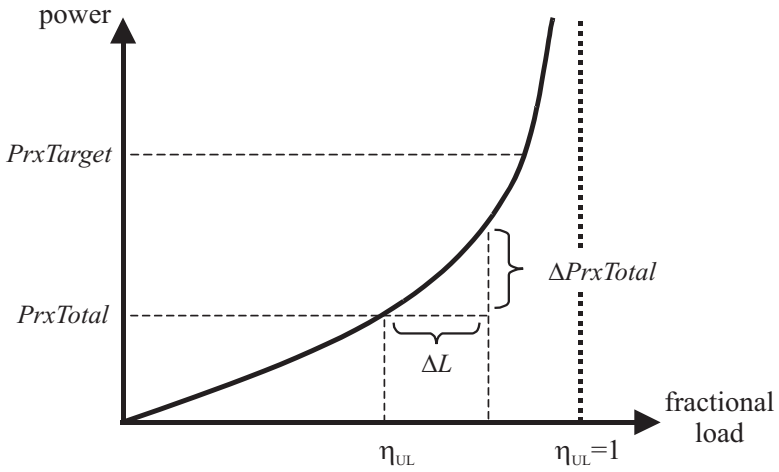

Figure B.1: Change in total received uplink power as a function of the fractional load change ΔL and of the fractional load η_{UL} in correspondence with the system operation point (PrxTotal).

In general, the fractional load η_j associated to user *j* can be derived from (3.2) as:

$$\eta_j = \frac{1}{1+\frac{W}{R_j \cdot \rho_j}} \tag{B.1}$$

In (B.1), *W* is the WCDMA chip rate, while *Rj* and ρ_j are the data rate allocated to user *j* and the estimated required energy-per-bit to noise ratio (E_b/N_0) for the corresponding NRT service, respectively.

From (B.1), the increase in fractional load caused by user *j* when its allocated data rate is increased from ${R_{old}}^j$ to ${R_{new}}^j$ can be written as in (B.2). Similarly, the fractional load to be reserved to an inactive user *j* with allocated data rate R_j can be expressed as in (B.3).

$$\Delta {L_{modified}}^j = \frac{1}{1+\frac{W}{{R_{new}}^j \cdot \rho_j}} - \frac{1}{1+\frac{W}{{R_{old}}^j \cdot \rho_j}} \tag{B.2}$$

$$\Delta {L_{inactive}}^j = \frac{1}{1+\frac{W}{R_j \cdot \rho_j}} \tag{B.3}$$

Defined $N_{modified}$ as the number of users whose allocated data rate is modified during the packet scheduling procedure, and $N_{inactive}$ as the number of NRT users for which inactivity is detected, the total fractional load variation ΔL in Figure B.1 is computed as:

$$\Delta L = \sum_{j=1}^{N_{modified}} \Delta {L_{modified}}^j + \sum_{j=1}^{N_{inactive}} \Delta {L_{inactive}}^j \tag{B.4}$$

After reserving uplink load to inactive NRT bearers, the PS starts upgrading the allocated data rate to users issuing a capacity request. At each step of the data rate upgrading procedure, the PS updates the value of the fractional load change ΔL and, using the power increase estimator

(B.8), estimates whether or not the allocation of additional resources causes the total received power to exceed the planned target. The packet scheduling procedure is terminated when the total available uplink power is exhausted, when there are no more capacity requests to be processed, or when the fractional load change due to modified radio bearers exceeds a predefined threshold value (see Table 3.2).

B.2 Power Increase Estimator

There are two methods for mapping an increase of the uplink fractional load to an equivalent increase in total received uplink power: The derivative method and the integrative method [Holma99]. Both power increase estimators are derived from the following relation, where P_{noise} is the background noise power.

$$PrxTotal = \frac{P_{noise}}{1-\eta_{UL}} \tag{B.5}$$

The equations to derive the change in the total received uplink power $\Delta PrxTotal$ (see Figure B.1) for the derivative and for the integrative methods are given in (B.6) and (B.7), respectively. A detailed derivation of these expressions can be found in [Holma99].

$$\Delta PrxTotal = \frac{\Delta L}{1-\eta_{UL}} \cdot PrxTotal \tag{B.6}$$

$$\Delta PrxTotal = \frac{\Delta L}{1-\eta_{UL}-\Delta L} \cdot PrxTotal \tag{B.7}$$

The power increase estimator deployed in the system level simulator is a weighted combination of the derivative and of the integrative methods.

$$\Delta PrxTotal = k \cdot \left(\alpha \cdot \frac{\Delta L}{1-\eta_{UL}} + (1-\alpha) \cdot \frac{\Delta L}{1-\eta_{UL}-\Delta L} \right) \cdot PrxTotal \qquad \begin{matrix} \alpha \in [0,1] \\ k \in [0,1] \end{matrix} \tag{B.8}$$

In (B.8), the parameter α defines the uplink power change estimation weight between the derivative and the integrative method. By adjusting the variable k, the power increase estimator can be forced to be more under estimating. Default values for α and k used in the system level simulator are $\alpha = 0.5$ and $k = 1$.

In the load control algorithm, the power decrease is estimated using in (B.8) *PrxTarget* instead of *PrxTotal*, and $|\Delta L|$ instead of ΔL. The estimated total received power after load control is then estimated by subtracting $\Delta PrxTotal$ to *PrxTotal*. The load control algorithm is completed when the estimated received uplink power is below the planned target.

Appendix C

Uplink transmission: DPDCH and DPCCH

This appendix outlines some of the main issues related to the mapping between link level and system level simulations. First, an introduction on the physical channel structure of WCDMA FDD uplink is presented. The method based on Actual Value Interface (AVI) is then shortly reviewed. Finally, the appendix presents a discussion on the impact that the model used in the system level simulator has on the performance assessment of WCDMA uplink packet access.

C.1 Introduction

WCDMA defines two types of dedicated physical channels for the uplink: The dedicated physical data channel (DPDCH) and the dedicated physical control channel (DPCCH). The DPCCH carries the physical layer control information, including pilot bits for channel estimation in the receiver, downlink power control commands, and information on the transport format combination used on the parallel DPDCH(s). The higher layer information, including user data, is carried on one or more DPDCHs. The maximum number of simultaneously transmitted DPDCHs is 6. The uplink dedicated physical channels are transmitted in parallel I-Q branches, using different codes and spreading factors. Figure C.1 presents the generic structure of an uplink transmitter according to 3GPP [TS25213]. The signals are multiplied by a channelisation code for channel discrimination and by a scrambling code for user discrimination. Additionally, the data and control channels are given different relative power strengths by means of the power scale factors β_c and β_d [TS25213]. On the DPDCH, the spreading factor can vary between 4 and 256, while the spreading factor for the DPCCH is fixed to 256 [TS25213].

C.2 Actual Value Interface (AVI) Method

The actual value interface (AVI) is a method to connect link and system level simulations. The performance of the link level algorithms is neither measured nor analysed during system level simulations, but its effect is included by means of AVI tables [Hämä97].

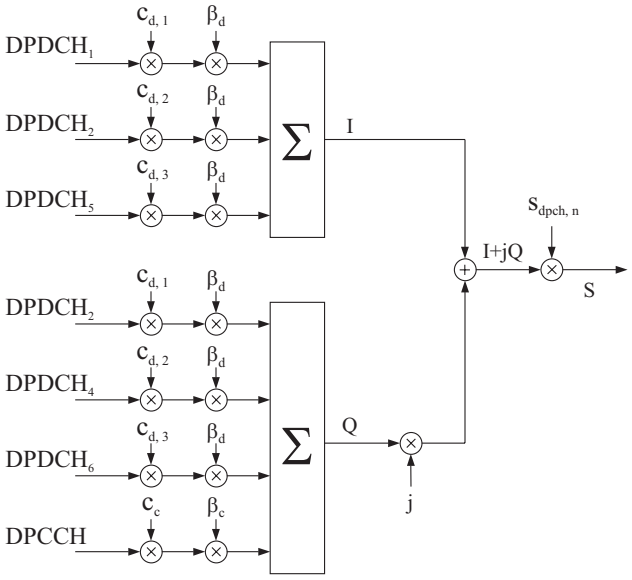

Figure C.1: Transmission of data through one or more DPDCHs and one DPCCH according to 3GPP [TS25213].

The generation of AVI tables for the performance assessment of WCDMA uplink evolution is out of the scope of this Ph.D. study. However, a good understanding of the method based on actual value interface is indispensable in order to assess the reliability of system level simulations when new features such as L1 HARQ with soft combining, combined time and code division scheduling, and 2 ms TTI are introduced.

Essentially, AVI tables are used in system level simulations to map a value of the per TTI average received E_b/N_0 (see definition [A 2.5]) to an equivalent block error probability for the transmitted radio frame. Figure C.2 plots the AVI tables used in this Ph.D. thesis for three different propagation and mobility scenarios: Vehicular A at 50 km/h, Vehicular A at 3 km/h,

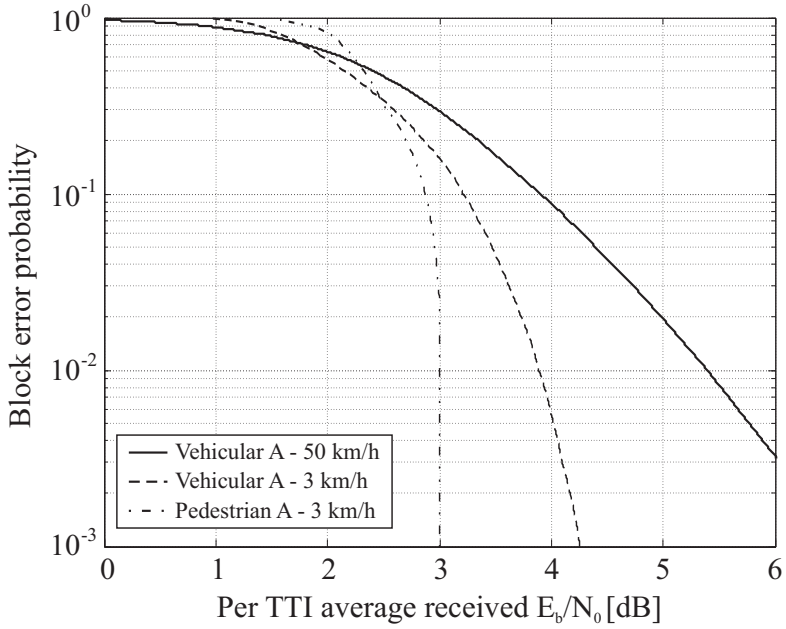

Figure C.2: Block error probability as a function of the average per TTI E_b/N_0 for Vehicular A channel profile at 3 and 50 km/h, and for Pedestrian A channel profile at 3 km/h. The AVI tables are obtained assuming packet-switched services at 64 kbps, 10 ms TTI, and include the effect of fast closed loop power control.

and Pedestrian A at 3 km/h [Outes04]. All the reported AVI results have been obtained assuming packet-switched services at 64 kbps (with a DPCCH to DPDCH power ratio of -5.46 dB), 10 ms TTI, and include the effect of fast closed loop power control.

From the definition of energy-per-bit to noise ratio (E_b/N_0) in [A 2.5], it is clear that the AVI tables used in this Ph.D. thesis include the combined operation of both DPDCH and DPCCH. I.e., AVI tables provide a block error probability value associated to the data part by taking as input the E_b/N_0 value that corresponds to the sum of the contributions from the DPDCH and the DPCCH.

When using the AVI tables in Figure C.2 for data rates different from 64 kbps, the impact of the changed DPCCH to DPDCH power ratio is not taken into consideration. The DPCCH to DPDCH power ratio also plays an important role in case of L1 HARQ schemes with soft combining of information received at different transmission instants of the same data frame. These and other issues concerning the use of AVI tables with 2 ms TTI are discussed more in detail in the following subsections.

C.3 Impact of the Use of the Same AVI Tables with Different Data Rates

Let $\rho[R]$ be the required E_b/N_0 as defined in [A 2.5] (i.e. including the contribution from both DPDCH and DPCCH) to meet a specific BLER target for a given data rate R. The corresponding E_b/N_0 associated to the data channel can be derived as:

$$\rho_{data}[R] = \frac{\rho[R]}{1+\gamma[R]} \tag{C.1}$$

In (C.1), $\gamma[R]$ is the DPCCH to DPDCH power ratio and is a function of the DPDCH data rate R. Now, let us assume that the performance with respect to the received E_b/N_0 on the data channel is independent of the selected data rate for transmission. I.e., the required E_b/N_0 on the DPDCH to meet the specified BLER target remains constant as the DPDCH data rate varies.

$$\rho_{data}[R] = \rho_{data} \quad \forall R \in \text{TFCS} \tag{C.2}$$

As a consequence, the following relation between the E_b/N_0 requirements for different data rates can be derived.

$$\frac{\rho[R]}{\rho[R']} = \frac{1+\gamma[R]}{1+\gamma[R']} \tag{C.3}$$

An error is made when the AVI tables in Figure C.2 are used to set the E_b/N_0 requirement for data rates different from 64 kbps, and the error depends on the particular value of $\gamma[R]$. 3GPP specifies different values of the DPCCH to DPDCH power ratio for different data rates [TS25101]. These must be interpreted as reference values for a given Transport Format Combination (TFC). When the user modifies the data rate on the DPDCH, it computes the gain factors β_c and β_d (see Figure C.1) based on the signalled settings for a reference TFC [TS25214]. According to [TS25101], whenever the data rate for transmission on the DPDCH is changed, the corresponding power step must be calculated so that the power transmitted on the DPCCH follows the inner loop power control. The reason for this is that power control is based on signal-to-interference plus noise ratio (SINR) measurements performed on the DPCCH at the base station receiver. As a consequence, when the DPDCH data rate is

changed, the DPCCH to DPDCH power ratio is updated so that the E_b/N_0 performance on the data channel is maintained. The SINR on the DPCCH can be derived from the E_b/N_0 requirement for a given data rate R as:

$$SINR_{control}[R] = \frac{R}{W}\rho[R]\frac{\gamma[R]}{1+\gamma[R]} \tag{C.4}$$

Imposing the SINR on the control channel to be equal independently of the DPDCH data rate, the following relation is obtained.

$$\frac{\gamma[R]}{\gamma[R']} = \frac{R'}{R} \tag{C.5}$$

Based on the reference DPCCH to DPDCH power ratio of -5.46 dB for 64 kbps [TS25101], the power ratios for different data rates are calculated according to (C.5). Then, the error made in the system level simulations when setting the E_b/N_0 requirement for different data rates using the AVI tables in Figure C.2 is derived substituting the obtained values for $\gamma[R]$ in (C.3). The ratio of the required E_b/N_0 with data rate R to the required E_b/N_0 with 64 kbps is reported in Table C.1 for different values of the DPDCH data rate. Due to the lower DPCCH to DPDCH power ratio, the required E_b/N_0 including both data and control channels generally decreases as the DPDCH data rate increases.

Data rate	$\rho[R]/\rho$[64 kbps]
64 kbps	0.00 dB
128 kbps	-0.51 dB
256 kbps	-0.79 dB
384 kbps	-0.87 dB
768 kbps	-0.99 dB

Table C.1: Offset in the required E_b/N_0 for different data rates with respect to the reference value for 64 kbps.

In Table C.1, the E_b/N_0 inaccuracy is only reported for data rates higher than 64 kbps. There are two main reasons for this: First of all, data rates lower than 64 kbps are hardly ever selected for transmission in the simulation scenarios considered in this Ph.D. thesis (see e.g. Figure 3.9, Figure 4.16, Figure 4.19, Figure 6.4, Figure 6.5, and Figure 6.14). Moreover, with data rates lower than 64 kbps and 10 ms TTI the channel coding performance starts to get worse because of the smaller block size at the input of the turbo coder. This means, the underlying assumption that the performance with different data rates only depends on the received E_b/N_0 on the data channel does not hold true.

It should be mentioned that the same assumption is in reality ideal also for data rates higher than 64 kbps, in which case the required DPDCH E_b/N_0 for the same BLER target is typically higher due to the increased inter-path interference. In [Holma04], it is shown that the degradation caused by inter-path interference in a frequency selective channel is about 0.6 dB for a BLER target of 10% and an uplink data rate of 512 kbps.

Moreover, as shortly introduced in definition [A 2.5], the system level simulator uses a fictitious data rate of 2 kbps in the case no data is transmitted on the DPDCH, i.e. transmission only takes place on the DPCCH. As a consequence, the transmission power of a

user switching from data transmission with rate R to no data transmission (only DPCCH) is reduced by a factor $R/2\cdot10^3$. To evaluate the accuracy of this assumption, let us define $P_{data}[R]$ the received power on the DPDCH when transmitting with data rate R, $P_{control}$ as the power received on the DPCCH, and I as the interference including background noise power at the base station receiver [11]. Then, the SINR on the DPCCH can be written as in (C.6) when data is transmitted on the DPDCH at a rate $R\neq0$ kbps, and as in (C.7) when no data is transmitted on the DPDCH.

$$SINR_{control}[R] = \left(\frac{P_{data}[R] + P_{control}}{I}\right)\frac{\gamma[R]}{1+\gamma[R]} \tag{C.6}$$

$$SINR_{control}[0\text{ kbps}] = \frac{P_{control}}{I} \tag{C.7}$$

The fictitious data rate R_0 to be used when scaling the transmission power of a user switching from data transmission with rate R to no data transmission can be derived by imposing the expressions in (C.6) and (C.7) to be equal.

$$R_0[R] = R\cdot\frac{P_{control}}{P_{data}[R]+P_{control}} = R\cdot\frac{\gamma[R]}{1+\gamma[R]} \tag{C.8}$$

Comparing the values of $R_0[R]$ from (C.8) with 2 kbps, it can be seen that an error is made in the system level simulator when setting the DPCCH power in case of no data transmission on the DPDCH. The values of the ratio between the fictitious data rate $R_0[R]$ and 2 kbps are reported in Table C.2 for different values of the DPDCH data rate R. Notice that the difference in the ratio $R_0[R]/2\cdot10^3$ between 64 kbps and a generic data rate R is exactly equal to the corresponding ratio $\rho[R]/\rho[64\text{ kbps}]$ reported in Table C.1. I.e., the overall error made in setting the DPCCH power in case of no data transmission on the DPDCH is not data rate dependent. This issue is clarified in more detail later on in this section.

Data rate	$R_0[R] / 2\cdot10^3$
64 kbps	8.50 dB
128 kbps	9.01 dB
256 kbps	9.29 dB
384 kbps	9.39 dB
768 kbps	9.49 dB

Table C.2: Offset between real and simulated DPCCH power whenever a user switches from data transmission at rate R to no data transmission (only DPCCH).

Though the error values in Table C.2 might seem quite significant, the power level when transmitting only on the DPCCH is much lower than with high DPDCH data rates, thus the impact on system level performance is expected to be minimum.

[11] Notice the since the power transmitted on the DPCCH is only supposed to follow the power control commands [TS25101], the power received on the control channel is assumed to be independent of the DPDCH data rate.

To better illustrate this issue, let us consider the variation in uplink load caused by using the fictitious data rate $R_0[R]$ derived in (C.8) to simulate transmission on the DPCCH compared to using a data rate of 2 kbps. To estimate the effect on the uplink fractional load, (B.2) can be used.

$$\Delta L_0 = \frac{1}{1+\frac{W}{R_0[R]\cdot\rho[R]}} - \frac{1}{1+\frac{W}{2\cdot 10^3\cdot\rho[64\,\text{kbps}]}} \tag{C.9}$$

As previously introduced, ΔL_0 does not depend on the DPDCH data rate R, since from (C.3), (C.5) and (C.8) the product $R_0[R]\cdot\rho[R]$ is a constant.

Similarly, we derive the uplink load variation caused by a user transmitting with data rate R, and whose E_b/N_0 requirement is determined using the AVI tables in Figure C.2 without an opportune modification according to the values in Table C.1. The same equation as before can be used:

$$\Delta L_R = \frac{1}{1+\frac{W}{R\cdot\rho[R]}} - \frac{1}{1+\frac{W}{R\cdot\rho[64\,\text{kbps}]}} \tag{C.10}$$

For different propagation and mobility scenarios, Table C.3 reports values of ΔL_0 and ΔL_R (R=384 kbps and R=768 kbps). The reference E_b/N_0 requirements for 64 kbps to be used in (C.9) and (C.10) are derived from the AVI tables in Figure C.2 for a BLER target of 10%.

	Veh A – 3 km/h	Ped A – 3 km/h	Veh A – 50 km/h
ΔL_0	0.0100	0.0085	0.0122
$\Delta L_{384\text{ kbps}}$	-0.0355	-0.0323	-0.0393
$\Delta L_{768\text{ kbps}}$	-0.0525	-0.0499	-0.0549

Table C.3: Variation in uplink load compared to the model used in the system level simulations for users transmitting at different data rates, and for various propagation and mobility scenarios.

With a more accurate model than the one used in the system level simulator, the increase in uplink load caused by a user that only transmits on the DPCCH is about 1%. At the same time, the decrease in uplink load caused by a user transmitting with high data rates is between 3% and 5%. I.e., with an accurate model the additional uplink load caused by 3 to 5 users that only transmit on the DPCCH is approximately compensated by the load decrease caused by a user transmitting with a high DPDCH data rate.

As a conclusion, the model used in the system level simulator can be assumed to be sufficiently accurate, especially for the generation of relative gain numbers.

C.4 Impact of AVI Tables on the Performance of L1 HARQ

With HARQ techniques such as CC and IR, different versions of the same data frame received at different transmission instants are combined at the receiver. In the system level simulator soft combining is modelled by adding the received E_b/N_0 to the cumulated E_b/N_0 from previous transmissions, including a certain combining loss [Fred02] (see Section 4.5.1).

The cumulated E_b/N_0 is than used as an input to the AVI tables to obtained the block error probability after combining. However, the E_b/N_0 from every single retransmission includes the energy from both the DPDCH and the DPCCH, whereas soft combining is only intended for the data channel.

Let ρ_n be the received E_b/N_0 at the n^{th} transmission of one data frame including the contribution of both data and control channels. Since at each retransmission only the DPDCH E_b/N_0 has to be added to the cumulated E_b/N_0, (4.23) should be rewritten as:

$$\rho_{cum,n} = \begin{cases} \rho_n & n = 1 \\ \rho_{cum,n-1} + \dfrac{\dfrac{\rho_n}{1+\gamma[R_n]}}{L_{comb}} & 1 < n \le N \end{cases} \qquad \text{(C.11)}$$

In (C.11), L_{comb} is the loss to due to soft combining that must be subtracted to the ideal combining gain, and was already included in (4.23). Moreover, M is the maximum number of L1 transmissions, and $\rho_{cum,n}$ is the cumulated E_b/N_0 after n transmissions. Differently from (4.23), (C.11) also includes a combining loss due to the transmission of the DPCCH. This loss is more significant for higher values of the DPCCH to DPDCH power ratio, i.e. for lower data rates. Assuming the same received E_b/N_0 at different transmission instants of the same data frame ($\rho_1=\rho_2=\ldots=\rho_M$), the loss due to the DPCCH after m retransmissions can be written as:

$$L_{control,m} = \frac{\rho_{cum,m+1}^{(4.23)}}{\rho_{cum,m+1}^{(C.11)}} = \begin{cases} \dfrac{2\cdot(1+\gamma[R])}{2+\gamma[R]} & m = 1 \\ \dfrac{(1+\gamma[R])\cdot\left(2+\sum_{i=1}^{m-1}(L_{comb})^i\right)}{2+\gamma[R]+\sum_{i=1}^{m-1}(L_{comb})^i} & 1 < m \le M-1 \end{cases} \qquad \text{(C.12)}$$

For a DPCCH to DPDCH power ratio of -5.46 dB (corresponding to a data rate of 64 kbps), the loss in the cumulated E_b/N_0 due to the control channel overhead is 0.51 dB after one retransmission. For data rates higher than 64 kbps the loss is lower, as the DPCCH to DPDCH power ratio decreases. For 64 kbps, the combining gain after one retransmission can be approximated as:

$$G_{comb,64\ kbps} = 3\ dB\ (ideal\ combining) - 0.2\ dB\ (L_{comb}) - 0.51\ dB\ (L_{control}) = 2.29\ dB \qquad \text{(C.13)}$$

The assumption of an ideal combining gain of 3 dB can be done since with fast power control the average received E_b/N_0 at different transmission instants can be assumed to be approximately constant. From the AVI tables in Figure C.2 and considering a BLER target at first transmission of 10%, it can be seen that a combining gain of 2.29 dB is sufficiently large to reasonably assume that a data frame will be correctly received after one retransmission with probability close to 1. Hence, modelling soft combining using (4.23) instead of (C.11) is expected to have a marginal impact on the performance assessment of L1 HARQ schemes, especially for low mobility scenarios.

C.5 Use of AVI Tables with 2 ms TTI

Another issue with AVI tables is related to 2 ms TTI operation and fast power control. Even assuming perfect power control with no delay, the instantaneous received E_b/N_0 differs from the planned target due to the discrete power step used in the power control procedure. As a consequence, the per TTI average received E_b/N_0 does not always equal the target E_b/N_0, and AVI tables typically allow for this effect. The standard deviation of the difference between the average received E_b/N_0 and the target E_b/N_0 depends on the power control step and on the number of power control commands in one TTI. In order to maintain approximately the same standard deviation as for 10 ms TTI, with 2 ms TTI the power control step is reduced (see Table A.1). In the simulated scenarios with 2 ms TTI and a low terminal speed this is not expected to have great impact on the power control performance, while it reduces the error made by using AVI tables generated assuming a frame size of 10 ms.

Appendix D

Traffic Modelling

D.1 Traffic Model

Traffic modelling plays a fundamental role in the performance assessment of packet scheduling strategies for NRT data services. Although different services are characterised by different data traffic profiles, it is possible to underline some features common to nearly all NRT services:

- At the start of a connection, some small messages are typically exchanged to setup the service.
- During the packet data session, packets are generated by the application level and transmitted over the air interface.
- At the end of the service often some small packages are exchanged between the peer entities.

Since both start and end phase are characterised by the transmission of a small amount of data in both uplink and downlink directions, data transmission in these phases is likely to take place on common channels (i.e. on either the RACH or the CPCH in uplink, and on the FACH in downlink). As the focus of this Ph.D. thesis is on packet scheduling on dedicated channels, the traffic model implemented in the system level simulator neither considers the start phase nor the end phase, but only models the main data session.

Figure D.1 shows the main characteristic of the source traffic model considered in this Ph.D. thesis. Similarly to other models, it defines a packet call arrival process and, within each packet call, a datagram arrival process. In the considered model, the packet session arrival process is not specified, and it is assumed that packet calls are generated indefinitely for the entire simulation time.

For the packet call arrival process, the packet call duration and the reading time (the time between packet calls) are specified. The reading time starts at the successful transmission of all datagrams generated during the previous packet call to emulate a closed loop transmission mode. I.e., it is imagined that before starting the reading time, the application running on the UE needs to await acknowledgement from the network peer.

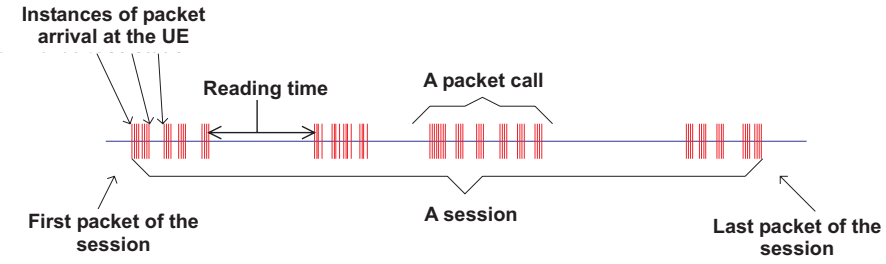

Figure D.1: A source packet data model with packets arriving as part of a packet call [TR25896].

For the datagram arrival process, the packet size and the interarrival time between datagrams are specified. The model for this is largely derived from the modified gaming model in [TR25896].

The traffic model and its closed loop feature are illustrated in Figure D.2. Essentially, the state of a simulated user with respect to the generation and the transmission of data packets can be divided into three main phases:

1. In the first phase, source data is generated in the user RLC buffer. During this first phase, data is transmitted based on the buffer occupancy and on the data rate allocated by the packet scheduler. This first phase is referred to as packet call.
2. During the second phase, the generation of source data in the user RLC buffer is terminated. At the same time, the terminal continues transmitting the data it has accumulated during the packet call period. The second phase is ended whenever all the buffered data has been successfully transmitted. The first and the second phase together form the 'on' period of the traffic model duty cycle.
3. Finally, during the third phase (reading time) no data is generated in the user RLC buffer. Since the buffer is empty when the third phase is started, during the reading time no data is transmitted on the dedicated physical data channel. The reading time corresponds to the 'off' period of the traffic model duty cycle.

The model is implemented in the system level simulator assuming infinite user RLC buffer size, as well as infinite lifetime of a packet in the buffer.

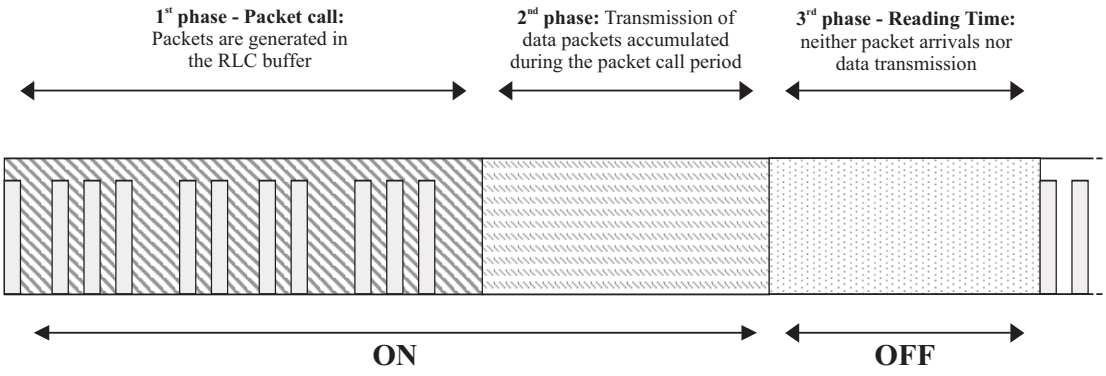

Figure D.2: Source traffic model and its closed loop feature.

				Default	Modified
Packet Call	Distribution of packet call period	Exponential	Mean	5 s	5 s
	Distribution of reading time	Exponential	Mean	5 s	5 s
Datagram	Distribution of inter-arrival time between datagrams	Log-Normal	Mean	40 ms	50 ms
			Standard deviation	38 ms	47 ms
	Size (Fixed)			1152 bytes	3000 bytes
Resultant average source rate during packet call periods				≅ 250 kbps	≅ 495 kbps

Table D.1: Parameter setup for the modified and the default traffic models.

In the performance assessment of WCDMA uplink packet access presented in this Ph.D. thesis, two different traffic model setups are used. A default traffic model is first introduced in Chapter 3, and also used for performance assessment of different packet scheduling strategies throughout Chapter 4 and Chapter 5. However, for the performance assessment of advanced system features such as peak data rates up to 768 kbps, 4-branch antenna diversity, and interference cancellation, a traffic model characterised by a higher average source data arte is needed. Therefore, a modified version of the default traffic model is introduced in Chapter 6, and referred to as modified traffic model.

The traffic model parameter setup for the default and for the modified traffic models is reported in Table D.1.

D.2 Packet Call Arrival Process

As shortly introduced in Section A.1.1, at the beginning of each simulation users are placed in the network, and for the entire simulation time users neither enter nor leave the system. Though the total number of users in the system is a fixed parameter, the number of users having data to transmit fluctuates during the simulation time due to the on/off nature of the traffic generated by each user. The users being in an ‘on’ period of their duty cycle are also referred to as active users.

To illustrate this issue, Figure D.3 gives a graphical representation of the packet call arrival process for the traffic model deployed in the system level simulator. It can be seen that the

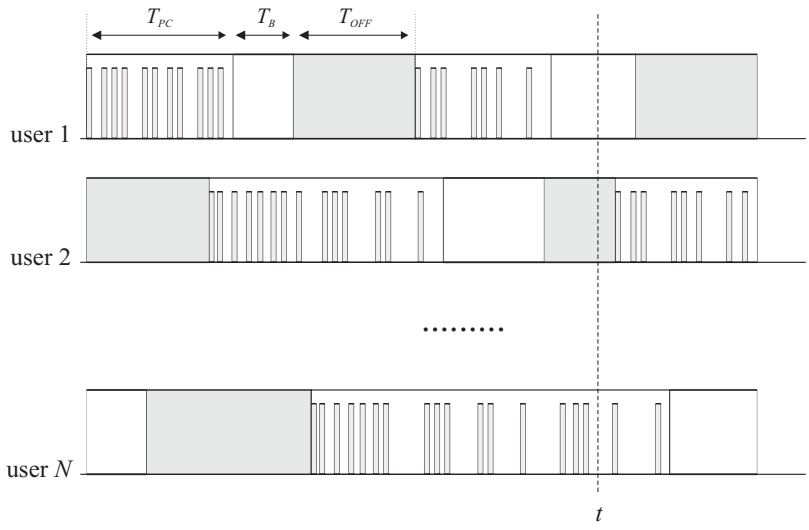

Figure D.3: Graphical representation of the packet call arrival process in the system level simulator.

number of active users at a generic time instant *t* can be described as a stochastic process, whose characteristics intrinsically depend on the packet call arrival process.

Figure D.3 also illustrates that the interarrival time between packet calls at one user is given by the sum of the packet call duration T_{PC}, the reading time T_{OFF}, and the time T_B the user needs for transmitting the data he has accumulated during the packet call period. While T_{PC} and T_{OFF} are two independent exponentially distributed random variables (see Table D.1), the distribution of T_B depends on a number of unknown factors. This makes it relatively complex to analytically characterise the packet call arrival process at each simulated user, and hence the overall packet call arrival process. However, an analytical derivation of the packet call arrival process for the considered traffic model is outside the scope of this Ph.D. thesis, and for this reason is left out of the presented analysis.